Università degli Studi di Padova

Dipartimento di Geoscienze

SCUOLA DI DOTTORATO DI RICERCA IN SCIENZE DELLA TERRA

CICLO XXVIII

VARIABILITY OF LATE-QUATERNARY TRANSGRESSIVE SEDIMENTATION IN THE NORTHERN ADRIATIC SEA

Direttore della Scuola: Prof. Fabrizio Nestola

Supervisore: Prof. Cristina Stefani

Co-supervisori: Dr. Annamaria Correggiari, Dr. Alessandro Fontana

Dottorando: Giorgia Moscon

TABLE OF CONTENTS

ABSTRACT

The Adriatic Sea is an epicontinental semi-enclosed basin characterized by a low axial gradient shelf in the northern and central part. In particular, during the post-LGM transgression, the northern Adriatic shelf was affected by huge drowning due to slight sea-level rise. In this context, different generation of barrier-lagoon systems were developed and preserved. Thus, these transgressive bodies, on the Adriatic seafloor, record different phases of the relative sea-level rise. In the last few decades, several authors focused their study on the last transgressive cycle to reconstruct the evolution of the last relative sea-level rise in order to identify and predict its impact on the present coastal and terrestrial environments. The aim of this PhD thesis was a detailed characterization of transgressive deposits sedimented and preserved during distinct phases of the last relative sea-level rise in the northern Adriatic shelf. These sedimentary bodies, indeed, are one of the more appropriate direct sea-level indicators and their study could be the key to better constrain the paleo sea-level and predict possible scenarios of environmental changes. Moreover, these transgressive deposits are identified as an economical resource because their sand portion, indicative of fossil shorelines, can be exploited for beaches nourishment. The characterization of different deposits was carried out with a multidisciplinary approach through the analyses of very high resolution seismic profiles, cores, bathymetric maps, petrographic samples, and XRF core scanner analysis.

To improve the sea-level Mediterranean curve with new data, a preserved transgressive deposit south of the Po River delta was studied in detail. This sedimentary body, formed in a portion of the shelf affected by strong sediment supply, recorded different environments. The high quality of the acquired data and the considerable preservation of this deposit allowed to recognize and date different peat and organic-rich layers that testify brackish lagoon facies representative of distinct paleo sea-level position. The new radiocarbon data permitted to calculate the rate of sedimentation and the rate of the relative sea-level rise during the deposition of the investigated body. In particular, these high resolution data could be used to detect centennial fluctuations and calibrate sea-level models.

Furthermore, to obtain new data on the paleogeography of the Adriatic shelf, eight starved and reworked transgressive deposits, northern of the present Po River delta, were investigated with petrographic and preliminary XRF core scanner analyses. The compositional results highlighted three sedimentary petrofacies (petrofaciesI, II, III) connected to different relative sea-level phases. In particular, the petrofacies I, indicative of the ancient sea-level phase, allowed to hypothesize a northward shifting of an ancient branch of the Po River; the Petrofacies II, highlighted a drowned shoreline characterized by different fluvial supply, and the petrofacies III, indicative of the more recent sea-level phase, and belonging to a transgressive deposit that have been already studied by other authors, confirmed a Tagliamento River supply. Furthermore, the XRF analysis, in support of the petrographic analysis, allowed to individuate geochemical proxies in order to distinguish marine sand portion from sorted sand portion. Moreover, through the XRF analysis was possible to identify geochemical variation related to different environments of sedimentation connected also to glacial-interglacial cycle.

The applied approach to the characterization of the northern Adriatic transgressive deposits allowed to obtain satisfactory results in order to improve the Adriatic relative sea-level curve and to recognize environmental changes in relation to the sea-level rise. At least, the results can provide a significant contribution in order to identify appropriate sand suitable deposits for beaches nourishment.

RIASSUNTO

Il Mare Adriatico è un bacino epicontinentale semi-chiuso caratterizzato da un basso gradiente della piattaforma nella zona centro settentrionale. In particolare, l'ultima risalita del mare, successiva all'ultimo massimo glaciale, provocò l'annegamento della piattaforma nord adriatica e conseguente sedimentazione e preservazione di diverse generazioni di sistemi costieri, che hanno quindi registrato diverse fasi di risalita del livello del mare. Negli ultimi decenni, più autori hanno focalizzato i loro studi sull'ultimo episodio trasgressivo per ricostruire in dettaglio i diversi momenti dell'ultima risalita relativa del livello del mare, per prevedere l'impatto che un innalzamento del livello del mare potrebbe avere nelle aree costiere attuali. Lo scopo di questa tesi di dottorato è stato quello di caratterizzare con estremo dettaglio i depositi trasgressivi sedimentati e preservati durante ultime fasi di risalita del mare nella piattaforma adriatica settentrionale. Questi corpi sedimentari sono infatti ottimi indicatori diretti del livello del mare e il loro studio potrebbe essere la chiave per delineare scenari futuri. Inoltre la porzione sabbiosa di questi depositi può costituire una risorsa economica sfruttabile per il ripascimento delle spiagge. Questi corpi sedimentari sono stati studiati con un approccio multidisciplinare che ha previsto l'analisi di profili sismici ad alta risoluzione, di carote, di mappe batimetriche, analisi compositive petrografiche su campioni di sabbia e analisi non distruttiva tramite spettrofotometria XRF in continuo su carote.

Un deposito a sud del Delta del Po meglio comprendere gli effetti del sollevamento del livello del mare in un ambiente di transizione e con questo fornire dati di maggior dettaglio alla curva di risalita del mare Adriatico. Questo corpo sedimentario, formatosi in un'area caratterizzata da apporti sedimentari consistenti, ha registrato lo sviluppo di diversi ambienti sedimentari. La qualità dei dati analizzati e la considerevole preservazione del deposito hanno permesso di riconoscere e datare livelli ricchi in materia organica che testimoniano facies lagunari e quindi sono ottimi indicatori di paleo livelli del mare. Inoltre, le nuove datazioni al radiocarbonio hanno permesso di calcolare sia il tasso di sedimentazione sia il tasso relativo di risalita del livello del mare durante la formazione del deposito stesso. Questo estremo dettaglio nella

ricostruzione delle fasi trasgressive potrebbe essere utilizzata in futuro per individuare fluttuazioni centenarie e calibrare i modelli di risalita del livello del mare.

Inoltre, sono stati analizzati otto depositi starvati e rimaneggiati, presenti a nord del Delta del Po, per ottenere nuovi dati sulla paleo geografia del nord Adriatico. Questi depositi sono stati studiati con analisi petrografiche e di spettrofotometria XRF. I risultati compositivi, hanno messo in evidenza tre petrofacies sedimentarie in relazione a diverse fasi della risalita del livello del mare. In particolare, la petrofacies I, indicativa della fase di risalita più antica, ha permesso di ipotizzare uno spostamento verso nord di un ramo fluviale del paleo Po; la petrofacies II ha messo in evidenza una paleo linea di costa caratterizzata da diversi apporti fluviali; mentre la petrofacies III, indicativa di un deposito trasgressivo studiato in precedenza da altri autori, ha confermato una provenienza legata al fiume Tagliamento. Inoltre, l'analisi XRF ha consentito di individuare proxies geochimici che hanno permesso di distinguere porzioni di sabbie marine da porzioni di sabbie ben cernite, con variazioni geochimiche che riflettono i diversi ambienti di sedimentazione.

I risultati ottenuti con lo studio di questi depositi hanno permesso di migliorare la curva dl livello relativo del mare Adriatico e di riconoscere cambiamenti ambientali legati alla risalita del livello del mare. Infine, questi risultati possono contribuire in modo cospicuo all'identificazione di corpi sabbiosi utilizzabili per il ripascimento delle spiagge.

CHAPTER 1
INTRODUCTION

In the last decades several authors have focused their attention on the Quaternary stratigraphic records of the Mediterranean Basin, in order to highlight the relative sea-level rise response which occurred during the last glacial-interglacial cycle. In particular, the sedimentary records of continental margins testify flooding transgression and subsequent regression due to withdrawals of the sea (Miller et al., 2011). The Mediterranean margins provide several examples of Quaternary high-frequency depositional cycles (Tesson et al., 1990; Trincardi and Field, 1991; Piper and Aksu, 1992; Skene et al., 1998) that are characterized by longer phases of sea-level fall, likely in response to the longer time required for the formation of ice caps (Hays et al., 1976). The resulting relative sea-level curve exhibits an asymmetric shape, reflecting low rates of sea-level fall (slow regressions; 125-18 kyr) and high rates of sea level rise (rapid transgressions; ~18-6 kyr). More in detail, the relative sea-level dropped about 120 m in the Adriatic Sea epicontinental basin during the Last Glacial Maximum (LGM; Trincardi et al., 1994), and the maximum shoreline displacement was about 250 km more southern than the nowadays. In this context, the present Adriatic shelf was a huge alluvial plain. Subsequently, between late-glacial and early-Holocene, it experienced a very rapid sea-level rise, causing significant basin widening which allowed the sedimentation and drowning of several generations of coastal wedges and barrier-lagoon systems (Trincardi et al., 1994; Correggiari et al., 1996a; 2011). The remnants of these sand barriers were recognized offshore (Trincardi et al., 1994; Fabbri et al., 2001; Correggiari et al., 2011; Trincardi et al., 2011) as isolated depositional bodies generally parallel to the present coastline and characterized by a complex facies architecture and peculiar seismic geometries.

This research focuses on the detailed characterization of the post-LGM transgressive deposits in the Northern Adriatic, aiming at the following goals:

1. The reconstruction of the paleogeography variation induced by the submersion of the coastal system affected by a rapid sea-level rise. This aspect is also considered as a correct approach to predict possible scenarios of environmental changes under rising sea-level conditions. Several authors (e.g. Blum and Tornqvist, 2000; Cattaneo and Steel, 2003) demostrated that the Quaternary deposits emplaced during the last sea-level cycle can represent a valid archive for this purpose.

2. A detailed reconstruction of the past relative position of the sea during the last transgression cycle. In this regard, the Adriatic basin, and in particular the transgressive deposits sedimented during the last glacial-interglacial cycle represent a good record to highlight detailed fossil sea-level positions. Their paralic portions, indeed, are characterized by lateral continuity peat and organic-rich layers, easily recognizable on high resolution seismic profiles, that testify brackish lagoon facies representative of paleo sea-level, confirmed also by a typical fauna assemblage. With this aim, high resolution AMS ^{14}C dates on peat layers, together with robust stratigraphic framework, could be used for assessing and calibrating the geophysical models predicting post-LGM sea-level corrected curves.

3. Identification of the exploitable deposits for the beach nourishment focusing on the sorted sand portions belonging to the shelf transgressive sediments. In the last 30 years the offshore aggregates have become an economic resource. Nowadays, beach erosion is a widespread problem due to the sea-level rise combined with reduced fluvial supply and intensified storminess. Moreover, the human impact related to heavy urbanization of the coastal areas and tourism have worsened the situation together with the landward retreat of the coast. In this setting, the nourishment operation exploiting sand belonging to the transgressive deposits offshore, can be a good strategy to preserve beaches from erosion. Furthermore, during this PhD work several sand samples were analysed in order to identify different sand compositions, thus, the compositional comparison between transgressive sand and present beach sand could be an improved approach useful to select exploitable areas for beach nourishment.

Taking as reference the points listed above, this PhD project wants to give a new contribution concerning the transgressive deposits characterization focusing on detailed architecture and composition analyses of the main transgressive bodies in the northern Adriatic Sea. Therefore, it focuses on the detailed characterization of some parasequences emplaced and partly preserved on the low-gradient northern Adriatic shelf, following a multi-disciplinary approach. The study was based on a large dataset of CHIRP-sonar profiles, bathymetric and isopach maps and integrated stratigraphic cores, provided by CNR-ISMAR (Bologna Section). In particular, during this work seismic facies analysis, core analysis and sand analysis were combined in order to obtain new information about the evolution and the response of some deposits in relation to the last relative sea-level rise.

Furthermore, this project allowed me to gain experience on two oceanographic cruises (NAD12 and AS14 on board Urania R/V organized by CNR-ISMAR Bologna Section) in order to acquire new data. Moreover, I took part in the first research campaign concerning the morphological mapping of the Po River delta with the ultra-high resolution multibeam bathymetry and backscatter data (June 2013), an activity related to the Ritmare Project, and I also took part in a research cruise (on board Astrea R/V organised by ISPRA) of a project to monitor and characterize sand marine quarries for beach nourishment. For the methodology I learnt to use the innovative XRF core scanner analyses at the NIOZ Institute (Netherlands) to acquire continuous geochemical composition for seven selected cores.

In order to identify the depositional environment and the rate of sedimentation in a transitional environment influenced by the sea-level rise, a transgressive deposit 40 km south of the present Po River delta was investigated (-38.5 to -34 m msl; Fig. 1.1). The transitional environments are mainly formed by clayey and silty sediments often rich in organic matter. These sediments are indicative of alluvial plain and lagoon facies. In particular, the AMS radiocarbon data of each peat layer allowed to calculate the rate of sedimentation. These accurate geochronological results on coastal and lagoon deposits have been used to improve the reconstruction of the curve of relative sea-level in the Adriatic Sea. As a second area of investigation, different transgressive deposits north of the Po Delta were analysed (Fig. 1.1). They

were formed during different phases of the sea-level rise and their study focused on the sandy portion, through the use of petrographic analysis under polarizing microscope. These results were used to distinguish among different sedimentary petrofacies and to recognize their provenance, producing new data to reconstruct the paleogeography evolution of the last part of the marine transgression.

XRF core scanner analyses are presented and discussed in the final part of the thesis. This new method, generally applied to fine or mud sediments, was tested in this PhD project for sandy sediments for the first time. The aim of this investigation through XRF analysis was to highlight different chemical signature in correspondence of different environment of sedimentation. In particular, this method was applied to distinguish continental sediments from transitional environments developing during the last sea-level rise. Furthermore, the XRF analysis of the sand portion pointed out different geochemical proxies in order to distinguish sediments affected by marine productivity and sediments influenced by a terrigenous supply.

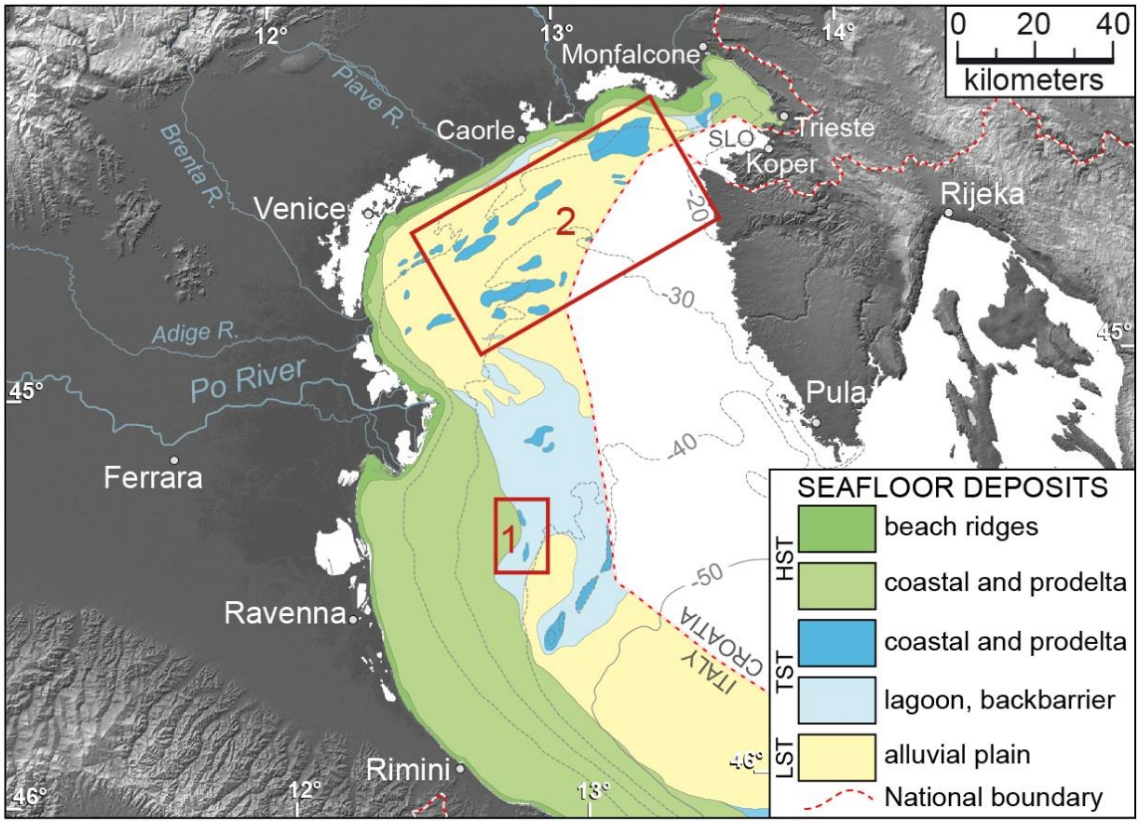

Fig. 1.1: Study area of this PhD project. 1: First investigated area, south of the Po River delta; 2: Second investigated area, north of the Po River delta.

OUTLINE

The work performed in the last three years, reflecting the above reported goals, is presented in this thesis as follow:

- ✓ Chapter 1) Introduction
- ✓ Chapter 2) Geomorphological setting
- ✓ Chapter 3) Instruments, methods and data
- ✓ Chapter 4) Moscon, G., Correggiari, A., Stefani, C., Fontana, A., Remia, A. (2015), “Very-high resolution analysis of a transgressive deposit in the northern Adriatic Sea (Italy).” Alpine and Mediterranean Quaternary, 28(2), 121-129.
- ✓ Chapter 5) Sediment provenance in some Holocene transgressive deposits in the northern Adriatic Sea
- ✓ Chapter 6) XRF core scanner results
- ✓ Chapter 7) Discussions and Conclusions

CHAPTER 2
GEOMORPHOLOGICAL SETTING

2.1 Adriatic seafloor morphology

The Adriatic Sea is located in the central Mediterranean, between the Italian peninsula and the Balkans and is characterized by a strong transversal and longitudinal asymmetry. It is a narrow semi-enclosed epicontinental shelf dominated by mud deposition and characterized by a narrow shape, with its major axis elongating for over 800 km in the NW-SE direction. Considering the shelf morphology, this basin can be divided into three different portions (Fig. 2.1). The northern section is characterized by a very shallow and slightly inclined shelf (0.02° dip), with an average depth of about -35 m msl, extending for about 350 km from the Gulf of Venice to the Mid Adriatic Deep (MAD). This area shows a complex microtopography, with metric size reliefs and scours which reach a depth of 4-5 m. The central portion is formed by several slope basins, including the MAD, a small slope basin about 250 m deep, characterized by a NE-SW trend. This basin is bounded eastward by a small platform and southward by the Gallignani-Pelagosa ridge (Ridente and Trincardi, 2006). The southern section, south of the Pelagosa sill, is characterized by a wide depression more than 1200 m deep and a complex slope morphology (Cattaneo et al., 2003). In particular, the Adriatic environment and its oceanography were subjected to dramatic changes during the eustatic oscillations which occurred during late Quaternary in particular during the last relative sea-level rise. Storm et al. (2008), reconstructing the Adriatic paleo environment through simple models, highlighted strong tidal influence related to low sea-level and higher wave progradation, close to the present coastline, connected to the last phases of the sea-level rise.

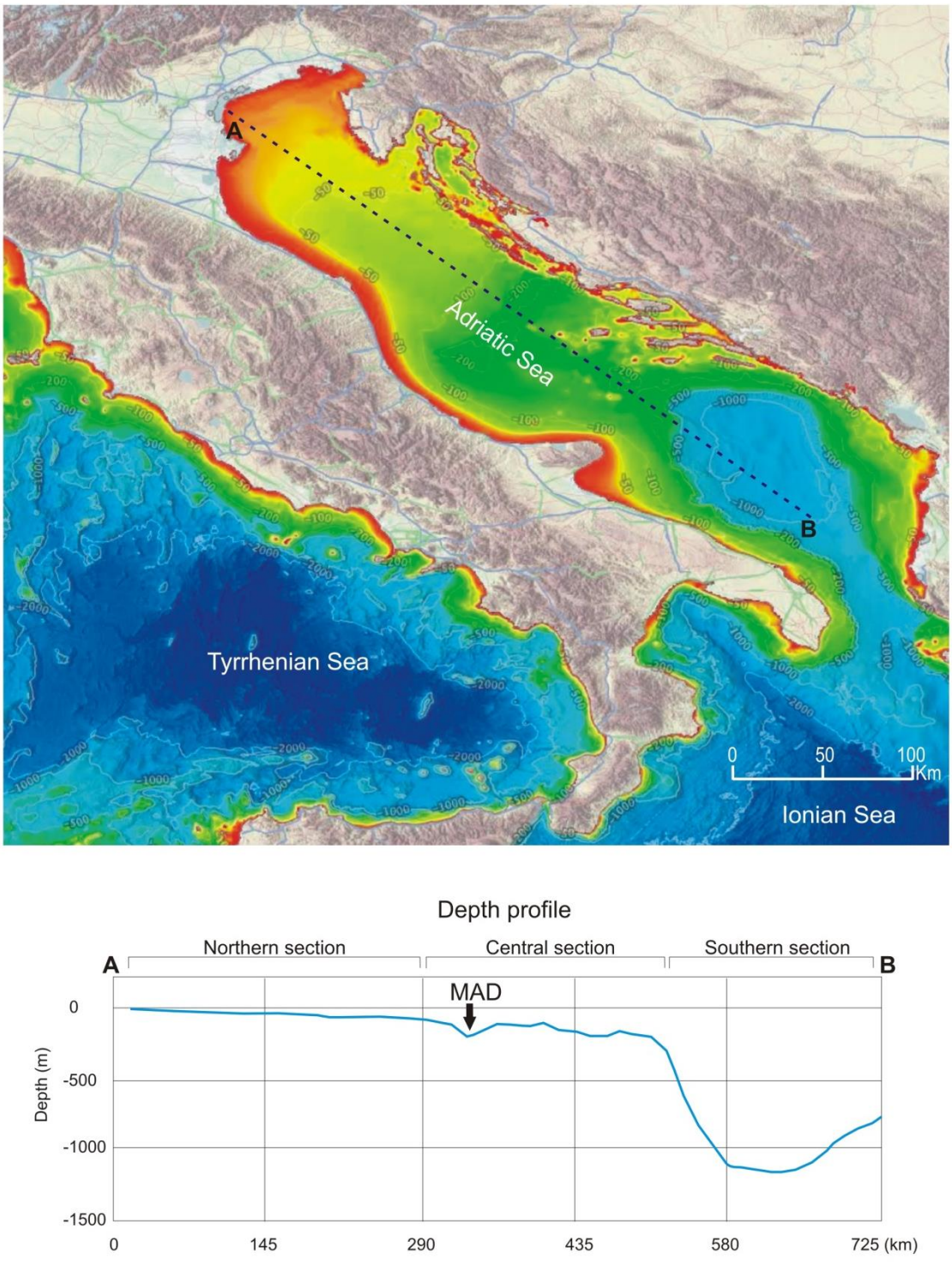

Fig. 2.1: Morphology and axial depth profile of the Adriatic basin. The depth profile highlights three different portions: a northern gently portion; a central part characterized by different slope basins including the Mid Adriatic Depression (MAD); and a southern wide depression more than 1200 m deep (from http//:www.emodnet.eu).

2.2 Oceanography

The Adriatic Sea is presently characterized by a microtidal regime with a tidal range lower than 1 m and dominated by a clockwise circulation pattern which is driven by thermoaline currents (Bondesan et al., 1995; Cattaneo et al., 2003). In particular, three water masses can be described: 1) a superficial temperature-mixed layer (0-30 m), 2) a Levantine Intermediate Water (30-130 m; LIW), 3) a bottom-water region (>130 m) with very dense waters that occasionally form in the northern Adriatic and sink towards the south (Northern Adriatic Dense Water circulation-NAdDW; Cattaneo et al., 2003; Fig. 2.2). The superficial water mass (1) consists of a large-scale counter clockwise baroclinic geostrophic structure with cyclonic gyres of thermoaline origin (Malanotte-Rizzoli and Bergamasco, 1983; Artegiani et al., 1997a-b). As a result of this counter clockwise circulation, a fine-grained sediment wedge, formed by sediment deriving from the Po and Apennine rivers, is dispersed southward and deposited in a narrow band along the Italian coastline down to the Gulf of Manfredonia, south of the Gargano promontory (Cattaneo et al., 2003. Moreover, the Adriatic circulation depends on three main components: a) river forcing, due to 5700 m^3s^{-1} fresh water input, causing heat loss and low-salinity water; b) wind forced at the surface, producing deep-water masses and seasonal changes in circulation; c) morphological forcing, due to the Otranto channel, controlling the effects of freshwater and salty water discharges (Cattaneo et al., 2003).

In particular, the superficial cyclonic circulation forces the fresh waters to flow along the western side of the basin. The along shore sediment transport, enhanced during winter by the strong catabatic Bora wind, causes two large gyres that involve the whole water column to flow towards SW along the Italian coast (Gacic et al., 1999). The dense and salty water mass of the LIW enters the south Adriatic on the eastern side and flows out southward along the slope in intermediate depths (Manca et al., 2002). However, the deeper water mass of NAdWM forms in winter moving southwards across the SW Adriatic slope (Trincardi et al., 2007).

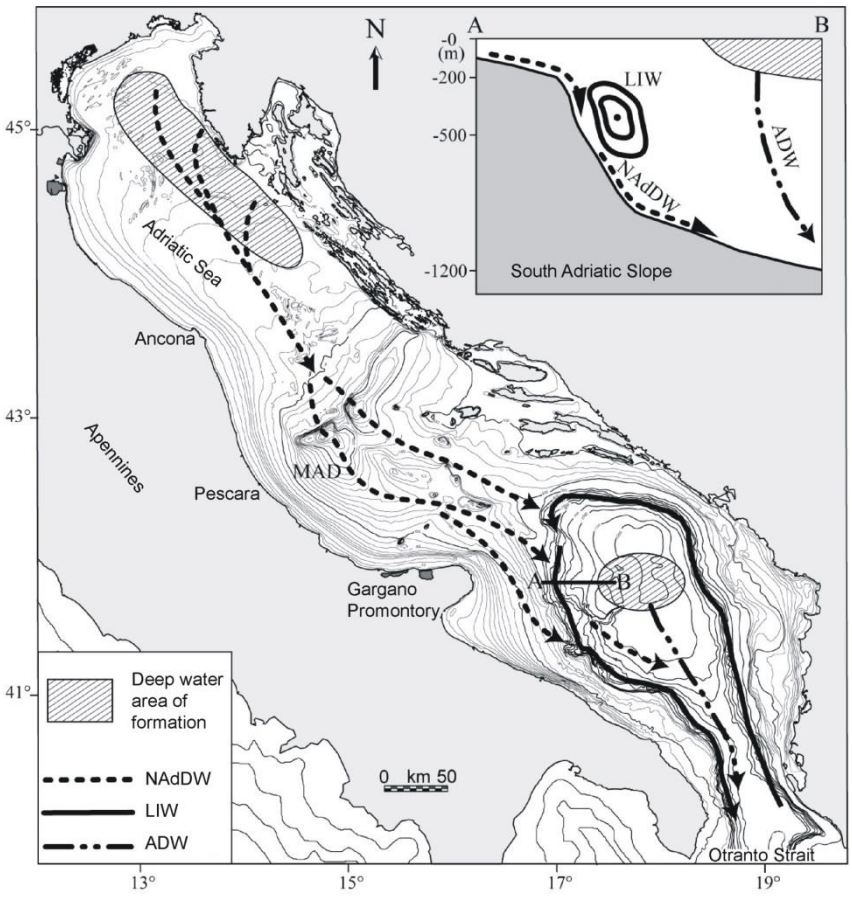

Fig. 2.2: Marine circulation of the Adriatic Basin (from Trincardi et al., 2011a; 2011b). NAdDW: Northern Adriatic Dense Water circulation; LIW: Levantine Intermediate Water; ADW: Adriatic Dense Water.

2.3 Geological setting of the Adriatic Sea

The Adriatic region is partly surrounded by mountain belts (Apennines, southern Alps and Dinarides-Hellenides) and corresponds to the foreland domain of these three orogens (Fig. 2.3; D'Argenio and Horvath, 1984; Ori et al., 1986; Ciabatti et al., 1987; Argnani and Frugoni, 1997). The Adriatic Sea represents the foredeep and foreland of the SW Apennine subduction (Carminati et al. 2003), the retrobelt foreland of the SE Alpine subduction (Doglioni and Carminati, 2002; Dal Piaz et al., 2003; Kummerow et al., 2004), and the foreland basin of the NE Dinaric subduction (Di Stefano et al., 2009). In particular, the western sector of the northern and central Adriatic represents a Plio-Quaternary foredeep basin, which is the last of a series of westward migrating foredeep basins formed during the Apennine orogenesis (Argnani and Ricci Lucchi., 2001; Trincardi et al., 2011; Fig. 2.4). The Plio-Quaternary Adriatic foredeep is characterized by two distinct depocentres separated by a

structural high in the area of Ancona (Ori et al., 1986; Argnani and Gamberi, 1996). These two depocentres correspond to areas of minimum Bouguer anomaly where the sediment fill reaches up to 8 km. During the late Quaternary the sedimentation was affected by high uplift rates of the Apennines that favoured high sediment supply rates, thus, inducing the load subsidence of the adjacent Po plain-Adriatic foreland basin (Pieri and Groppi, 1981; Bally et al., 1986). The northern Apennine front affects the Po Plain with four thrust systems: the Monferrato, the Emilia and the Ferrara-Romagna arcs and the Adriatic fold (Pieri and Groppi, 1981; Trincardi et al., 2011). Southeastward the external front of the Apennine accretionary prism is traced a few kilometres offshore, in the area between the cities of Ancona and Pescara. In this sector, the Adriatic Plio-Quaternary foredeep is formed by two depocentres located north of Ancona and offshore Pescara (Argnani and Frugoni, 1997).

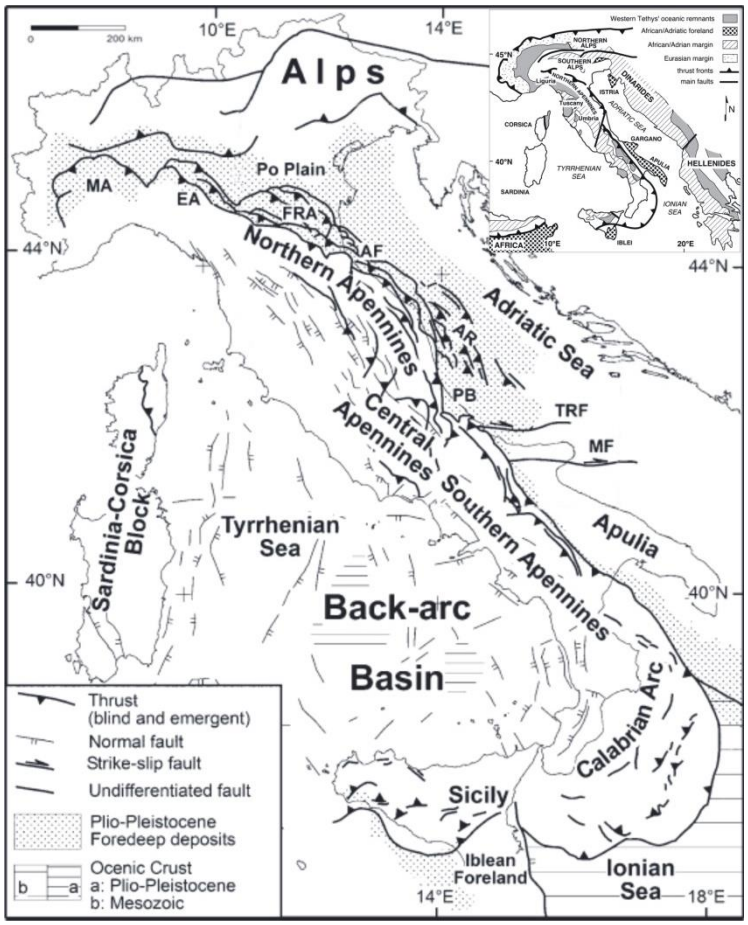

Fig. 2.3: Main structural features and orogens of Italy (modified by Scrocca et al., 2007). MA: Monferrato Arc; EA: Emilia Arc; FRA: Ferrara-Romagna Arc; AF: Adriatic Folds; AR: Adriatic Ridge; PB: Pescara Basin; TRF: Tremiti Fault; MF: Mattinata Fault.

The central Adriatic thrust front is separated by the southern Apennine chain by a lithospheric fault, indicative of the Tremiti-Pianosa structural high. This is a tectonic lineament which allowed the accommodation of different tectonic behaviour between the northern subsiding Adriatic margin and the uplifting Apulia region (Doglioni et al., 1994). Below, the Gargano area is characterized by a deformation induced by a N-S and a NE-SW stress field due to the pushing activity of the Dinaric front (Bertotti et al., 1999).

The geological history of the Adriatic basin highlights the evolution from a Mesozoic carbonate passive margin to a Cenozoic foreland basin system as a consequence of the collision between the African and European plates (D'Argenio and Horvath, 1984). The deep exploration boreholes allowed to highlight the stratigraphic evolution from the carbonate platform of the Triassic and Early Jurassic, to the carbonate pelagic sedimentation of Middle Jurassic-Late Cretaceous. This stratigraphy recorded the rifting and subsequent continental break up that led to the opening of the Tethys Ocean. A significant change in sedimentation occurred during the Tertiary, when the hemipelagic clastic sedimentation was characterized by a progressive increasing, recording the compressive deformation produced by the convergence of the African and European plates. In particular, the seismic and well log data collected for hydrocarbon exploration, allowed the reconstruction of the progressive fill of confined basins of tectonic origin, that recorded the foredeep deposition during the growth and eastward migration of the Apennine chain since the Oligocene (Ori et al., 1986; Ricci Lucchi, 1986). The eastward migration of the Apennine thrust front produced a series of piggyback basins that were filled by Late Pliocene to Early Pleistocene sediments (Ori and Friend, 1984). During the Quaternary the Adriatic basin became increasingly dominated by progradational deposits advancing along the major axis of the basin, from the Po Plain toward SE direction (Ori et al., 1986) marked by cyclical glacio-eustatic sea-level fluctuations (Trincardi and Correggiari, 2000; Ridente and Trincardi, 2002).

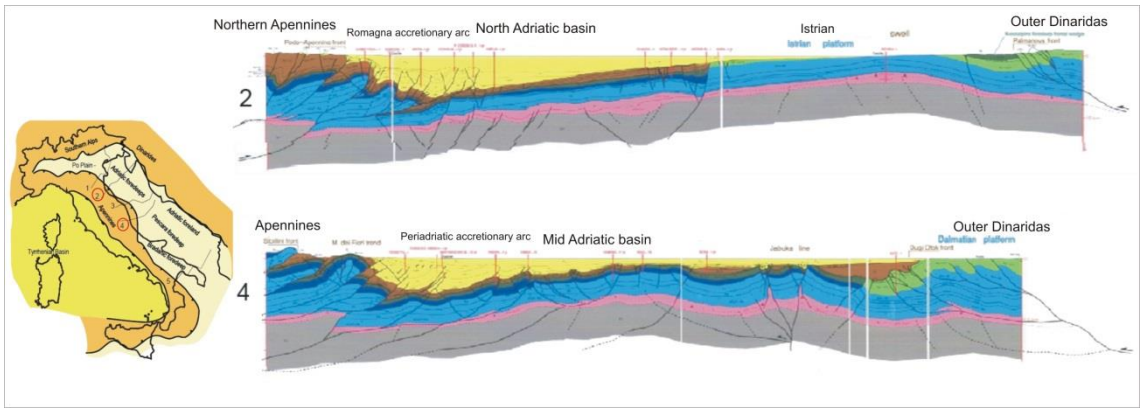

Fig. 2.4: Geological cross-sections from the Apennine foldbelt through the north and central Adriatic basin (modified by Cazzini et al., 2015, after Fantoni and Franciosi, 2010).

2.4 Subsidence

The natural subsidence is controlled by two types of process: sedimentation/compaction and tectonics, that act on geological time scale and climate processes that act on tens of thousands of years (Carminati et al., 2003). The reconstruction of the sea-level rise curve requires the knowledge of the subsidence history of the study area. The northern Adriatic sea highlights important subsidence mainly in the Venice and Ravenna areas, related to geodynamic forcing due to the eastward rollback of the subduction hinge (Doglioni et al., 1994) and the consolidation of recent late-Holocene compressible low-permeable deposits (Teatini et al., 2011). In particular, the north Adriatic subsidence rate for the last 125 kyr is on the order of 1 mm/yr (Massari et al., 2004; Maselli et al., 2010). More in detail, several authors have pointed out that the Italian coasts are characterized by variable tectonic styles, the maximum subsidence rate, with 1.2 mm/yr, was calculated in the northern Adriatic sector (Massari et al., 2004), whereas the southern part is characterized by uplift rate on the order of 0.2-0.3 mm/yr (Ferranti et al., 2006; Lambeck et al., 2006; Maselli et al., 2010). The north Adriatic coastal and shelf area are affected by locally anthropogenic ground subsidence caused by fluid removal from subsurface reservoirs in the form of gas, and groundwater (Gambolati et al., 2006). Both natural and anthropogenic land subsidence, and eustasy in the northern Adriatic have caused 23 cm of relative land subsidence, with respect to the mean sea-level over the last 100 years (Fabris, et al., 2014; Lambeck et al., 2011).

2.5 Quaternary evolution of the Adriatic Basin

During the Quaternary, cyclical changes in orbital parameters led to variations in solar radiation reaching the Earth surface and causing important climatic oscillations (Martinson et al., 1987; Ruddiman, 2006). On time-scales of centuries and millennia, sea-level change is mainly affected by eustatic related to all types of water variations, glacio-hydro-isostatic and tectonic factors. The Quaternary period was characterized by repeated growth and melting of large continental ice sheets in the northern and southern hemisphere and the sea-level reached a maximum elevation of 5-10 m above present sea level at least three times and dropped to more than 100 m below the present sea level at least five times (Waelbroeck et al., 2002; Siddall et al., 2006; Fig. 2.5).

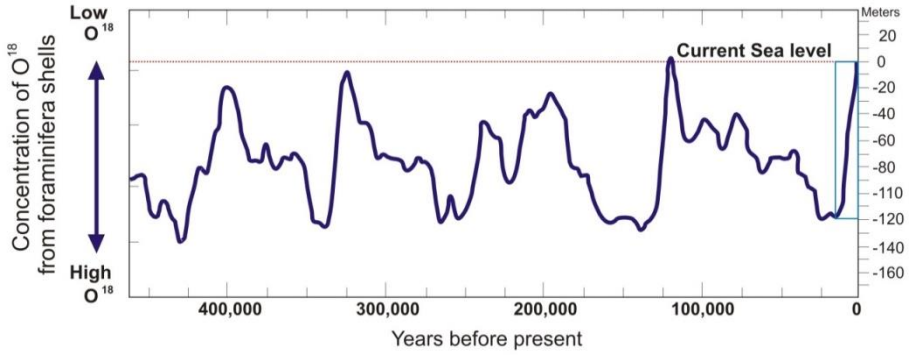

Fig.2.5: Global sea-level changes in the last 600 kyr (modified by Siddall et al., 2006). The light-blue rectangle, on the right margin, highlights the last sea-level rise.

The morphological evolution of the Adriatic basin was strongly influenced by the sea-level variations during the last 800,000 years. The glacio-eustatic cycles, affected the continental margin deposition and the coastal dynamic, due to their amplitude (> 100 m) and frequency. During middle and late Quaternary, the duration of the glacial/interglacial cycles was about 100 kyr (Shackleton, 2000), and the mean time between one glacial trough and the succeeding interglacial marine peak was about 20 kyr. These successions of glacial and temperate conditions led to delineate the sea-level curve with long periods of sea-level falling, related to the growth of ice caps and inlandsis, interrupted by sea-level rises induced by the melting of ice caps and the thermal expansion of water (Trincardi et al., 2011a).

The most recent glacial-interglacial cycle began with the general sea-level fall which followed the last interglacial (MIS 5e, 132,000-116,000 years

BP, +6 ±3 m msl; Ferranti et al., 2006), intercalated by some periods of minor sea-level rise (as MIS 3, 58,000-29,000 years BP, around -60 m msl) and with a peak corresponding to the Last Glacial Maximum, 29,000-19,000 years BP, -125 m msl (Martinson et al., 1987, Bard et al., 1990; Lambeck et al., 2014). The melting of ice caps after the end of the Last Glacial Maximum caused a rapid eustatic rise of ca. 125 m and the consequent drowning of continental shelves (Fairbanks, 1989; Bard et al., 1990; Lambeck et al., 2002; 2004; 2014; Fig. 2.6; Fig. 2.7). The post LGM has not been characterized by a monotonic climate, but was punctuated by two main steps of enhanced ice melting and by minor eustatic events (Fairbanks, 1989). At first, about 19,000 years cal. BP, an early sea-level rise of 15-20 m took place, due to a partial melting of the northern-hemisphere ice sheets (Clark et al., 2004). Consequently, sea-level rise highlighted two main steps connected to two intervals of enhanced fresh water discharge, called Meltwater pulses 1A (MWP-1A) and 1B (MWP-1B), starting at 14,200 years cal. BP and 11,300 years cal. BP, respectively (Fairbanks, 1989; Bard et al., 1996).

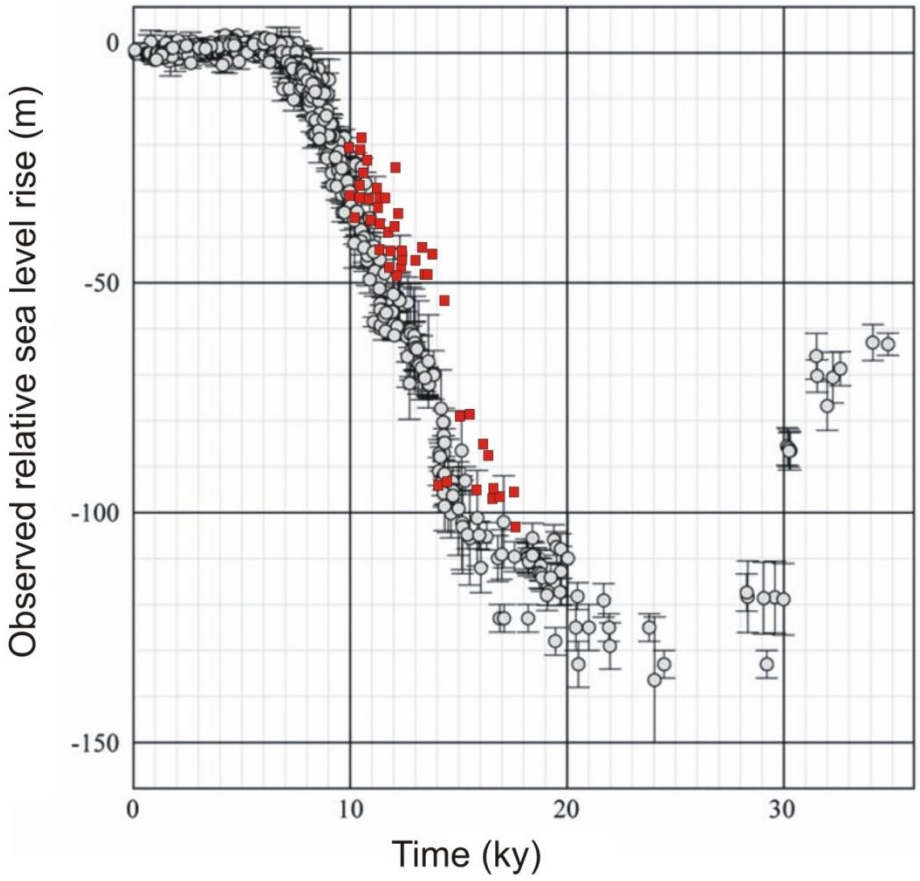

Fig. 2.6: Sea-level curve for the post-LGM time interval (modified by Lambeck et al., 2014). The radiocarbon data obtained for paralic Adriatic samples are plotted in red squares.

The sea-level, during MWP-1A, rose about 25 m in 1500 years, whereas during MWP-1B sea-level rose about 15 m in 500 years. The Meltwater pulses were separated by a strong and short cold phase, known as the Younger Dryas, that brought the climate to almost LGM conditions between 12,500 and 11,700 BP (Allen et al., 1999). The last relative sea-level rise took place in the Adriatic basin over the low gradient alluvial plain which originated during the LGM and the maximum marine ingression was reached ca. 5500 years cal. BP when the basin reached its maximum extent.

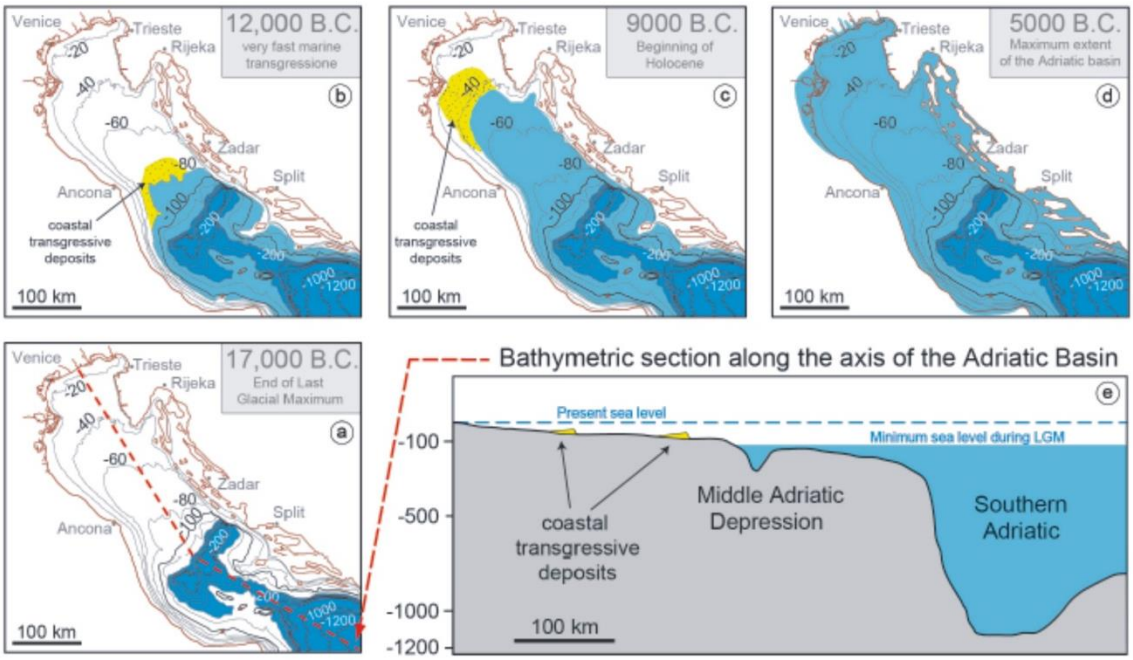

Fig. 2.7: Post-LGM sea-level rise phases (from Fontana et al., 2014).

2.6 Late Quaternary Sequence stratigraphic framework of the Adriatic basin

In the Adriatic shelf the stratigraphic analysis highlighted four sequences of forced-regression deposits, characterized by similar internal organization and thickness, that respond to a dominant eustatic cyclicity (Trincardi and Correggiari, 2000). These sequences, named from 1 to 4 (from the youngest to the oldest) accumulated during the last 450 kyr and they are separated by unconformities (ES1-ES4). Each depositional sequence represents a distinct transgressive-regressive cycle, and is essentially composed of thicker regressive deposits and less thick transgressive units, with a patchy distribution on the shelf (Ridente and Trincardi, 2002). On the base of a dense grid of very high resolution seismic profiles and cores the Adriatic seafloor can be divided into two different domains: the shallower portion, landward, is characterized by a clinoform of late Holocene deposits, due to the sediment supply delivered towards the basin by the Po and Apennine rivers after the maximum marine ingression (Cattaneo et al., 2003; Cattaneo et al., 2007). The offshore area of the northern Adriatic shelf is instead characterized by low-stand alluvial plain sediments covered by sand deposits of barrier-island systems, formed during the last sea-level rise (Correggiari et al., 1996b). Thus, the Adriatic seafloor stratigraphy can be summarized into three different sedimentological units bounded by stratigraphic discontinuity surfaces, strongly related to the last glacial-interglacial cycle (Trincardi et al., 1994; Cattaneo and Steel, 2003; Fig. 2.8).

- ✓ The Prograding Pleistocene wedges, truncated at their top by a regional erosional surface [ES1, identified as Ts-Transgressive surface- in the Geological Map of the Italian Seafloor, Trincardi, (2011a,b)], that records a regressive phase from MIS 5e to the base of the Last Glacial Maximum (Trincardi and Correggiari, 2000; Ridente and Trincardi, 2002).

- ✓ The Transgressive System Tract, that rests on ES1, highlights different phases of sea-level rise (Cattaneo and Trincardi, 1999) and reflects short-term variations of sediment supply and dispersal, likely accompanied by changes in the oceanographic regime of the basin (Asioli et al., 2001).

- ✓ The High stand System Tract consists of a shore-parallel prograding mud prism younger than 5.5 cal kyr BP, formed above a regional downlap surface (MFS; Correggiari et al., 2001).

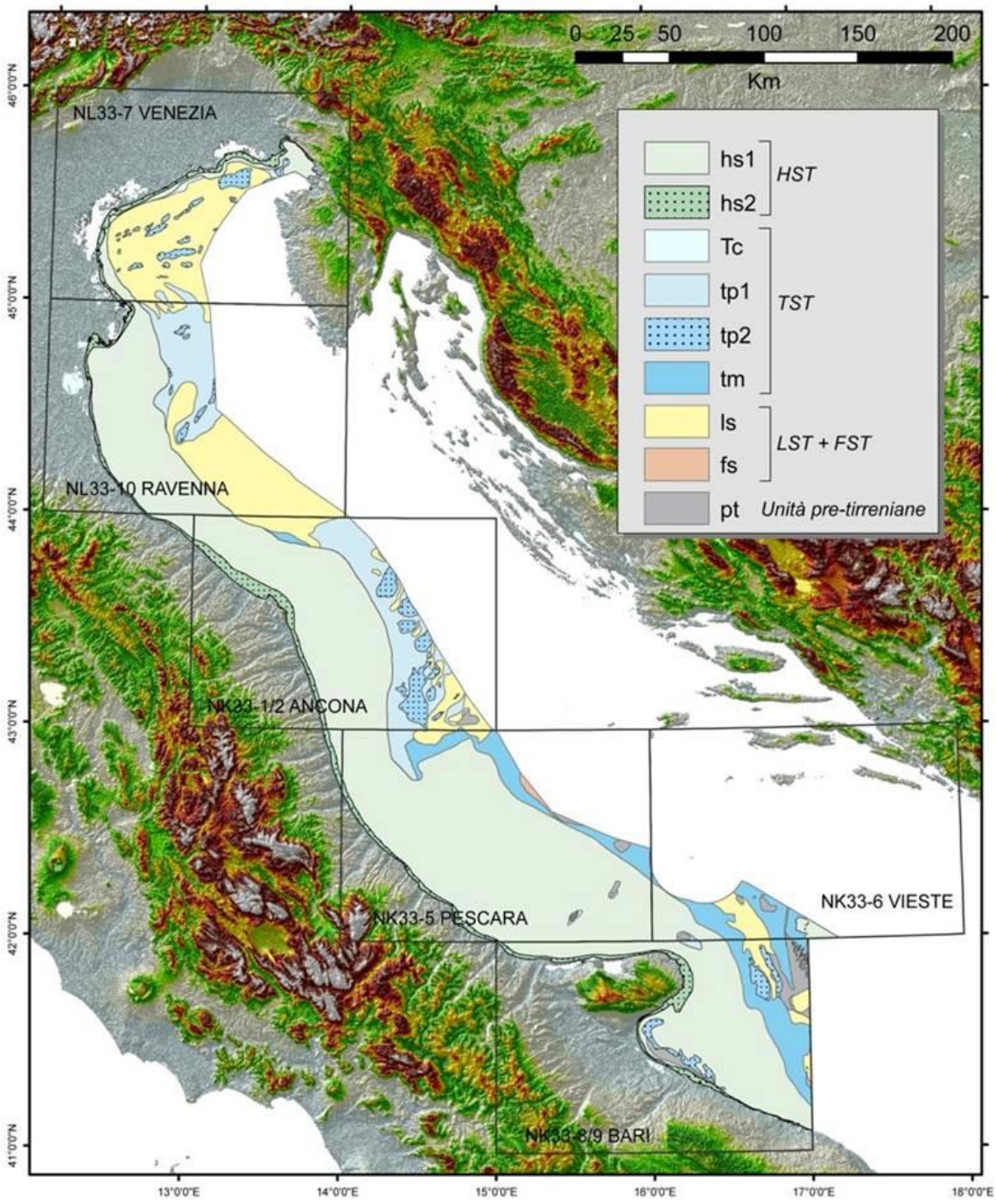

Fig. 2.8: Geological Map of the Italian Sea (from Trincardi et al., 2011c), superficial geology of the Adriatic basin. In green: high-stand deposits; in light-blue: transgressive deposits; in yellow: low-stand deposits.

In particular, during the LGM, the northern and central Adriatic areas were an alluvial plain partly characterized by a main fluvial system, referred to as “Mega Po” river with Alpine and Apennine rivers as tributaries, terminating in a low-stand delta located at the northern edge of the MAD (De Marchi, 1922; Correggiari et al., 1996b; Cattaneo and Steel, 2003; Ridente and Trincardi, 2005; Amorosi et al., 2015). The sediment carried by the fluvial system progressively filled the western side of the MAD, forming a low-stand sedimentary body thicker than 200 m (Trincardi et al., 1994; 2004; Maselli et al., 2011). After this period, during the late-glacial to early-Holocene transgression, the sea level rose about 120 m and caused a substantial basin widening. This process was accompanied by landward migration of barrier-lagoon systems, drowned progressively due to the gradual sea ingression. In particular, the deposition and preservation of these deposits is linked to several parameters including the morphology of the shelf and the rate of sea-level rise (Trincardi and Correggiari, 2000; Fabbri et al., 2001). These transgressive bodies rest on the transgressive surface and are topped by a wave-ravinement surface that often coincides with the maximum flooding surface. Successively, as a final phase, the maximum ingression and the HST phase resulted in a shore-parallel prograding prism, consisting of mud and which formed a regional downlap surface over the previous units (MFS; Correggiari et al., 2001).

2.6.1 Adriatic Systems Tract

2.6.1.1 Falling-stage system tract (FSST) and low-stand system tract (LST)

The FSST is the product of a forced regression and includes all the regressive deposits that accumulate after the onset of a relative sea-level fall; this system tract is bounded at the top by a composite surface that includes the subaerial unconformity, its correlative conformity, and the youngest portion of the regressive surface of marine erosion (Catuneaneu et al., 2011).

The LST includes deposits that accumulated after the onset of early-rise normal regression and it is bounded by the top of the falling-stage systems tract at the base, and by the maximum regressive surface at the top (Catuneaneu et al., 2011). Taking as reference the Italian Sea Geological Cartography (scale 1:250000; http://www.isprambiente.gov.it/it/cartografia/carte-geologiche-e-geote

matiche/carta-geologica-dei-mari-italiani-alla-scala-1-a-250000; Fig. 2.8), the sedimentary bodies belonging to FSST and LST deposits are assimilated to the same body because of the not easy recognizable reflector in correspondence of the basal boundary. In the Adriatic basin these deposits are mainly characterized by yellowish-grey stiff clays with continental fauna as *Planorbidae* spp., *Psidium* sp., *Bythinia* sp.. This unit is indicative of an alluvial plain environment with fluvial systems and swamps, which represents the paleo environment of the Adriatic shelf during the LGM. The low-stand deposits of the LGM are mainly confined off shelf and within the MAD, where a very thick low-stand wedge prograded from NW along the axis of the Adriatic basin on top of a set of acoustically transparent seismic units (Trincardi et al., 2004). The LGM low-stand wedge is more than 200 m in thickness and pinches out towards SE on the southern flank of the MAD slope basin (Trincardi et al., 2004).

2.6.1.2 Transgressive system tract (TST)

The TST is characterized by deposits accumulated from the onset of transgression until the time of maximum transgression of the coast. The TST lies on the maximum regressive surface, which truncates older low-stand deposits, formed at the end of the regression and is overlain by the maximum flooding surface (MFS), that formed when marine sediments reach their most landward position (Cattaneo et al., 2011).

In the Adriatic basin the TST deposits are mostly formed by several backstepping barrier-lagoon and incised valley systems in the low gradient northern shelf, while mud sedimentary bodies thicker than 25 m are present in the western side of the central Adriatic shelf (Cattaneo and Trincardi, 1999; Maselli et al., 2011, Trincardi et al., 2013; Fig. 2.8). The seismic and core data highlighted a basal delta plain environment with distributary channel and at the top a paralic environment, passing through tidal regulated barrier-lagoon estuary systems (Correggiari et al., 1996a; Trincardi et al., 2011).

2.6.1.3 High-stand system tract (HST)

The HST includes the progradational deposits that form when sediment accumulation rates exceed the rate of increase in accommodation during the late stages of relative sea-level rise. The HST lies directly on the MFS formed when marine sediments reached their most landward position (Correggiari et

al., 2001; Catuneaneu et al., 2011; Fig. 2.8). The late-Quaternary HST deposits in the Adriatic basin are constituted by a prograding unit indicative of a prodelta pelitic body variably bioturbated, gradually intercalated with sandy layers that mark the transition toward the modern beach environment.

2.6.2 Sequence stratigraphy surfaces

2.6.2.1 Transgressive Surface (TS)

The TS is a stratigraphic surface that marks a change in stratal stacking patterns from low-stand normal regression to transgression. It corresponds to the paleo seafloor at the end of low-stand normal regression, and its correlative surface within the non-marine setting (Catuneaneu et al., 2011; Fig. 2.9). Moreover, this surface does not always represent the boundary between continental and marine deposits, but may also separate continental deposits which are the product of distal variations of the sea-level.

2.6.2.2 Maximum Flooding Surface (MFS)

The maximum flooding is a stratigraphic surface that marks a change in stratal stacking patterns from transgression to high-stand normal regression. It is the paleo seafloor at the end of transgression, and its correlative surface within the non-marine setting (Catuneaneu et al., 2011; Fig. 2.9). The maximum flooding surface is often expressed as a downlap surface in seismic stratigraphic terms, as it is typically downlapped by the overlying high-stand clinoforms which record progradation (Catuneaneu et al., 2011).

2.6.2.3 Ravinement Surface (Rs)

The Rs is an erosive surface that gets scoured off as the “front” of the sea makes its way landwards. This surface is diachronous, younging towards the basin margin (Catuneaneu et al., 2011; Fig. 2.9). Ideally this surface represents the boundary between the transgressive beach deposits and the above transgressive shoreface deposits. Typically on the Rs a mixed deposit called transgressive lag can be found (Catuneanu, 2006).

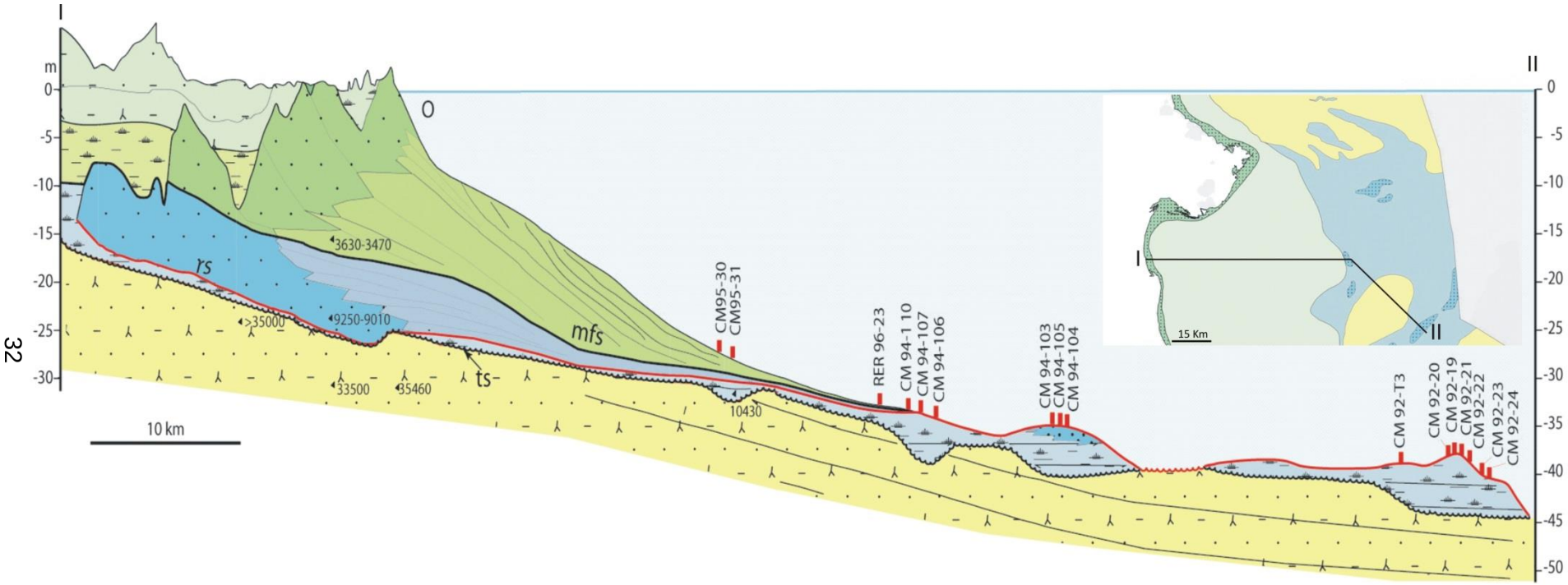

Fig. 2.9: Example of sequence stratigraphy relation in a cross-section of the post-LGM deposits subdivided in system tracts (modified from Trincardi et al., 2011a).

2.6.3 Transgressive deposits and their preservation

The transgressive deposits are indicative of sediments deposited at or near the coastline in response to relative sea level rising and landward migration of the shoreline. They can be fully marine, eustuarine/lagoonal or fluvial, and can include other facies such as coal and eolian deposits with a variability driven by changes in rate of sea-level rise, sediment supply, textural character of the sediments, shelf gradient or basin features (Cattaneo and Steell, 2003). Through high resolution seismic profiles and correlated cores they can be highlighted with the overall retrogradational stacking pattern (Van Wagoner, 1990). Moreover, they can be identified with an abrupt upward-deepening of facies covered at the top by the MFS. Barrier or shoreface retreat (Swift, 1968; Sanders and Kumar, 1975) occurs when the base of the shoreface migrates landwards, truncating by the action of waves the pre-existing deposits and creating a ravinement surface (Cattaneo and Steel, 2003). Coeval transgressive deposits may be preserved below and above the ravinement surfaces (Fig. 2.10). The transgressive deposits below the Rs, on the landward side, are paralic deposits, while the transgressive deposits above the Rs, on the basinward side, are marine deposits (Nummedal and Swift, 1987). In particular, the ravinement surface erodes mainly upper and middle shoreface strata, leaving the basal shoreface to the fossil record, and disperses the eroded sediments both landwards to lagoon (or estuarine, whashover deposits) environments and offshore to deeper areas.

In particular, the preservation of transgressive deposits, during the transgression is influenced by different factors, that are: 1) sea-level rise; 2) sediment supply; 3) gradient of the substrate and 4) morphology of the coastal systems (Tortora and Crowell, 2005).

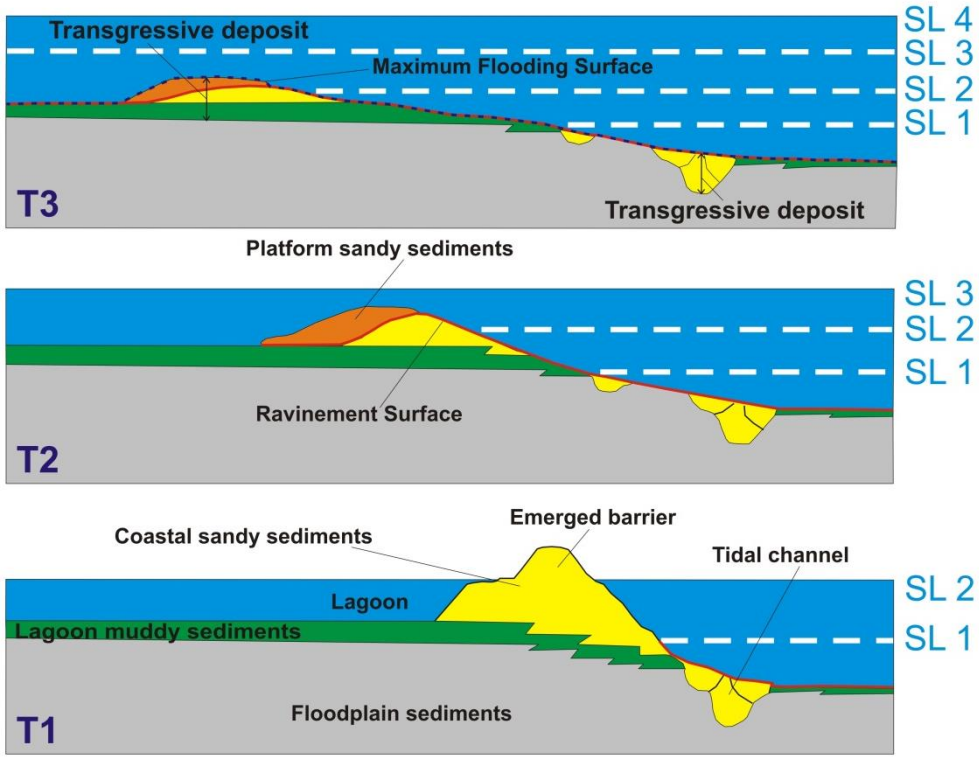

Fig. 2.10: Sedimentation, reworking and preservation of one transgressive deposit in a low gradient shelf. T1: sedimentation and aggradation of one transgressive deposit; T2: drowning and reworking of the transgressive deposit, due to the relative sea-level rise; T3: preservation of the deposit below the maximum flooding surface (MFS).

2.6.3.1 Shoreline trajectory

The shoreline trajectory is the path taken by the shallow shelf margin facies as they change position when during rising and falling relative sea-level affect sedimentary basin (Helland-Hansen and Gjelberg, 1994). There are three main scenarios characterized by different shoreline trajectories: 1) the shoreline trajectory coincides or is at a lower angle than the older surface. This situation is characterized by a low sedimentation or absence of transgressive deposits accommodation (Cattaneo and Steel, 2003); 2) when the shoreline trajectory diverges upwards from the transgressed topography, transgressive sediments are accumulated if high sediment supply is provided behind the shoreface (Cattaneo and Steel, 2003); 3) the shoreline trajectory could have a zig-zag pattern if transgression is characterized by punctuated shoreline movement (Cattaneo and Steel, 2003). Thus, the preservation of transgressive deposit could occur in relation to a zig-zag pattern when the shoreline trajectory is steeper than the original topography (Cattaneo and Steel, 2003; Fig. 2.11).

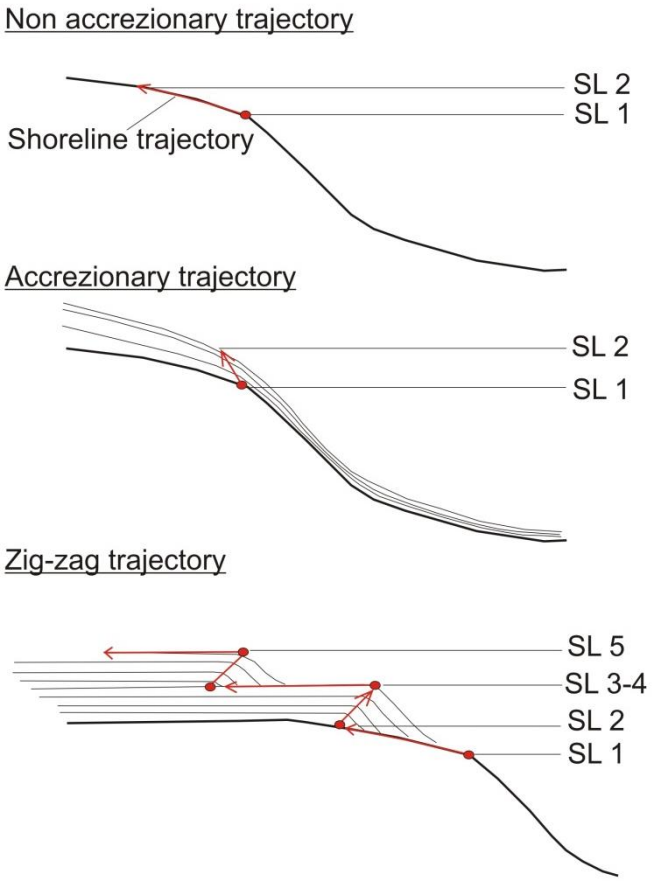

Fig. 2.11: Three main classes of transgressive shoreline trajectories. The shoreline trajectory depends on changes in relative sea level, sediment supply and basin morphology (redrawn by Cattaneo and Steel, 2003).

2.6.3.2 Sediment supply

Cattaneo and Steel (2003) highlight that the thickness and the internal architecture of the transgressive deposits strongly depend on to the rate of sediment supply, rate of sediment transport, textural composition and rate of relative base-level rise. In particular, the rate of sediment transport is due to currents pattern against coastal promontories or morphological barriers, whereas the rate of sediment supply depends on tectonic causes or fluctuation in climatic changes resulting in the catchment area modification or changes in longshore currents (Cattaneo and Steel., 2003). Furthermore, the sediment characters depends on source areas and also are due to the sediment distribution caused by alongshore transport or basin widening.

2.6.3.3 Original topography

The transgression occurs on older sediments forming the original substrate and the role of ancient topography is considered in terms of its gradient and roughness (Belknap and Kraft, 1985; Cattaneo and Steel, 2003). In particular, a transgression across a high-gradient platform causes a slow landward shifting of the coastline producing reworking sediments in the adjacent areas (Fig. 2.12), whereas, a transgression across a low-gradient platform causes a more rapid landward shifting of the shoreline and a later drowning of the previous transgressive deposits if the rate of relative sea-level is sufficiently high (Fig. 2.12; Sanders and Kumar, 1975).

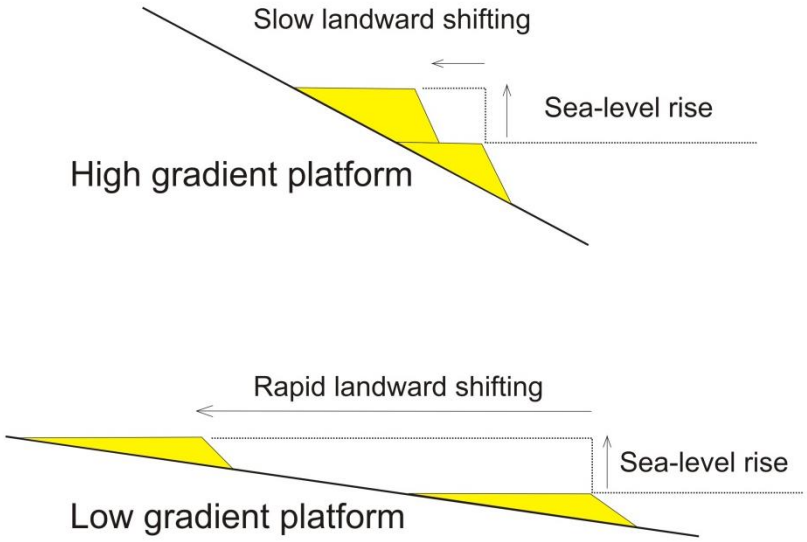

Fig. 2.12: Sea-level rise in relation to different gradient of the platform. High gradient scenario is characterized by slow landward shifting and reworking in adjacent areas; low gradient scenario influences rapid horizontal translation and drowning of transgressive deposits.

Cattaneo and Steel (2003), from Curray (1964) diagram, had described the transgressive processes in relation to accommodation and supply, highlighting that the thickness of transgressive deposits depends on the interplay of accommodation (A) and supply (S), and it is maximum if the A/S ratio is close to 1. The preservation of transgressive deposits landward of the shoreline depends on the amount of erosion by ravinement. Thus, at the shoreface, the maximum preservation potential of transgressive deposits occurs where the trajectory of the ravinement surface is steeper, close to the transgression-to-regression turnaround point. Moreover, for example, Belknap and Kraft (1981) showed that transgressive deposits are well preserved within incised valleys,

where an idealised valley-fill succession is characterized by fluvial deposits at the bottom, upper bay marsh, lower bay tidal inlet/flood-tidal delta and offshore marine units at the top. However, the spatial relationships between the sequence boundary and the overlying wave ravinement surface is indicative of the degree of preservation of transgressive deposits (Belknap and Kraft, 1985).

2.6.4 Transgressive deposits: Classification

In order to highlight the physical elements forming the transgressive deposits, Cattaneo and Steel (2003) proposed a classification that summarizes their main features. In particular, the authors highlighted 5 different groups of transgressive deposits (T-A, T-B, T-C, T-D and T-E; Fig. 2.13), emphasizing that the inherited physiography of the basin is a critical parameter, especially in relation to the transgressive deposits thickness.

- ✓ T-A is indicative of transgressive deposits developed below the Rs, preserved in low-gradient setting where the ravinement trajectory is steeper than the pre-existing topography.
- ✓ T-B (sand prone than T-A) is indicative of transgressive deposits developed above the tidal ravinement surface and below the wave ravinement surface. They are formed in tide-dominated setting and the local separation or slight divergence between tidal and wave ravinement surfaces allows estuarine sand bodies to develop.
- ✓ T-C is indicative of transgressive deposits developed above the wave ravinement surface in low gradient setting. These deposits are due to shoreface erosional products during transgression. The T-C transgressive deposits group transgressive lags or shelf sand ridges resulting from the transgressive reworking of older sand-rich systems.
- ✓ T-D is indicative of transgressive deposits developed above the wave ravinement surface in high gradient and high sediment supply setting. In this context, coarse-grained transgressive lithosomes can aggradationally developed because all the eroded and newly supplied sediment is redeposited locally above a high gradient wave ravinement.

- ✓ T-E is indicative of transgressive deposits without evidence of ravinement surfaces. These transgressive deposits are indicative of low-energy coastline and are typically developed in mud-dominated environment.

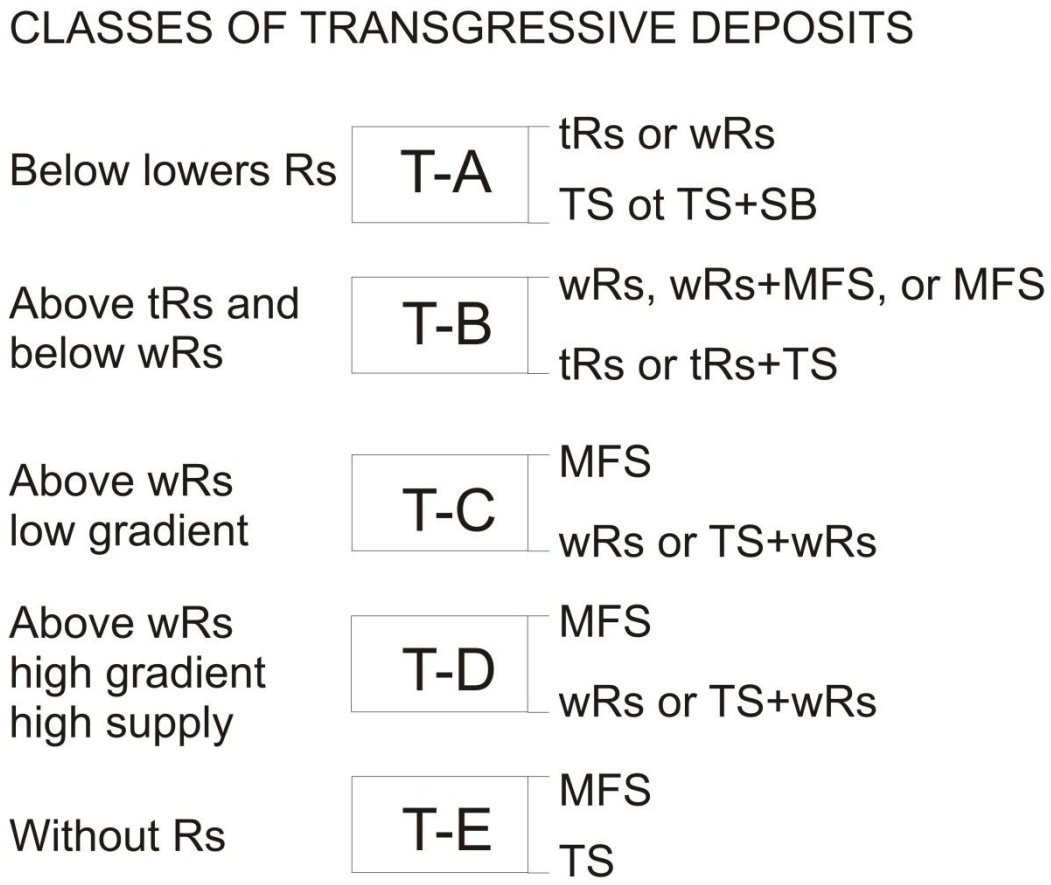

Fig. 2.13: Classification of transgressive deposits from Cattaneo and Steel (2003). Summarizing of all possible combinations.

2.6.5 *Late Pleistocene-Holocene transgressive deposits in the Adriatic Sea*

In the Adriatic Sea the transgressive deposits of late-Pleistocene and Holocene were deposited in a short time of high-amplitude and high-rate relative sea-level rise, recording the interval between ca. 19 and 5.5 kyr BP (Cattaneo and Trincardi, 1999). On the northern Adriatic shelf the transgressive deposits are few meters thick and are characterized by different generation of patchy barrier islands and incised valley system (Correggiari et al., 1996a; Storm et al., 2008), whereas on the central Adriatic platform, the transgressive deposits are formed by a sedimentary progradational body thicker than 25 m, divided into three portions, composed of backstepping wedges of marine deposits that onlap an erosional transgressive surface (Cattaneo and Trincardi, 1999; Maselli et al.,2011). In particular, the Fig. 2.14 highlights the classification of the transgressive deposits, proposed by Cattaneo and Steel (2003), related to the transgressive deposits identified in the Adriatic shelf.

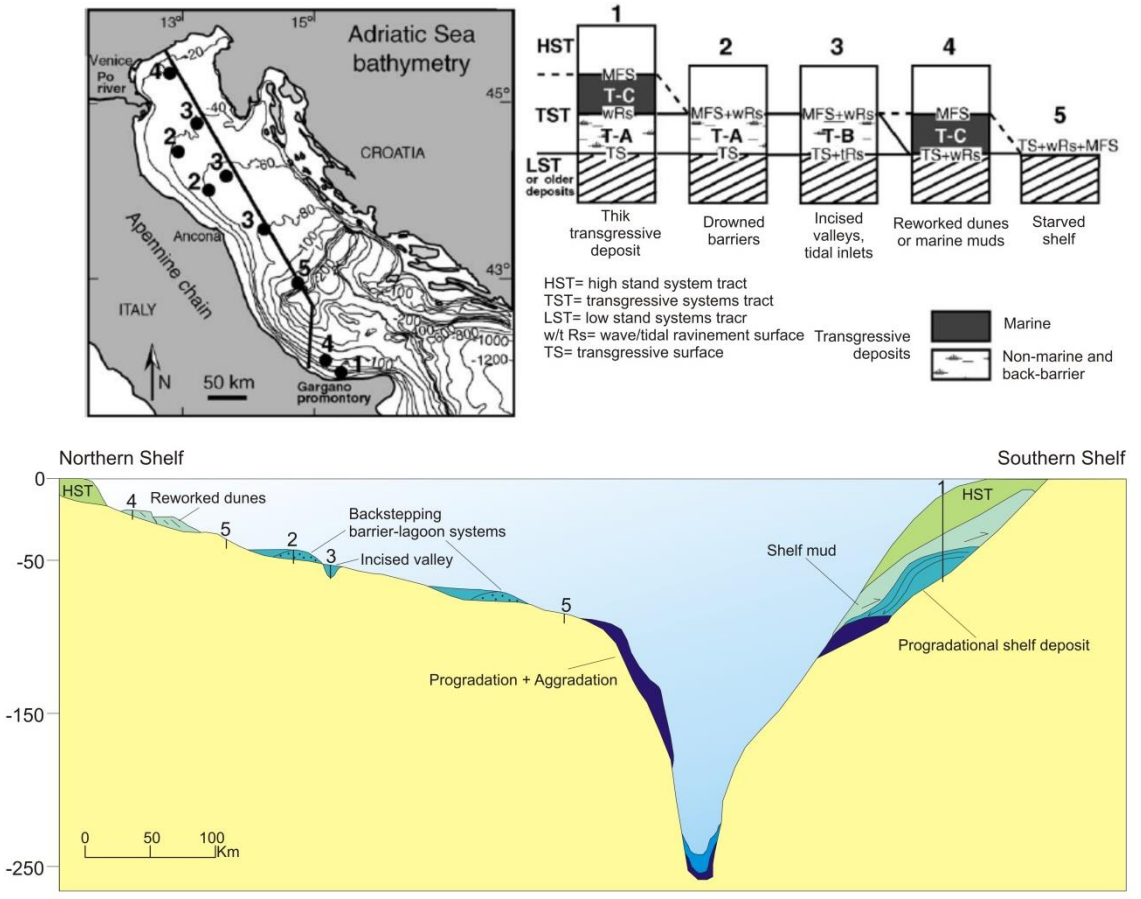

Fig. 2.14: Adriatic Sea morphology and examples of five stratigraphic columns showing the variability of transgressive deposits (modified from Cattaneo and Steel, 2003).

2.6.5.1 TST Central Adriatic Sea

In the central sector of the Adriatic shelf, each unit part of the transgressive deposit records a distinct phase of the last relative sea-level rise. The basal and top units record an abrupt landward shift of the shoreline, while the middle unit is prograding seawards and represents a regressive sedimentary body within the TST (Cattaneo and Trincardi, 1999). Moreover, the three TST units are separated by two prominent and extensively erosional surfaces (S1 and S2 surfaces, Cattaneo and Trincardi, 1999; Maselli et al., 2011; Fig. 2.15). In particular, the lower unit records the early stages of relative sea-level rise in an over-supplied setting; this unit is a 10 m muddy thick prograding wedge, with aggradational component deposited between 18 and 14.5 cal. kyr BP (Cattaneo and Trincardi, 1999). The middle unit records a landward shift of the coastal onlap respect to the lower unit, but also represents a phase of increased supply and seaward progradation in the southern area (Trincardi et al., 1996), it is formed by continuous unit of marine mud in the MAD and is characterized by two sub-units separated by an erosional surface (Si), that probably, records a minor sea-level fall during the Younger Dryas period (Maselli et al.,2011; Pellegrini et al., 2015). The upper unit, extending further landwards compared to the middle unit, records the last phase of sea-level rise, following the Meltwater pulse 1B, and is characterized by marine muddy sediments (Trincardi et al., 1996), rich in planktonic foraminifera indicative of outer-shelf to upper-slope environment (Amorosi et al., 2015).

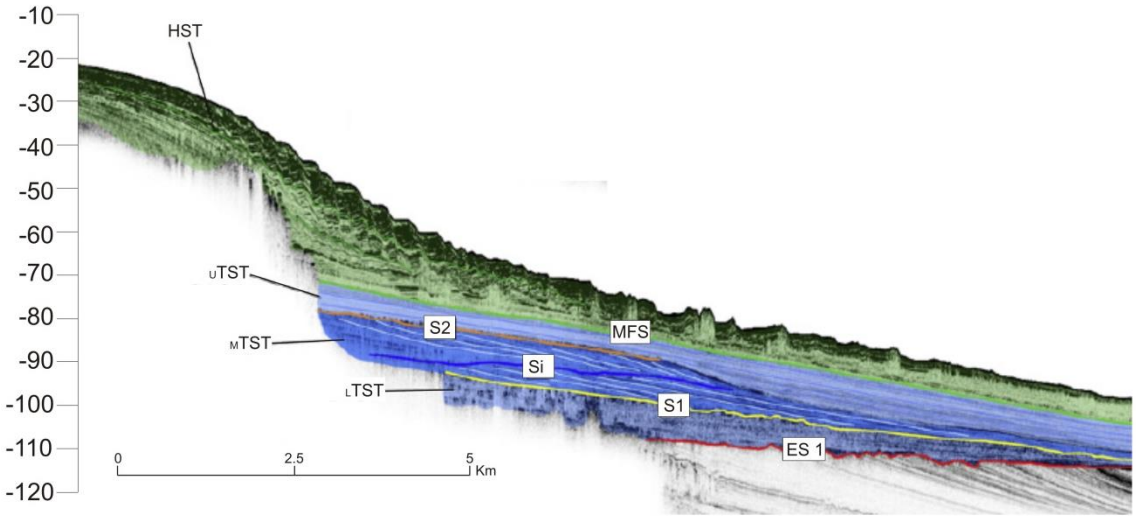

Fig. 2.15: Central Adriatic stratigraphy along CSS700 seismic profile (from Maselli et al., 2011). In blue the Transgressive System Tract, and in green the High-stand System Tract.

2.6.5.2 TST Northern Adriatic Sea

The low gradient of the northern Adriatic shelf, together with the sea-level rise, favoured the deposition and the submersion of different generation of barrier-lagoon systems. These transgressive deposits, present in the shelf as isolated body between -45 and -10 m msl, are preserved as elongated and undulating elevations, almost parallel to the present coastline. These transgressive bodies have generally a small size and are discontinuous, due to the reworking action of the ravinement surface. Furthermore, some transgressive sandy bodies with a thickness of 3-5 m, were preserved in the northern Adriatic shelf representing relicts of preserved basal shoreface (Correggiari et al., 1996a; Trincardi et al., 2011). Moreover, at 20-24 m msl, some transgressive deposits are characterized by fields of asymmetric sand dunes with variable wave-length, up to 700 m. In this shallow part of the north Adriatic shelf the transgressive reworking is maximized as the result of decrease rate of accommodation space at the end of the sea-level rise and of decrease of sediment supply together with a stronger oceanographic regime in response to the widening of the semi-enclosed basin (Trincardi et al., 1994; Correggiari et al., 1996b).

In particular, the northern Adriatic shelf is characterized by paralic and marine transgressive deposits.

- ✓ The Paralic deposit are related to transitional environments connect to the sedimentation and the subsequent drowning of barrier-lagoon system. These paralic bodies rest on a TS, that is indicative of the incipient sea-level rise on a substrate exposed to subaerial erosion, and are truncated by the Rs at the top, thus, they correspond to the T-A transgressive deposits described by Cattaneo et al. (2003) (Fig. 2.14; 2.16). The paralic deposits are mainly formed by clay and silty-clay, rich in organic matter, alternating with peat layers characterized by lateral continuity. The fossils association, with dominant *Cerastoderma glaucum*, *Ventrosia ventrose* and *Hydrobia*, is indicative of a brackish back-barrier setting. These deposits record delta plain environments with distributary channels, bay fill and lagoons (Correggiari et al., 2011; Fabbri et al., 2001; Trincardi et al., 2011). Moreover, a sandy-silty coarsening upward interval can be preserved above the silty-clay sediments; this

portion consists of very-fine to fine sorted sand representing a basal shoreface portion reworked by the wave action (Rs) during the sea-level rise. In particular, in the northern Adriatic Sea, the ravinement surface, a coarser layer less than 30 cm thick, characterized by marine shelly fragments, often coincides with the MFS (Trincardi et al., 1994). In this case, the transgressive deposits record only a paralic backstep wedge that represents partial preservation of drowned barrier-lagoon-estuary systems (Trincardi et al., 1994).

- ✓ The marine deposits rest on the ravinement surface and are capped by the MFS; they correspond to the T-C transgressive deposits described by Cattaneo et al. (2003) (Fig. 2.14; 2.16). In particular, these deposits are present in the northern Adriatic Sea both, as prodelta facies and as bioclastic sand facies. The former (Fig. 2.14 schematic log 1) are marine wedges parallel to the present coastline, below to the high-stand deposits and are mainly characterized by pelitic sediments. The latter (Fig. 2.14 schematic log 4), are generally characterized by bioclastic sand gradually shifting upwards to pelitic sediments. Moreover, they are confined in few outcrops and are preserved as the result of transgressive reworking of older sand-rich systems or as simple transgressive lags, commonly bioturbated if immediately overlain by deeper water shale, that contain pebbles and shell fragments (Cattaneo et al., 2003).

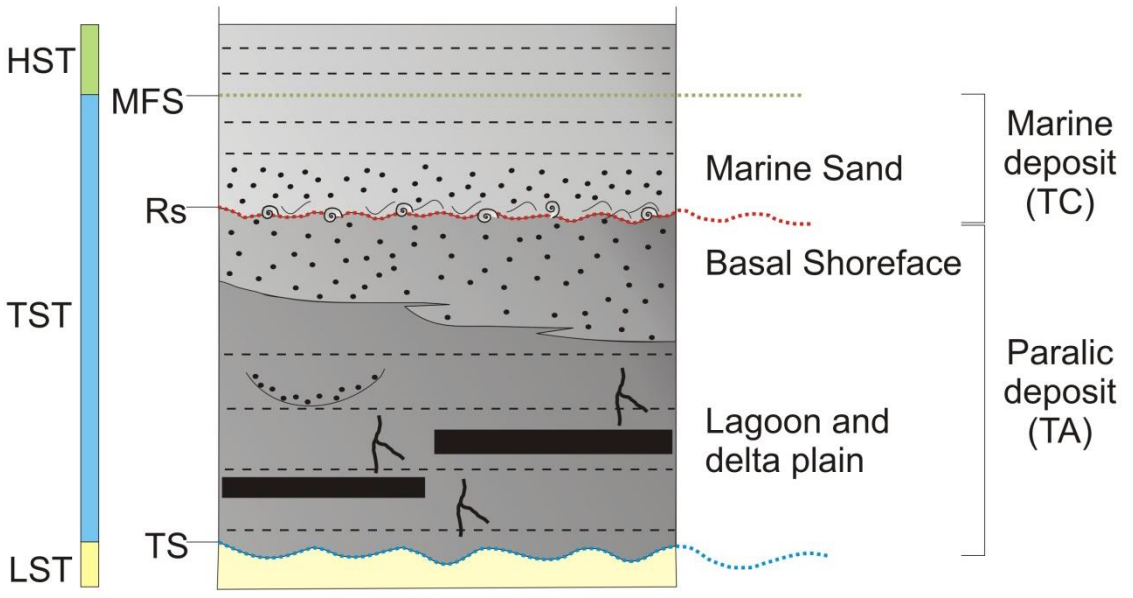

Fig. 2.16: Schematic log of paralic and marine transgressive deposits in the northern Adriatic Sea.

2.6.6 Shelf sand deposits for nourishment

To protect the coastal areas from the erosion the artificial nourishment is the more indicated operation. In the recent years, several studies were carried out focussing on the offshore sand as main source for the beaches nourishment. In particular, the transgressive bodies, sedimented and preserved in the northern Adriatic shelf during the last relative sea-level rise, are an economic resource because their significant amount of sorted sand. Thus, these deposits represent fossil coastal bodies reworked by the last transgression and are characterized by variable size and sand thickness. In order to identify a proper dragging area, several analyses are required. In particular, study on measurements and volumes calculation must be associated with grainsize and compositional analyses to obtain accurate data on amount and quality of sand. More in detail, the characteristics of sand have to satisfy some aspects, such as, low mud content (<5%), medium-fine sand grainsize and same composition of the coastal area chosen for the nourishment. The Adriatic Regional technical offices responsible for the coastal plan protection since 1990 work with CNR-ISMAR in collaboration project to find sand deposits potentially useful to offshore borrow site for beach nourishment (Correggiari et al., 2011).

CHAPTER 3
INSTRUMENTS, METHODS AND DATA

The characterization of the investigated deposits was based on a large dataset of CHIRP-sonar profiles, bathymetric and isopach maps of the Late Pleistocene-Holocene deposits on the Adriatic shelf. Moreover, these data were validated and integrated with stratigraphic and compositional analyses from sediment cores, allowing a very high chronological resolution.

3.1 CHIRP Sonar

The CHIRP Sonar is a Sub Bottom Profiler that provides quantitative, high-resolution, low-noise subbottom data and allows to investigate the first meters of loose sediment of the substrate. The CHIRP Sonar used is a Teledyne Benthos CHIRP-III SBP, characterized by 16 low-frequency transducers (2-7 kHz) inserted in the keel of the Urania research vessel. This instrument transmits a limited bandwidth signal with a defined transmission length with Linear Frequency Modulation. The vertical resolution is proportional to the bandwidth of the signal and, thus, the longer the signal the larger the bandwidth, the higher is the image resolution (Correggiari et al., 2011). The adopted configuration of the system is characterized by a pulse length of 5 or 10 ms and a trigger rate from 0.25 to 1.5 s depending on the seafloor depth. The obtained geophysical data were recorded as .XTF extension by the SwanPRO 1.60 software, produced by Communication Technology. This software is directly interfaced to the differential GPS in order to track the exact position of the seismic profile with a centimetric to decimetric accuracy.

3.1.1 Data description and software tools applied

The .XTF recorded data were converted in .SEGY extension with a tool included in SwanPRO v. 2.00 by Communication Technology (*http://www.comm-tec.com/Prods/mfgs/CommTech/swanpro/SwanPro.html*).
The .SEGY extension is an open standard file format used for reading and processing seismic profiles by different software.

Two software were used for the visualization, interpretation and the processing of the data.

- ✓ **Kogeo v. 2.7** is an open software developed by the Institute for Biogeochemistry and Marine Chemistry of the University of Hamburg. This software was mainly used for the visualization (Fig. 3.1), and stretching of the seismic profiles. Moreover, this software allows to import the navigation data in order to identify the coordinate position and the distance (millisecond) from the instrument to the seafloor.

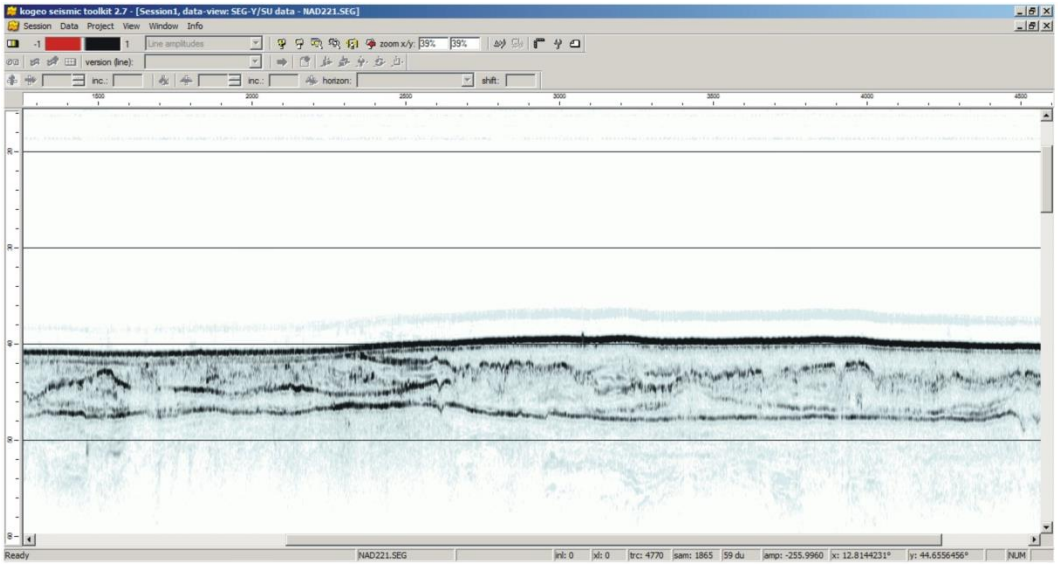

Fig. 3.1: Example of one seismic profile visualization provided by Kogeo v. 2.7.

- ✓ **SeisPrho** is an open software developed by ISMAR-CNR institute (Bologna Section; Stanghellini and Gasperini, 2009; *http://software.bo.ismar.cnr.it/seisprho*). This software is usefull for processing and interpreting high-resolution seismic reflection profiles. The main feature of SeisPrho is its interactive graphic interface, that provides the user with several tools for interpreting the data, such as reflector picking and map digitizing. SeisPrho was mainly used to digitize by picking seismic key reflectors previously identified (Fig. 3.2). In particular, the files obtained by the picking, showing the coordinate and the millisecond (ms) depth per each picked point, are text files with a .dgt extension.

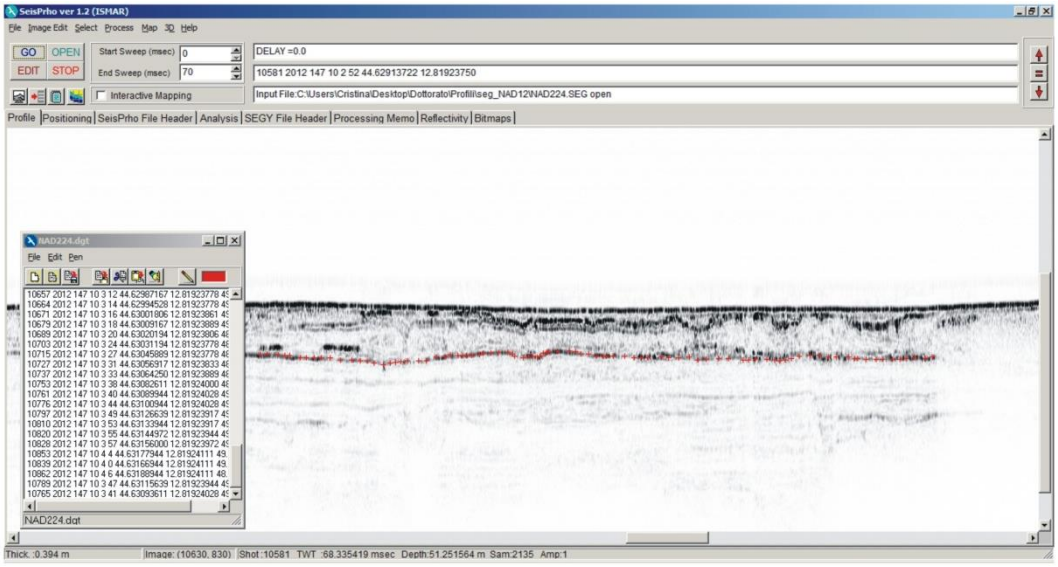

Fig. 3.2: Example of one seismic profile visualization provided by SeisPrho, and digitalization of one key surface.

3.1.2 Very High Resolution (VHR) seismic profiles interpretation

The seismic profiles allowed to visualize with high resolution the first meters depth from the seafloor and, as a consequence, the seismic analysis allowed to describe in detail the transgressive deposits. According to Stoker et al. (1997), the analysed VHR seismic profiles highlight different values of amplitude, frequency and continuity, thus lithological boundaries will only be detected if the acoustic impedance changes across the boundary. In particular, the reflection amplitude depends on the acoustic impedance contrast between the layers. For example, the Quaternary successions are characterized by interbedded alternations of sand and clay with high amplitude, associated to peat layers (Stoker et al., 1997). The reflection frequency depends on layer thickness in relation to different breadth of the signal. The changes of the vertical thickness can be used to identify sequence boundaries, whereas lateral variation can suggest change of facies. The reflection continuity is related to the layer continuity and can suggest facies interpretation; in particular, high continuity is indicative of low-energy environments, while low continuity corresponds to high energy environments (Stoker et al., 1997). Moreover, the low continuity can be affected by the presence of gas within the sediments, that can absorb the signal producing noise and discontinuity reflectors.

The VHR seismic profiles highlighted three dominant seismic facies (Fig. 3.3): 1) a semi-transparent unit associated to plane-convex bodies,

characterized by low amplitude and low continuity due to scarce penetration of the signal and a discontinuous base; 2) an interbedded transparent seismic facies with parallel and subparallel irregular and discontinuous reflectors, that suggest variation in amplitude and 3) regular and continuous reflectors indicative of high amplitude and continuity, easily traceable along the seismic profile.

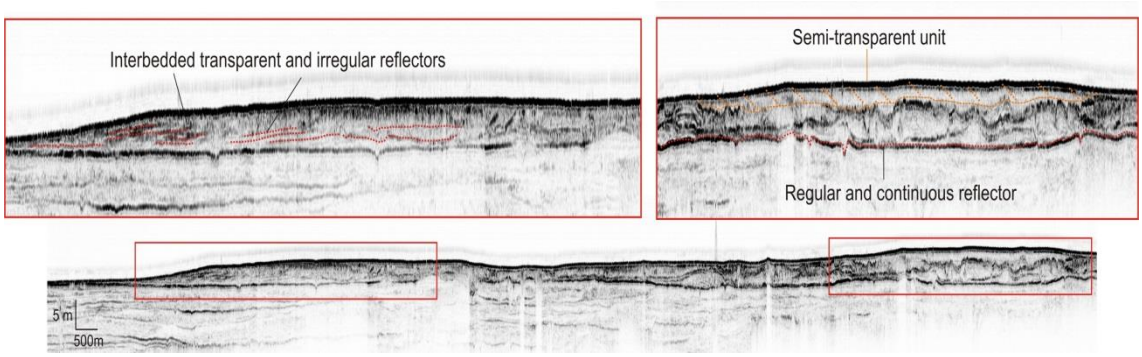

Fig. 3.3: Main seismic facies highlighted in the seismic profiles. Semi-transparent units, regular and continuous reflectors and interbedded transparent and irregular reflectors are identified.

3.2 Multibeam Eco-sounder System

The Multibeam is a sounder used for very high resolution seabed mapping, measuring the seafloor depth generating a short pulse of sound (ping) and recording the echo of the pulse produced by the bottom. The multi-beam sonar system can plot the bottom depth for dozens to hundreds of points in a line perpendicular to the direction route of the ship (swath width; SeaBeam Instruments Manual, 2000; Fig. 3.4A). This system is highly advantageous because travelling through paths close enough to keep the swath length linked, a detailed and complete bathymetric map can be obtained (Fig. 3.4B). The Multibeam must be calibrated with an accurate sound velocity profile of the water column (CTD). In particular, the analysed seafloor maps were recorded by a Kongsberg EM170 multibeam system characterized by ping transmission frequency ranging from 70 to 100 kHz and a swath width of 140° and maximum coverage up to five times the water depth. Furthermore a DGPS was connected to the Kongsberg Seatex Seapath 200 and to the Kongsberg Seatex MRU5 motion sensors in order to track the vessel path more efficiently.

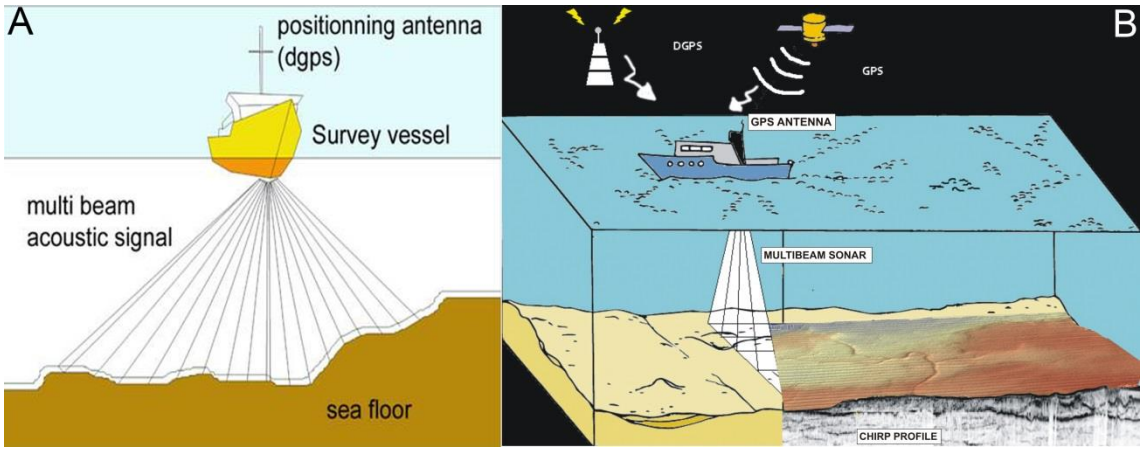

Fig. 3.4: A: Multibeam sonar footprint below the ship. B: Schematic bathymetric map obtained by the Multibeam allowed by the swath length overlapping.

3.2.1 Multibeam data (NAD12 oceanographic cruise)

The obtained maps highlight a detailed morphology of the seafloor in several areas of the Adriatic Sea. In particular, during the NAD12 oceanographic cruise, one transgressive deposit south of the Po River delta was investigated with the Multibeam device. This sedimentary body, which extends 15 km NS and 8 km WE, was investigated through seismic profiles network spaced 120 m each other and maximum coverage up to five time the water depth that permitted to produce a detailed bathymetric map with resolution of 1 m. The obtained digital elevation map shows with detail morphological highs, depressed areas, channel systems and a dredged area (Fig. 3.5).

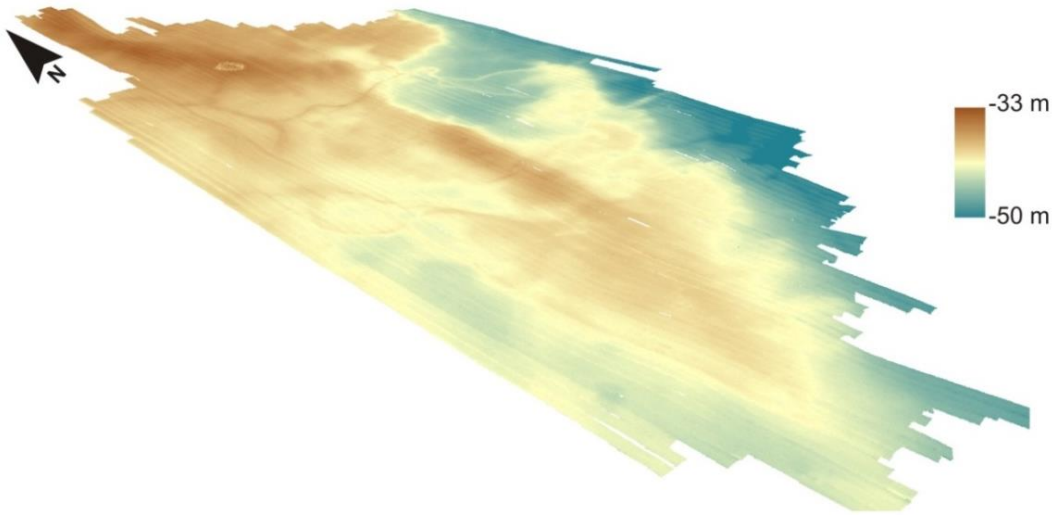

Fig. 3.5: Detailed DEM (1 m resolution) of one investigated area south of the Po delta, acquired through Multibeam data NAD12 oceanographic cruise.

3.3 Sediment corers

The analysed cores were collected both with gravity corer and vibro-corer. About 140 stratigraphic cores were described and calibrated with seismic profiles in order to identify the main core facies, and to correlate them with the seismic facies. Moreover, about 100 core samples were selected for grain-size and petrographic analyses and 20 core samples were selected for radiocarbon dating.

- ✓ **Gravity corer**

  The gravity corer was used in order to sample loose sediment bodies with a low resistance to penetration. This is a device formed by a head characterized by a cylindrical weight, a steel pipe with a removable lining of PVC tubing and a nose including a catcher that allows to keep the sediment inside the liner (Fig. 3.6). In particular the gravity corer used to collect the analysed cores has a 600 kg head and a 6 m long steel case with an inner plastic liner with a diameter of 90 mm.

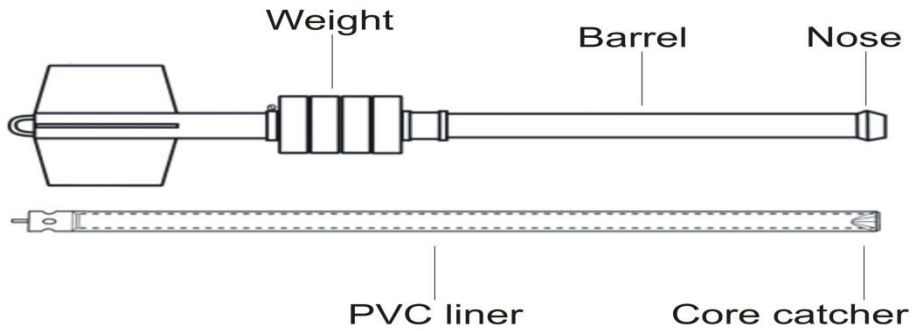

Fig. 3.6: Example of a gravity corer used to collect some analysed cores; modified from Lee and Clausner, (1979).

- ✓ **Vibro corer**

  The vibro corer was used to sample sand sediments that generally canno't be passed, by a gravity corer. This device, through vibration, produces a mobilization of a thin layer of sediment, allowing the penetration of the corer. This instrument is characterized by the same components of the gravity corer except for the heavy head that is replaced with a vibrating head (Fig. 3.7). The vibrocorer used is a Vibrocorer Rossfelder P5 powered by 440-460 V and 60 hertz.

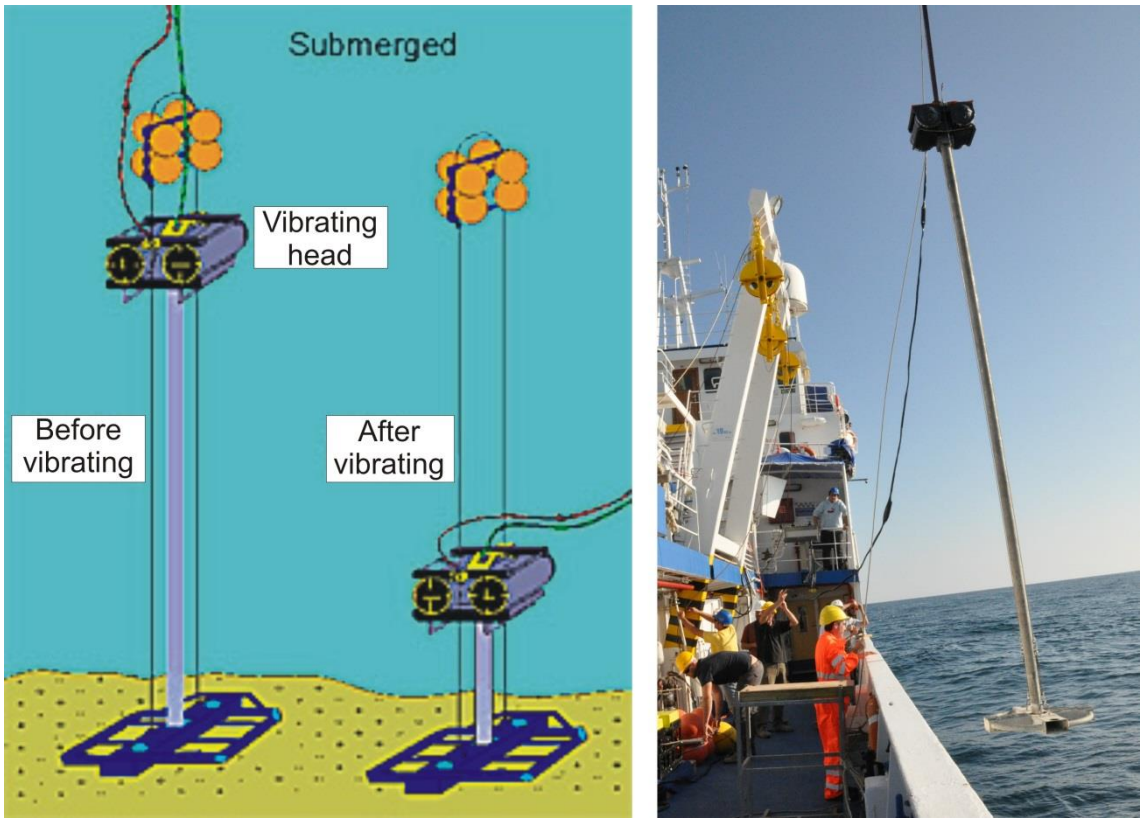

Fig. 3.7: Example of a vibro corer used to collect some analysed cores. On the left: picture from http://www.rossfelder.com/buyonet-rigid.html; on the right: core collected during AS14 oceanographic cruise (on board Urania R/V).

3.3.1 Data description

In order to identify different sedimentary facies forming the transgressive deposits, 140 cores were selected and described. The cores that highlight more than one sedimentary facies are the longer ones, and consist of a top layer of approximately 30 cm of silty and sandy clay that rests on a reworked surface mainly formed by shell fragments. The sediments below this peculiar and easily recognizable surface present a coarsening-upward trend with basal grey-clay and peat layers characterized by carbonaceous frustules, organic matter and shells. The dominant fossils association is characterized by *Cerastoderma glaucum*, *Ventrosia ventrose* and *Hydrobia*; and upper sand layers (from 1.5 to 2 m) and is formed by fine and sorted sand with low content of shell fragments and with rare clay hollow. Moreover, the top of the sand portion occasionally bioturbated at contact with the reworked surface. Furthermore, the longest cores reach basal sediments, deposited below clay and peat sediments. The latter are made of clay sediments, but stiffer and pale yellow in colour that allow to distinguish them (Fig. 3.8; Appendix A).

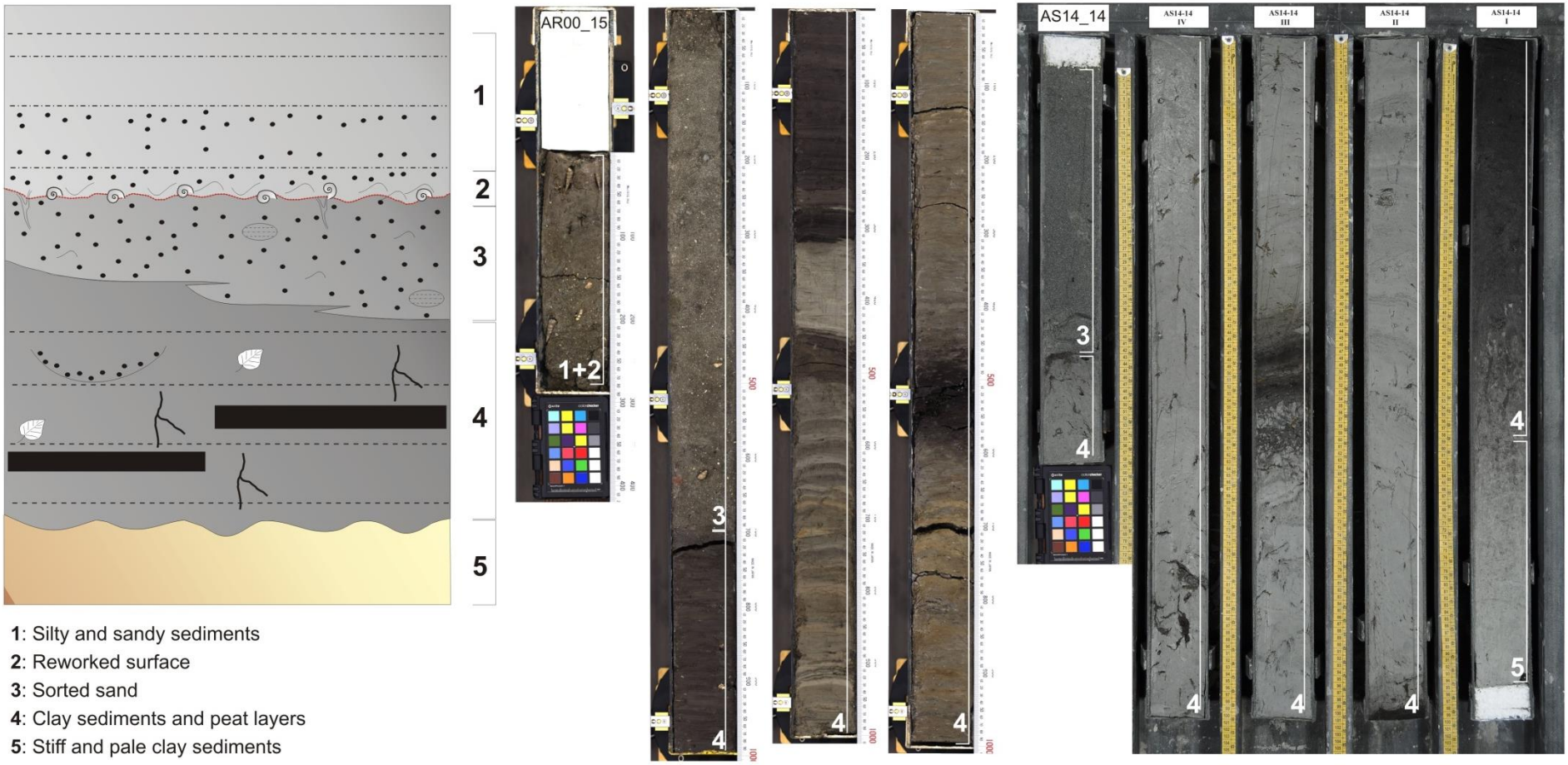

Fig. 3.8: Schematic log of one analysed core and examples of two collected cores.

3.4 AMS Radiocarbon analysis

In order to geochronologically constrain some of the studied deposits, wood fragments, organic-rich sediments, and peat layers were sampled from selected cores.

The AMS Radiocarbon dating analysis were carried out by the Ion Beam Laboratory at the ETH Institute in Zurich, and the radiocarbon calibration was performed using CALIB14 Radiocarbon Calibration Program of Stuiver and Reimer (1993). The Accelerator Mass Spectrometry (AMS) is a highly sensitive methods of counting atoms. It is used to detect very low concentrations of natural isotopic abundances of both radionuclides and stable nuclides. The main advantages of AMS compared to conventional radiometric methods are the use of smaller samples (mg and even sub-mg size) and a shorter measuring time (less than 1 hour). Radiocarbon dating uses the amount of Carbon 14 (^{14}C) available in living creatures as a measuring stick. All living things maintain a content of ^{14}C in equilibrium with that available in the atmosphere, right up to the moment of death. When an organism dies, the amount of ^{14}C available within it begins to decay at a half-life rate of 5730 years, In fact, it takes 5730 years for ½ of the ^{14}C available in the organism to decay. Comparing the amount of ^{14}C in a dead organism to available levels in the atmosphere, produces an estimate of when that organism died. By measuring the radiocarbon age of tree rings of known or other independently dated samples it is possible to construct calibration datasets. The current calibration datasets including IntCal04, Marine04, and SHCal04 is recommended for general use (Stuvier and Reimer, 1993; Reimer et al., 2004). The results were corrected for isotopic fractionation, but no correction for oceanic reservoir was made because the dated samples are plant and sediments of terrestrial origin. The obtained data were plotted in a Depth vs. Age graph which groups Adriatic ^{14}C age data from Fabbri et al. (2001), Antonioli et al. (2009) and Trincardi et al. (2011a-b).

3.5 Grain-size analysis

The grain-size analysis was performed in order to identify particle-size classes of the sand and the amount of clay. Initially the samples were treated with a solution H_2O_2 30% diluted and kept under a hood for at least three days

in order to disintegrate the organic matter. Then the samples were washed with 63µm sieve to separate the sand from silt and clay. The sand portion was collected in a ceramic bowl and was heated in the oven at 60 ˚C, whereas the clay portion was collected in a beaker and left to decant. Once the sand portion has been dried, it was after separated through a stack of sieves from 2000 to 63 µm, and the sediment held within each sieve was weighted. Once the clay portion has been decanted at the base of the baker, the water was removed through syphoning, and subsequently the clay portion was heated in the oven at 40 ˚C and weighed.

The statistical analysis was performed through the Gradistat software (Blott and Pye, 2001), written in Microsoft Virtual Basic and integrated into the Excel spreadsheet, that allows to calculate mean diameter, median, mode, sorting, skewness, kurtosis per each samples through the obtained data from sieve.

3.6 Petrographic analysis

About 70 sand samples, from selected cores belonging to the study deposits, were selected for a quantitative compositional study in order to delineate their composition. The sand samples selected for analysis were split and a small portion of sand was impregnated in an epoxy resin according to the methodology described by Gazzi et al. (1973), to obtain a thin section for microscopic analysis. All the thin sections were stained with alizarine-red solution to facilitate distinction of calcite and dolomite during the modal analyses. Sand point counts, under polarizing microscope, were performed following the Gazzi–Dickinson technique (Gazzi, 1966; Dickinson, 1970; Ingersoll et al., 1984), modified by Zuffa (1987), with the aim of minimizing the influence of grain size on the composition. Initially, a counting chart was created, consisting of four main grain classes (Quartz, Feldspar, Lithic fragments, Extrabasin Carbonates) highlighting a division of components according to composition and texture features. The point-counting method consists of separating coarse-grained lithic fragments (single crystals >0.0625 mm) from fine grained lithic fragments (single crystal grains <0.0625 mm). Due to the lack of interstitial components, 300 points were determined for each thin

section using a 0.5 mm grid spacing and the percentage of main classes was calculated and plotted in a triangular diagram. In order to better distinguish the different composition of the deposits, the point-counting wass counted for a selected number of samples until at least 200 rock fragments (both fine and coarse-grained) were determined.

3.7 XRF analysis

Seven cores from different transgressive deposits were selected for the XRF core scanner analysis in order to track downcore changes in chemical composition. The XRF core scanner analysis is one of the greatest innovation that have been developed in the last decades in order to collect high resolution continuous downcore records of element distribution (Rothweel et al., 2006). The X-ray fluorescence is a spectrometry technique that highlights the chemical elements forming the analysed sample. When the sample surface is exposed to X-ray, the component atoms are stimulated and ionization takes place. Incident X-rays eject an electron from the inner shell of the atom, and the resulting vacancy is filled by an electron falling back from an outer shell. The electron releases its surplus energy in the form of electromagnetic radiation, that highlights characteristic energy and wavelength spectra different for each atom (Fig. 3.9; *http://www.handheldxrf.com.au/technology_handheld_xrf.php*), thus the intensity and the energy of the emitted X-ray are analysed and compared against standard in order to determine the elemental composition.

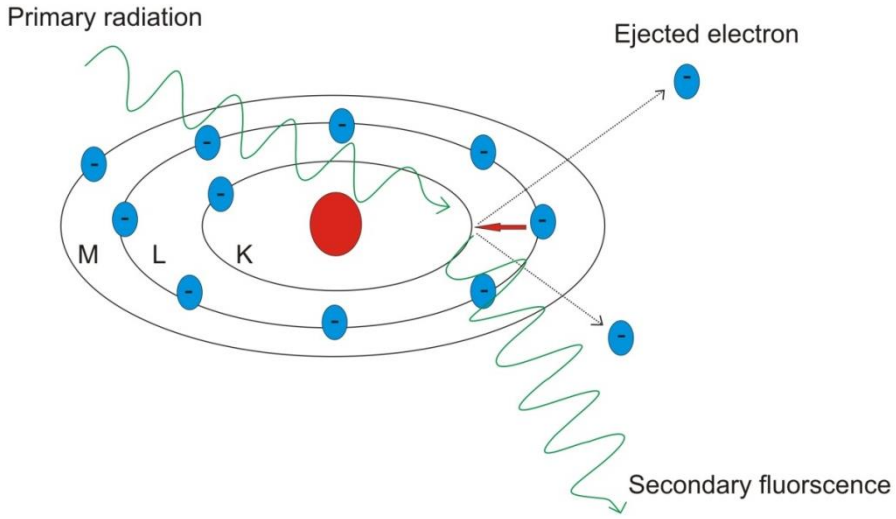

Fig. 3.9: Physics of X-ray fluorescence in a schematic representation.

Moreover, for the XRF core scanner analysis the response depth of elements to incoming X-ray radiation must be considered for its dependence to wavelength of emitted radiation. In Moseley's law, the elements with higher atomic numbers emit X-rays with relatively high fluorescent energy that are less susceptible to absorption and scatter along their path lengths to the detector. Hence emergent fluorescent radiation intensity and response depth are closely linked to atomic number, with progressively deeper response depths for heavier elements (Fig. 3.10). Thus, the response depth ranges from 0.05 mm for Aluminium (Al, Z 13) to 2-4 mm for Barium (Ba, Z 56) (Wihelms-Dick et al., 2012).

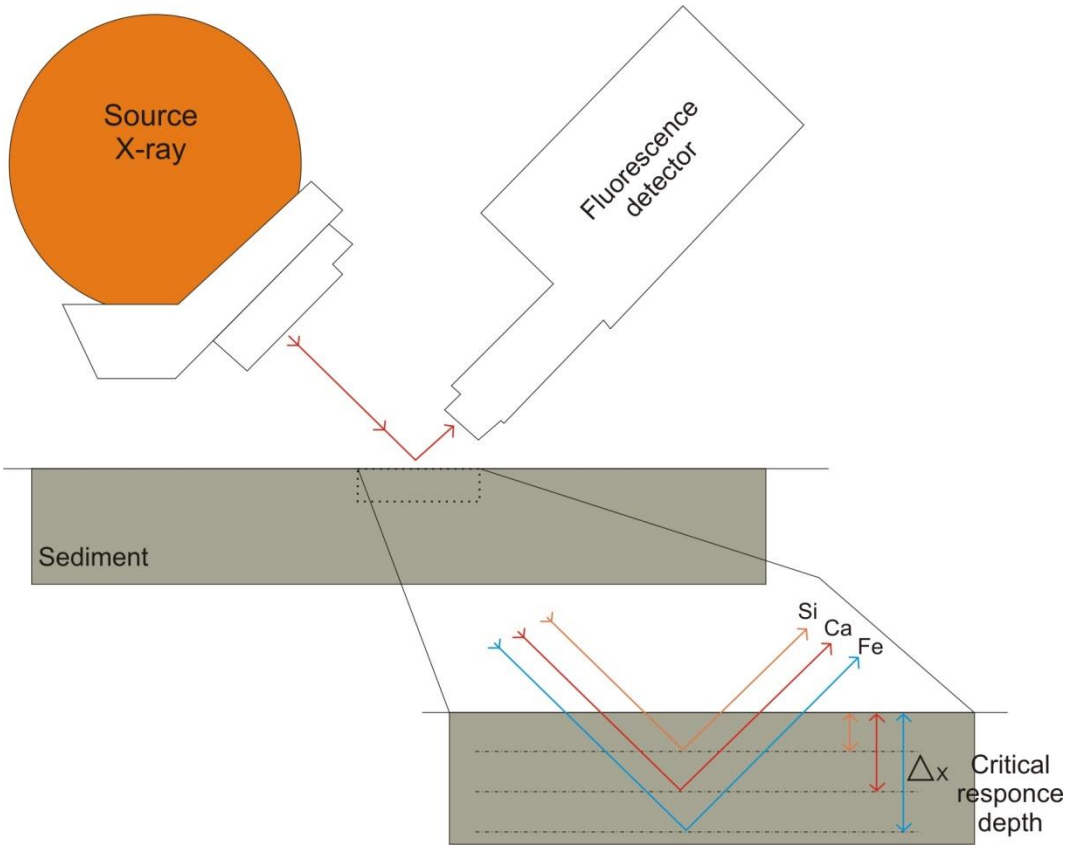

Fig. 3.10: Fluorescence critical depth, closely linked to atomic number. Lighter elements are characterized by shallow response depths, whereas heavier elements by deeper response depth.

The analysis was performed with an Avaatech XRF core scanner at the Royal Netherlands Institute for Sea Research (NIOZ). The measurement are non-destructive and require very limited sample preparation. The core sediment is covered by a thin high-purity polypropylene film (typically 1,5-6 µm thick) to prevent the core drying in order to avoid shrinkage and cracking. Moreover the XRF device needs a flat and homogeneous surface of the core to work properly.

In particular, the sample inhomogeneity and surface roughness are strongly pronounced for sediments containing abundant medium-coarse sand sediment, particles such as shell fragments in coastal environments or foraminifera in deep-sea setting (Richter et al., 2006), that produce a signal-noise increasing. Accordingly to these, the more appropriate cores for the XRF analysis are characterized by fine-grained clay sediments. The split cores were scanned at 1 cm resolution. The elemental range determined by the instrument starts from Aluminium to Uranium in concentrations from 100% down to ppm levels. The X-ray tube has variable power between 10 to 50 kV in order to measure, under optimal conditions, the whole range of elements (Tab. 1). The incident X-ray beam interacts with small sample volumes and, thus, the emitting characteristic X-rays contain only information from a thin superficial layer.

Tube Voltage (kV)	Count Time (s)	Tube Current (uA)	Filter	Elements
10	10	500	No Filter	Al, Si, P, Cl, K, Ca, Ti, Mn, Fe
30	10	500	Pd Thin	Br, Rb, Sr, Zr
50	40	750	Cu	Rb, Sr, Zr, Ba

Tab.1 : X-ray tube power and filter

The geochemical data obtained are generally expressed as count per second. It is worth noting that, this analysis is considered to be semi-quantitative, thus its interpretation must be considered carefully. Therefore, in order to have a more precise measure, the elemental ratio rather than direct counts is preferred.

3.8 Digital Elevation Map (DEM)

DEMs are obtained by the interpolation of a discrete number of points representing the key surfaces belonging to two transgressive deposits. These DEMs highlight the areal distribution and, thus, the paleo topography of each key surface. In particular, the good resolution, highlighted by the Digital Elevation Maps, was due to a grid of parallel seismic profiles spaced 120 m

from each other. The dense amount of data allowed to identify and trace in each seismic profile several key surfaces.

Firstly, from the .xls file obtained by digitalization, a rapid conversion from millisecond using a sound velocity of 1,500 m/s to convert travel times to depth value in m was done using the simple relation :

$$z(m) = (ms * (-0.75)) - 3.5$$

Where z is the depth, in meters, from the sea-level; 0.75 m corresponds to 1 ms (S=Vxt/2) and -3.5 m is the position under the sea level where the hull mounted CHIRP sonar is located on the ship. The obtained files were converted in ASCII file, easily readable by GIS software. The picking points were interpolated through the ArcGIS software in order to achieve a morphological map for each key surface. This software is a geographic information system designed to work with map and geographic information. In particular, the ArcCatalog software allowed to transform the ASCII file in shape files of the picking points. These shape files contain all the picked points that are characterized by the longitude, latitude and elevation parameters, moreover, the chosen coordinate system was the WGS84. Then, with the Geostatistical Analyst toolbox of ArcMap, the shape files were converted to raster files. This tool, indeed, allows to create continuous surfaces or maps that can be used to visualize, analyse and understand spatial phenomena.

3.9 Geodatabase

This PhD work, focused on detailed VHR seismic profiles and cores analyses, was possible thanks to seismic profiles and sediment cores dataset organized in a geodatabase made available by the CNR-ISMAR (Bologna Section). The CNR-ISMAR geodatabase, indeed, groups all data collected in the Adriatic basin during oceanographic cruises organized in the last twenty years (Fig. 3.11). In particular, data from CM94; AR00; VE04; VE05; RV08; RV11; NAD12 and AS14 oceanographic cruises have been analysed. Moreover, the NAD12 and AS14 oceanographic cruises, on which I took part, played a significant role in order to collect high resolution data allowing a total coverage of key areas, 1 and 2 of the Fig. 1.1.

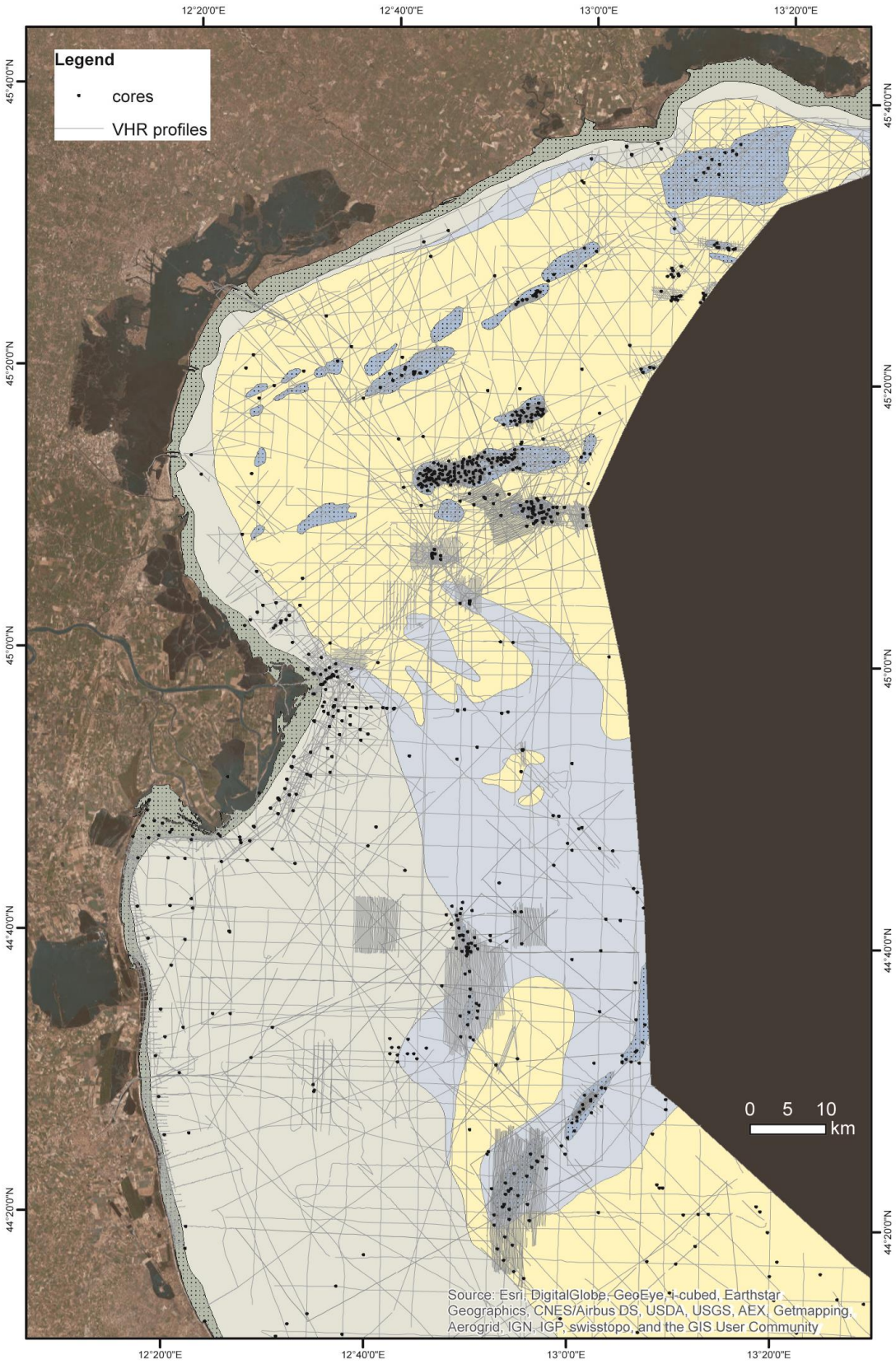

Fig. 3.11: Geodatabase grouping VHR seismic profiles and cores of the Adriatic basin made available by CNR-ISMAR (Bologna Section) for this PhD project.

CHAPTER 4

VERY-HIGH-RESOLUTION ANALYSIS OF A TRANSGRESSIVE DEPOSIT IN THE NORTHERN ADRIATIC SEA (ITALY)

4.1 Overview

This chapter is a journal paper published in Alpine and Mediterranean Quaternary. The characterization of one transgressive deposit in the Northern Adriatic Sea (Italy), located offshore Ravenna at 34 m w.d. is presented in order to emphasize in detail its evolution during the last transgressive cycle focusing on the transitional environments response in relation to the relative sea level rise.

4.2 Paper

GIORGIA MOSCON[1], ANNAMARIA CORREGGIARI[2], CRISTINA STEFANI[1], ALESSANDRO FONTANA[1], ALESSANDRO REMIA[2]

[1]*Dipartimento di Geoscienze, Università degli Studi di Padova, Via G. Gradenigo 6, 35131 Padova, Italy*

[2]*Istituto di Scienze Marine - CNR, Via Gobetti 101, 40129 Bologna, Italy*

4.2.1 Abstract

The Adriatic Sea is characterized in the northern and central shelf by different generation of isolated transgressive bodies formed and drowned in-place during the last relative sea-level rise. The continental shelf is characterized by a low gradient and, within the transgressive deposits the episodic variations in sea level and sediment supply caused the formation of backstepping parasequences. The transgressive bodies have been studied in detail because they have considerable amount of sorted sand exploitable for beach nourishment. A transgressive deposit, located south of the Po Delta, offshore Ravenna at depth of 34-35 m, has been investigated with a total coverage of very-high resolution (VHR) seismic profiles and high number of cores in order to understand the stratigraphic evolution during the late

Quaternary sea-level rise. The transgressive body is composed of four seismic units separated by high-amplitude and high continuity reflectors, corresponding to peat and organic-rich layers indicating different depositional phases. The core analysis confirmed the presence of different units showing sediment variation from clay with peat-layer at the base to fine-grained sand at the top of the deposit. Furthermore, the core analysis gave information about the thickness of the deposit. The thickness of the transgressive body is from 3 to 5 m and each unit varies from 1 to 2 m. In particular, the sand portion reached a maximum thickness of 1.5 meters. The seismic analysis and the digital elevation model constructed for key surfaces highlighted the channel system direction was towards ENE during Last Glacial Maximum and during sedimentation of Unit 1 and 2, while it shifted toward ESE during the formation of Unit 3. Moreover, to constrain the chronology of the sedimentary evolution, some peat and organic-rich samples, have been dated with ^{14}C method. These organic horizons are evident seismic reflectors and correspond to key surfaces. They are characterized by brackish lagoon facies and could be a proxy indicator for the relative paleo sea-level. Along with the previous data, they indicated that the sedimentation of the studied transgressive body occurred around 10,000 cal. a BP.
Keywords: Quaternary, sea-level rise, sequence stratigraphy, beach nourishment, CHIRP-sonar.

4.2.2 Introduction

The late glacial and Holocene (Post 18,000 a) sea-level rise is well recorded in the Adriatic Sea due to the peculiar physiographic and sedimentary setting of the basin (Correggiari et al., 1996). During the last sea-level rise the Northern Adriatic Sea was characterized by the formation of different generation of barrier-lagoon systems. These bodies, drowned in-place and partly preserved, crop out in the northern Adriatic seafloor as elongated build-ups parallel to the present coastline. They are interpreted as patches of ancient coastal wedges which have considerable amount of sorted sand and are a significant resource exploitable for beaches nourishment. The sand portion of the transgressive deposits has been studied in detail with grain-size analysis, petrographic analysis, sedimentary architecture and volumes calculation in

order to use this resource for coastal nourishment. The detailed characterization of a transgressive deposit located south of the Po Delta, through very-high resolution seismic profiles and facies analysis can shed new lights on the formation and evolution of the transgressive deposits. In particular, as the formation of the transgressive bodies is strongly related to the changes of relative sea level, their multidisciplinary study can produce important data in the reconstruction of the past relative position of the sea level (Antonioli et al., 2009) and detect centennial fluctuations.

4.2.3 Geological Setting

4.2.3.1 The Adriatic Sea

The Adriatic Sea is an epicontinental semi-enclosed basin (Fig. 4.1) surrounded by three thrust-and-fold-belts: the NE-verging Apennines, the S-verging Southern Alps and the SW-verging Dinarides. The basin records the evolution from a passive margin, during the Mesozoic, to a foreland basin system, during the Cenozoic (D'Argenio and Horvath, 1984; Ori et al., 1986; Ciabatti et al., 1987; Argnani and Frugoni, 1997). During Quaternary sea-level fluctuations the basin has been shaped by huge change of the oceanographic regime and sedimentary dynamics (Trincardi et al., 1994, 1996).

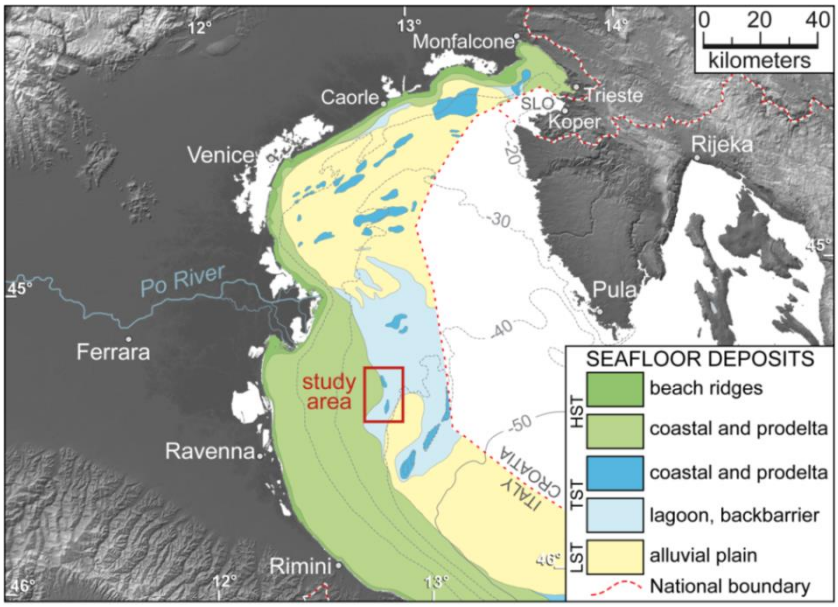

Fig. 4.1: Location of the study area in the Adriatic Sea. Bathymetry and superficial geology modified from the Geological Map of Italian seafloor (Fabbri et al., 2001; Trincardi et al., 2011 a, Trincardi et al., 2011 b).

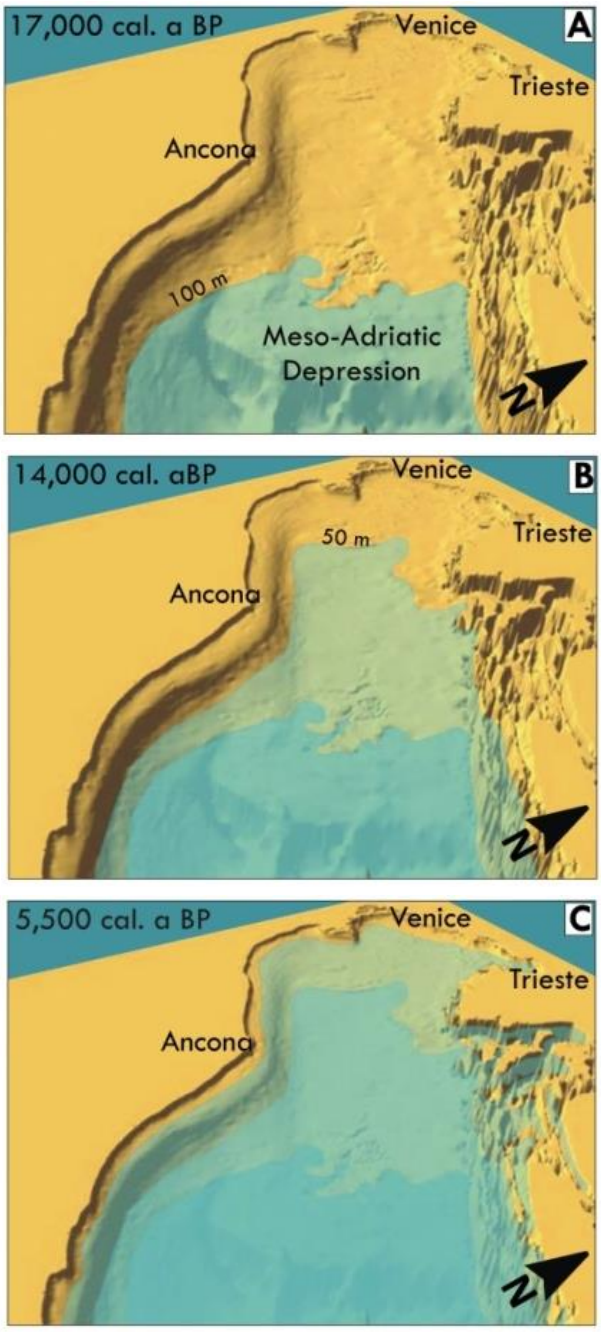

Fig. 4.2: Widening of the Adriatic basin during the last transgressive cycle. (A) Sea-level during the LGM, an extensive portion of the Adriatic sea was in subaerial condition, while the Meso-Adriatic-Depression (MAD) was a semi-enclosed basin receiving high amount of sediment (Correggiari et al., 1996). (B) Rapid sea-level rising after the LGM. (C) Maximum marine ingression reached 5500 cal. a BP.

During the Last Glacial Maximum (LGM, 30,000-19,000 ^{14}C a BP; Lambeck and Purcel, 2005; Clark et al., 2009) the sea-level was about 120-130 m lower than today and the northern continental shelf was completely in subaerial conditions (Fig. 4.2A). In this environment several river networks formed, consisting of by a main trunk river (Paleo Po River) and Alpine and Apennines tributaries; the fluvial system terminated in a low-stand delta located at the northern edge of the Meso-Adriatic-Depression, southeast of Ancona (De Marchi, 1922; Correggiari et al., 1996; Ridente and Trincardi, 2005). During the late-glacial to early-Holocene transgression, a glacio-eustatic, non-steady sea-level rise of approximately 120 meters caused substantial basin widening coupled by changes in energy regimes across the basin (Cattaneo and Steel, 2003) (Fig. 4.2B). The low gradient of the northern Adriatic shelf, together with the sea-level rise (approximately 10-15 mm/a), favoured the deposition and drowning of different generations of transgressive barrier-lagoon system sedimentary bodies. In contrast, the steeper topographic gradient of the southwestern Adriatic shelf has been characterized by the deposition of thick transgressive progradational deposits (Cattaneo and

Trincardi, 1999; Maselli et al., 2011). The maximum marine ingression was reached ca. 5500 cal. a BP when the basin occupied much wider area than during the low-stand (Fig. 4.2C). During high-stand the anticlockwise circulation characterizing the Adriatic caused southward transport of sediment along the entire western side of the basin as documented in surficial geology maps of the Adriatic (Fabbri et al., 2001; Trincardi et al., 2011a; Trincardi et al., 2011b; Fig. 4.1). Our study focused on a transgressive deposit, located 50 km from Ravenna at 34-35 m water depth (Fig. 4.1). This transgressive deposit showed a dominant longshore trend parallel to the modern coastline, it extends NS for about 20 km and is 8 km wide. Its thickness varies from 1 m near the boundary areas to 4 meters in the depocenters.

4.2.3.2 Transgressive deposits

The late-glacial and Holocene transgressive deposits (Transgressive System Tract, TST) in the Adriatic basin were formed by backstepping barrier-lagoon and incised valley systems in the low gradient northern shelf, while mud sedimentary bodies thicker than 25 m are present in the central Adriatic shelf (Cattaneo and Trincardi, 1999; Maselli et al., 2011, Trincardi et al., 2013) (Fig. 4.1). The TST rests on an erosive surface of regional extent (transgressive surface, TS) that truncates older low-stand deposits (LST), and is below the maximum flooding surface (MFS) (Fig. 4.3). Available ^{14}C data show that the time interval encompassed by the TST spans about 11,000 years, between 16,000 and 5500 cal. a BP (Correggiari et al., 1996; Trincardi et al., 1996; Cattaneo and Trincardi, 1999, Correggiari et al., 2001, Maselli et al., 2011). The transgressive deposits in the northern Adriatic shelf are located at sea bottom between -45 m to -10 m water depth, and they are preserved as elongated undulating elevations almost parallel to the present coastline. The complex geometry and their preservation is probably due to a combination of different factors such as the rate of sea-level rise, the low gradient of the shelf and the coastal dynamics (Belknap and Kraft, 1981, Correggiari et al., 2011). In the northern Adriatic Sea, transgressive deposits are generally associated to a barrier-lagoon system, that is typically characterized by clayey-silty lagoon deposits associated with sandy beach deposits (Fabbri et al., 2001) (Fig. 4.3).

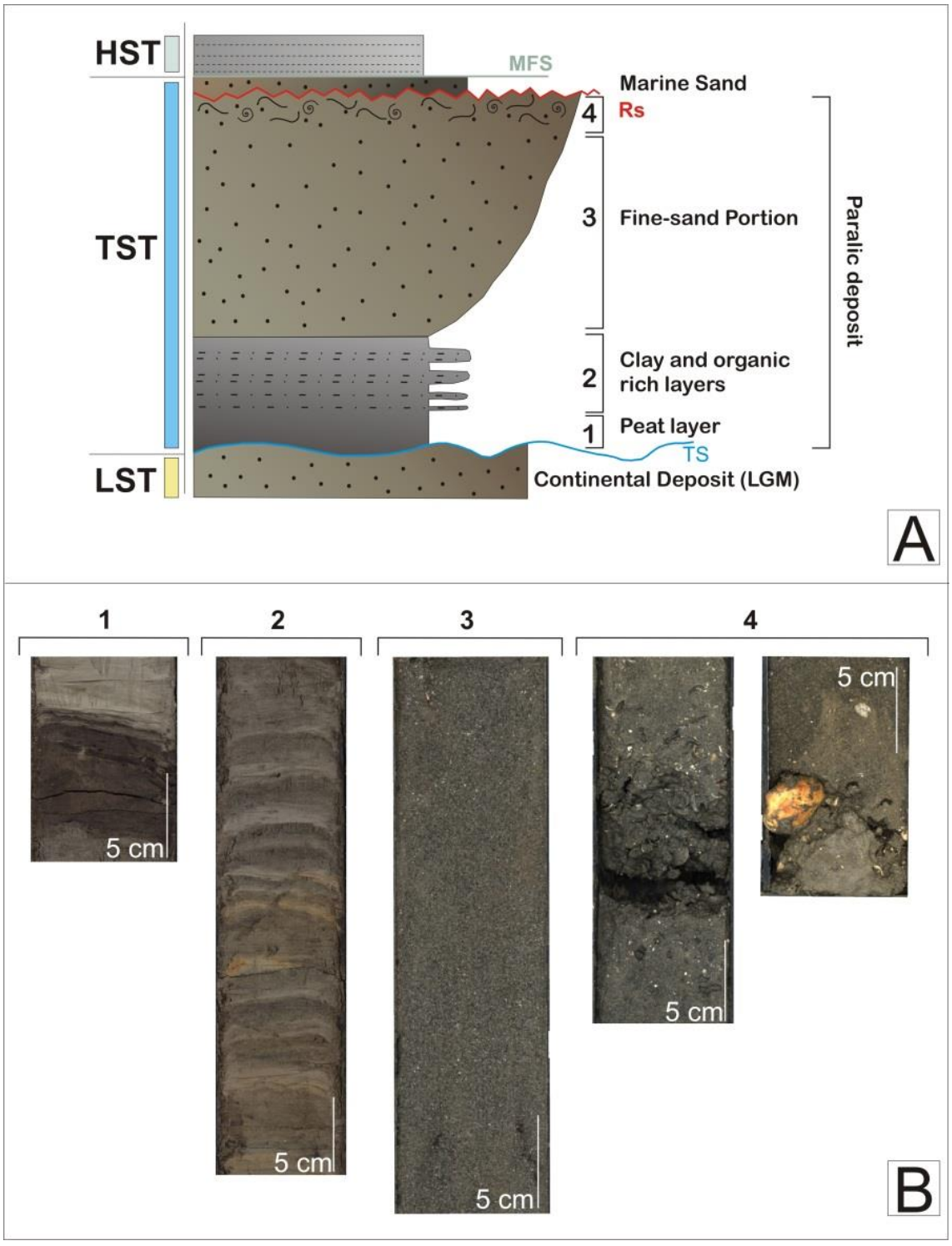

Fig. 4.3: Main cores facies description. (A) Simplified log of most representative cores. The TST deposits rest on the Transgressive Surface. The paralic deposit is characterized at the base by clay sediment, peat and organic-rich layers and at the top by a sand portion. This deposit ends with ravinement surface. (B) Example of cores facies. 1: Peat layer; 2: Interbedded clayey and silty layers; 3: Sand portion; 4: ravinement surface (Rs).

4.2.4 Methods

The transgressive deposit has been examined with a multi-disciplinary approach through very high resolution (VHR) seismic profile analysis and vibrocorer samples, digital elevation model (DEM) of most significant surfaces and 14C dating. All the analysed data have been collected during oceanographic cruises carried out in the last 20 years by CNR-ISMAR onboard Urania R/V. VHR seismic profiles have been acquired with Sub Bottom Profiler CHIRP-Sonar with 16 low-frequency transducers. About 750 km of VHR seismic profiles, oriented NS and spaced 120 meters each other, covered the transgressive deposit (Fig. 4.4A). The seismic profiles have been processed and interpreted with SeisPrho (Gasperini & Stanghellini, 2009).

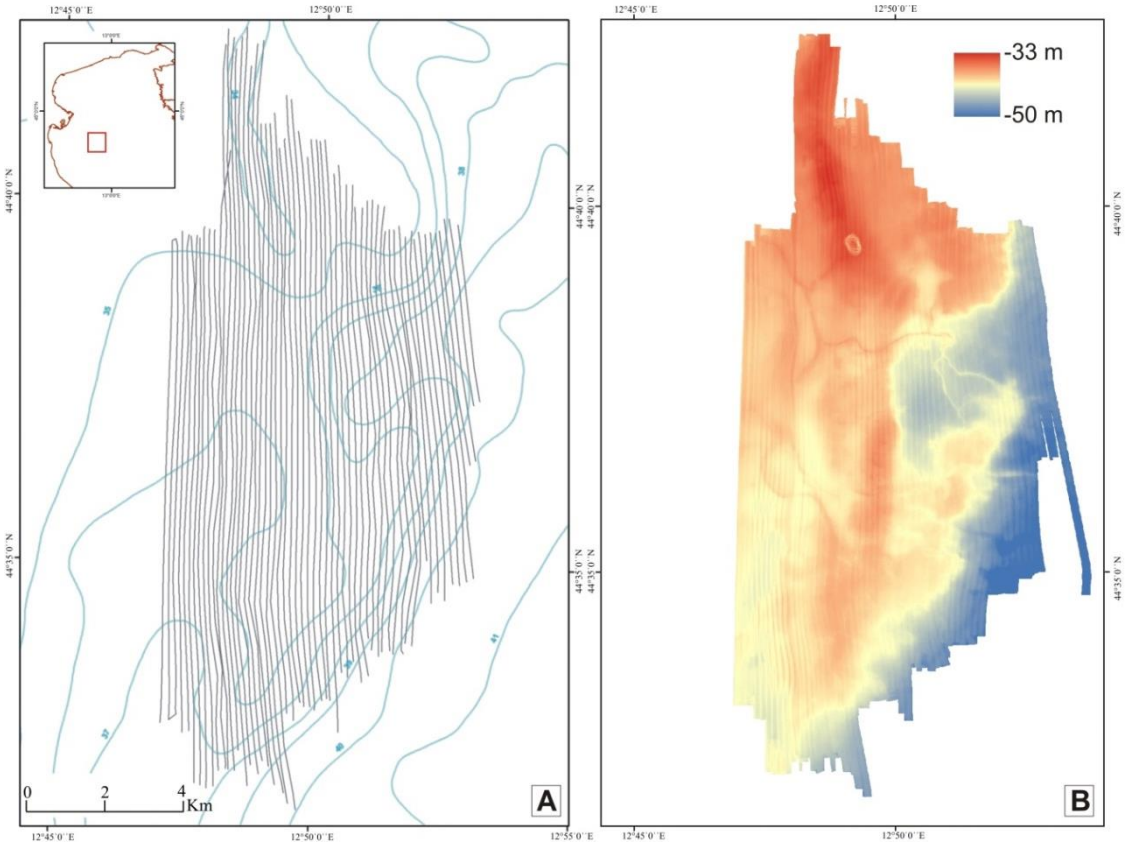

Fig. 4.4: Study Area detail. (A) Tracks of VHR seismic profiles, acquired in 2012, covering the study area. (B) Seafloor bathymetry (image resolution of 10 m). Evidence of the ESE channel system trend.

Cores have been collected by Vibrocorer Rossfelder P5, with a vibrating head and a steel corer 6-m long and 10-cm wide. DEMs of key seismic surfaces, obtained from Conversion Tools ASCII to Raster of ArcMap 10.1 software, have been used to map their areal distribution. Furthermore the top of the transgressive deposit, coinciding with the seafloor, has been analysed with the

Digital Elevation Model of the multibeam bathymetry (with image resolution of 10 m) acquired during the NAD12 (in 2012) oceanographic cruise onboard Urania R/V (Fig. 4.4B). The device used is an EM 710 Multibeam echosounder with 70-100 kHz. The geochronological constrains of the geological evolution have been provided by the ^{14}C dating of 3 samples of organic-rich and peat layers, in the core AR00_22. The AMS analysis has been done at the Ion Beam Laboratory at the ETH Institute in Zurich. Our data have been integrated with those from core CM94_107 (Fabbri et al., 2001). The radiocarbon ages from AR00_22 and CM94_107 cores have been calibrated using CALIB14 Radiocarbon Calibration Program of Stuiver and Reimer (1993). The results have been corrected for isotopic fractionation, but no correction for oceanic reservoir was made because the dated layers are of terrestrial origin.

4.2.5 Results

4.2.5.1 Seismic analysis

The seismic profiles analysed, were collected during the oceanographic cruises NAD12. The detailed seismic-stratigraphic analysis highlighted three different seismic facies: 1) a semi-transparent unit, due to scarce penetration of the acoustic signal, indicative of sandy sediments, characterized by an irregular, erosive base; 2) an interbedded transparent seismic facies with parallel and subparallel irregular and discontinuous reflectors related to fine-grain deposits with thin fine sand or silty layers; 3) regular and continuous reflectors interpreted as peat and organic-rich layers. In each profile five key surfaces have been identified and traced in order to define the geometry of deposits and to investigate the formation and evolution of the transgressive parasequences. The key surfaces, easily visible and traceable along the entire profile, correspond to organic rich and peat layers. The seismic reflector interpreted as transgressive surface marks a different response in the seismic profile and has been traced correlating the dated peat layers from published data (Fabbri et al., 2001; Correggiari et al., 2011). The TS is an erosional surfaces that marks the first major flood of the margin. It rests on the low-stand deposit formed during the LGM where the top was dated at 20,000-21,000 ^{14}C a BP by radiocarbon

dating of peat samples southern than the investigated deposit by Trincardi et al. (1994); Fabbri et al. (2001); Cattaneo and Steel, (2003).

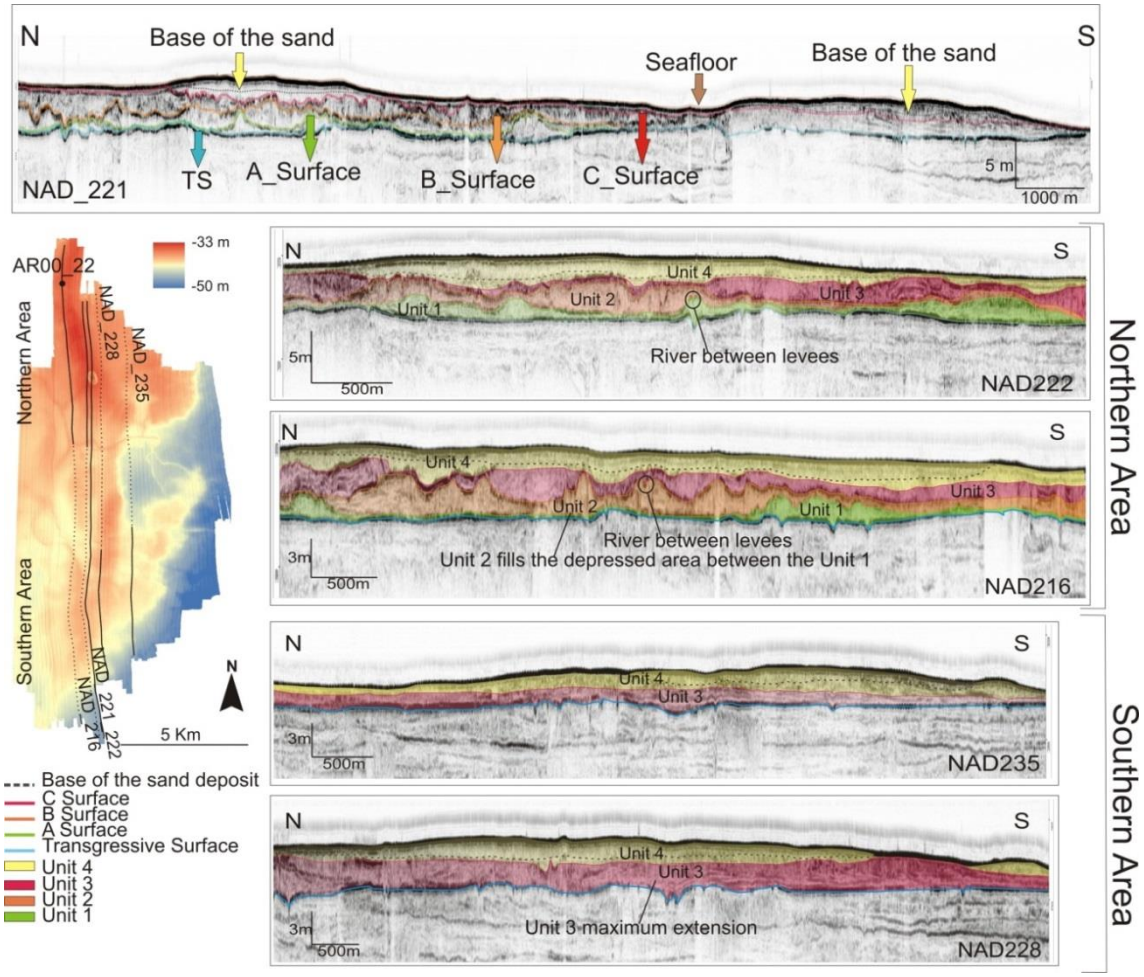

Fig. 4.5: Evidence of the key surfaces and units within the sedimentary transgressive body.

The studied transgressive body rests on the TS. In addition to the TS other three key reflectors have been identified within the transgressive deposit (A surface, B surface, C surface and Seafloor surface at the top, Fig. 4.5); these surfaces border four different units (from Unit 1 at the base, to Unit 4 at the top) that mark four different depositional environments during the sedimentation of the transgressive deposit (Fig. 4.5). Moreover within the most recent unit an additional key surface has been identified at the base of the sandy portion. The Unit 1, 2 and 3 were delimited by the digitized key surfaces, corresponding to peat layers, and were characterized by interbedded transparent and discontinuous seismic reflectors, which were more regular within the unit 3. At the top of both the Unit 1 and the Unit 2 seismic profiles revealed the presence

of some channels bordered by levees. The Unit 4, was delimitated at the base by the C key surface and at the top by the seafloor. Additional key surface within Unit 4 divided the base with irregular and discontinuous seismic reflectors and at the top a semi-transparent seismic facies indicative of sandy sediments.

4.2.5.2 Digital elevation models of key surfaces

The digital elevation models showed the morphology of the surfaces highlighting the occurrence of the channel system network existing when each of them was exposed and active (Fig. 4.6). Thus, each DEM represents one step in the formation of the transgressive deposit. The TS lies higher to the west and lower towards east, characterized by channels with ENE direction (Fig. 4.6A). At first, the sedimentation over the TS occurred in the north/northeast and western areas and shows an ENE channel progradation. This situation was highlighted by the DEM of the A surface (top of the Unit 1) and the DEM of the B surface (top of the Unit 2) (Fig. 4.6B/C), and then the sedimentation of the transgressive body shifted to the south/southwest. The DEM of the C surface (top of the Unit 3) highlighted the filling of the southern area together with the variation of the channel direction from ENE to ESE (Fig. 4.6D). The transgressive body ended at the top with Unit 4, that correspond to the basal clay lagoon layer resting on the C surface, filling and flattening the transgressive body. The seafloor bathymetry (Fig. 4.4B), that coincides with the top of the Unit 4, maintained the same ESE channel trend as highlighted for Unit 3.

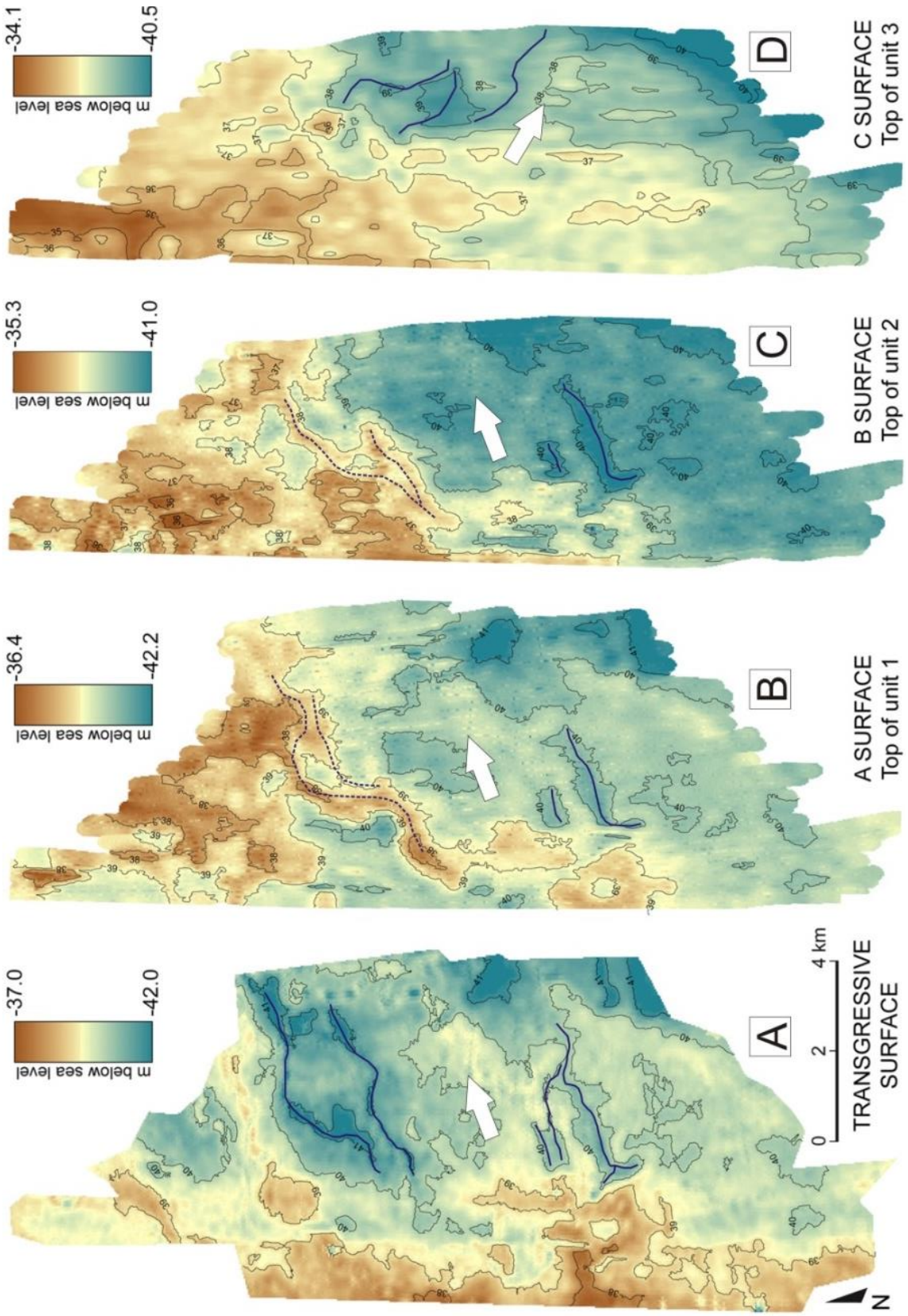

Fig. 4.6: DEMs with isopach of the key surfaces obtained from Conversion Tools ASCII to Raster of ArcMap 10.1 program. Comparison of DEM. Variation in channel system trend and preservation of each unit. The channels depicted in each surface have been traced in blue, while the dashed rivers represent the leveed channel systems elevated above the underlying surface.

4.2.5.3 Cores facies analysis and calibration of seismic units

30 cores collected during the oceanographic cruises CM94 and AR00 (in 1994 and 2000) onboard Urania R/V (CNR-ISMAR) have been described to define the depositional environment corresponding to the sedimentation of the transgressive body. The cores had a length spanning between 1.5-4 m and generally showed coarsening-upward trend with a thin fining-upward layer at the top. The basal portion was formed by clay with some peat layers. This unit was overlain by fine-sand that was capped by an erosional surface. The TST deposit was covered with thin layer (about 15-30 cm) of silty-clay representing a recent distal Po prodelta high-stand deposit (Correggiari et al., 2005; Correggiari et al., 2011) (Fig. 4.3). The Unit 1 rests on the transgressive surface and is capped by the A surface (Fig. 4.5), it was found only in the northern part of the investigated area and it is organized in elongated river systems that are elevated above the TS and oriented towards ENE. These systems lie on the ancient fluvial system highlighted by the TS, and in the seismic profiles it was possible to recognise some leveed channel systems. The Unit 1 was mainly formed by clay with organic matter and millimetric plant debris interbedded with peat layers (Fig. 4.7), farther few cores highlighted a fine-sand to silty layer at the top of this unit. The fossil content belonging to this unit was characterized by the mollusc association consisting of *Cerastoderma glaucum*, *Abra segmentum* and *Lentidium*. The Unit 2 was bounded at the base by the A surface and at the top by the B surface (Fig. 4.5), it was mainly present in the northern and western part of the investigated area and it filled the depressed zones formed between the Unit 1 channel systems. This unit was similar to the Unit 1, characterized by clay with organic matters and carbonaceous frustules, while the top was an easily recognizable layer of peat with a thickness of 10-15 cm (Fig. 4.7). The fossil content was the same as of the Unit 1. The Unit 3 was bounded at the base by the B surface if present or by the TS surface where it was not present and at the top by the C surface (Fig. 4.5). Unit 3 was mostly developed in the southern part of the area, while in the northern sector was limited to a thin layer below the Unit 4. The southern portion of the Unit 3 was characterized by 2-2.5 meters of clay layers with millimetric plant debris interbedded with parallel-laminated silty layers (Fig. 4.7). The northern portion of the Unit 3 was formed of a thin layer of clay that filled and smoothed the underlying depressed areas.

The paleontological association was characterized by *Cerastoderma glaucum*, *Abra segmentum* and *Lentidium sp*. The Unit 4 was bounded at the base by the C surface and at the top by the seafloor (Fig. 4.5), its geometry showing two convex landforms with a gentle trough in the middle of the deposit. In this unit a significant amount of sorted sand has been found within the two build ups above a thin clayey layer. The sand portion, that reached up to 1.5 m of thickness, ended with a bioclastic sand layer representing the ravinement surface (Rs) (Fig. 4.7). The analysis on the sand below the Rs showed a mean diameter between 0.25-0.35 mm and a very scarce content of silt and clay (Correggiari et al., 2011). The top of the deposit is locally characterized by a very thin 15-30 cm layer of clay.

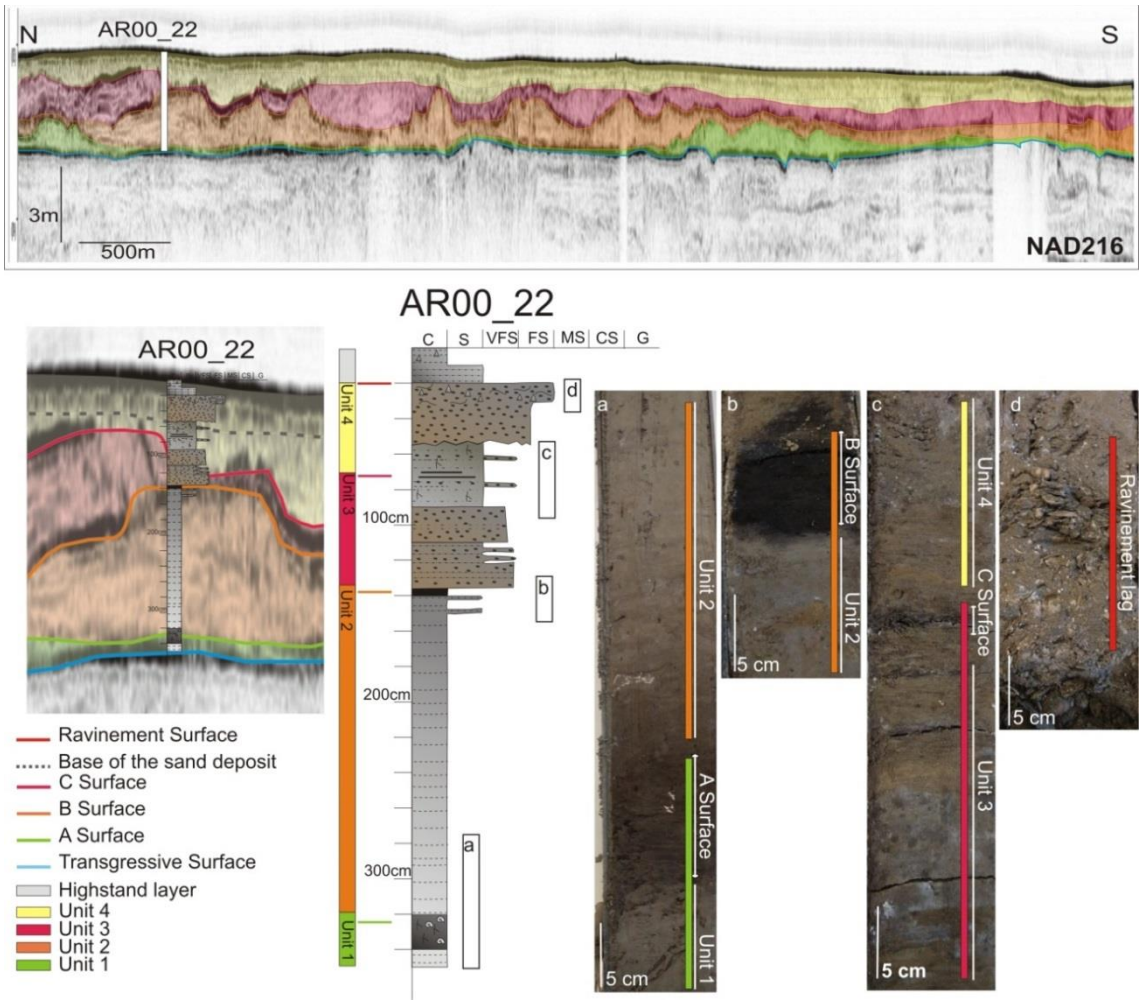

Fig. 4.7: AR00_22 core log plotted on NAD216 seismic profile, location in Fig. 4.5 . On the left, the picture shows the position of AR00_22 in the seismic profile, the seismic units in color bordered by the key surfaces. On the right, the picture shows the description of the AR00_22 core, their core facies, highlighted by the photos, corresponding to the white panels a, b, c, d close to the core log.

4.2.6 Discussion

The combined seismic and core analyses allow us to reconstruct the evolution of the transgressive deposit. The four units, forming the transgressive body, show different environment of sedimentation. The basal units (Unit 1, Unit 2 and Unit 3), consisting of silty-clay sediment with organic matter and interbedded peat layers, are indicative of lower delta plain environments with distributary channels and lagoon. The paleontological content, recognized in clay layers belonging to Unit1, 2 and 3, is indicative of euryhaline association of bivalves peculiar of transitional environment from fresh to brackish water. The more recent unit (Unit 4) consists of basal thin layer of clays formed in a lagoon environment, covered by two plano-convex bodies of basal beach sand. This unit represents a patch of barrier-lagoon system capped by the ravinement surface formed by bioclastic sand. The combined study of seismic profiles and cores emphasizes a marked difference between the basal and the superficial portion of the deposit in terms of sedimentary environment and preservation potential. The buried units, belonging to an inner coastal environment compared to the Unit 4, indicate back-barrier environment. The analysis of the seismic profiles highlighted a local aggradation of the Unit 1, 2 and 3 that filled the morphological depressions inherited from of the previous topography. On the contrary, Unit 4, which was strongly affected by marine processes, was characterized by erosion and reworked sediment, as highlighted by the ravinement surface. The comparison among DEMs of the surfaces confirmed limited erosion in Units 1, 2 and 3, while marked reworking occurred at the top of Unit 4. The buried units were characterized by erosion due to the activity of washover fans or fluvial floods, while Unit 4 was subjected to shallow marine processes such as wave activity. Moreover, the seafloor DEM, which shows the present bathymetry, highlights that the path of channels is in relief. This setting suggests differential erosion within Unit 4 with the removal of softer or less stiff sediment.

The radiocarbon data constrains the time of sedimentation of the transgressive deposit between 11,000 to 9800 cal. a BP, in the time interval following the Melt Waters Pulse 1B (Fairbanks, 1989). This was characterized by both the strong influx of freshwater and the increased sediment loads by rivers, especially the Po (Ariztegui et al., 2000). The dating samples (Tab. 2)

gave information about the rate of sedimentation in each unit. The Unit 1 (thickness up to 1 meter) was deposited in about 500 years, the Unit 2 (thickness up to 2 meters) in about 300-500 years, while the Unit 3 (thickness up to 1 meters) was deposited in about 200 years.

Sample	Core	Latitude WGS84	Longitudine WGS84	Seafloor bathymetry (m asl)	Depth from seafloor (m)	Corrected Depth (m asl)	Lab. Code	Method
AR00_22 67-68 cm	AR00_22	44°41.5003	12°48.2207	34,2	0,67	34,9	ETH-57129	AMS
AR00_22 135-136 cm	AR00_22	44°41.5003	12°48.2207	34,2	1,35	35,7	ETH-57130	AMS
CM94_107 311-321 cm	CM94_107	44°39,0322	13°42,6896	34,9	3,11	37,9	-	AMS
AR00_22 338-339 cm	AR00_22	44°41.5003	12°48.2207	34,2	3,38	37,7	ETH-57131	AMS
CM94_107 363-365 cm	CM94_107	44°39.0322	13°42.6896	34,9	3,63	38,6	-	AMS

Sample	Material	Conventional radiocarbon age	Error (years, ±)	Calibrated age 2σ 95.2% prob. (a cal. BP)	Error	Calibrated medium age 2 sigma (a BP)	δ13C‰ PDB
AR00_22 67-68 cm	Macrofossils	8828	32	9730-9960 cal. A BP	115	9845	-27,3
AR00_22 135-136 cm	Macrofossils	8869	23	9895-10160 cal. A BP	132,5	10027,5	-25,9
CM94_107 311-321 cm	Peat	9110	60	10180-10430 cal. A BP	125	10305	-
AR00_22 338-339 cm	Macrofossils	9307	23	10480-10580 cal. A BP	50	10530	-28,3
CM94_107 363-365 cm	Peat	9600	70	10730-11180 cal. A BP	225	10955	-

Tab.2 : AMS and calibrated dating from CM94_107 (Fabbri et al. 2001) and AR00_22 cores.

The obtained data were plotted in a Depth vs. Age plot which groups Adriatic ^{14}C age data from Fabbri et al. (2001), Antonioli et al. (2009) and Trincardi et al. (2011a-b) (Fig. 4.8). The new data coincide with the published curves showing in particular 1110 years gap between the base of the Unit 1 and the C Surface. Considering an average thickness of about 4 meters, the estimated, relative sea-level rise was about 0.4 cm/a. Moreover the detailed study of this transgressive deposit showed that the variation of the channel system trend from ENE to ESE, coincides with the incipient sea-level rise.

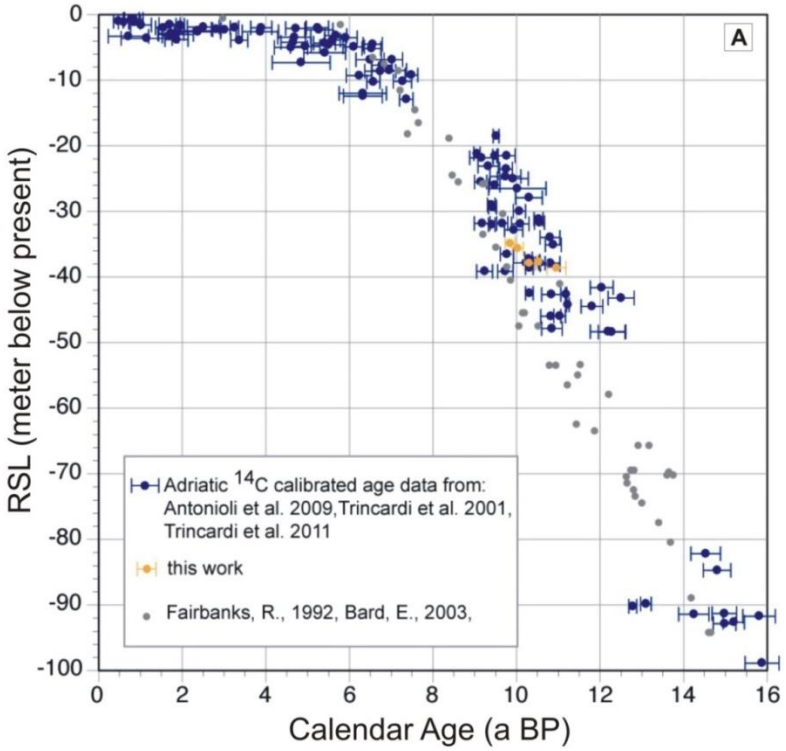

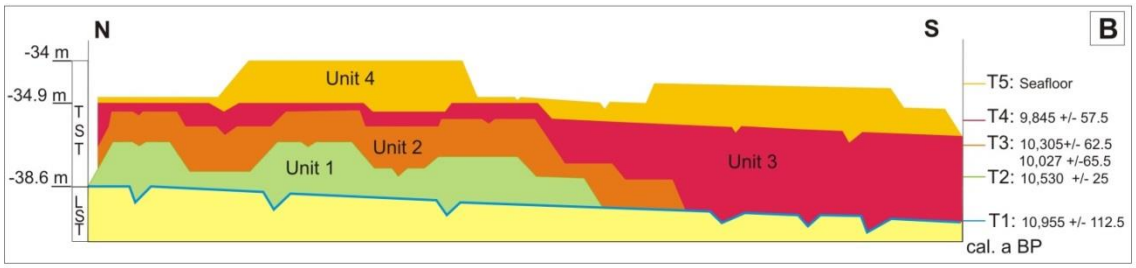

Fig. 4.8: Depth vs. Age Plot. In blue are represented the Adriatic 14C data from composite table in Antonioli et al. (2009) and from Geological Map of the Italian Sea (Fabbri et al., 2001; Trincardi et al., 2011 a-b). In orange are represented the Radiocarbon dating from this work. In grey are represented Th/U data from Fairbanks (1992) and Bard (2003). B: Simplified scheme of the transgressive deposit with water depth and age of each unit.

4.2.7 Conclusions

The VHR seismic profiles, acquired in the northern Adriatic shelf during the NAD12 oceanographic cruise, supported key information to characterize in detail the transgressive deposit located offshore Ravenna at depth of 34-35 m. The combined study of VHR seismic data and cores gave new information about the sedimentation, evolution and age of the deposit.

- ✓ The transgressive deposit consists of four units, each one of them representing an evolutionary step. The lower units (Unit 1, Unit 2 and Unit 3) correspond to delta plain setting with some distributary channels and a lagoon, while the upper unit (Unit 4) represents a barrier-lagoon system with patches of ancient beach at the top.
- ✓ The sedimentation of the transgressive deposit occurred between 11,000 to 9800 cal. a BP. In particular the radiocarbon data allowed to estimate the rate of relative sea-level rise and sedimentation rate of each unit. Moreover, the dated layers correspond to peat or organic-rich horizons of brackish lagoon facies, thus, they are representative of the paleo sea-level and mark the aggradation steps of each unit.
- ✓ The variation of the channel system trend from ENE to ESE occurred during the sea-level rise and it brought to the change of the coastal paleogeography. At the beginning the coast was growing eastward, then the basin flooding (recorded by the Unit 3 at 35 m water depth) caused a preliminary drowning of the investigated area and a consequent variation of the channel system trend. The detailed study of this transgressive body shows not only its evolution but also the paleogeography variation of the surrounding areas due to both sea-level rise and the fluvial pattern.

CHAPTER 5

SEDIMENT PROVENANCE IN SOME HOLOCENE TRANSGRESSIVE DEPOSITS IN THE NORTHERN ADRIATIC SEA

5.1 Overview

This chapter is a journal paper almost ready to be submitted to Journal of Sedimentary Research. In this chapter, some transgressive deposits, sedimented in the northern Adriatic Sea, are characterized with petrographic analysis in order to delineate their composition and to propose a preliminary reconstruction of the paleogeography of the northern Adriatic shelf during the last relative sea-level rise.

5.2 Paper

GIORGIA MOSCON[1], CRISTINA STEFANI[1], ALESSANDRO FONTANA[1], ANNAMARIA CORREGGIARI[2], ALESSANDRO REMIA[2]

[1]*Dipartimento di Geoscienze, Università degli Studi di Padova, Via G. Gradenigo 6, 35131 Padova, Italy*

[2]*Istituto di Scienze Marine - CNR, Via Gobetti 101, 40129 Bologna, Italy*

5.2.1 Abstract

The low gradient Northern Adriatic shelf recorded different generation of partially preserved transgressive barrier-lagoon systems, sedimented and drowned in-place during the last relative sea-level rise. These transgressive deposits are isolated and elongated high grounds on the Northern Adriatic seafloor showing a dominant longshore trend similar to the modern high-stand deposits. In particular, they lay on an erosive surface of regional extent (transgressive surface) that truncates older low-stand deposits and are below a ravinement surface, often coinciding with the maximum flooding surface. Furthermore, they generally are formed by a basal portion of silt-clayey layers interbedded with peat and organic-rich layers and a top portion of fine-grained sorted sands. The identification and characterization of these deposits has been

carried out analysing a large dataset of Very High Resolution (VHR) seismic profiles, cores, bathymetric and isopach maps; moreover the sand portion of these transgressive deposit has been and is still object of detailed studies, because it is a significant resource for beach nourishment.

The sand portion of eight distinct bodies, located offshore between -35 and -10 m msl, was studied with petrographic analysis in order to delineate their composition. Three different petrofacies (Petrofacies I, II, III), characterized by distinct terrigenous supplies were recognized, linked to different phases of sea-level rise. In particular, the petrographic analysis allowed to support a potential northward shifting of a branch of the paleo Po River during the deposition of the transgressive deposits belonging to the Petrofacies I; moreover, the transgressive deposits belonging to the Petrofacies II were interpreted as ancient coastline emphasized by mixed composition of several supplies, reworked by marine currents. Besides, petrographic data regarding the transgressive deposit belonging to the Petrofacies III , previously interpreted by other authors as an ancient Tagliamento River delta, highlights and confirms a Tagliamento River supply. The petrographic results permit a preliminary paleogeography reconstruction of the northern Adriatic shelf during the last relative sea-level rise. Furthermore, our petrographic results can be useful to support sand exploitations in order to identify correlation between the sand portion of the deposits and the sand belonging to the present coastline.

Keywords: Transgressive deposits, northern Adriatic sea, sea-level rise, petrographic analysis, sand sediments.

5.2.2 Introduction

In the Mediterranean basin, the continental shelf has a large extent only in a few selected areas (northern Adriatic Sea in Italy; Gulf of Gabes in Northern Tunisian coast; Fig.5.1). During the post-LGM transgression, these areas were characterized by huge drownings associated to slight sea-level rise. This process, due to the low gradient of the shelf, caused the formation of different generation of barrier-island systems, subsequently drowned in-place and partly preserved. Thus, the north Adriatic is one of the few setting in the Mediterranean Sea characterized by late-glacial and holocenic transgressive bodies. In particular, these deposits are interpreted as patches of ancient coastal wedges and document different phases of relative sea-level rise. Up to now, these offshore transgressive deposits have been studied in detail with grain-size analysis, sedimentary architecture and volumes calculation because their sand portion is a potential resource for coastal nourishment (Correggiari et al., 2011), but no evaluation on their sand composition has never carried out. In this work we consider the transgressive deposits located in the northern Adriatic shelf between -10 to -35 m msl, and focus on their transgressive sand portion. In particular, we have studied their composition and provenance variations in order to delineate a preliminary framework of the paleogeography and the paleo drainage pathways using a large dataset of vibrocores, Very High Resolution CHIRP sonar seismic profiles and bathymetric maps acquired in the last ten years by CNR-ISMAR (Bologna Section).

Fig. 5.1: Mediterranean extent of the continental shelf exposed at the maximum sea-level regression (from: http://antiquity.ac.uk/projgall/sakellariou334/).

5.2.3 Geological setting

The north-western sector of the Adriatic Sea represents the Cenozoic to Quaternary sedimentary infilling of the subsiding foreland basin related to the opposing thrust belt chains of the Southern Alps and the Northern Apennines (Doglioni 1993). In the Pliocene and early Holocene the Po Plain corresponded to the Apennine foredeep (Scrocca et al., 2007), characterized by deep marine sedimentation. Since middle Pleistocene the fluvial systems fed by the southern Alps experienced a strong progradation, largely supported by the erosive action played by the glacial in the mountain valleys (Muttoni et al., 2003). The Quaternary evolution of the Venetian-Friulian Plain, which is the eastern boundary of the Po Plain, is strongly related to the response of alluvial systems to climate and sea-level changes (Fontana et al., 2010; 2014). In particular, during the Last Glacial Maximum (LGM, 29,000-19,000 yr cal. BP; Lambeck and Purcell, 2005; Clark et al., 2009) the Northern Adriatic shelf has been exposed under continental conditions and the alluvial plain enlarged over 300 km south of the present Venetian coast (Correggiari et al., 1996a; Fontana et al., 2008). In this context, it is generally accepted that the alluvial plain was characterized by a river network which converged in a “Mega Po” trunk river (Storm et al., 2008). This fluvial system terminated in a low-stand delta located at the northern edge of the Meso-Adriatic Depression (MAD) (Trincardi and Correggiari, 2000; Ridente and Trincardi, 2006; Maselli et al., 2011). At the same time landwards, the glaciers hosted in the main south-eastern Alpine valleys debouched into the plain leading to the formation of huge terminal moraines in the piedmont belt (Castiglioni 2004). The Alpine glaciers fed with their water and sediment discharge the glacio-fluvial systems of Isonzo, Tagliamento, Piave, Brenta and Adige leading to the formation of alluvial megafans (Fontana et al. 2008; Fig. 5.2). These large depositional features are characterized by a proximal sector, consisting of gravels and sandy gravels, and a fine-dominated distal sector (Fontana et al., 2008). Megafans extended onto the North Adriatic shelf with their distal sector, that can be recognized up to 15-20 km from the present coast between Venice Lagoon and Friuli, while downstream of this belt a homogeneous alluvial plain can be described (Fontana et al., 2014). The stratigraphy of the LGM deposits is dominated by silt and clay with isolated bodies of fine-to-medium sand with a thickness of 1-2 m

and rather common presence of layers of peat. These have a centimetric to decimentric thickness and correspond to fen environments that developed in some sectors of the distal floodplain (Miola et al., 2006).

At the climatic transition between LGM and Late-glacial a dramatic decrease in the sedimentary supply occurred and a strong phase of incision affected all the megafans in the Venetian–Friulian Plain (Fontana et al. 2008). The Alpine rivers entrenched respect the LGM megafan surface and, thus, fluvial activity was confined along incised river valleys, through which the sediments passed and deposited on the Adriatic shelf (Fontana at al., 2014). This resulted in a sedimentary hiatus marked by an overconsolidated calcic horizon, locally called caranto paleosoil (Gatto and Previatello, 1974; Tosi, 1994; Mozzi et al. 2003; Fontana et al., 2014).

Since the end of LGM the melting of Arctic and Antartic ice sheets prompted the marine transgression (Bard et al., 1996; Lambeck et al., 2014). The sea-level rise took place over the alluvial plain formed during the low-stand, characterized by a gentle topographic gradient. This setting favoured the deposition and the subsequent drowning of different generations of transgressive barrier-lagoon systems (Fig. 5.2, Trincardi et al., 1994; Correggiari et al., 1996 a; Cattaneo at al., 2003).

Since about 7 kyr cal BP, the Adriatic coast was located in a position comparable to present (Lambeck et al., 2004; Amorosi et al., 2008), and was subjected to the formation of several deltas and lagoons which built a coastal wedge onlapping on the LGM plain.

The post-LGM transgressive sediments present in the Adriatic Sea were deposited while the coastline shifted about 250 km northwards since the last relative sea-level rising (Trincardi et al., 1994). They are characterized by backstepping barrier-lagoon and incised valley systems in the low gradient northern shelf, while mud sedimentary bodies thicker than 25 m are present in the central Adriatic shelf (Cattaneo and Trincardi, 1999; Maselli et al., 2011). In the axial portion of Adriatic shelf, these deposits are preserved in a narrow area between -100 m to -10 m msl, and they consist of a lower wedge composed of a paralic portion and an upper wedge of marine deposits, separated by a ravinement surface and bordered at the base by the transgressive surface (Fig. 5.3, Trincardi et al., 1994). They are preserved as elongated reliefs almost

parallel to the present Adriatic coastline and are generally a few meters thick and mainly formed of sorted sand. Moreover, ^{14}C dating from peat layers belonging to the lower paralic portion permit to refer their sedimentation between 9500 to 7000 yr cal. BP time interval (Correggiari et al., 1996a, b; Trincardi et al., 2011; Moscon et al., 2015).

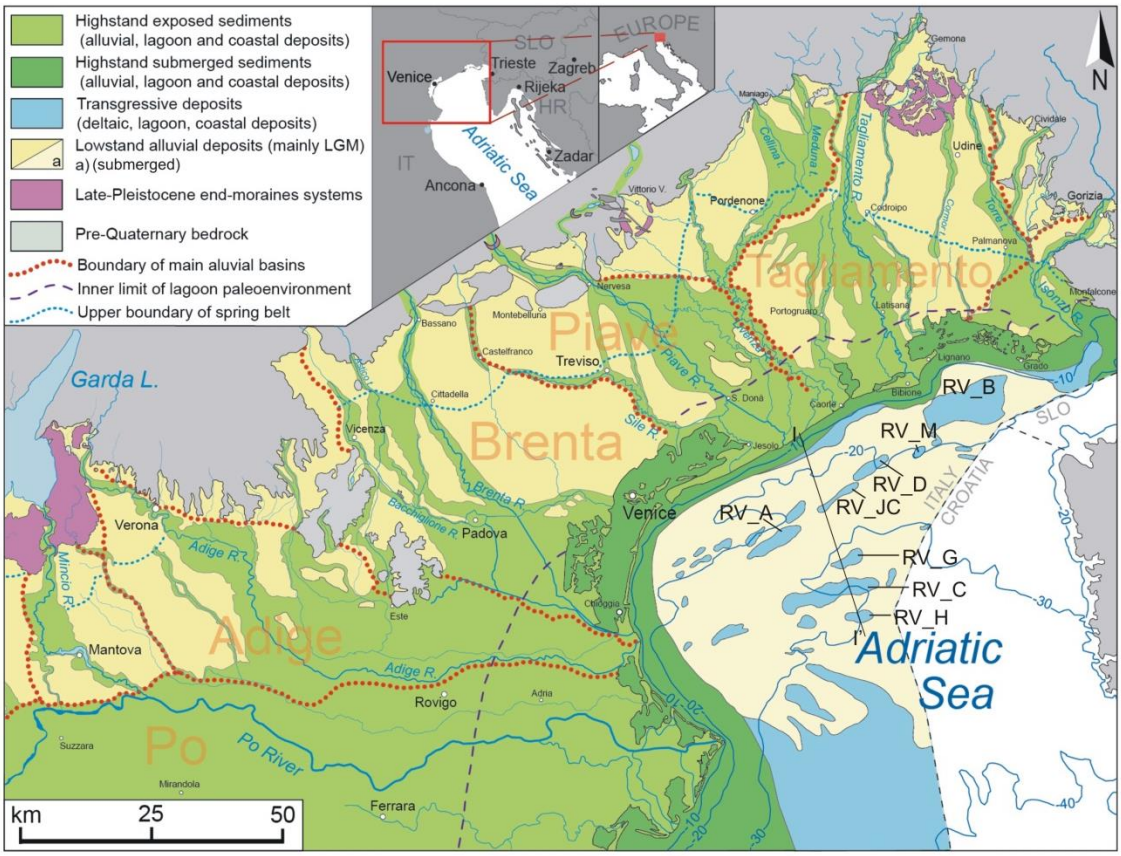

Fig. 5.2: Late Quaternary depositional system of the Venetian-Friulian Plain and the Northern Adriatic shelf. In blue, isolated transgressive deposits examined in this work.

5.2.4 Methods

The transgressive deposits chosen for this study were selected from the Geological Map of the Italian Seafloor (Fabbri et al., 2001; Trincardi et al., 2011a). From SW to NE they are RV_H, RV_C, RV_G, RV_A, RV_JC, RV_D, RV_M, RV_B (Fig. 5.2). We are processing precise radiocarbon data per deposits, then we took as reference the sea-level curve from Correggiari et al. (1996a) and Lambeck, (2004), where they fall from 9500 to 7000 yr cal. BP in respect to their water depth. A large dataset of CHIRP-sonar profiles, gravity cores and vibro-corers, bathymetric and isopach maps of the Late Pleistocene-Holocene deposit on the Adriatic shelf collected and conceded by CNR-ISMAR

(Bologna-Section), allowed to characterized these deposits with a multi-disciplinary approach. At first, these bodies were analysed with Very High Resolution (VHR) seismic profiles in order to highlight their sedimentary architectures focussing on their sand portion. The seismic profiles were acquired with a CHIRP Sonar profiler with 16 transducer and low frequency (2-7 kHz). This instrument, through an emission of a modulate acoustic pulse, returns an image of acoustic impedance structure, that investigates only the first few meters of the substrate allowing high resolution comparable to a sediment core length. Moreover a detailed description of 140 cores collected in the last years was carried out during oceanographic cruises (R/V Urania, CNR-ISMAR), and high number of samples belonging to the transgressive paralic sand portion have been selected for compositional analysis. The sandy fraction selected for petrographic analysis has been split and impregnated in an epoxy resin according to the methodology described by Gazzi et al. (1973), in order to obtain thin sections. All thin sections were stained with alizarine-red solution to facilitate the distinction of calcite and dolomite during the modal analyses. Sand point counts were performed following the Gazzi–Dickinson technique (Gazzi, 1966; Dickinson, 1970; Ingersoll et al., 1984), modified by Zuffa (1987), with the aim of minimizing the influence of grain size on composition. This point-counting method consists of separating coarse-grained lithic fragments (single crystal within grains >0.0625 mm) from fine grained lithic fragments (single crystal within grains <0.0625 mm). Due to the lack of interstitial components, 300 points were determined for each thin section using a 0.5 mm grid spacing. Secondly, in order to obtain more information about source areas the point-counting was continued for a selected number of samples per deposit until at least 200 rock fragments were determined. The data are reported in Tab.3 and 4. In addition, assuming a similar source area to the present and no significant changes regarding the provenance due to diagenetic processes or important geological changes in source areas, our data were compared to those from recent literature of present-day rivers (Gazzi et al., 1973; Marchesini et al., 2000; Monegato et al., 2010), in order to highlight the signature of the different sand bodies. Beside, in order to distinguish different inputs relative to distinct fluvial supplies the linear mixing model was tested, according to the method proposed by Weltje and Prins, (2003); Garzanti et al., (2005; 2007); Vezzoli and

Garzanti, (2009). This method is useful to compare detrital signatures with end-member compositions in order to discriminate the main contributions belonging to different sand deposits. With this aim, the fluvial composition reported by Gazzi et al. (1973) was considered as an end-member for the Po River and for eastern alpine fluvial supplies. The program, written on a Microsoft Excel spreadsheet, through the regressive analysis, allows to compare the end-members with the analysed sand samples, and calculates the multiple correlation index R. The latter is closest to 1 if it corresponds to one end-member, but if samples are indicative of a mixed supply, the R index must be reconstructed as a weighted average of primary end-members (Vezzoli and Garzanti, 2009), and it is satisfactory for R values ≥0.8 (Vezzoli and Garzanti., 2009).

5.2.5 Results

5.2.5.1 Seismic facies analysis

Several VHR seismic profiles were analysed in order to evaluate the transgressive deposits extension and delineate their bases (Fig.5.3). Generally, the seismic profiles highlight semi-transparent units, characterized by low reflection amplitude and continuity, due to scarce signal penetration, indicative of sandy sediments, alternating with more continuous and high amplitude reflectors interpreted as peat and organic-rich layers.

The RV_H deposit, located at 28-32 m msl., extends about 15 km EW and 6 km NS. The VHR seismic profiles highlight two different units. On top a transparent seismic unit with no internal reflectors, indicative of sandy sediments, reaches up to 3.5 m in thickness. This unit rests on a discontinuous and irregular reflector interpreted as peat layers. The scarce penetration of the acoustic signal, due to the thicker sand body at the top, masks the underlying seismic unit. However, it is possible to recognize a 1.5 m thick basal unit which is bordered at the base by a couple of strongly discontinuous seismic reflectors (Fig. 5.3).

	Deposit	RV_C									RV_H														
	Data base sample	ADR_4	ADR_6	ADR_7	ADR_10	ADR_11	ADR_13	ADR_14	ADR_15	ADR_16	ADR_9	ADR_17	ADR_18	ADR_19	ADR_48	ADR_49	ADR_50	ADR_53	ADR_54	ADR_59	ADR_60	ADR_61	ADR_62	ADR_63	ADR_64
	Present work	1	2	3	4	5	6	7	8	9	10	11	12	13	14	15	16	17	18	19	20	21	22	23	24
	Petrofacies					I												I							
Q	Monocrystalline Quartz	40.0	30.3	28.7	37.0	23.3	31.7	33.3	41.3	43.3	28.7	38.0	42.7	36.3	32.3	40.0	39.7	32.7	33.3	44.7	34.7	37.3	32.3	48.0	40.0
	Polycrystalline Quartz	12.0	10.3	12.7	6.3	13.7	5.3	3.0	6.3	8.0	14.3	9.3	1.7	2.0	13.3	8.7	6.3	4.7	6.3	4.3	5.7	2.3	3.7	8.0	5.7
	Quartz in metamorphic rock fragments	13.0	13.0	21.7	15.0	9.3	9.7	12.3	10.0	10.0	12.3	11.3	9.0	11.0	8.7	8.0	7.3	12.0	13.0	5.7	11.0	10.7	10.0	7.3	10.0
	Quartz in acidic volcanic r. f.	1.7	3.7	4.3	3.0	5.3	3.0	4.3	2.3	4.7	2.0	4.0	1.7	2.0	2.0	0.3	1.0	1.7	2.3	2.0	3.0	0.7	1.7	0.3	1.7
	Quartz in arenites/siltstones	-	0.3	0.7	0.3	0.7	-	-	0.7	-	-	-	-	0.3	-	-	-	-	-	-	-	-	-	-	-	-
F	K-feldspar monocrystalline	0.7	5.7	1.0	1.0	4.0	11.0	7.3	8.3	6.7	4.7	3.3	4.3	4.3	10.7	13.0	12.7	12.3	11.7	6.7	7.3	13.0	11.0	3.7	7.3
	K-feldspar in granitic/gneissic r.f.	0.3	0.7	0.7	-	-	1.0	0.7	0.3	0.7	0.3	0.3	-	0.7	-	0.7	2.7	1.0	1.0	0.7	0.3	0.3	0.3	-	0.7
	K-feldspar in acidic volcanic r.f.	0.3	1.0	0.3	-	1.7	1.7	1.3	2.3	0.7	1.3	1.0	0.7	1.3	1.0	1.0	-	0.3	0.3	0.7	2.0	1.3	0.7	0.3	1.3
	Monocrystalline Plagioclase	2.3	2.7	2.0	2.7	2.3	3.0	2.7	2.3	1.0	2.0	1.3	1.3	1.0	1.7	1.3	1.7	0.7	1.7	1.0	0.7	1.0	2.0	1.0	3.0
	Plagioclase in acidic volcanic r.f.	0.3	0.3	-	-	0.7	-	-	-	-	-	0.3	-	-	1.0	-	0.3	-	0.3	0.3	-	-	-	-	-	-
L	Low-grade metamorphic r.f.	-	0.3	-	-	0.7	2.7	0.7	0.7	0.3	1.0	0.7	0.3	0.3	0.3	0.7	1.0	0.3	0.7	1.0	1.0	0.3	0.3	1.0	1.0
	Quartzose metamorphic r.f.	1.3	1.7	2.0	2.0	4.3	3.7	1.3	2.3	1.7	3.7	3.0	2.7	3.7	5.3	3.7	2.0	4.7	1.7	2.7	1.7	1.3	1.3	2.0	0.7
	Micaschist	0.7	1.0	3.7	1.3	2.3	2.0	0.3	1.0	0.7	2.0	1.0	1.0	5.0	1.3	2.3	2.0	2.0	3.0	1.0	1.7	2.3	2.3	1.0	0.3
	Schistose serpentinite	1.3	1.0	2.0	-	2.3	1.3	0.3	1.3	0.3	0.7	1.0	1.0	1.3	-	1.0	-	1.3	0.7	0.7	1.3	1.0	1.3	1.3	0.3
	Acidic volcanic r.f.	1.0	1.7	2.7	3.3	2.7	4.0	3.3	2.3	1.0	0.7	5.3	0.7	1.3	1.3	1.0	0.3	0.7	1.0	-	1.0	0.7	0.3	1.7	0.7
	Intermediate volcanic r.f.	-	1.0	1.0	0.3	1.0	1.0	0.7	0.7	0.7	0.3	0.3	0.7	0.7	0.7	2.7	2.3	2.3	2.0	3.0	2.3	1.7	2.0	2.7	3.0
	Siliciclastic siltstone	0.7	2.0	1.0	2.4	2.0	-	0.7	-	0.3	1.4	1.0	0.3	0.7	3.7	-	0.7	1.3	0.3	1.3	1.3	0.3	0.3	0.7	0.7
	Chert	-	-	0.3	0.7	1.0	-	0.3	-	-	0.3	-	-	0.7	-	-	-	-	-	-	0.3	0.3	-	-	-
	Micas and chlorite	1.0	1.7	2.3	6.0	2.7	0.7	2.0	1.7	2.3	3.0	2.7	5.3	8.7	5.0	1.3	2.7	1.3	2.7	4.0	1.3	6.7	4.3	2.0	2.3
	Micas and chlorite in granitic/gneissic r.f.	0.3	1.0	1.3	0.7	-	-	-	-	-	1.7	-	-	0.3	-	-	-	-	-	-	-	-	-	-	-	-
	Micas and chlorite in volcanic r.f.	-	-	-	-	-	-	-	-	-	-	-	-	-	-	-	-	-	-	-	-	-	-	-	-	-
	Other minerals	3.3	6.3	2.0	1.7	6.7	3.0	3.7	3.7	3.7	4.0	2.3	3.7	2.0	4.0	2.3	2.0	3.3	3.7	5.3	5.3	1.3	3.3	3.3	4.0
CE	Dolostone monocrystalline grain	5.0	2.0	1.3	3.0	-	3.0	6.0	0.3	1.7	-	1.7	6.7	2.0	0.7	2.0	3.3	5.3	1.7	3.0	2.3	4.7	4.0	1.7	2.0
	Dolostone polycrystalline grain	4.0	1.0	1.7	1.7	-	4.0	4.0	2.0	1.7	-	3.7	5.7	2.3	-	5.3	6.3	5.3	1.7	1.0	3.3	3.3	3.0	2.7	1.7
	Monocrystalline calcite spar	0.7	1.0	0.3	1.0	0.3	0.3	-	1.7	3.0	1.7	2.0	1.3	3.7	-	-	-	-	1.3	2.3	0.7	0.7	0.7	1.0	1.0
	Sparitic and microsparitic limestone	2.3	3.3	4.3	4.7	7.0	5.3	9.3	5.0	4.0	6.0	3.7	6.3	3.7	4.0	0.3	-	2.0	4.0	4.7	6.3	4.3	8.7	6.3	6.3
	Mudstone - wackestone	6.3	3.7	1.3	4.0	2.7	2.0	0.7	1.0	2.7	5.0	1.7	1.7	3.3	2.3	4.0	3.3	3.3	4.0	3.7	3.7	4.0	4.3	3.0	3.7
	Bioclasts	0.7	0.7	-	1.6	0.7	0.3	1.3	1.0	0.7	-	-	0.3	0.3	0.7	0.3	2.0	1.3	1.3	-	0.3	-	0.7	0.3	2.3
	Peloids	-	0.3	-	-	-	-	-	-	-	2.0	-	-	-	-	-	-	-	-	-	-	-	-	-	-
	Green particles	-	-	-	-	-	-	-	-	-	-	-	-	-	-	-	-	-	-	-	-	-	-	-	-
	Opaque minerals	0.7	2.3	0.7	0.3	2.7	0.3	0.3	1.3	0.3	1.0	1.0	1.0	1.0	-	-	0.3	-	0.3	0.3	1.3	0.3	1.3	0.7	0.3
	Total	100.0	100.0	100.0	100.0	100.0	100.0	100.0	100.0	100.0	100.0	100.0	100.0	100.0	100.0	100.0	100.0	100.0	100.0	100.0	100.0	100.0	100.0	100.0	100.0

Tab.3 : Modal analysis (300 points determined) of sand samples belonging to transgressive deposits (northern Adriatic Sea)

Deposit	RV_G								RV_A				RV_JC					RV_D		RV_M				RV_B					
Data base sample	ADR_20	ADR_41	ADR_42	ADR_43	ADR_44	ADR_45	ADR_46	ADR_47	ADR_21	ADR_22	ADR_34	ADR_35	ADR_31	ADR_32	ADR_33	ADR_67	ADR_68	ADR_26	ADR_27	ADR_29	ADR_30	ADR_39	ADR_40	ADR_23	ADR_24	ADR_25	ADR_36	ADR_37	ADR_38
Present work label	25	26	27	28	29	30	31	32	33	34	35	36	37	38	39	40	41	42	43	44	45	46	47	48	49	50	51	52	53
Petrofacies	II								II				II					II		II				III					
Monocrystalline Quartz	26.3	19.3	21.3	31.7	28.3	25.3	29.7	34.3	16.0	16.7	14.7	16.3	22.0	18.0	16.7	13.3	16.7	19.0	28.3	27.0	30.0	23.0	32.3	4.3	12.3	17.0	5.3	6.3	10.7
Polycrystalline Quartz	4.0	5.0	5.3	2.0	2.0	4.0	8.7	4.0	4.0	3.3	3.0	4.3	4.3	6.7	6.3	3.3	6.3	3.3	1.0	3.0	1.7	3.3	1.3	1.7	2.0	-	5.0	2.7	3.0
Quartz in metamorphic rock fragments	5.0	5.3	4.7	3.3	7.3	6.0	6.0	8.0	4.0	3.7	5.0	3.3	6.0	6.3	4.0	2.7	6.0	4.7	3.3	5.0	0.7	3.0	3.7	1.0	1.0	-	1.3	-	1.7
Quartz in acidic volcanic r. f.	0.7	1.3	0.7	1.3	2.3	0.7	1.7	3.0	1.7	2.7	1.7	1.7	2.0	3.3	1.7	1.7	1.3	2.3	1.3	1.3	1.3	3.3	2.7	0.3	1.3	0.7	0.3	0.3	0.7
Quartz in arenites/siltstones	-	-	-	-	-	-	-	-	0.3	-	-	-	-	-	-	-	-	-	-	-	-	-	-	-	-	-	-	0.7	-
K-feldspar monocrystalline	4.7	11.3	9.3	5.7	5.7	7.7	5.3	12.3	3.7	4.0	3.0	4.3	5.7	2.7	3.3	5.7	8.0	1.7	5.3	4.3	5.0	2.0	3.7	-	1.7	2.3	1.3	-	0.7
K-feldspar in granitic/gneissic r.f.	-	1.0	0.7	1.0	0.3	1.0	0.3	-	-	0.3	0.3	-	0.3	0.3	-	0.7	1.0	-	-	-	-	-	-	-	-	-	-	-	-	-
K-feldspar in acidic volcanic r.f.	0.7	-	1.0	1.7	0.7	0.7	0.3	0.7	0.3	1.7	0.3	0.7	-	0.7	1.0	-	-	0.7	-	0.3	0.3	0.3	-	-	-	-	0.3	-	-
Monocrystalline Plagioclase	1.0	0.3	0.3	0.3	0.7	0.7	1.0	1.0	0.7	0.3	-	1.0	0.7	0.7	1.0	0.3	0.3	0.3	2.0	0.3	0.7	1.0	0.7	-	-	-	-	-	0.7
Plagioclase in acidic volcanic r.f.	-	0.3	-	-	-	-	0.3	-	0.3	-	0.3	0.3	-	0.3	-	-	-	-	-	0.3	-	0.3	-	-	-	-	-	-	-
Low-grade metamorphic r.f.	-	1.7	0.7	-	-	-	1.0	1.3	0.3	-	-	-	-	-	-	-	0.7	-	0.3	-	-	0.3	1.0	-	-	-	-	-	-
Quartzose metamorphic r.f.	1.7	1.3	1.0	2.7	2.7	2.0	0.7	1.7	4.7	2.7	3.0	1.3	1.7	3.7	3.0	1.7	2.3	2.7	0.7	0.7	1.7	1.0	1.7	2.3	3.3	2.7	0.7	0.3	-
Micaschist	2.0	1.3	1.0	1.3	1.3	2.3	1.3	1.3	-	1.0	0.7	1.3	2.0	1.7	-	1.0	1.7	0.7	1.3	0.7	0.7	-	2.0	-	-	-	-	-	-
Schistose serpentinite	-	-	-	0.3	-	0.7	-	-	-	-	-	-	-	-	-	-	-	-	-	-	-	0.7	-	-	-	-	-	-	0.3
Acidic volcanic r.f.	2.3	1.7	0.7	5.3	3.0	3.3	2.7	5.3	5.7	4.3	7.0	9.7	12.0	5.3	5.0	0.7	-	8.3	4.0	5.0	2.3	3.7	3.3	3.0	5.0	1.3	0.3	0.7	-
Intermediate volcanic r.f.	1.0	2.3	6.0	1.7	1.3	1.7	2.3	3.7	0.7	0.3	1.7	1.3	-	2.3	0.3	3.0	4.3	-	0.3	2.0	-	3.0	-	-	-	0.3	0.3	0.3	1.7
Siliciclastic siltstone	-	0.3	0.3	-	0.3	1.0	2.0	2.3	1.0	-	1.0	1.3	0.3	1.0	-	1.3	0.3	2.3	-	-	-	1.0	-	0.3	-	0.3	0.7	0.7	0.3
Chert	1.0	-	-	-	0.3	-	-	-	0.3	-	-	0.3	1.0	-	0.7	-	-	-	0.3	-	-	0.3	0.7	-	1.3	-	0.3	-	0.3
Micas and chlorite	1.3	3.0	2.0	0.7	0.3	1.0	1.3	4.3	0.3	-	-	-	0.7	1.0	0.3	-	1.7	0.3	-	0.3	1.0	0.7	2.3	-	-	0.3	-	-	-
Micas and chlorite in granitic/gneissic r.f.	-	-	-	-	-	-	-	-	-	-	-	-	-	-	-	-	-	-	-	-	-	-	-	-	-	-	-	-	-
Micas and chlorite in volcanic r.f.	-	-	-	-	-	-	-	-	-	-	-	-	-	-	-	-	-	-	-	-	-	-	-	-	-	-	-	-	-
Other minerals	1.0	1.3	1.3	2.3	1.0	2.3	2.3	2.3	1.0	0.3	0.3	0.3	0.3	0.3	1.0	1.3	0.7	0.7	2.0	1.3	2.0	1.3	-	-	0.7	-	-	-	-
Dolostone monocrystalline grain	15.0	11.7	15.3	11.3	10.0	12.0	2.7	3.3	7.0	11.0	3.3	7.3	7.0	6.0	6.0	8.7	8.7	11.0	18.3	11.0	18.7	9.7	12.3	15.7	12.3	34.0	3.3	4.3	6.7
Dolostone polycrystalline grain	15.3	15.3	15.0	9.3	11.7	10.3	3.7	1.0	24.0	26.3	18.0	18.0	14.3	20.3	23.7	25.0	16.3	22.0	15.0	12.3	8.3	14.7	9.3	43.0	18.3	24.7	15.7	25.0	25.7
Monocrystalline calcite spar	0.3	-	-	0.3	-	-	-	-	1.7	-	1.0	0.3	-	3.3	0.7	-	-	-	1.3	1.0	1.3	0.3	-	-	4.0	-	2.3	1.3	1.3
Sparitic and microsparitic limestone	4.3	0.3	-	9.7	7.7	5.7	6.3	6.0	5.7	0.3	9.0	8.3	-	8.3	4.7	12.0	9.3	1.3	10.7	7.3	11.3	9.0	11.3	0.3	18.0	-	40.3	40.3	33.0
Mudstone - wackestone	11.7	15.3	12.7	8.0	10.7	11.7	9.3	4.0	14.0	13.0	24.3	16.7	13.3	5.7	20.0	17.0	13.3	12.0	4.0	16.3	11.7	14.0	11.0	24.7	14.0	15.0	20.3	16.7	13.3
Bioclasts	-	-	-	-	1.7	-	10.7	-	2.0	8.0	-	1.7	6.3	2.0	0.7	-	0.3	6.3	-	-	0.7	4.0	0.7	3.3	4.7	1.3	2.0	0.3	-
Peloids	-	-	-	-	-	-	0.3	-	-	-	-	-	-	-	-	-	-	-	-	-	-	-	-	-	-	-	-	-	-
Green particles	-	-	-	-	-	-	-	-	-	-	-	-	-	-	-	-	-	0.3	-	-	-	-	-	-	-	-	-	-	-
Opaque minerals	0.7	0.3	0.7	-	0.7	-	-	-	0.7	-	2.3	-	-	-	-	0.7	0.7	-	0.3	0.3	0.7	-	-	-	-	-	-	-	-
Total	100.0	100.0	100.0	100.0	100.0	100.0	100.0	100.0	100.0	100.0	100.0	100.0	100.0	100.0	100.0	100.0	100.0	100.0	100.0	100.0	100.0	100.0	100.0	100.0	100.0	100.0	100.0	100.0	100.0

Tab.3 : Modal analysis (300 points determined) of sand samples belonging to transgressive deposits (northern Adriatic Sea)

Rock fragment type\Deposit	ADR17 H	ADR_19 H	ADR_53 H	ADR_60 H	ADR_7 C	ADR_11 C	ADR_6 C	ADR_10 C	ADR_20 G	ADR_42 G	ADR_43 G	ADR_44 G
Metamorphic	41.5	49.3	49.0	44.5	56.5	50.5	46.0	47.1	15.5	14.0	14.5	20.5
Volcanic	19.0	12.4	12.5	15.0	16.0	20.5	15.0	9.8	8.0	15.5	19.0	13.5
Sedimentary	38.5	36.8	35.5	40.0	26.0	28.5	36.0	39.7	76.5	69.5	64.5	65.5
Granitic/Gneissic	1.0	1.5	3.0	0.5	1.5	0.5	3.0	3.4	-	1.0	2.0	0.5

Rock fragment type\Deposit	ADR_21 A	ADR_22 A	ADR_34 A	ADR_35 A	ADR_31 JC	ADR_32 JC	ADR_33 JC	ADR_68 JC	ADR_26 D	ADR_27 D
Metamorphic	12.6	10.9	11.3	8.3	16.5	17.0	9.9	16.0	11.8	9.0
Volcanic	12.1	13.4	14.3	19.0	23.0	17.5	11.3	9.5	16.7	9.0
Sedimentary	75.3	75.2	73.9	72.7	59.5	65.0	78.8	73.0	71.6	82.0
Granitic/Gneissic	-	0.5	0.4	-	1.0	0.5	-	1.5	-	-

Rock fragment type\Deposit	ADR_29 M	ADR_30 M	ADR_39 M	ADR_40 M	ADR_23 B	ADR_24 B	ADR_25 B	ADR_36 B	ADR_37 B	ADR_38 B
Metamorphic	10.0	5.0	8.5	14.0	3.7	5.5	3.4	2.3	0.4	2.4
Volcanic	13.5	7.5	16.5	9.5	3.7	8.1	3.0	1.5	1.5	2.7
Sedimentary	76.5	87.5	75.0	76.5	92.6	86.4	93.7	96.1	98.2	94.9
Granitic/Gneissic	-	-	-	-	-	-	-	-	-	-

Tab.4 : Abundance of rock fragments.

The RV_C deposit located at 26-32 m msl extends about 14 km EW, 4 km NS and it is approximately 6 m thick. This deposits is characterised by different overlapping transparent units indicative of alternate sand bodies with regular and continuous reflectors representing peat or organic-rich layers. Moreover this deposit rests on the same couple of seismic reflectors that bound the RV_H deposit, respectively dated by Trincardi et al., (2011a) 27,947 and 26,926 cal. yr BP (LGM deposits; Fig. 5.3).

The RV_G deposit located at 30-31 m msl extends about 6 km EW, 3 km NS and it reaches up to 3 m in thickness. It is characterized by an acoustically transparent unit, interpreted as sand portion, bordered by a discontinuous seismic reflector at the base (Fig. 5.3).

The RV_A, RV_JC, RV_D and RV_M extend parallel to the present coastline at 20-24 m msl. The seismic profiles show the seafloor morphology consisting of ridges and troughs. The former are characterized by a transparent seismic facies interpreted as sand bodies with thickness up to 3.5 m, that rest on interbedded continuous and irregular reflectors respectively indicative of organic rich and clayey-silty layers (Fig. 5.3). These deposits are interpreted as a sand-waves system with the crests oriented NW-SE, formed during the last relative sea-level rise, as a result of reworking sediments belonging to a coastal lithosome (Correggiari et al., 1996b).These sand bodies reach up to 3 m in thickness.

The RV_B deposit located at 11-16 m msl extends about 18 km WE and 13 km NS. The seismic profiles highlight to the top a 4 m thick transparent seismic facies that rests on interbedded discontinuous and irregular reflectors (Fig. 5.3). Moreover, the southern side of the deposit is formed by a dune field due to the reworking of a coastal wedge during the last relative sea-level rise.

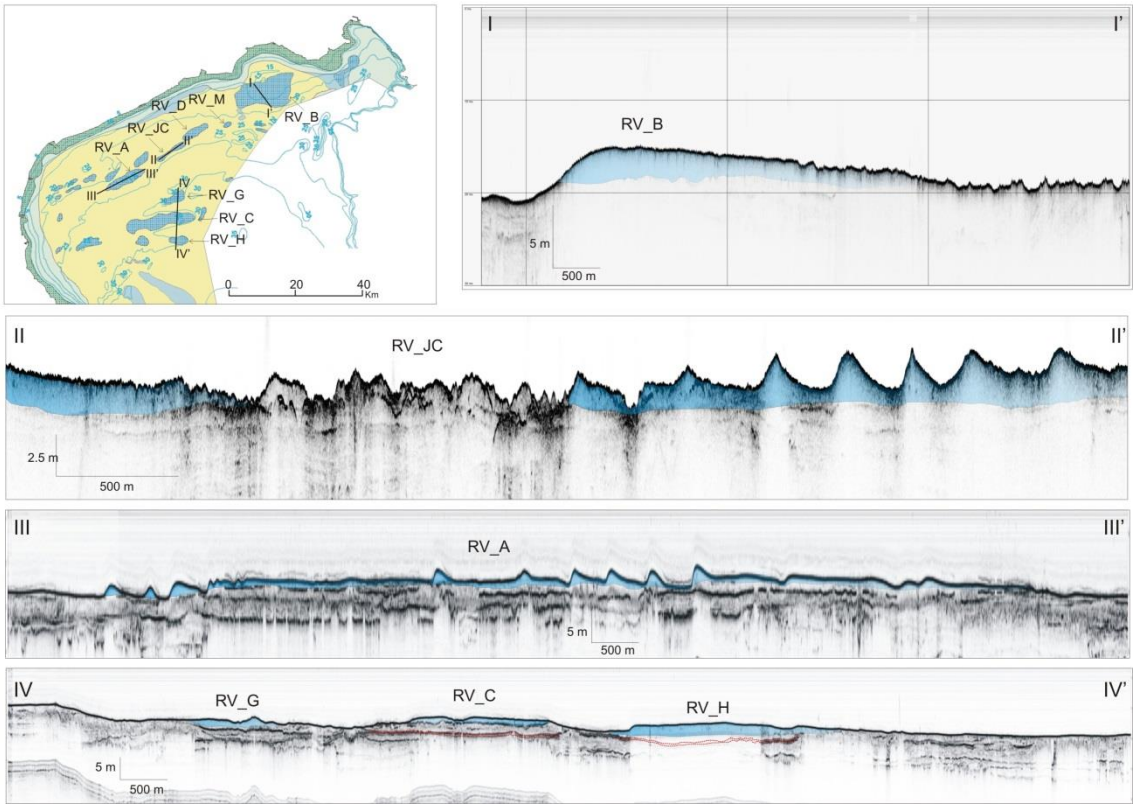

Fig. 5.3: Example of some analysed seismic profiles. In blue are represented the semi-transparent sand portion of the transgressive deposits, bordered at the base by strong and continuous high amplitude reflectors. The red dashed line is indicative of the same reflector that define the RV_ and RV_C base.

5.2.5.2 Core analysis

The seismic analysis was integrated with core analysis, in order to correlate the identified seismic facies with core sedimentary facies. Moreover, the core analysis allowed to recognize the more recent sand portion related to the last relative sea-level rise. The analysed cores, from 0.8 to 4.2 m long, consist of fine and very-fine sand.

One schematic core representing the facies succession of this bodies is showeded in Fig.5.4 and its description and interpretation are considered indicative of a common observed sediment organization. The basal portion (Fig.5.4; A) is made off hard pale-grey clays separated by an erosional surface

by dark-grey clays (Fig.5.4; B) with organic matter remains and millimetric plant debris. This mud portion is characterized by alternating peat layers and scattered small sand pockets. The fauna of this portion is scarce but predominated by *Cerastoderma glaucum*, *Ventrosia ventrose* and *Hydrobia* indicative of a brackish back-barrier environment. The upper sediments (Fig.5.4; C), from 1 to 3.5 m thick, are characterized by very fine to fine sorted sand with scattered content of shell fragments and sporadic clay chips, this portion is truncated on the top by an erosional and irregular surface with abundant shell fragments. Thin layers of very-fine sand and silt (Fig.5.4; D) often rest on this erosional surface and are capped by a mud veneer. The core is usually capped by a thin layer of clay sediment (Fig.5.4; E). The sediments at the base of the core (Fig.5.4; A) are interpreted as low-stand deposits bordered at the top by a transgressive surface. The coarsening upward sediments, at the top of the TS, are indicative of paralic sediments (Fig.5.4; B-C), and in particular, the thicker sand body is considered a relict form of ancient shoreline partially preserved and capped by a ravinement surface (Rs). The sand portion on the top of the Rs represents marine sand (Fig.5.4; C) and is capped by the maximum flooding surface (MFS). The cores are generally characterized at the top by a thin layer of high-stand deposits represented by mud (Fig.5.4; E).

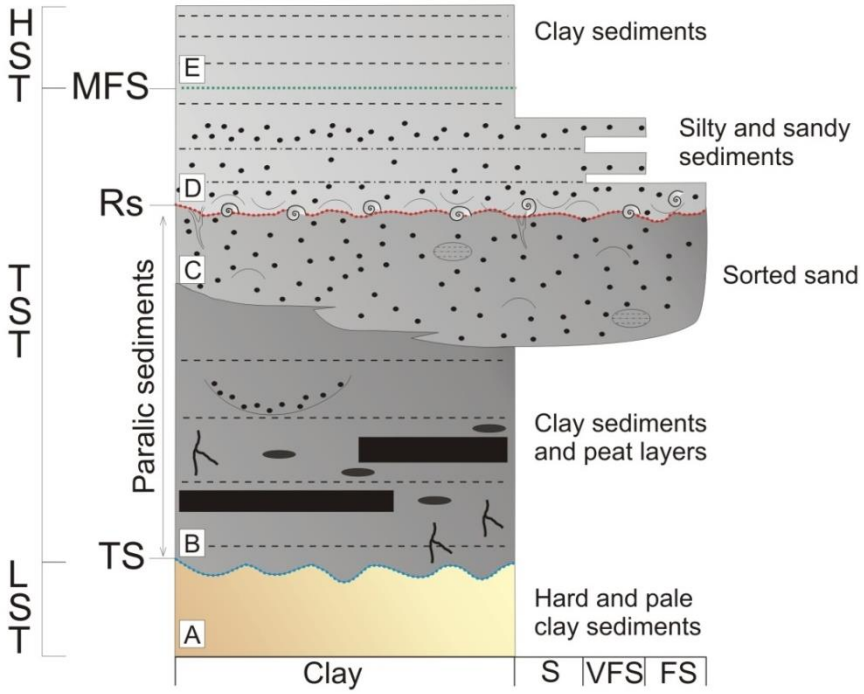

Fig. 5.4: Example of one study core.

5.2.5.3 Compositional results

About fifty sandy samples examined vary from fine to very-fine grained, with grains ranging from poorly to well rounded. The sediments analysed are a mixture of monocrystalline and polycrystalline terrigenous grains supplied in different percentages by trunk rivers and very small quantities of carbonate intrabasinal grains. For this reason, only the terrigenous fraction is considered in analysing our results. Data of Tab. 3 were elaborated to obtain the end-members for the ternary diagram (Fig. 5.5) Q, F, L+CE, where Q indicates the total quartz, F the feldspars and L+CE the fine-grained lithic fragments (L) plus the extrabasinal carbonates (CE). Modal composition of all samples highlighted by classic triangle diagrams fall in the litharenitic field. The siliciclastic fraction varies from 10% to 85% and is characterized by a high percentage of quartz and a significant contribution of feldspar and volcanic and metamorphic rock fragments. The terrigenous carbonate fraction, as well as the siliciclastic fraction, range from 10 to 85% and consists of limestone and dolostone grains. In the siliciclastic fractions, quartz occurs both as monocrystalline and polycrystalline grains and as a phaneritic component in metamorphic and granitic rock fragments. Feldspar grains are commonly present as single crystals and, in a few cases, within coarse-grained rock fragments derived from magmatic rocks. Metamorphic rock fragments are represented by abundant micaschists, quartz-micaschists and schistose serpentinites. Volcanic rock fragments are characterized by felsic grains with microphenocrysts of quartz or feldspars and acid and glassy ground mass which are usually altered with abundant oxides. Phyllosilicates are present in a small percentage of white mica, biotite and chlorite. The other mineral class comprises garnets, pyroxene, epidotes, and amphiboles including alkaline ones. In the carbonate terrigenous fraction rounded grains of micritic limestone and single and polycrystalline dolomitic clasts are mainly present. The intrabasinal component is largely represented by fragments of molluscs and echinoids. Furthermore, Fig. 5.6 highlights the percentage of the lithic component in relation to each deposit. The different types of rock fragments comprise both coarse and fine-grained lithics. In detail, metamorphic lithic fragments (M) range from 50 to 10%, volcanic lithic fragments (V) are relatively constant with maximum values reaching 16% and minimum values reaching 4%, sedimentary lithic fragments (S) range from 35 to

93%, and gneissic or granitic rock fragments (G) are rare due to the fine-size of the studied sand. The combination of bulk composition and lithic fragments analyses allowed us to distinguish three distinct petrofacies (Fig. 5.5; Fig. 5.6). Moreover, the composition of some present-day river supplies from literature (Gazzi et al., 1973; Marchesini et al., 2000; Monegato et al., 2010) are reported in Fig. 5.5 with the aim to compare our data with fluvial supplies.

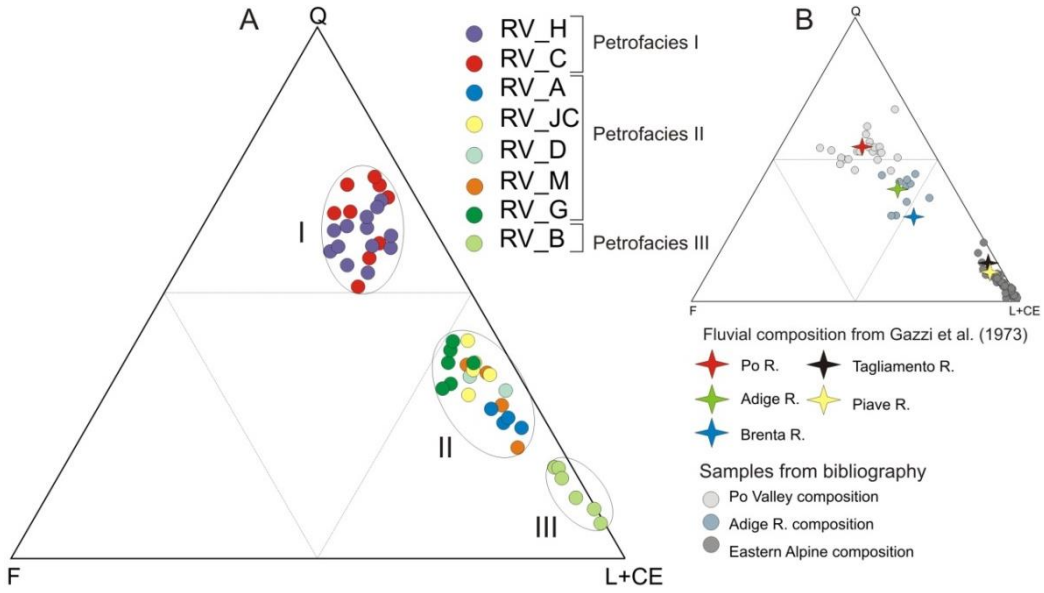

Fig. 5.5: Ternary diagram (A), F, L+CE (Quartz, Feldspar, Fine-grained ithic Fragments + Extrabasinal Carbonate). Identification of three different Petrofacies (Petrofacies I, II, III) and comparison with literature data (B).

The mean composition for each deposit is reported in Tab. 5 with their main sedimentological characteristics.

Deposit	Depth of Water (m)	Thickness of sand portion	Sand %	Mean composition	Sedimentary Supplies
RV_H	28-32	Up to 3.5 m	80-97	$Q_{61}F_{9}L+CE_{30}$	Po River Valley
RV_C	26-32	Up to 2 m	75-97	$Q_{61}F_{13}L+CE_{26}$	Po River Valley
RV_G	30-31	Up to 3 m	57-70	$Q_{37}F_{10}L+CE_{53}$	Hybrid
RV_A	20-24	Up to 2 m	89-97	$Q_{27}F_{6}L+CE_{67}$	Hybrid
RV_JC	20-24	Up to 2 m	93-97	$Q_{31}F_{7}L+CE_{62}$	Hybrid
RV_D	20-24	Up to 1 m	80-98	$Q_{33}F_{5}L+CE_{62}$	Hybrid
RV_M	20-24	Up to 1 m	85-93	$Q_{37}F_{5}L+CE_{58}$	Hybrid
RV_B	11-16	Up to 4 m	70-98	$Q_{14}F_{1}L+CE_{85}$	Tagliamento R.

Tab.5 : Summary of the main sedimentary characteristics of each deposits.

Petrofacies I (Q_{63} F_{11} L+CE_{26}). This petrofacies, including all samples belonging to RV_C and RV_H bodies, shows a quartzolithic composition, with a quartz grain predominance and subordinate amounts of feldspar. The lithic fraction is characterized by a considerable variety of grains both coarse and fine-grained as micaschists, schistose serpentinite and volcanic grains with microphenocrysts. The carbonate terrigenous fraction always has values lower than 20%, with calcite clasts prevailing on dolomite ones. Furthermore, relative high amounts of heavy minerals characterize this petrofacies (Appendix 1). Moreover, the point-counting of the rock fragments emphasizes a predominance of metamorphic fragments (around 50%), with subordinate sedimentary (35%) and volcanic (16%) fragments (Tab. 4; Fig. 5.6).

The composition and the lithic fragments analyses of the Petrofacies I suggest a supply mainly linked to the Po River input due to the presence of schistose serpentinites, a high content other minerals and among them the scattered presence of alkaline amphiboles. The Po River supply is also highlighted by the linear mixing model with R value higher than 0.950 both for RV_H and RV_C deposits (Tab. 6). Moreover, the comparison of our data with literature data (Gazzi et al., 1973; Marchesini et al., 2000) supports this interpretation.

Petrofacies II (Q_{33} F_7 L+CE_{60})**.** This petrofacies shows a litharenitic composition characterized by lower a percentage of quartz compared to Petrofacies I but higher than Petrofacies III. The carbonate terrigenous fraction is characterized by both carbonate and dolostone grains with predominance of dolostone grains, whereas other lithic fragments are characterized by felsic volcanic and low-grade metamorphic grains (Appendix 1). Furthermore, the point-counting on the lithic fraction emphasizes high values (73%), but not comparable with Petrofacies III, of sedimentary fraction, and low values of metamorphic and volcanic fractions, both around 13 % (Tab. 4; Fig. 5.6). Moreover a small percentage of intrabasinal grains is present. The petrofacies II comprises all samples belonging to RV_G, RV_A, RV_JC, RV_D, RV_M deposits that are geographically located between the RV_B deposit belonging to the Petrofacies III and RV_H and RV_C deposits belonging to the Petrofacies I. The composition of this petrofacies suggests a hybrid composition deriving from a commingling of several river supplies, even confirmed by the linear

mixing model, highlighting Brenta and Piave River contributions for the RV_A, RV_JC, RV_D and RV_M deposits and Adige, Brenta and Piave River components for the RV_G body (Tab. 6). The low number of available samples does not permit a more precise source distinction.

Petrofacies III (Q_{14} F_1 L+CE_{85}). This petrofacies highlights a litharenitic signature with carbonate fraction ranging from 60% to 87%, with a high amount of both dolostone and micritic limestone grains (Appendix 1). Other lithic fragments are represented by felsic volcanic rocks and by low-grade metamorphic rocks. In particular, the lithic component is characterized by significant values of sedimentary fragments and negligible values of volcanic and metamorphic fragments, whereas, quartz and feldspar are present in low percentages (Tab.4; Fig. 5.6). All samples belonging to the RV_B deposit mark this petrofacies for which the linear mixing model empathizes R value higher than 0.950 in relation to a Tagliamento River supply, possibly slightly affected by the Isonzo River input (Tab.6). Again, the comparison of our data with literature data (Gazzi et al., 1973; Monegato et al., 2010) confirms this interpretation, suggesting a Tagliamento River supply.

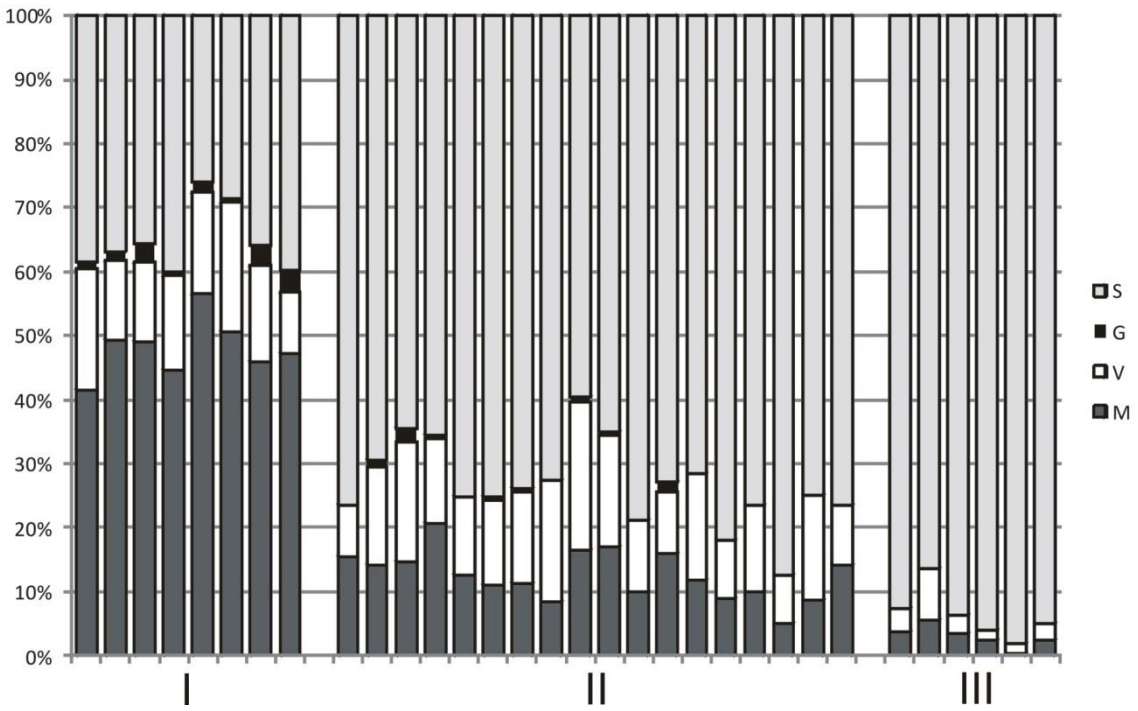

Fig. 5.6: Lithic fragments percentage in relation to the three different petrofacies. S: sedimentary lithic fragments; G: granitic lithic fragments; V: volcanic lithic fragments; M: metamorphic lithic fragments.

Petrofacies	*I*	*I*	*II*	*II*	*II*	*II*	*II*	*III*
Deposit	*RV_H*	*RV_C*	*RV_G*	*RV_A*	*RV_JC*	*RV_D*	*RV_M*	*RV_B*
R value	R=0.981	R=0.968	R=0.934	R=0.917	R=0.944	R=0.872	R=0.972	R=0.986
Po R.	**1**	**1**	0	0	0	0	0	0
Adige R.	0	0	0.4	0	0	0	0	0
Brenta R.	0	0	0.4	0.6	0.5	0.2	0.2	0
Piave R.	0	0	0.2	0.4	0.5	**0.8**	**0.8**	0
Tagliamento R.	0	0	0	0	0	0	0	**0.9**
Isonzo R.	0	0	0	0	0	0	0	**0.1**

Tab.6 : Comparison among composition of each deposit with the fluvial sands according to the R mixing model.

5.2.6 Discussion

Results of this research permit to delineate the internal organization of several Holocene transgressive deposits located in the northern Adriatic Sea and the differences of their composition contribute to delineate a paleogeography scenario of the northern Adriatic Sea during the last sea-level rise. All the considered deposits have a litharenitic composition mainly characterized by different quartz percentages and lithic content. Taking into account both bulk composition and rock fragments analyses three petrofacies have been recognized, and considering the very short time interval between the oldest (RV_H) to the younger deposits (RV_B) it is possible to relate each petrofacies to different supplies.

The RV_H and RV_C, belonging to the Petrofacies I are the oldest transgressive deposits among those here considered (Fig. 5.7). These two sedimentary bodies with positive bathymetry, consist of sand lenses on top and fine organic matter rich sediments at the base. In particular we focus on the uppermost sand units formed during the last relative sea-level rise. From petrographic results these deposits are referred to sediments furnished by the Po River even if are located northern than the present delta latitude. Thus, a presence of a paleo branch of the Po River, flowing more northward than the present has been suggested. This hypothesis is supported by different evidence. In particular, the two deposits were sedimented over a low gradient platform on which a slight morphological variation could cause a significant drainage shift. Moreover, the deepest area of the basin, during the last relative sea-level rise, was close to the NE Adriatic coast (Italy, Istria and Croatia coasts), due to a pronounced subsidence (Antonioli et al., 2009). Thus, it is possible to hypothesize a northeast Po fluvial trend, already pointed out in a transgressive barrier lagoon system (-32 m msl) south of the actual Po Delta

belonging to a previous phase of sea-level rise (Moscon et al., 2015). Furthermore, a northern paleo branch of the Po River has been also suggested by results of other authors (e.g. Castiglioni, 1978; Piovan et al., 2010).

The RV_G and RV_A, RV_JC, RV_D, RV_M deposits, belonging to the Petrofacies II, are isolated patches showing a longshore trend similar to the modern sea-level high-stand deposits (Fig. 5.2). Apart from the RV_G the other sedimentary bodies belonging this petrofacies are relatively small compared with the others. They are bounded to the base by peat layers and are characterized by sandy made of fine to medium sand. These deposits point out two different sea-level phases (subsequent to the RV_H and RV_C drowing; Fig. 5.7), and they record two different coastal lithosomes that mark the last steps of the Holocene transgression. The mixed composition, highlighted by petrographic results, is connected to sediment dispersion linked to long-shore drifting marine currents during the formation of the ancient coastlines. In particular, the linear mixing model highlights variation in dominant component moving from W to E. In a more recent coastline, represented by RV_A, RV_JC, RV_D and RV_M deposits, a decrease of the Brenta River component was observed, from W to E, associated with an increase of the Piave River component. Furthermore, the more recent coastal lithosome has never been affected by the Tagliamento sediments. These results may suggest a dominant clockwise marine current, with sediments moving longshore from W to E opposite to the present.

The RV_B, belonging to the Petrofacies III, is a transgressive deposit at 15 m msl in front of the modern Tagliamento mouth, and it is the younger sedimentary body studied in this work. This transgressive body, previously studied by Gordini et al. (2002), Fontana et al. (2004) and recently by Zecchin et al. (2015), has a top portion of sands interpreted as a delta front body and a basal portion of laminated silt and clay layers alternated with silt-sand layers interpreted as a prodelta facies (Zecchin et al., 2015). This deposit has been referred to as an ancient wave-dominated delta of the Tagliamento River developed when the sea-level was lower than the present one and probably drowned before 7 cal. yr BP (Zecchin et al., 2015). Our petrographic interpretation results support the previous interpretation focusing on a local area connected to its ancient coastline.

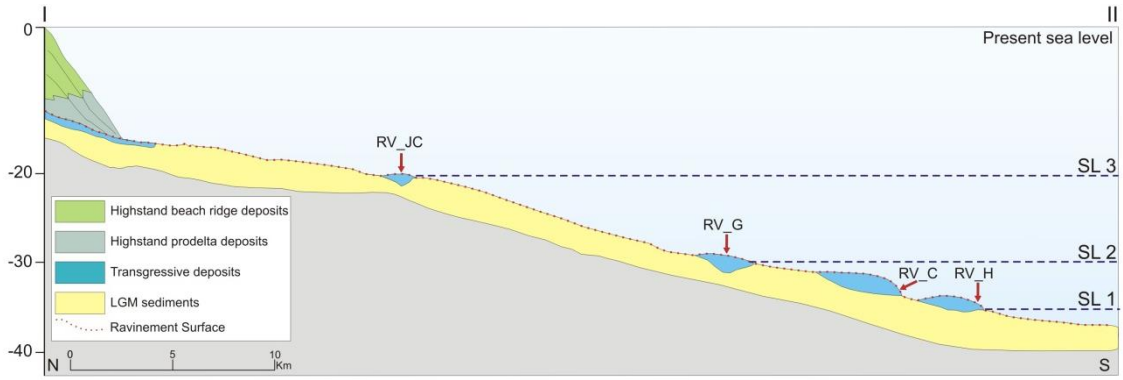

Fig. 5.7: Simplified section of different phase of the last relative sea-level rise in relation to the studied transgressive deposits. Location of the section in Fig. 5.2.

5.2.7 Conclusion

Sand petrography has been the proper approach in order to highlight different petrographic supplies in the transgressive deposits drowned and preserved in the northern Adriatic shelf. On the base of core analyses, geographic position and composition, a possible scenario for the northern Adriatic Sea, during Holocene transgression, is proposed. In detail, the petrographic analysis allowed to identify three petrofacies reflecting distinct supplies related to different phases of the last relative sea-level rise.

Considering the literature data focusing on present fluvial sand composition and that of the present northern Adriatic Italian beaches, a clear correlation, with fluvial supplies is delineated. Although the lack of radiocarbon dating didn't allow us to accurately constrain these transgressive deposits, it is possible to assume that the paleo drainage during the sedimentation of the studied transgressive deposits was similar to the present. Moreover, the petrographic analysis allowed to highlight some remarks:

- ✓ RV_H and RV_C transgressive deposits (Petrofacies I) record two wrecks of coastal lithosome indicative of two close sea-level rising phases; furthermore, considering that their sand composition suggests a Po River supply, they testify a potential northward shifting of a paleo Po trunk River when the sea level was 30 m below the present one.
- ✓ RV_G and RV_A, RV_JC, RV_D, RV_M deposits (Petrofacies II) are indicative of two coastal lithosomes, thus recording two different phases of the sea level rise. Their hybrid composition reveals different river supplies from Eastern Alpine rivers, moreover, the linear mixing model

analysis emphasizes variations in the Brenta and Piave Rivers contributions for the younger lithosome, and predominant Adige and Brenta River contributions for the ancient fossil lithosome.

- ✓ RV_B deposit (Petrofacies III), located in front of the present Tagliamento River mouth, and previously interpreted as a fossil Tagliamento delta (Gordini et al., 2002; Fontana et al., 2005 and Zecchin et al., 2015) points out an Eastern Alpine supplies mainly referable to Tagliamento River and in a small amount with a signature Isonzo River. In particular, our new petrographic results confirm the previous interpretation.

Finally, the results of this study can be useful in order to better identify the exploitable offshore sand deposits, for beach nourishment, in relation to different characterization of beache affected by erosion and sediment removal.

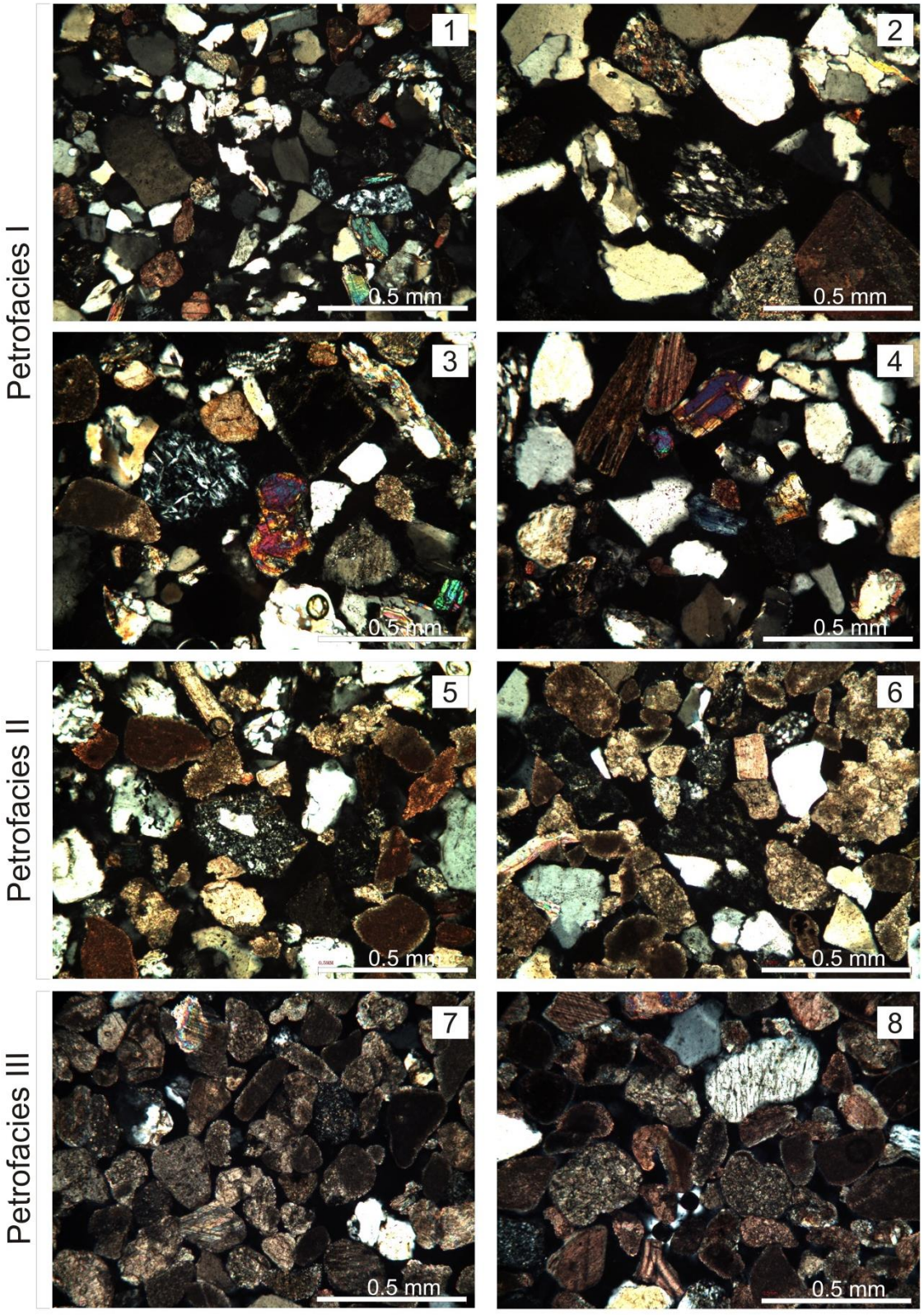

Appendix 1: Petrographic features of the analysed sand. Petrofacies I (1, 2, 3, 4 photos) has a quartzolithic composition, note the presence of heavy minerals. Petrofacies II (5,6 photos) shows a litharenitic composition. Petrofacies III (7, 8 photos) shows a litharenitic composition with carbonate fraction dominant.

CHAPTER 6

XRF CORE ANALYSIS

6.1 Overview

This chapter is a journal paper in preparation. In this chapter, XRF core scanner analysis is carried out in mixed sediments cores in order to identify peculiar geochemical proxies that can support environmental interpretation, geochemical characterization of the sediments and eventually climatic changes.

6.2 Literature

Since 1970 the X-Ray Fluorescence analysis has been a technique for analysing marine sediments. In particular, the XRF Core Scanner is a device built for high resolution and non-destructive determination of the chemical composition of sediment core samples, split in length. With this tool it is possible to obtain a continuous record along the sediment section in order to highlight the variation of the sediment's property during time.

In the last 20 years, XRF core scanner has been used in paleo environmental research worldwide. High resolution studies on continuous sedimentary archives are crucial for understanding climate change on seasonal to millennial scales (Rothwell and Croudace, 2015). A major application of XRF scanning of marine corers has been to determine changes in sediment composition, largely relating to climatic changes and glacial-interglacial cycles (Moreno et al., 2002; Lebreiro et al., 2009).

In particular, as the XRF analysis supplies a continuous data range along the split cores, its use has been applied in a wide variety of marine/lacustrine science applications summarized by Rothwell and Croudace, (2015).

This technique allows:

- ✓ description and characterization of cores;
- ✓ evaluation of climatic changes that are reflected in $CaCO_3$ or Fe fluctuations;

- ✓ sedimentological applications, as identification of ash layers, turbidites, ice-rafted debris and earliest stages of marine influences;
- ✓ studies of sediment provenances based on chemical differences in source areas;
- ✓ diagenetic studies;
- ✓ environmental impact studies.

Rothwell and Croudace, (2015) have reported that as the XRF core scanner provides rapid acquisition of high-resolution elemental dataset it has often been the first analytical tool used after opening and splitting cores. But the lack of standardised protocol for parameters setting, may reduce data quality compared to what might be achieved with chemical analyses of a smaller number of samples. Accordingly with this observation, it is fundamental to identify geochemical proxy to obtain meaningful paleoclimate data. As, Ca, Fe, Sr, K and Ti are commonly occurring elements in marine sediments, they are extensively used as tracers in environmental reconstructions (Gebhardt et al., 2008). Fe, Ti, Si, K and Al occur mainly in terrigenous silicates and oxides, they are indicative of detrital load derived from the erosion of continental rocks and they are indicative of sediment transport from land to sea. Si and Ca may be supplied by surface water productivity and are volumetrically substantial (Rothwell and Croudace, 2015). The two main parameters measured are Fe, as a proxy for terrigenous input (Vidal et al., 2002; Grutzner et al., 2005), and Ca, as measure of biogenic production (Solignac et al., 2011). Moreover, Rotweel et al. (2006) pointed out that high values in Si, Al, K and Ti correspond to glacial-fluvial sandy mud, whereas a decrease in Si, AL, K, Ti and an increase in S correspond to peat development. Furthermore, fluctuations of Ca and S suggest an oscillating coastline position. The authors conclude that transgressive sediment characteristics are most precisely highlighted by XRF core scanning results, through increase of K, Ti, Si. Furthermore, a number of factors related to the sediment matrix, such as water content, organic matter, grain size, mineral crystallinity and porosity may have a significant impact on the production and the detection of fluorescent photons (Weltje and Tjallingii, 2008). Results are usually presented as spectral peak areas or counts per second (cps) and can be calibrated to concentration. But the use of element ratios and

the plotting of XRF curves (in cps), together with discrete sample analyses obtained using destructive techniques, such as inductively-coupled plasma or other conventional techniques are two ways to improve the results (Francus et al., 2009). The importance of using the element ratios was verified by several authors in the various applications.

Major elemental proxies and some relative elemental ratio grouped and described by Rothwell and Croudace, (2015) are listed below:

Calcium

Ca/Fe, Ca/Ti, Ca/Al

May be biogenic or detrital, although biogenic sources have a volumetrically greater importance. Calcium content is a recognised proxy for oceanic productivity, and its variation typically reflects $CaCO_3$ stratigraphy in pelagic cores. This component is generally lower during glacials and higher during interglacials (Arz et al., 2003; Rooij van et al., 2007; Gebhardt et al. 2008). Thus, Ca is commonly an effective indicator for climate and efficient tool for establishing stratigraphic frameworks. However, Ca variation, particularly in marginal environments, may reflect dilution by terrigenous material rather than productivity changes.

Ca/Fe and Ca/Ti are useful proxies for assessing relative changes in biogenic versus lithogenic sedimentation, in particular Ca reflects marine production while Fe and Ti reflect terrigenous input.

Ca/Al represents the biogenic/detrital ratio so is a potential proxy for measuring changes in terrigenous sediment contribution too.

Strontium

Sr/Ca

Sr is an alkaline earth metal fixed by calcifying organisms at same time as Ca. Hence Sr is a marker for biogenic origin. As Ca can be supplied from terrigenous sources (e.g. feldspars and clays) co-variation of Ca and Sr suggests Ca mainly sourced from biogenic $CaCO_3$.

Sr/Ca is used as proxy for aragonite, thus enhanced Sr may indicate presence of high-Sr aragonite which requires a shallow-water source (Rotweel et al., 2006).

Iron

Fe/Al

Is the most common element on Earth, and the fourth most abundant element in the crust, after O, Si and Al. In marine sediments, Fe commonly highlights changes in carbonate/clay ratios. Fe variation is generally related to sediment's terrigenous fraction and or dilution of $CaCO_3$.

Fe, like Ti, has been widely used to document variations in terrigenous sediment delivery. As redox-sensitive element, Fe can identify secondary diagenetic features. Considering that Fe and Ti are closely related in terrigenous fractions, but Fe is partly prone to diagenetic remobilisation in pore waters and Ti is inert, good correlation of Fe to Ti suggests little diagenetic influence. Elevated Fe/Al, with high S, is indicative of anoxic bottom water (Spofforth et al., 2008).

Aluminium

Al/Si

Al is the most abundant metal in the Earth's crust and third most abundant element, after O and Si, but too reactive to be found pure, and is instead found as oxides and silicates. Aluminosilicates are a major component of kaolin (one of the most common clay minerals), other clay minerals and zeolites. Other aluminosilicate minerals include andalusite, kyanite, sillimanite, beryl, garnet, spinel, and turquoise.

Al/Si has been used as a proxy for chemical weathering, in particular, decreases in Al/Si is indicative of less chemical weathering.

Silicon

Si/Sr

Measured by mass, Si makes up 27.7 % of Earth's crust and is the second most abundant element, only O having greater abundance. Si may be detrital, derived from mechanical weathering of crustal rocks, or biogenic, derived from siliceous phytoplankton (diatoms, silicoflagellates), protozoans and

protists (radiolarians and ebridians) and sponge spicules. Moreover, quartz (SiO_2) is a major component of sand and silt derived through physical weathering of continental crust. Si may be detrital, derived from mechanical weathering of crustal rocks, or biogenic, derived from siliceous phytoplankton (diatoms, silicoflagellates), protozoans and protists (radiolarians and ebridians), plant phytoliths, some scolecodonts (polychaete worm jaws) and sponge spicules.

Like Fe and Ti, Si used as a proxy for terrigenous sediment delivery (Blanchet et al. 2007; Kleiven et al. 2007). Si/Sr used to identify layers poor in biogenic carbonate and relatively rich in detrital silicates (quartz, feldspar etc.; Hodell et al., 2008).

Titanium

Ti/Ca

Ti is conservative element that generally varies directly with the coarse-grained terrigenous fraction. A common constituent of rocks, such as gneisses or schists, it primarily indicates a terrigenous continental source. Moreover Ti occurs in all minerals commonly associated with sand and silt fractions. Ti is widely used to record terrigenous sediment delivery, it commonly co-varies with Fe, but is arguably a better proxy for terrigenous sediment delivery than Fe as it is redox-insensitive (Calvert and Pedersen 2007; Yarincik et al. 2000).

Ti/Ca records relative variation of terrigenous input and marine carbonate (e.g. Bahr et al. 2005, 2008; Hoang et al. 2010). It has been used to record changes from fluvial to marine deposits, for example, in incised-valley-fill sediments (Tjallingii et al. 2010).

Potassium

K/Ti

Is generally associated with terrestrial siliciclastics and potassium feldspar.

K/Ti has been used to emphasize provenance differences of detrital material tracing the relative importance of both terrigenous sources (Diekmann et al. 2008; Richter et al. 2006), with the proxy being useful with sediment supplied largely by weathering of schists and slates.

Barium

Ba/Al

Ba is important proxy for export paleo productivity. Its relationship to productivity is well established. Relatively high concentrations of tiny Ba-rich particles (< 2 μm in diameter) occur in near-surface waters (Dehairs et al. 1980 and others) especially in areas of high productivity (Dehairs et al. 1992; Cardinal et al. 2005). This Ba is commonly associated with biogenic aggregates and constitutes most of the suspended Ba in water column.

Ba/Al is used to determine the productivity. Productivity often strongly modulated by climate. For example, Jaccard et al. (2005) interpreted low biogenic Ba at glacial maxima at ODP Site 882 (N Pacific Ocean) as reflecting decreased nutrient supply.

Sulphur

Fe/S

S is closely linked to organic matter with S residing in biomass of marine plants and mineralised S in their dead remains. Within sediments organic S may be oxidised to sulphate and returned to seawater, or buried as organic S, sulphate or sulphide, through bacterial reduction (Ivanov 1981). S, thus serves as proxy for oxygen depletion in bottom water (Harff et al. 2011). High S contents, together with high Fe/S ratio, indicate reducing conditions.

Bromine

Br does not occur naturally but occurs as bromide compounds in diffuse amounts in crustal rocks. Terrestrial organic matter is comparatively poor in Br, then Br is widely used to quantify marine organic matter and related productivity (e.g. Caley et al. 2011; Ren et al. 2009; Ziegler et al. 2008, 2009), in order to discriminate marine and freshwater conditions.

6.3 XRF Avaatech core scanner analysis

The main goal of this study expected to investigate cores collected in the northern Adriatic Sea in some deposits that have been already characterized with different methods, such as petrographic analysis and seismic facies analysis. Being a previous knowledge of the sedimentary bodies under examination, an interpretative approach has been attempted, even if the analysed cores mainly consist of fine-sand sediments that generally cause a signal-noise increasing. This innovative methodology, tested in mixed sediments, was applied to assess whether the obtained data could be used for supporting the environmental interpretation, geochemical characterization of the sediments and eventually the recognition of climatic changes.

The selected cores, are RV08_B138, RV08_A80, RV11_G96, RV11_H113 and RV11_C34 (Fig. 6.1), in particular, these cores were collected during two oceanographic cruise in 2008 and in 2011 in order to identify the quality and the amount of sand per transgressive studied deposit north of the Po River delta. The cores have been collected with a vibrocorer, having a length from 2 to 4 m, and are characterized by up to 1 m of fine to very fine sand. Furthermore, two cores, AR00_C15 and AS14_14, belonging to a transgressive deposit south of the Po delta (described in Moscon et al., 2015) were selected for the XRF analysis. The AR00_C15, collected in 2000, is characterized by 100 cm of sand and 230 cm of organic-rich clay and peat layers. The AS14_14, collected in 2014, is characterized by 30 cm of sand at the top and 430 cm of clay and peat layers. Thus these two cores were investigated as one composite core with at the top AR00_C15, in order to highlight elements and ratios response in correspondence of a transitional environment.

Taking as references the elemental proxies, described above, some considerations were highlighted and in particular, where possible; elemental ratios with Al and Ti as denominators, were used rather than the direct counts (other elements and geochemical ratios are present in the Appendix B).

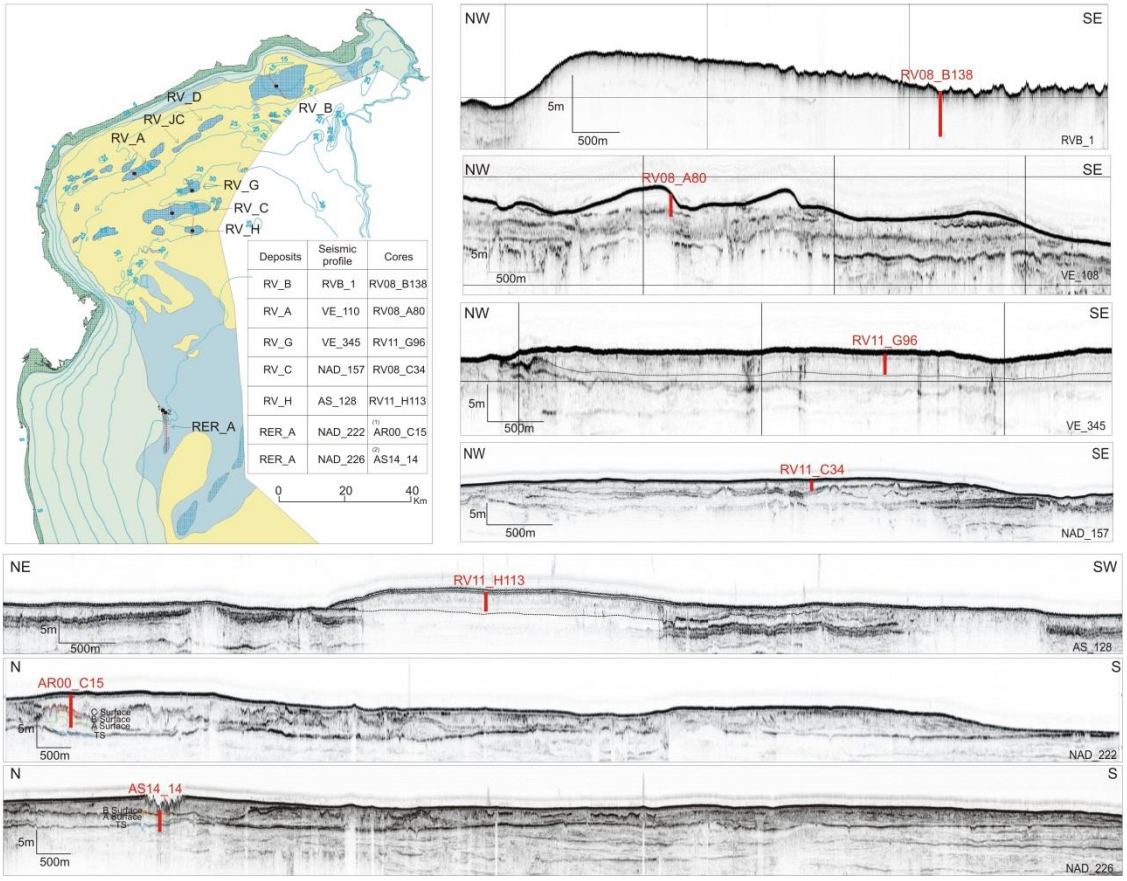

Fig. 6.1: Cores location and related seismic profiles of the analysed cores with the XRF core scanner. In correspondence of the AR00_C15 and AS14_14 are traced the key surfaces highlighted in Moscon et al., 2015; (zoomed image at the end of the thesis).

RV08_B138

The RV08_B138 was cored in the RV_B area up to the depth of 420 cm and it is characterized by fine and very-fine sand, with presence of shell fragments in the first 50 cm, and significant amount of silt in the basal portion. The RV_B deposit, previously studied by different authors (Gordini et al., 2002; Fontana et al., 2006; and recently by Zecchin et al., 2014), was interpreted as a delta front body in the top portion, shifting towards prodelta facies in the basal portion. The XRF analysis highlights three different units, marked by variation in ratio of selected elements established and used as geochemical proxies. (Fig. 6.2). The most recent unit, from 0 to 40 cm, is characterized by a noise signal with higher values of Ca/Ti, Ca/Fe and Ba/Al compared to the lower unit (middle unit). The middle unit, from 40 to 320 cm, in characterized by a stable pattern, whereas the deeper unit, from 320 to 420 cm, is characterized by a significant variation in chemical values response. Ba/Al, Br/Al and Ca/Al ratios, used as proxies for the paleo productivity, show high values corresponding to the upper and the basal unit. Si/Ti, Ca/Ti, Ca/Fe ratios, used as indicator of terrestrial influence, highlight constant values in the middle unit and low values in the deeper unit. Moreover the deeper unit is characterized by an increase in Fe/Al and S, probably related to reduce condition and high values in the ratio Sr/Ca may be indicative of shallow water environment (cf. Rothwell and Croudace, 2015; Fig. 6.2). Considering the known environment of sedimentation and the results obtained by the XRF analysis, the RV08_B138 core records three different sand units belonging to marine environment. In particular, the basal unit records a marine sand unit, indicative of shallow water environment highlighted by high values of Sr/Ca ratio, with high values relating to the productivity proxies and low values relating to terrestrial influence proxies. Moreover, the increasing Fe/Al values suggest a suboxic environment. The middle sand unit highlights a deepening of the system, and it is characterized by significant values associated to terrigenous supply proxies. Thus, this sand unit records the system response to the relative sea-level rise, due to a significant terrigenous supply allowing the deposit aggradation. The upper sand unit records the more recent marine units strongly influenced by marine processes, as documented by very low values associated to terrigenous supply proxy and high values related to the productivity proxies.

RV08_A80

The RV08_A80, belonging to the RV_A area, is a 300 cm long core and it is characterized by a top portion (0-200 cm) of fine transgressive sand with about 14% of medium sand, that rests on 100 cm of stiff clay and peat layers. In particular, the transgressive deposit of RV_A records asymmetric sand waves, with a westward steep side. This is elongated NNW-SSE due to reworking of coastal lithosome during the last phase of the Holocene sea-level rise (Correggiari et al., 1992; 1996b). In this core two units were identified according to the significant variation in the signal response which corresponds to the lithological change (Fig. 6.3). Regarding the upper sand portion, the XRF analysis did not show evident variation, however, some consideration, taking as reference the productivity and terrigenous proxies, were carried out. The Ba/Al highlights values comparable to the marine sand portion of the RV11_G96 and RV11_H113 cores. Moreover, the terrigenous indicators, show constant values but no evidence in variation of sediment supply was recorded. The signal homogeneity, both in Ba/Al, K/Ti ratio and in Al/Ti, probably is due to the strong reworking of the sediment in a starved area. Only Ca/Fe records a circa-sinusoidal trend that could be associate to different accretion phases during the development of the sand waves (Fig. 6.3). Concerning the basal portion, it is characterized by 30 cm of bioturbated organic silty-clay with bioclasts, that rests on a peat layer of 20 cm on top a stiff ochraceous clayey layer until the end of the sampled section. The lithological change between sand and clay show a significant decreasing in Ca, Ca/Fe, Ca/Al, this abrupt anti-correlate change is associated to glacial-interglacial transitions (Rothweel et al., 2006), moreover the peat layer emphasizes the negative peak, highlighting values close to 0 (Fig. 6.3). Therefore, the XRF analysis on RV08_A80 highlighted a sand portion with constant values both in productivity and terrigenous supply proxies due to deep reworking. A basal portion, that marks conspicuous changes in lithology and elemental response, is indicative of a continental environment formed during the LGM.

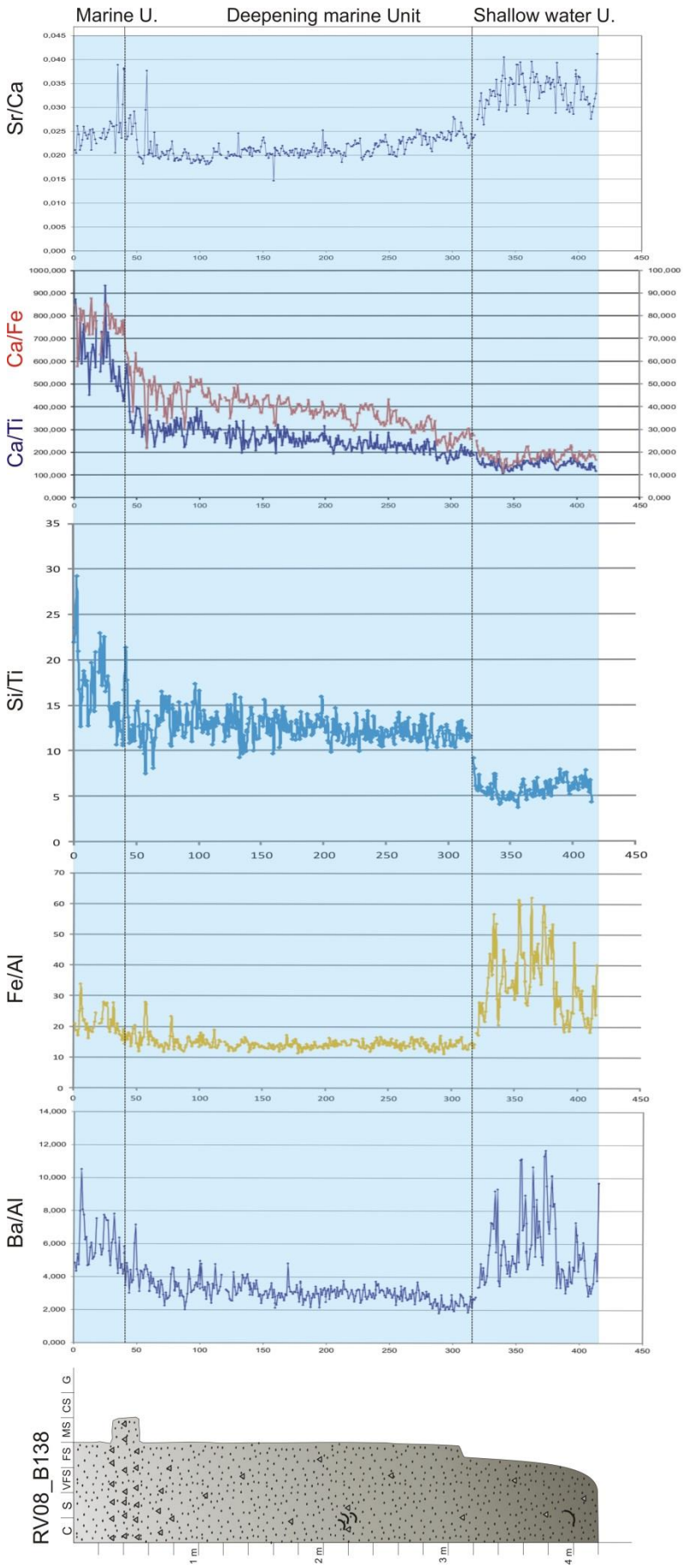

Fig. 6.2: Standard geochemical ratios highlighted by the XRF core scanner in order to describe the RV08_B138 core. Ba/Al, is used as productivity proxy, while Si/Ti, Ca/Ti, Ca/Fe are used as indicator of terrestrial influence. Fe/Al is used as proxy in order to identify suboxic environments, while Sr/Ca is used as proxy to individuate shallow water environments. Three different marine units are distinguished that record a deepening environment.

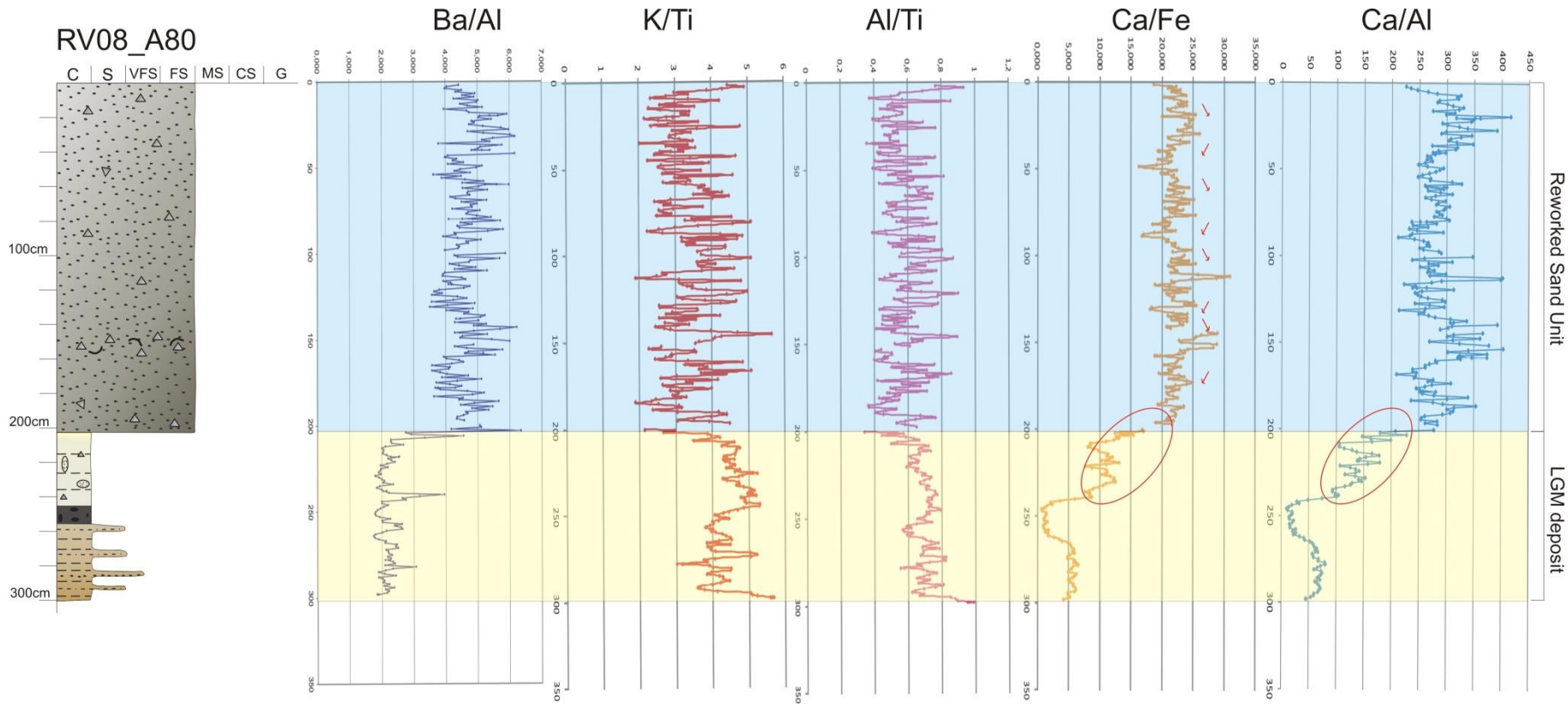

Fig. 6.3: Standard geochemical ratios highlighted by the XRF core scanner in order to describe the RV08_A80 core. Ba/Al, K/Ti and Al/Ti highlight a signal homogeneity in correspondence of the sand portion of the core, while Ca/Fe records a simil-sinusoidal trend. Ca, Ca/Fe and Ca/Al record an abrupt anti-correlate decreasing in relation to a pale-clay layer. In particular, two different units are highlighted: a reworked sand unit at the top and a continental (LGM deposit) unit at the base.

RV11_G96

The RV11_G96, belonging to the RV_G area, is 248 cm long and is characterized by a coarsening upward trend from very-fine to fine sand. Moreover, the upper portion is characterized by shell fragments, whereas the basal portion, about 2 meters below the sand deposit, is characterized by thin organic-rich layers alternating with sandy layers. Integrating the study of different proxies, three sand units seems to be recorded (Fig. 6.4). In particular, Ba/Al, Br/Al and Ca/Al were chosen as productivity proxy, whereas K/Ti, Al/Ti and Si/Ti as proxy indicative of terrigenous supply and variation in terrigenous material. The productivity proxies recorded high values at the top, from 0 to 10 cm. This thin layer is associated to marine sand, whereas, considering the terrigenous proxies, they heavily increase from 85 cm to the base of the core and this basal unit is characterized by sorted sand with high values of K and Si. The middle unit, from 10 to 85 cm, shows high values in Ba/Al, but not high enough to compare it with the upper unit, while K and Si values are lower than in the basal unit. However, this unit is associated to marine sand because its Ba/Al values are comparable with Ba/Al values displayed by core RV11_H113. Thus, the middle unit, can be merged with the upper unit even if it could record an increasing in terrigenous supply.

RV11_C34

The RV11_C34, belonging to the RV_C area, is 210 cm long and is characterized by a top portion (0-139 cm) of fine sand, that rests on 70 cm of clay and organic-rich layers. Considering that the RV11_C34 is characterized by different sediment grainsize, obviously, the XRF analysis highlights two easily recognizable units related to the sand portion and the clay and organic-rich layers portion, respectively at the top and at the base of the core (Fig. 6.5). Regarding the sand portion, especially Br/Al, used as proxy for the productivity, allowed to distinguish two different units (Fig. 6.5). The upper one, from 0 to 13 cm, with high values of Ba/Al, is indicative of marine sand, therefore affected by marine processes; while the basal unit, from 13 to 139 cm, with relatively high K/Ti and Al/Ti highlighting the terrestrial influence, is indicative of sorted sand with bioclastic fragments. Concerning the basal portion, it is characterized by 10 cm of silty-clay sediment, 6 cm of pale-clay layer and about 50 cm of alternating organic rich and peat layers. A significant peak, with high values of Ca, Ca/Fe

and Ca/Ti is observed in correspondence of the pale-clay layer (Fig. 6.5). Considering that abrupt anti-correlate changes in Ca, Fe and Ti are indicative of glacial-interglacial transitions (Rotweel et al., 2006), the recorded peak, associated to change in lithology and sediment lightness, could suggest continental sediments formed during the LGM.

RV11_H113

The RV11_H113, belonging to the RV_H area, is 320 cm long and it is characterized by very-fine sand with shell fragments in the upper portion and by fine sand in the basal portion. The XRF analysis emphasizes two different sand units (Fig. 6.6), that were not highlighted by previous analyses (core description, grain-size analysis, petrographic analysis, seismic facies analysis). The Ba/Al, used as proxy to determine the productivity, together with Br/ Al, point out two different units, the upper one from, 0 to 120 cm, and the basal one, from 120 to 320 cm. In particular, this strong variation highlights a marine sand unit at the top and a sorted sand with bioclastic unit at the base that records a different environment of sedimentation. Moreover, other elemental ratios highlight the same two units. Si/Ti, K/Ti and Al/Ti, that are proxy for terrigenous sediment delivery and are used to emphasize provenance differences of detrital material, highlight low values in correspondence of the marine unit and higher values in correspondence of the sorted sand unit (Fig. 6.6). Furthermore, Si/Ti ratio, in core RV11_H113, increasing in correspondence of the sorted sand unit, supports the previous results of petrographic analysis of the entire transgressive deposit, highlighting a strong terrigenous input controlled by high amount of quartzolithic supply.

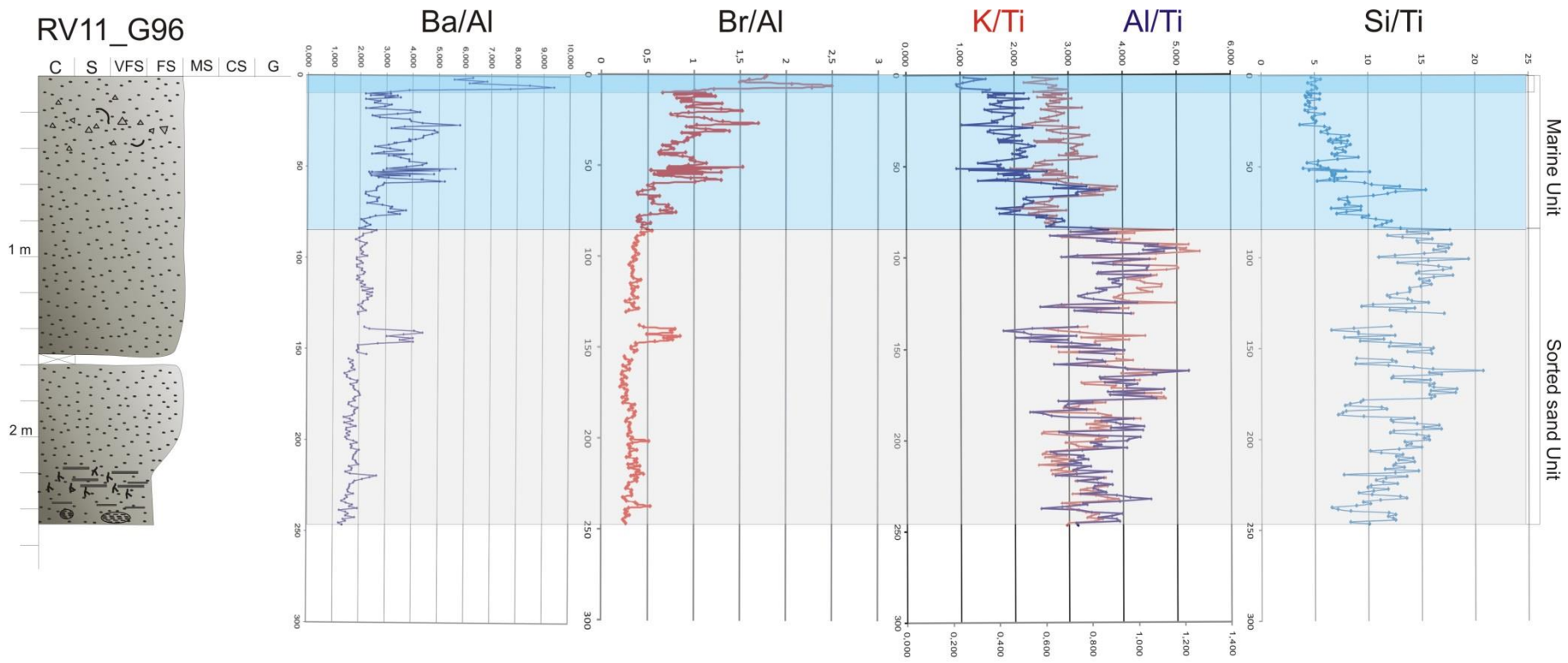

Fig. 6.4: Standard geochemical ratios highlighted by the XRF core scanner in order to describe the RV11_G96 core. Ba/Al and Br/Al are used as productivity proxies, while Si/Ti, Al/Ti and K/Ti are used as terrigenous sediment supply proxies. Two different units are distinguished: at the top a marine unit with a strong peak in the first centimeters of the core, and at the base a sorted sand unit.

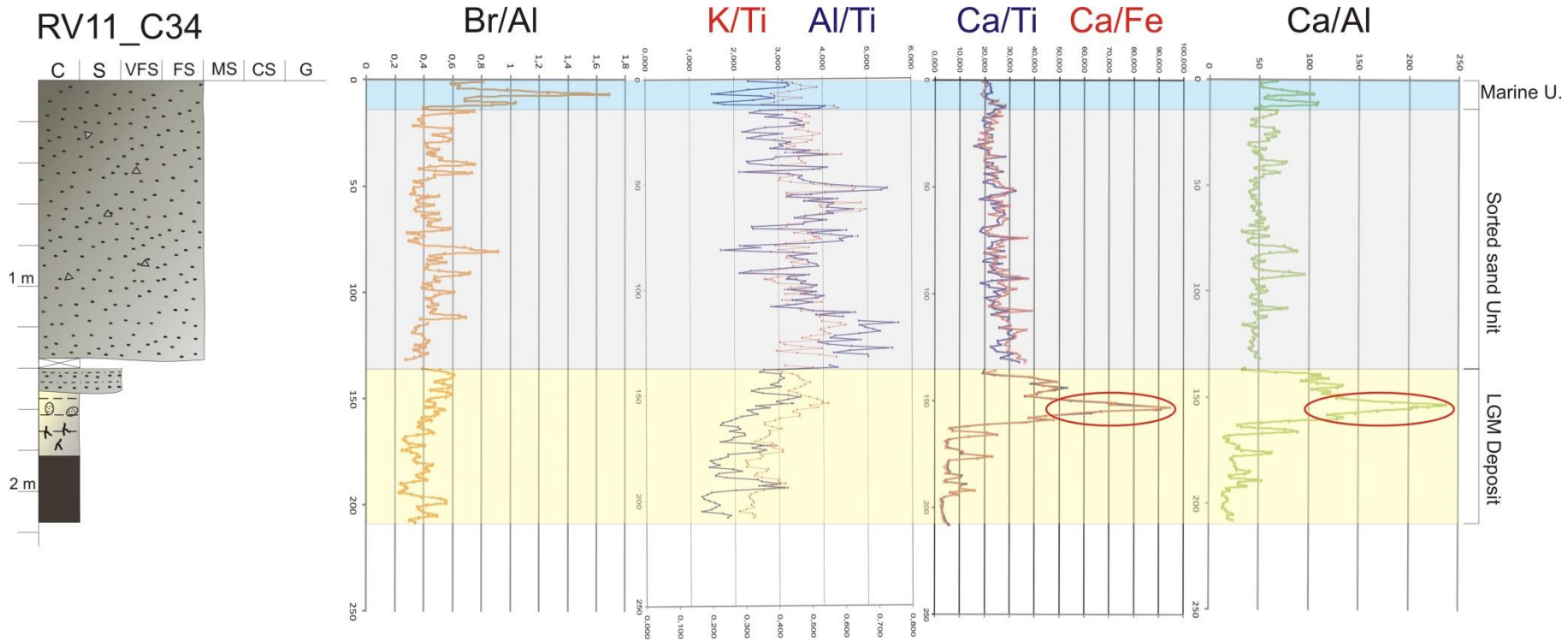

Fig. 6.5: Standard geochemical ratios highlighted by the XRF core scanner in order to describe the RV11_C34 core. Ba/Al is used as productivity proxy, while Al/Ti and K/Ti are used as terrigenous sediment supply proxies. Moreover, Ca, Ca/Fe and Ca/Ti emphasize a strong peak related to a pale-clay layer. In particular, three different units are identified: a marine unit at the top, a sorted sand unit in the middle, and a continental (LGM deposit) unit at the base.

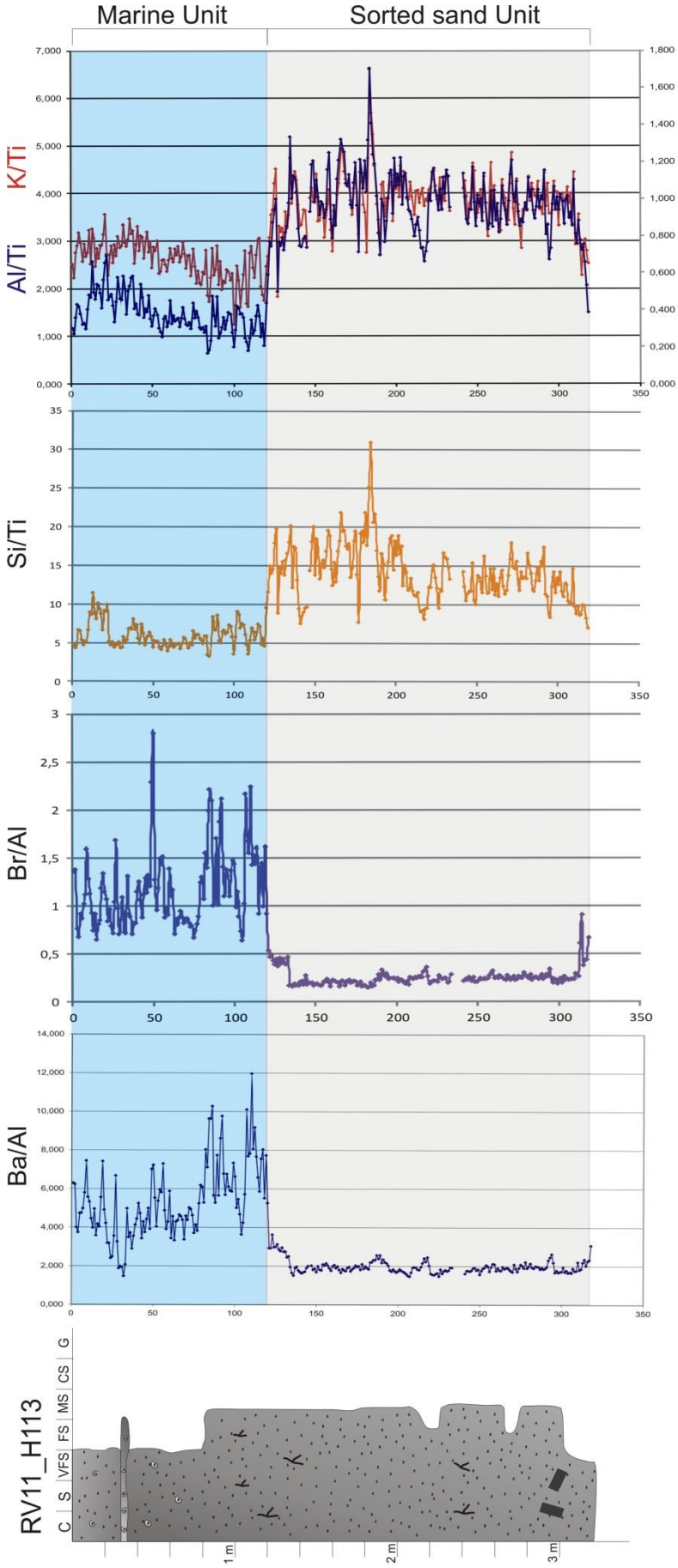

Fig. 6.6: Standard geochemical ratios highlighted by the XRF core scanner in order to describe the RV11_H113 core. Ba/Al and Br/Al are used as productivity proxies, while Si/Ti, Al/Ti and K/Ti are used as terrigenous sediment supply proxies. Two different units are recognized: at the top a marine unit, at the base a sorted sand unit.

The transgressive deposit south of the Po delta was investigated with the cores AR00_C15 and AS14_14, that can be composed together in order to identify the geochemical behaviour related to a transitional environment. This deposit, considered in detail in Moscon et al. (2015), is formed by a paralic unit at the top, and three transitional units at the base. The top unit corresponds to a barrier lagoon environment, characterized by a sorted sand portion and basal mud and organic-rich layers. The lower units are indicative of lagoon and delta plain environments, mainly characterized by clay sediments and bordered by peat and organic-rich layers. Moreover, this transgressive deposit is delimited at the base by the transgressive surface which marks a strong variation in depositional environments. In this case, the XRF analysis mainly focus on the transitional sediments recorded below to the sand portion, in order to identify a possible correlation between transgressive units.

AR00_C15

The AR00_C15 is 330 cm long and it is characterized at the top by a thin layer of clay sediment that rests on 90 cm of fine sand, and a 220 cm long basal portion of clay and peat layers. The thin layer of clay sediment at the top is indicative of high-stand deposit and, below this unit, the XRF analysis highlights two main units forming the sand portion and four main units forming the basal clay and the peat layers portion (Fig. 6.7). Considering the sand portion, Ba/Al and Ca/Fe productivity proxies record higher values at the top, from 10 to 40 cm, that are indicative of marine sand. The terrigenous proxies, Si/Ti Al/Ti and K/Ti, have high values in correspondence of the basal sand unit, even if the ratio decrease downward due to the episodic deposition of organic matter. This unit is representative of paralic sand affected in the basal portion by the variation in lithology. Regarding the four units identified below to the sand body, they are bounded by peat layers, that record low values of Ca/Ti and Ca/Fe and high values of Fe/Al, S and Sr/Ca (Fig. 6.7). The Ca/Fe, in this case, was the more suitable proxies showing relatively high values in correspondence of the clay layers and low values in correspondence of the underlying peat layers.

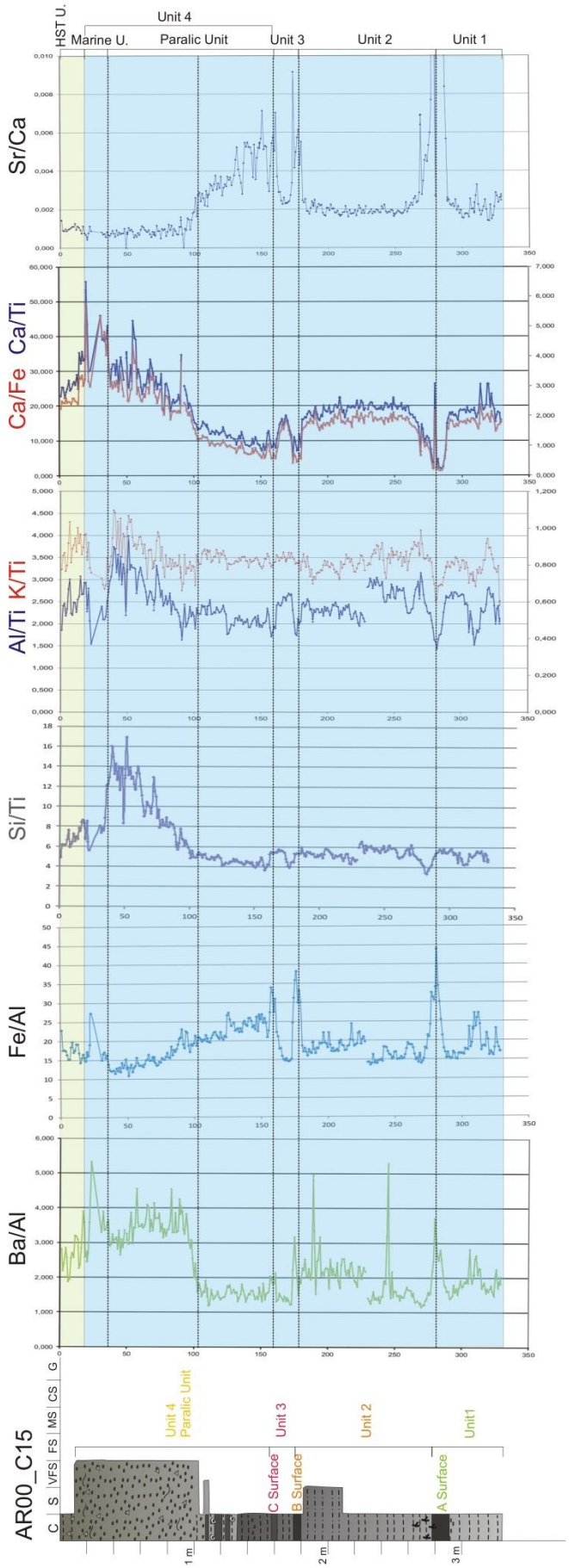

Fig. 6.7: Standard geochemical ratios highlighted by the XRF core scanner in order to describe the AR00_C15 core. Ba/Al and Ca/Fe are used as productivity proxies, while Si/Ti, Al/Ti and K/Ti are used as terrigenous sediment supply proxies. Ca/Ti and Ca/Fe record low values while, Fe/Al and Sr/Ca record high values in correspondence to peat and organic rich layers. Five different units are identified, especially, three transitional units at the base and a paralic unit, formed by a clay portion and a sand portion, and a marine unit at the top.

AS14_14

The AS14_14, belonging to the same transgressive deposit of AR00_C15, has a length of 455 cm and it is characterized by 30 cm of fine sands that rest on alternating peat and clay layers. This core was collected in a dragging area, about 2 km south of the AR00_C15 core, in order to reach the base of the transgressive deposit. The core AS14_14 is characterized by a record similar to AR00_C15, but reaches deeper sediments. In order to compare AS14_14 with AR00_C15, Ca/Fe, Sr/Ca and Fe/Al were analysed (Fig. 6.8). Fe/Al and Sr/Ca, as in AS14_14, highlight significant peak in correspondence of the peat layers, and Ca/Fe allowed an optimal correlation with AR00_C15 insofar as records relatively high values at clay layers and low values at peat layers. Moreover, at the basal portion of the core, abrupt and anti-correlated peak, related to stiff clay sediment, was observed. This significant peak highlights a different environment of sedimentation connected to the transition from glacial to interglacial conditions. The basal stiff clay is indicative of a continental environment formed during the LGM, whereas the whole AS14_14, except the basal portion, and the AR00_C15 are indicative on a transitional environment formed during the last transgressive cycle.

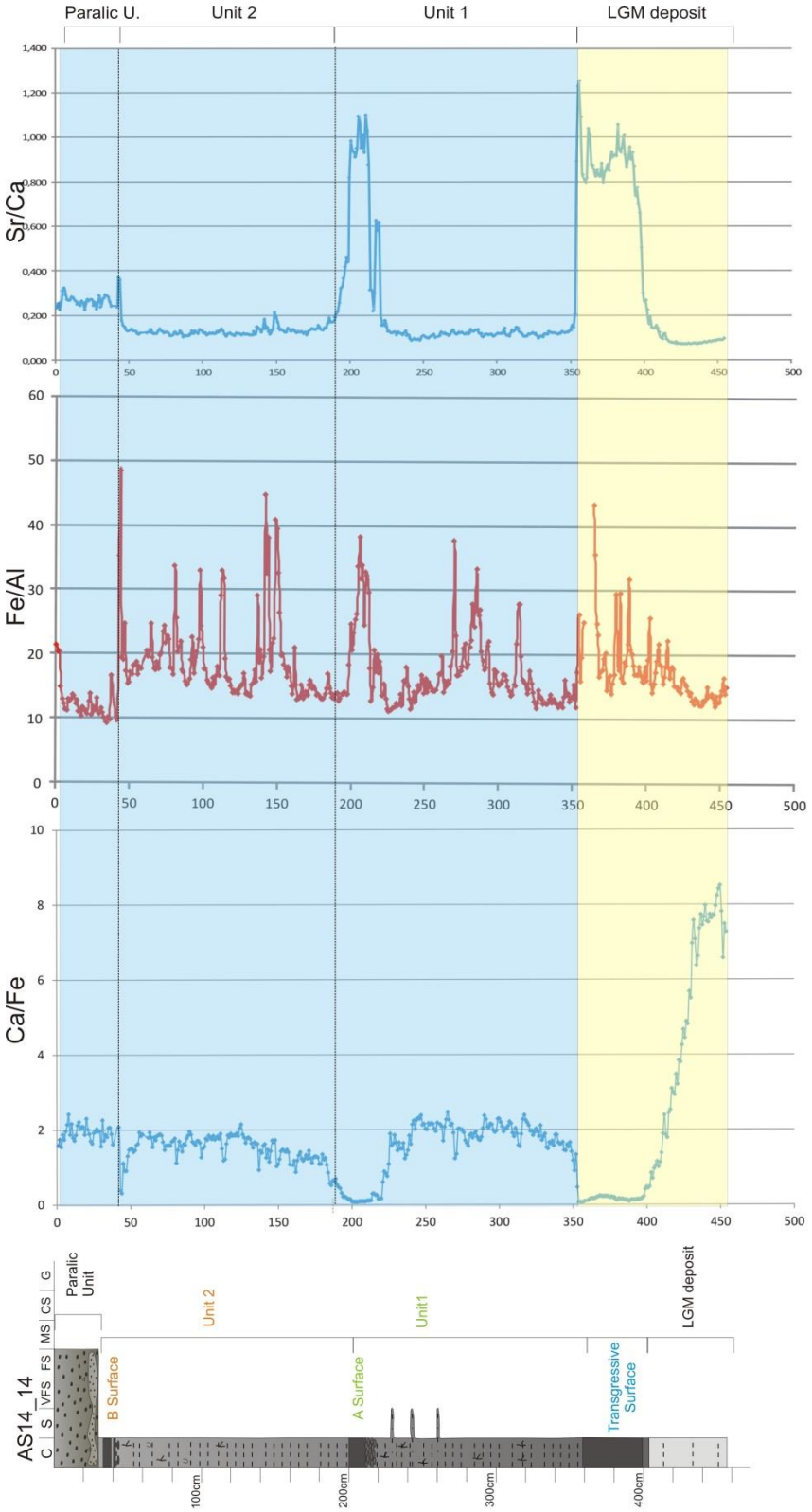

Fig. 6.8: Standard geochemical ratios highlighted by the XRF core scanner in order to describe the AS14_14 core. Ca/Fe, as in core AR00_C15, records low values in correspondence to peat and organic rich layers, while Fe/Al and Sr/Ca record high values. Moreover, Ca/Fe emphasizes a strong and anti-correlated peak related to a stiff clay layer at the base of the core. Four unit are highlighted: a small paralic unit at the top, two transitional unit in the middle and a continental (LGM deposit) unit at the base.

The XRF analysis, on AR00_C15 and AS14_14, allowed to clearly identify the geochemical variation connected with different environment of sedimentation related to the transition from glacial to interglacial conditions. Moreover, as described in Moscon et al., (2015), this method allowed to recognize the four units forming the deposit on the base of the geochemical variations. In particular, this transgressive deposit is characterized by a marine sand unit at the top that rests on paralic sediments formed by a sand unit indicative of beach environment and basal clay and peat layers unit indicative of lagoon environment. Below the paralic portion three different units were distinguished. These units, recording transitional environment of alluvial plain and lagoons, are characterized by clay sediments bordered at the top by peat and organic rich layers.

Thus, this innovative method, together with core facies analysis, allowed to identify the appropriate proxies in order to highlight transitional environments formed during the last relative sea-level rise and discriminate them by continental deposits. Moreover, Ca/Fe, Fe/Al and Sr/Ca emphasized different transitional units, whereas Ca/Fe proxy was utilized to identify strong geochemical variation in relation to the transition from glacial to interglacial conditions.

6.4 Geochemical proxies in the northern Adriatic Sea

The XRF core scanner analysis gave new interesting results in order to identify the proper proxies for the geochemical characterization of transgressive environments in the northern Adriatic Sea. The more significant elements and ratios were highlighted, both to describe the upper sand portion and the basal clay and organic rich layers portion. In particular for the sand portion, the most important results were emphasized by the productivity proxy that allow to distinguish marine sand from sorted sand. Ba/Al points out the best response, recording high and similar values per each sand portion analysed, in correspondence to the marine sand. Especially, Ba/Al ratio highlights the sand portions affected by marine processes, accordingly, the higher values are related to water/sediment interface. Concerning the terrigenous proxy, Al/Ti,

K/Ti and Si/Ti highlighted significant results. They generally mark increasing values in correspondence of the sorted sand portions, moreover their values varies in relation to the changes in terrigenous supply. Below the sand portion, the sediments were mainly described by Ca/Fe and Fe/Al ratios. Significant peaks of Fe/Al and S were identified in correspondence of peat or organic-rich layers that are indicative of suboxic-anoxic environment, which allows to preserve the organic matter. Whereas, the Ca/Fe proxy was used to distinguish different units forming the transitional environment, but, above all, was essential in order to identify continental sediments related to climatic change. Moreover, Sr/Ca ratios recorded strong pecks related to peat layers in transitional environments. Besides this result, in the sandy portion significant values of Sr/Ca ratio are indicative of shallow water environment.

Summarizing the obtained results, the marine sand that belong to the transgressive deposits highlight comparable values of Ba/Al in the northern Adriatic Sea; the terrigenous proxies show varying values in response of the terrigenous supply, but an increase connected with the sorted sand portions was documented in all the considered cores. Whereas, the Ca/Fe and Ca/Al proxies, allowed to distinguish different transitional units related to relative sea-level rise and allowed to identify LGM continental sediments, showing abrupt and anti-correlate peaks.

CHAPTER 7
DISCUSSIONS AND CONCLUSIONS

In the last decades several authors have focused their study on the stratigraphic evolution of the Adriatic basin in order to investigate and understand the impact of the late Quaternary fluctuations (Trincardi et al., 1994; Correggiari et al., 1996a; Ridente and Trincardi, 2008). The sea-level rise is a currently urgent and outstanding issue due to its potential impacts as coastal erosion, salinization of surface and ground waters, and drowning of coastal land and increasing flooding frequency. Thus, the past sea-level reconstruction could be a proper approach in order to predict more confidently what is going on in the near future. The relative sea-level variations have a significant impact on the continental margin architecture, and in particular, on the barrier-lagoon and delta coastal systems (Penland et al., 1988). The northern Adriatic shelf has been identified as a favourable geological laboratory to study in detail different generation of drowned transgressive deposits, that represent fossil record of different sea-level phases during the last transgression cycle. The low gradient of the northern Adriatic shelf, indeed, favoured the preservation of paleo shorelines, as few meters of sea-level rise caused the rapid landward shift of the shoreline for several tens of kilometres. The characterization of these preserved fossil deposits, that are the results of strong reworking and subsequent drowning and testify the last relative sea-level rise can highlight different environments response in relation to the relative sea-level rise. Moreover, they can evidence a more detailed knowledge of the last transgressive cycle.

In this research several transgressive deposits in the northern Adriatic Sea were considered.

A key area, previously identified by Correggiari et al., (2011), was analysed through a huge dataset of VHR seismic profiles and cores. This deposit, located south of the present Po River delta (Fig. 1.1), was sedimented in a portion of the shelf affected by strong sediment supply fed by an ancient

channel belt of the Po River, that allowed an early aggradation phase of the system. In particular, the extraordinary preservation of this sedimentary body was related to several factors such as its position (close to the Po River delta), the low gradient of the shelf, and the rapid drowning of the system. Therefore, the study of this transgressive deposit allowed to reconstruct and chronologically constrain its evolution in relation to the last relative sea-level rise. This transgressive deposit recorded initially an aggradation phase testified by the transitional units dating, from 10,950 to 9,800 yr cal. BP. Moreover, the organic-rich and peat layers radiocarbon data allowed to calculate the rate of sedimentation per unit. In particular, Unit 1, up to 1 m thick, was deposited in 500 yr, Unit 2, up to 2 m thick, was deposited in 300-500 yr and Unit 3, up to 1 m thick, was deposited in 200 yr. Afterwards, when the sea-level reached the transgressive deposit position, a barrier-lagoon system took place, corresponding to by the paralic unit. The rapid relative sea-level rise, estimated about 0.4 cm/yr, drowned the investigated transgressive deposit causing erosion and sediment removal in the top paralic body. The accurate reconstruction of a drowned coastal system response, emplaced in a low gradient shelf highlighting the rate of sea-level rise, the rate of aggradation and the environment evolution, was carried out with the aim to reconstruct the past relative position during the last transgression and predict a possible scenario of environmental changes under rising sea-level conditions.

The second phase of the research considered other transgressive deposits that are located north of the Po River delta and hve been sedimented and reworked during more recent sea-level rise phases (Fig. 1.1). These deposits, sedimented in a dynamic environment characterized by different fluvial input, recorded distinct paleo shorelines that testify the last phases of the transgression. Their sand portions were analysed with petrographic analysis in order to highlight their provenance and clarify fluvial supplies. The compositional results, stressed by the rock fragments determination, allowed to define three petrofacies reflecting distinct fluvial provenances in relation to different sea-level phases. On the base of the previous ground-truth and accurate seismic and compositional analysis, allowed a preliminary paleogeography reconstruction of the northern Adriatic shelf during the last relative sea-level rise. In particular, 1) through composition analysis a potential

northward shifting of a paleo Po trunk river was detected when the sea-level was -30 m msl. 2) Different fluvial contributions were distinguished along a fossil shoreline (between -20 and -24 m msl) that had been affected by possible clockwise long-shore drifting currents. 3) An ancient Tagliamento deltaic lithosome at -11 m msl was identified. Also in this case, the preliminary paleogeography reconstruction was carried out in order to trace environmental changes and evolution which occurred in the past.

The characterization of relict transgressive deposits in a low-gradient shelf is also important to identify the exploitable sand deposits for beaches nourishment by volumes calculation, grain-size and composition analysis. Nowadays, beach erosion is an existing problem as much as the sea-level rise, and the exploitation of the sand portion of the transgressive deposits is a reasonable method to reduce coastal erosion, prevent flooding and maintain a wide recreational beach. With the purpose of evaluating the sand portion geochemical characteristics, the XRF core scanner was tested on 5 selected cores. This innovative method highlighted interesting results in order to differentiate sand portion belonging to different sedimentary process, that was not possible to distinguish with other methods. Moreover, some geochemical proxies, related to marine sand and sorted sand were detected. In particular, Ba/Al ratio, indicative of the productivity proxy, recorded the best response in correspondence to the marine sand. On the contrary, Al/Ti, K/Ti and Si/Ti, indicative of terrigenous supply proxies, recorded the best response in relation to the changes in terrigenous supply. Furthermore, the investigations carried out through XRF core scanner on the cores collected in the southern deposits allowed to recognize the proper proxies for the geochemical characterization of transitional environments (Ca/Fe and Sr/Ca) in the northern Adriatic Sea. Moreover, these analyses evidenced the proxies to identify the geochemical variation connected with different environments of sedimentation related to glacial-interglacial cycle (Ca/Fe and Ca/Al).

The results obtained from this thesis could be the starting point for future improvements. Focussing on the transgressive sand portion as an economical resource, the construction and implementation of a georeferenced database related to the sand characterisation in terms of composition, petrographic signature and colour properties could be an efficient tool to identify

the best areas for exploitation of relict offshore sand bodies, managing the information related to grainsize, petrographic and geochemical composition. Furthermore, a detailed sand characterization and an accurate comparison between present beach sand with offshore transgressive sand could improve the geodatabase. This information could improve the existing geodatabase suite (in_Sand and env_Sand) recently implemented to exploit offshore sand deposits by CNR-ISMAR and regional Adriatic administrations (Correggiari et al., 2011; Correggiari et al., 2015; Grande et al., 2016). At the same time, a detailed characterization of other transgressive deposits could improve the Adriatic sea-level curve and the reconstruction of paleo environmental variation that occurred during the last sea-level rise.

This PhD thesis contributes to increase the knowledge of the transgressive deposits in northern Adriatic, which represent an important data source to reconstruct the environmental changes that occurred in a low-gradient shelf. Transgressive deposits are an interesting and exploitable economic resource for nourishing the present beaches, in order to reduce the coastal erosion and at the same time maintain the touristic resource available.

Summarising, the main results are:

- ✓ Detailed characterization of one transgressive deposit sedimented on a portion of the shelf favourable to the preservation. In particular, three aggradational transitional units were identified at the base of the deposit, each of them capped by organic-rich layers, whereas a paralic unit was present at the top. The radiocarbon data of the organic-rich layers allowed to temporally constrain the deposit and permitted to calculate the rate of sedimentation of each unit and to estimate the rate of the relative sea-level riseduring their deposition. Thus, this study allows to reconstruct with a high detail tract of the relative sea-level curve, that was not well-defined in the pre-existing literature of all Mediterranean Sea.
- ✓ Petrographic analysis on eight transgressive deposits was carried out in order to highlight their composition and obtain a preliminary

paleogeography reconstruction in relation to three different sea-level phases. Fluvial drainage and provenance variation were highlighted in a low-gradient shelf fed by Alpine rivers characterized by low sediment supply. In particular, the composition of the transgressive deposits belonging to the ancient sea-level phase allowed to suggest a northward shifting of a paleo Po trunk River; the transgressive deposits belonging to the second sea-level phase recorded a fossil shoreline characterized by different fluvial contributions; while the composition of the transgressive deposit belonging to the more recent sea-level phase confirms a Tagliamento River supply. Moreover the petrographic results can be processed in order to identify the exploitable sand deposits in relation to different coastal areas affected by erosion and sediment removal.

- ✓ The sand portion of the transgressive and transitional deposits was also investigated through XRF core scanner to acquire geochemical proxies. The study tested this innovative method to support environmental interpretation related to climatic changes which occurred in the past. Ba/Al ratio recorded the best response in relation to marine sand units, Al/Ti, K/Ti and Si/Ti recorded the best response in relation to sorted sand units. Furthermore, Ca/Fe allowed to highlighted different transitional units related to sea-level rise and permitted to distinguish LGM continental sediments.
- ✓ The results of this thesis are reported in a paper that has been selected for the “AIQUA Nagoya Award” (Moscon et al., 2015), a second paper will be submitted shortly and a third regarding the XRF data is in progress.

BIBLIOGRAPHY

Allen, J.R.M., Brandt, U., Brauer, A., Hubberten, H.W., Huntley, B., Keller, J., Kraml, M., Mackensen, A., Mingram, J., Negendank, J.F.W., Nowaczyk, N.R., Oberhänsli, H., Watts, W.A., Wulf, S., and Zolitschka, B., 1999, Rapid environmental changes in southern Europe during the last glacial period: Nature, v. 400, p. 740–743.

Amorosi, A., Fontana, A., Antonioli, F., Primon, S., and Bondesan, A., 2008, Post-LGM sedimentation and Holocene shoreline evolution in the NW Adriatic coastal area: GeoActa, v. 7, p. 41-67.

Amorosi, A., Maselli, V., and Trincardi, F., 2015, Onshore to offshore anatomy of a late Quaternary source-to-sink system (Po Plain–Adriatic Sea, Italy): Earth Science Reviews, in press, doi:10.1016/j.earscirev.2015.10.010

Antonioli, F., Amorosi, A., Fontana, A., Bondesan, A., Braitenberg, C., Dutton, A., Ferranti, L., Fontolan, G., Furlani, S., Lambeck, K., Mastronuzzi, G., Monaco, C., Orrù, P., 2009, A review of the Holocene sealevel changes and tectonic movements along the Italian coastline: Quaternary International, v. 206, p. 102-133.

Argnani, A., and Frugoni, F., 1997, Foreland deformation in the Central Adriatic and its bearing on the evolution of the Northern Apennines: Ann. Geof., v. 40, p. 771-780.

Argnani, A., and Gamberi, F., 1996, Stili strutturali al fronte della catena appenninica nell'Adriatico centro-settentrionale: Studi Geologici Camerti Volume Speciale, 1995/1, p. 19–27.

Argnani, A., and Ricci Lucchi, F., 2001, Tertiary Siliciclastic Turbidite Systems. In: Vai, G.B., and I.P. Martini (Eds.), Anatomy of an Orogen: the Apennines and adjacent Mediterranean basins, Kluwer Academic Pubblication, p. 327-350, Dordrecht, Netherlands.

Ariztegui, D., Asioli, A., Lowe, J.J., Trincardi, F., Vigliotti, L., Tamburini, F., Chondrogianni, C., Accorsi, C.A., Bandini Mazzanti, M., Mercuri, A.M., Van der Kaars, S., McKenzie, J.A., and Oldfield, F., 2000,Palaeoclimate and the formation of sapropel S1: inferences from Late Quaternary lacustrine and marine sequences in the central Mediterranean region: Palaeogeography, Palaeoclimatology, Palaeoecology, v. 158, p. 215–240.

Artegiani, A., Bregant, D., Paschini, E., Pinardi, N., Raicich, F., and Russo, A., 1997a, The Adriatic Sea general circulation. Part I Air-sea interactions and water mass structure: J. Phys. Oceanogr., v. 27, p. 1492–1514.

Artegiani, A., Bregant, D., Paschini, E., Pinardi, N., Raicich, F., and Russo, A., 1997b, The Adriatic Sea general circulation. Part II Baroclinic circulation structure: J. Phys. Oceanogr., v. 27, p. 1515–1532.

Arz, H.W., Pätzold, J., Müller, P.J., and Moammar, M.O., 2003, Influence of Northern Hemisphere climate and global sea level rise on the restricted Red Sea marine environment during termination: Paleoceanography, v. 18, p. 1053. doi:10.1029/2002PA000864

Asioli, A., Trincardi, F., Lowe, J.J., Ariztegui, D., Langone, L., and Oldfield, F., 2001, Sub-millennial climatic oscillations in the Central Adriatic during the last deglaciation: paleoceanographic implications: Quaternary Science Reviews, v. 20, p. 33–53.

Bahr A, Lamy F, Arz H, Kuhlmann H, Wefer G (2005) Late glacial to Holocene climate and sedimentation history in the NW Black Sea: Mar Geol 214:309–322. doi:10.1016/j.margeo. 2004.11.013

Bahr, A., Lamy, F., Arz, H.W., Major, C., Kwiecien, O., and Wefer, G., 2008, Abrupt changes of temperature and water chemistry in the late Pleistocene and early Holocene Black Sea: Geochem Geophys Geosyst, v. 9, Q01004.

Bally, A., Burbi, L., Cooper, C., and Ghelardoni, R., 1986, Balanced sections and seismic reflection profiles across the Central Apennines: Mem. Soc. Geol. Ital., v. 35, p. 257–310.

Bard, E., Hamelin, B., and Fairbanks, R.G., 1990, U-Th ages obtained by mass spectrometry in corals from Barbados: sea level during the past 130000 years: Nature, v. 346, p. 456-458.

Bard, E., Hamelin, B., Arnold, M., Montaggioni, L., Cabioch, G., Faure, G., and Rougerie, F., 1996: Deglacial sea-level record from Tahiti corals and the timing of global meltwater discharge, Nature, v. 382, p. 241-244.

Bard, E., 2003, Tahiti Deglacial Relative Sea Level Reconstruction, IGBP PAGES/World Data Center for Paleoclimatology Data Contribution Series 2003-028. NOAA/NGCD Paleoclimatology Program, Boulder CO, USA.

Belknap, D.F., and Kraft, J.C., 1981, Preservation potential of transgressive coastal lithosomes on the U.S. Atlantic shelf: Marine Geology, v. 42, p. 429–442.

Belknap, D.F., and Kraft, J.C., 1985. Influence of antecedent geology on stratigraphic preservation potential and evolution of Delaware's barrier systems: Marine Geology, v. 63, p. 235– 262.

Bertotti, G., Casolari, and E., Picotti, 1999, The Gargano promontory: A Neogene contractional belt within the Adriatic plate: Terra Nova, v. 11, p. 168–173.

Blanchet, C.L., Thouveny, N., Vidal, L., Leduc, G., Tachikawa, K., Bard, E., and Beaufort, L., 2007, Terrigenous input response to glacial/interglacial climatic variations over southern Baja California: a rock magnetic approach: Quat Sci Rev, v. 26, p. 3118–3133.

Blott, S.J., Pye, K., 2001, Gradistat: A grain size distribution and statistics package for the analysis of unconsolidated sediments: Earth Surf. Proces. Landf., v. 26, p. 1237–1248.

Bondesan, M., Castiglioni, G.B., Elmi, C., Gabbianelli, G., Marocco, R., Pirazzoli, P.A., and Tomasin, A., 1995, Coastal areas at risk from storm surges and sea-level rise in northeastern Italy: Journal of Coast. Res., v. 11, p. 1354-1379.

Caley, T., Malaizé, B., Zaragosi, S., Rossignol, L., Bourget, J., Eynaud, F., Martinez, P., Giraudeau, J., Charlier, K., and Ellouz-Zimmerman, N., 2011, New Arabian Sea records help decipher orbital timing of Indo-Asian monsoon: Earth Planet Sci. Lett., v. 30, p. 433–444.

Calvert, S.E., and Pedersen, T.F. 2007, Elemental proxies for palaeoclimatic and palaeoceanographic variability in marine sediments: interpretation and application, In: Hillaire-Marcel C, De Vernal A (eds) Proxies in Late Cenozoic Paleoceanography: Dev Mar Geol, Elsevier, p. 567–644.

Cardinal, D., Savoye, N., Trull, T.W., Andre, L., Kopczynska, E.E., and Dehairs, F., 2005, Variations of carbon remineralisation in the Southern Ocean illustrated by the Baxs proxy: Deep Sea Res., v. 52, p. 355–370.

Carminati, E., Doglioni, C. and Scrocca, D. 2003, Apennines subduction-related subsidence of Venice: Geophysical Research Letters, v. 30 (13): 1717, doi: 10.1029/2003GL017001.

Castiglioni, G.B., 1978, Il ramo più settentrionale del Po nell'antichità: Atti e Memorie Accademia Patavina Scienze, Lett. Arti, v. 90, p. 157–164.

Castiglioni, G.B., 2004, Quaternary glaciations in the eastern sector of the Italian Alps, in Elhers, J., and Gibbard, P.l., eds., Quaternary Glaciations–Extent and Chronology–Part I: Europe, p. 209–215. Elsevier, Amsterdam.

Cattaneo, A., and Trincardi, F., 1999, The late-Quaternary transgressive record in the Adriatic epicontinental sea: Basin widening and facies partitioning, In: Bergman, K. and J. Snedden (Eds.), Isolated Shallow Marine Sand Bodies: Sequence Stratigraphic Analysis and Sedimentologic Interpretation: SEPM Spec. Publ. Soc. Sediment. Geol., v. 64, p. 127-146, Tulsa, Oklahoma.

Cattaneo, A., Correggiari, A., Langone L., and Trincardi, F., 2003, The late-Holocene Gargano subacqueous delta, Adriatic shelf: Sediment pathways and supply fluctuations: Marine Geology, v. 193, p. 61-91.

Cattaneo, A., Steel, R.J., 2003, Transgressive deposits: a review of their variability: Earth-Science Reviews, v. 62, p. 187–228.

Cattaneo, A., Trincardi, F., Asioli A., and Correggiari, A., 2007, The Western Adriatic shelf clinoform: energy-limited bottomset: Continental Shelf Research, v. 27, p. 506-525.

Catuneanu, O., 2006, Principles of Sequence Stratigraphy: Elsevier, Amsterdam, p. 375.

Catuneanu, O., Galloway, W.E., Kendall, C.G.St.C., Miall, A.D., Posamentier, H.W., Strasser, A., and Tucker, M.E., Sequence stratigraphy: methodology and nomenclature: Newsletters on Stratigraphy, v. 44, p. 173–245.

Cazzini, F., Dal Zotto, O., Fantoni, R., Ghielmi, M., Ronchi, P., and Scotti, P., 2015, Oil and gas in the Adriatic foreland, Italy: Jornal of Petroleum Geology, v. 38, p. 255-279.

Channell, J.E.T., D'Argenio, B., and Horvath, F., 1979, Adria, the African Promontory, in Mesozoic Mediterranean paleo- geography, Earth Science Rev., v. 15, p. 213-292.

Chiocci, F.L, Ercilla, G., and Torres, J., 1997, Stratal architecture of Western Mediterranean Margins as the result of the stacking of Quaternary lowstand deposits below glacio-eustatic fluctuation base-level: Sediment. Geol., v. 112, p. 195-217.

Ciabatti M., Curzi P.V., and Ricci Lucchi F., 1987, Quaternary sedimentation in the central Adriatic Sea: Giornale di Geologia, v. 3, p. 113-125.

Clark, P.U., Marshall McCabe, A., Mix A.C., and Weaver, A.J., 2004, Rapid rise of sea level 19000 years ago and its Global implications: Science, v. 304, p. 1141-1144.

Clark, P.U., Dyke, A.S., and Shakun, J.D., 2009, The last glacial maximum: Science, v. 325, p.710-714.

Correggiari, A., M. Roveri, and F. Trincardi, 1992, Regressioni forzate, regressioni deposizionali e fenomeni di instabilità in unità progradazionali tardo-quaternarie (Adriatico centrale): G. Geol., v. 54, p. 19–36.

Correggiari, A., Roveri, M., and Trincardi, F., 1996a, Late Pleistocene and Holocene evolution of the North Adriatic Sea: Il Quaternario, v. 9, p. 697-704.

Correggiari, A., Field, M. and Trincardi, F., 1996b, Late Quaternary transgressive large sand dunes on the sediment starved Adriatic shelf, In: De Baptist, M., and P. Jacobs (Eds.), Geology of Siliciclastic Shelf Seas: Geological Society Special Publications, v. 117, p. 155-169.

Correggiari, A., Trincardi, F., Langone, L., and Roveri, M., 2001, Styles of failure in heavilysedimented high-stand prodelta wedges on the Adriatic shelf: Journal of Sedimentary Research, v. 71, p. 218-236.

Correggiari, A., Cattaneo, A., and Trincardi, F., 2005, The modern Po delta system: lobe switching and asymmetric prodelta growth: Marine Geology, v. 222–223, p. 49–74.

Correggiari A., Aguzzi M., Remia A., and Preti, M. 2011, Caratteristiche sedimentologiche e stratigrafiche dei giacimenti sabbiosi in Mare Adriatico Settentrionale utilizzabili per il ripascimento costiero: Studi Costieri, v. 19, p. 11-31.

Correggiari, A., Remia, A., Foglini, F., Perini, L., Luciani, P., Piazza, P., and Pinato, T. 2015, Ricerca di depositi sabbiosi offshore come risorsa per le strategie di ripascimento costiero: nuove prospettive e architettura del geodatabase in_Sand utilizzato in nord Adriatico: Workshop, La risosrsa sabbia offshore per Il ripascimento costiero, 28/04/2015 Bologna (Italy).

Croudace, I.W, Rindby, A., and Rothwell, R.G., 2006, ITRAX: description and evaluation of a new multifunction X-ray core scanner. In: Rothwell RG (ed) New techniques in sediment core analysis: Geological Society Special Publication, v. 267, p. 51–63.

Curray, J.R., 1964, Transgressions and regressions. In: Miller, R.L. (Ed.), Papers in Marine Geology. Macmillan, New York, p. 175– 203.

Dal Piaz, G.V., Bistacchi, A., Massironi, M., 2003: Geological outline of the Alps, v. 26, p. 175–180.

D'Argenio, B., and Horvath, F., 1984, Someremarksonthedefor- mation history of Adria, from the Mesozoic to the Tertiary: Ann. Geophys., v. 2, p. 143-146.

Dehairs, F., Chesselet, R., and Jedwab, J., 1980, Discrete suspended particles of barite and the barium cycle in the open ocean: Earth Planet. Sci. Lett., v. 49, p. 528–550.

Dehairs, F., Baeyens, W., and Goeyens, L., 1992, Accumulation of suspended baite at mesopelagic depths and export production in the Southern Ocean: Science, v. 254, p.1332–1335.

De Marchi L., 1922, Variazioni di livello dell'Adriatico in corrispondenza delle espansioni glaciali: Atti della Accademia Scientifica Veneta-Trentino-Istriana, v.12-13, p. 3-15.

Dickinson, W.R., 1970, Interpreting detrital modes of greywacke and arkose: Journal of Sedimentary Petrology, v. 40, p. 695-707.

Diekmann, B., Hofmann, J., Henrich, R., Fütterer, D.K., Röhl, U., and Wei, K.Y., 2008, Detrital sediment supply in the southern Okinawa Trough and its relation to sea level and Kurishio dynamics during the late Quaternary: Mar. Geol., v. 255, p. 83–95.

Di Stefano, R., Kissling, E., Chiarabba, C., Amato, A., and Giardini, D., 2009, Shallow subduction beneath Italy, Three-dimensional images of the Adriatic-European-Tyrrhenian lithosphere system based on high quality P wave arrival times: Journal Geophysical Research, 114, doi: 10.1029/2008JB005641.

Doglioni, C., 1993, Geological evidence for a global tectonic polarity: Journal of the Geological Society of London, v. 150, p. 991-1002.

Doglioni, C., Mongelli, F., and Pieri, P., 1994, The Puglia uplift (SE Italy): An anomaly in the foreland of the Apenninic subduction due to buckling of a thick continental lithosphere: Tectonics, v. 13, p. 1309-1321.

Doglioni, C., and Carminati, E., 2002, The effects of four subductions in NE Italy. Transalp conference, Mem. Soc. Geol., v. 54, p. 1-4.

Fabbri A., Argnani A., Bortoluzzi G., Correggiari A., Gamberi F., Ligi M., Penitenti D., Roveri M., and Trincardi, F., 2001, Note Illustrative della Cartografia Geologica dei mari italiani scala 1:250.000: Foglio NL 33-10 Ravenna.

Fabbri, A., Argnani, A., Bortoluzzi, G., Correggiari, A., Gamberi, F., Ligi, M., Marani, M., Penitenti, D., Roveri, M., and Trincardi, F., 2002, Carta geologica dei mari italiani alla scala 1:250.000. Guida al rilevamento. Presidenza del Consiglio dei Ministri, Dipartimento per i Servizi Tecnici Nazionali, Servizio Geologico: Quaderni serie III, 8, p. 1–93.

Fabris, M., Achilli, V., Menin, A., 2014, Estimation of Subsidence in Po Delta Area (Northern Italy) by Integration of GPS Data, High-Precision Leveling and Archival Orthometric Elevations:International Journal of Geosciences, v. 5, p. 571-585.

Fairbanks, R.G., 1989, A 17.000-yr glacio-eustatic sea level record: influence of glacial melting rates on the Younger Dryas event and deep-ocean circulation: Nature, v. 342, p. 637-642.

Fairbanks, R.G., 1992, Barbados Sea Level and Th/U 14C Calibration. IGBP PAGES/World Data Center for Paleoclimatology Data Contribution Series 92-020. NOAA/NGDC Paleoclimatology Program, Boulder CO, USA.

Fantoni, R., and Franciosi, R., 2010, Mesozoic extension and Cenozoic compression in Po Plain and Adriatic foreland. In: Sassi FP (ed) Nature and Geodynamics of the Lithostere in Northern Adriatic, Rendiconti Lincei - Scienze Fisiche e Naturali.

Ferranti, L., Antonioli, F., Mauz, B., Amorosi, A., Dai Pra, G., Mastronuzzi, G., Monaco, C., Orrù, P., Pappalardo, M., Radtke, U., Renda, P., Romano, P., Sansò, P., and Verrubbi, V., 2006, Markers of the last interglacial sea level high-stand along the coast of Italy: tectonic implications: Quaternary International, v. 145–146, p. 30–54.

Fleming, K.P., Dan Zwartz, J., Yokoyama, Y., Lambeck, J., and Chappell, J., 1998, Refining the eustatic sea-level curve since the Last Glacial Maximum using far- and intermediate-field sites: Earth and Planetary Science Letters, v. 163, p. 327-342.

Fontana, A., Mozza, P., and Bondesan, A., 2004, L'evoluzione geomorfologica della Pianura Veneto-Friulana, In: Geomorfologia della provincia di Vicenza, Bondesan, A., Meneghel, M., ed. Esedra, Padova, p. 113-138.

Fontana, A., 2006, Evoluzione geomorfologica della bassa pianura friulana e sue relazioni con le dinamiche insediative antiche (with enclosed the Geomorphological map of the Friulian low plain, scale 1:50,000): Monografie Museo Friulano Storia Naturale 47, Udine, p. 288.

Fontana, A., Mozzi, P., and Bondesan, A., 2008, Alluvial megafans in the Venetian–Friulian Plain (north-eastern Italy): evidence of sedimentary and erosive

phases during Late Pleistocene and Holocene: Quaternary International, v.189, p. 71-90.

Fontana, A., Mozzi, P., and Bondesan, A., 2010, Late Pleistocene evolution of the Venetian–Friulian Plain: Rendiconti Lincei, v. 21, p. 181-196.

Fontana, A., Mozzi, P., and Marchetti, M., 2014, Alluvial fans and megafans along the southern side of the Alps: Sedimentary Geology, v. 301, p. 150-171.

Francus, P., Lamb, H., Nakagawa, T., Marshall, M., Brown, E., and Suigetsu Project Members, 2009, The potential of high-resolution X-ray fluorescence core scanning: Pages News, v. 17, p. 93-96.

Gacic, M., Civitarese, G., Ursella, L., 1999, Spatial and seasonal variability of water and biogeochemical fluxes in the Adriatic sea, In: Malanotte-Rizzoli, P., Eremeev, V.N. (Eds.), The eastern Mediterranean as a laboratory basin for the assessment of contrasting ecosystems, Kluwer Academic Publishers, p. 335–357.

Gambolati, G., Teatini, P., and Ferronato, M., 2006, Anthropogenic Land Subsidence: In. Encyclopedia of Hydrological Sciences, Chapter 158,v. IV, M.G. Anderson (ed), J. Wiley, 2444-2459, 2005.

Garzanti, E., Vezzoli, G. Andò, S., Paparella, P., and Clift, P.D., 2005, Petrology of Indus River sands: a key to interpret erosion history of the Western Himalayan Syntaxis: Earth and Planetary Science Letters, v. 229, p. 287-302.

Garzanti, E., Doglioni, C., Vezzoli, G., and Andò, S., 2007, Orogenic belts and orogenic sediment provenances: Journal of Geology, v. 115, p. 315-334.

Gasperini L., Stanghellini, G., 2009, SEISPRHO: An interactive computer program for processing and interpretation of high-resolution seismic reflection profiles: Computers & Geosciences, v. 35, p. 1497-1507.

Gatto, P., and Previatello, P., 1974, Significato stratigrafico, comportamento meccanico e distribuzione della laguna di Venezia di un’argilla sovraconsolidata nota come “caranto”: CNR-ISDMG, V. 70.

Gazzi, P., 1966, Le arenarie del flysch sopracretaceo dell’Appennino modenese: correlazioni con il Flysch di Monghidoro: Mineralogy Petrography Acta, v. 12, p. 69-97.

Gazzi, P., Zuffa, G.G., Gandolfi, G., and Paganelli, L., 1973, Provenienza e dispersione litoranea delle sabbie delle spiagge adriatiche fra le foci dell’Isonzo e del Foglia: inquadramento regionale: Memorie della Società Geologica Italiana, v. 12, p. 1-37.

Gebhardt, H., Sarnthein, M., Grootes, P.M., Kiefer, T., Kühn, H., Schmieder, F. and, Röhl, U., 2008, Paleonutrient and productivity records from the subarctic North Pacific for Pleistocene glacial terminations I to V: Paleoceanography, v. 23, PA4212. doi:10.1029/2007PA001513.

Gordini, E., Marocco, R., and Vio, E., 2002, Stratigrafia del sottosuolo della Terrazza Grande (Adriatico-Settentrionale): Gortania, v., 24, p. 31-63.

Grande, V., Proietti, R., Foglini, F., Remia, A., Correggiari, A., Paganelli, D., Targusi, M., Franceschini, G., La Valle, P., Berducci, M.T, La Porta, B., Lattanzi, L., Lisi, I, Maggi, C., Loia, M., Pazzini, A., Gabellini, M ., and Nicoletti, L., 2015, Sistema Informativo per il monitoraggio ambientale della risorsa sabbiosa offshore nei progetti di protezione costiera: geodatabase env_Sand, ISPRA: Manuali e Linee guida, 127/2015.

Grützner, J., Hillenbrand, C.D., and Rebesco, M.A., 2005, Terrigenous flux and biogenic silica deposition at the Antarctic continental rise during the late Miocene to early Pliocene: implications for ice sheet stability and sea ice coverage, Glob Planet Change, v. 45, p. 131–149.

Harff, J., Endler, R., Emelyanov, E., Kotov, S., Leipe, T., Moros, M., Olea, R., Tomczak, M., and Witkowski, A., 2011, Late Quaternary climate variations reflected in Baltic Sea sediments, In: Harff J, Björck S, Hoth P (eds) The Baltic Sea Basin, v. 3, p. 99–132.

Hays, J.D., Imbrie, J., and Shackleton, N.J., 1976, Variations in the Earth's orbit: pacemaker of the ice ages: Science, v. 194, p. 1121–1132.

Helland-Hansen, W., Gjelberg, J.G., Conceptual basis and variability in sequence stratigraphy: a different perspective: Sedimentary Geology, v. 92, p. 31–52.

Hoang van, L., Clift, P.D., Schwab, A.M., Huuse, M., Nguyen, D.A., Zhen, S., 2010, Large-scale erosional response of SE Asia to monsoon evolution reconstructed from sedimentary records of the Song Hong-Yinggehai and Qiongdongnan basins, South China Sea: Geol Soc Spec Publ, v. 342, p. 219–244.

Hodell, D.A., Channell, J.E.T., Curtis, J.H., Romero, O.E., and Röhl, U., 2008, Onset of 'Hudson Strait' Heinrich events in the Eastern North Atlantic at the end of the Middle Pleistocene transition (~ 640 ka)?: Paleoceanography, v. 23, PA4218.

Ingersoll, R.V., Bullard, T.F., Ford, R.L., Grimm, J.P., Pickle, J.D., and Sares, S.W., 1984, The effect of grain size on detrital models: a test of Gazzi-Dickinson point-counting method: Journal of Sedimentary Petrology, v.54. p. 103-116.

Instruments, L.-C.S., 2000, Multibeam sonar theory of operation, available at: www.mbari.org/data/mbsystem/sonarfunction/SeaBeamMultibeamTheoryOperation.pdf

Ivanov, M.V., 1981, The global biogeochemical sulphur Cycle. In: Likens GE (ed) Some perspectives of the major biogeochemical cycles SCOPE, p. 61–78.

Jaccard, S.L., Haug, G.H., Sigman, D.M., Pedersen, T.F., Thierstein, H.R., and Röhl, U., 2005, Glacial/interglacial changes in Subarctic North Pacific stratification: Science, v. 308, p. 1003–1006.

Kleiven, H.F., Kissel, C., Laj, C., Ninnemann, U.S., Richter, T.O., and Cortijo, E., 2007, Reduced North Atlantic Deep Water coeval with the Glacial Lake Agassiz fresh water outburst: Science, v. 319, p. 60–64.

Kummerow, J., Kind, R., Oncken, O., Giese, P., Ryberg, T., Wylegalla, K., and Scherbaum, F., 2004, A natural and controller source seismic profile through the Eastern Alps: TRANSALP: Earth and Planetary Science Letters, v. 225, p. 115–129.

Lambeck, K., Yokoyama, Y., and Purcell, T., 2002, Into and out of the Last Glacial Maximum: sea level changes during Oxygen Isotope Stage 3 and 2: Quaternary Science Reviews, v. 21, p. 343-360.

Lambeck, K., Antonioli, F., Purcell, A., and Silenzi, S., 2004, Sea-level change along the Italian coast for the past 10,000 yr: Quaternary Science Reviews, v. 23, p. 1567-1598.

Lambeck, K., and Purcell, A, 2005, Sea-level change in the Mediterranean Sea since the LGM: model predictions for tectonically stable areas: Quaternary Science Reviews, v. 24, p. 1969-1988.

Lambeck, K., Purcell, A., Funder, S., Kjær, K.H., Larsen, E., and Möller, P., 2006, Constraints on the Late Saalian to early Middle Weichselian ice sheet of Eurasia from field data and rebound modelling: Boreas, v. 35, p. 539–575.

Lambeck, K., Rouby, H., Purcell, A., Sun, Y., and Sambridge, M., 2014, Sea level and global ice volumes from the Last Glacial Maximum to the Holocene: Pnas, v. 111, p. 15296-15303.

Lambeck, K., Antonioli, F., Anzidei, M., Ferranti, L., Leoni, G., Scicchitano, G. and Silenzi, S., 2011, Sea Level Change along the Italian Coast during the Holocene and Projections for the Future: Quaternary International, v. 232, p. 250-257.

Lebreiro, S.M., Voelker, A.H.L., Vizcaino, A., Abrantes, F.G., Alt-Epping, U., Jung, S., Thouveny, N., and Gràcia, E., 2009, Sediment instability on the Portuguese continental margin under abrupt glacial climate changes (last 60 kyr): Quat Sci Rev, v. 28, p. 3211–3223. doi:10.1016/j.quascirev.2009.08.007.

Lee, H. J. and Clausner, J. E., 1979, Seafloor Soil Sampling and Geotechnical Parameter Determination: Handbook, Technical Report, Civil Engineering Laboratory, Port Hueneme, California, TR-873, p. 128.

Malanotte-Rizzoli, P., and Bergamasco, A., 1983, The dynamics of the coastal region of the northern Adriatic Sea: J. Phys. Oceanogr., v. 13, p. 1105-1130.

Manca, B.B., Kovačević, V., Gačić, M., and Viezzoli, D., 2002, Dense water formation in the southern Adriatic Sea and spreading into the Ionian Sea in the period 1997–1999: J. Mar. Syst., v. 33–34, p. 133–154.

Marchesini, L., Amorosi, A., Cibin, U., Spadafora, E., Zuffa, G.G. and Preti, D., 2000, Detrital supply versus facies architecture in the Late Quaternary deposits of the south-eastern Po plain (Italy): Journal of Sedimentary Research, v. 70, p. 829-838.

Martinson, D.G., Pisias, N.G., Hays, J.D., Imbrie, J., Moore, T.C., and Shackleton, N.J., 1987, Age dating and the Orbital theory of Ice Ages: Development of a high-resolution 0 to 300,000 year chronostratigraphy: Quaternary Research, v. 27, p. 1-29.

Maselli, V., Trincardi, F., Cattaneo, A., Ridente, and D., Asioli, A., 2010, Subsidence pattern in the central Adriatic and its influence on sediment architecture during the last 400 kyr: Journal of Geophysical Researc, v. 115, B12106. doi:10.1029/2010JB007687

Maselli, V., Hutton, E.W., Kettner, A.J., Syvitski, J.P.M., and Trincardi, F., 2011, High-frequency sea level and sediment supply fluctuations during Termination I: An integrated sequence-stratigraphy and modelling approach from the Adriatic Sea (Central Mediterranean): Marine Geology, v. 287, p. 54-70.

Massari, F., Rio, D., Serandrei Barbero, R., Asioli, A., Capraro, L., Fornaciari, E., and Vergerio, P., 2004, The environment of Venice area in the past two million years: Palaeogeography, Palaeoclimatology, Palaeoecology, v. 202, p. 273–308.

Miller, E.L., Kuznetsov, N., Soboleva, A., Udoratina, O., Grove, M.J., and Gehrels, G., 2011, Baltica in the Cordillera?: Geology, v. 39, p. 791–794.

Miola, A., Bondesan, A., Corain, L., Favaretto, S., Mozzi, P., Piovan, S., and Sostizzo, I., 2006, Wetlands in the Venetian Po Plain (north-eastern Italy) during the

Last Glacial Maximum: vegetation, hydrology, sedimentary environments: Paleobotany and Palynology, v. 141, p. 53–81.

Monegato, G., Stefani, C., Zattin, M., 2010, From present rivers to old terrigenous sediments: the evolution of the drainage system in the eastern Southern Alps: Terra Nova, v. 22, p. 218-226.

Moreno, A., Nave, S., Kuhlmann, H., Canals, M., Targarona, J., Freudenthal, T., and Abrantes, F., 2002,Productivity response in the North Canary Basin to climate changes during the last 250000 years: a multi-proxy approach: Earth Planet Sci Lett, v. 196, p. 147–159.

Moscon, G., Correggiari, A., Stefani, C., Fontana, A., Remia, A., 2015, Very-high resolution analysis of a transgressive deposit in the Northern Adriatic Sea (Italy): Alpine and Mediterranean Quaternary, v. 28, p. 121-129.

Mozzi, P., Bini, C., Zilocchi, L., Becattini, R., and Mariotti Lippi, M., 2003, Stratigraphy, palaeopedology and palinology of Late Pleistocene and Holocene deposits in the landward sector of the lagoon of Venice (Italy), in relation to the 'caranto' level: Il Quaternario – Italian Journal of Quaternary Sciences, v. 16, p. 193–210.

Muttoni, G., Carcano, C., Garzanti, E., Ghielmi, M., Piccin, A., Pini, R., Rogledi, S., and Sciunnach, D., 2003, Onset of major Pleistocene glaciations in the Alps: Geology, v. 31, p. 989-992.

Nummedal, D., Swift, D.J.P, 1987, Transgressive stratigraphy at sequence-bounding unconformities: some principles derived from Holocene and Cretaceous example ,In: D Nummedal, O.H Pilkey, S.D Howard (Eds.), Sea level Fluctuation and Coastal Evolution, SEPM Special Publication, vol. 41, p. 241–260.

Ori, G.G., and Friend, P.F., 1984, Sedimentary basins formed and carried piggyback on active thrust sheets: Geology, v. 12, p. 475-478.

Ori, G.G., Roveri, M., and Vannoni, F., 1986, Plio-Pleistocene sedimentation in the Apenninic- Adriatic foredeep (central Adriatic Sea, Italy), In: Allen, P., and P. Homewood (Eds.), Foreland Basins, Int. Ass. Sediment., Spec. Pub., v. 8, p. 183-198, Blackwell Sci., Oxford, United Kingdom.

Pellegrini, C., Maselli, V., Cattaneo, A., Piva, A., Ceregato, A., and Trincardi, F., 2015, Anatomy of a compound delta from the post-glacial transgressive record in the Adriatic Sea: Mar. Geol., v. 362, p, 43–59.

Penland, P., Boyd, R., and Suter, J.R., 1988, Transgressive depositional systems of the Mississippi delta plain: a model for barrier shoreline and shelf sand development: Journal of Sedimentary Petrology, v. 58, p. 932-949.

Pieri, M., and Groppi, G., 1981, Subsurface geological structure of the Po Plain, Italy: Progetto Finalizzato Geodinamica, CNR Publ., v. 414, pp. 23, Roma, Italy.

Piper, D.J.W., and Aksu, A.E., 1992, Architecture of stacked Quaternary deltas correlated with global oxygen isotopic curve: Geology, v. 20, p. 415–418.

Piovan, S., Mozzi, P., and Stefani, C., 2010, Bronze Age Palaeohydrography of the Southern Venetian Plain: Geoarcheology, v. 25, p. 6-35.

Ren, J., Jiang, H., Seidenkrantz, M.S., and Kuijpers, A., 2009, A diatom-based reconstruction of Early Holocene hydrographic and climatic change in a southwest Greenland fjord, Mar Micropaleontol, v. 70, p. 166–176.

Remier, P.J.,Baillie, M.G.L.,Bard, E., Bayliss, A., Beck, J.W., Bertrand, C.J.H., Blackwell, P.G., Buck, C.E., Burr, G.S., Cutler, K.B., Damon, P.E., Edwards, R.L., Fairbanks, R.G., Friedrich, M., Guilderson, T.P., Hogg, A.G., Hughen, K.A., Kromer, B., McCormac, F.G., Manning, S.W., Ramsey, C.B., Reimer, R.W., Remmele, S., Southon, J.R., Stuiver, M., Talamo, S., Taylor, F.W., van der Plicht, J., and Weyhnmeyer, C.E., 2004, IntCal04 terrestrial radiocarbon age calibration, 26-0 cal kyr BP: Radiocarbon, v. 46, p. 1087-1092

Ricci Lucchi, F, 1986, The Oligocene to recent foreland basins of the Northern Apennines, In: Allen, P.A., and P. Homewood (Eds.), Foreland Basins, Int. Ass. Sediment., Spec. Pub., v. 8, p. 105-139, Blackwell Sci., Oxford, United Kingdom.

Richter, T.O., Van der Gaast, S., Koster, B., Vaars, A., Gieles, R., de Stigter, H.C., de Haas, H., and van Weering, T.C.E., 2006, The Avaatech XRF core scanner: technical description and applications to NE Atlantic sediments. In: Rothwell RG (ed) New techniques in sediment core analysis: Geol Soc Spec Publ, v. 267, p. 39–50.

Ridente, D., and Trincardi, F., 2002, Eustatic and tectonic control on deposition and lateral variability of Quaternary regressive sequences in the Adriatic basin (Italy): Marine Geology, v. 184, p. 273-293.

Ridente, D., and Trincardi, F., 2005, Pleistocene “muddy” forced-regression deposits on the Adriatic shelf: A comparison with prodelta deposits of the late Holocene high-stand mud wedge: Marine Geology, v. 222-223, 213-233.

Ridente, D., and Trincardi, F., 2006, Active foreland deformation evidenced by shallow folds and faults affecting Late Quaternary shelf-slope deposits (Adriatic Sea, Italy): Basin Research, v. 18, p. 171-188.

Ridente, D., Trincardi, F., Piva, A., Asioli, A., and Cattaneo, A., 2008, edimentary response to climate and sea level changes during the past ~400 ka from borehole PRAD1–2 (Adriatic margin): Geochemistry, Geophysics, Geosystems, v. 9, p. Q09R04.

Rooij van, D., Blamart, D., Richter, T., Wheeler, A., Kozachenko, M., and Henriet, J.P., 2007, Quaternary sediment dynamics in the Belgica mound province, Porcupine Seabight: ice-rafting events and contour current processes: Int. J. Earth Sci., v. 96, p. 121–140.

Rothwell, R.G, Hoogakker, B, Thomson, J, and Croudace, I.W., 2006, Turbidite emplacement on the southern Balearic Abyssal Plain (W. Mediterranean Sea) during marine isotope stages 1–3; an application of XRF scanning of sediment cores in lithostratigraphic analysis. In: Rothwell RG (ed) New techniques in sediment core analysis, v. 267, Geological Society Special Publication, London, p. 51–63.

Rothwell, R.G., and Croudace, I.W., 2015, Micro-XRF studies of sediment cores: a perspective on capability and application in the environmental sciences, In: Croudace IW, Rothwell RG (eds) Micro-XRF studies of sediment cores, Springer, Dordecht.

Ruddiman, W.F., 2006, Orbital changes and climate: Quaternary Science Reviews, v. 25, p. 3092-3112.

Sanders, J.E., Kumar, N., 1975, Evidence of shoreface retreat and in-place “drowning” during Holocene submergence of barriers, shelf off Fire Island, New York: Geological Society of America Bulletin, v. 86, p. 65–76.

Scrocca, D., E. Carminati, C. Doglioni and D. Marcantoni, 2007, Slab retreat and active shortening along the Central-Northern Apennines, in Lacombe, O., J. Lavu, F. Roure and J. Verges, Eds., Thrust belts and Foreland Basins: from fold kinematics to hydrocarbon systems: Frontier in Earth Science, p. 471-487.

Shackleton, N., 2000, The 100,000-years ice-age cycle identified and found to lag temperature, carbon dioxide, and orbital eccentricity: Science, v. 289, p. 1897-1902

Sidall, M., Stocker, T.F., Spahni, R., Blunier, T., McManus, J., and Bard, E., 2006, Using a maximum simplicity paleoclimate model to simulate millennial variability during the last four glacial cycles: Quaternary Science Review, v. 25, p. 3185-3197.

Skene, K.I., Piper, D.J.W., Aksu, A.E., and Syvitski, J.P.M., 1998, Evaluation of the global oxygen isotope curve as a proxy for Quaternary Sea level by modeling of delta progradation: J. Sediment. Res., v. 68, p. 1077–1092.

Solignac, S., Seidenkrantz, M.S., Jessen, C., Kuijpers, A., Gunvald, A.K., and Olsen, J., 2011, Late-Holocene sea-surface conditions offshore Newfoundland based on dinoflagellate cysts: Holocene, v. 2, p. 539–552. doi:10.1177/0959683610385720

Spofforth, D.J.A., Pälike, H., and Green, D., 2008, Paleogene record of elemental concentrations in sediments from the Arctic Ocean obtained by XRF analyses: Paleoceanography, v. 23,PA1S09.

Stoker, M.S., Pheasant, J.B., and Josenhans, H., 1997, Seismic methods and interpretation, In Davies, T.A., Bell, T., and Cooper, A.K., (Eds.), Glaciated Continental Margins, An Atlas of Acoustic Images, Chapman and Hall, London, p. 9–26.

Storms, J.E.A., G.J. Weltje, G.J. Tierra, A. Cattaneo and F. Trincardi, 2008, Coastal dynamics under conditions of rapid sea-level rise: Late Pleistocene to Early Holocene evolution of barrier-lagoon systems on the northern Adriatic shelf (Italy): Quaternary Science Reviews, v. 27, p. 1107-1123.

Stuiver M., Reimer, P. J., 1993, Extended 14C database and revised CALIB radiocarbon calibration program: Radiocarbon, v. 35, p. 215-230.

Surić, M., Juračić, M., Horvatinčić, N., Krajcar Bronić, I., 2005, Late Pleistocene–Holocene sea-level rise and the pattern of coastal karst inundation: records from submerged speleothems along the Eastern Adriatic Coast (Croatia): Marine Geology, v. 214, p. 163-175.

Swift, D.J.P, 1968, Coastal erosion and transgressive stratigraphy: Journal of Geology, v. 76, p. 444–456.

Tesson, M., Gensous, B., Allen, G.P., and Ravenne, Ch., 1990, Late Quaternary deltaic lowstand wedges on the Rhône continental shelf, France: Mar. Geol., v. 91, p. 325–332.

Teatini, P., Tosi, L., and Strozzi, T., 2011, Quantitative evidence that compaction of Holocene sediments drives the present land subsidence of the Po Delta, Italy: J. Geophys. Res.,116, B08407, doi:10.1029/2010JB008122.

Tjallingii, R., Stattegger, K., Wetzel, A., Van Phach, P., 2010, Infilling and flooding of the Mekong River incised valley during deglacial sea-level rise: Quat Sci Rev, v. 29. P. 1432–1444.

Tortora P., and Cowell P.J., 2005, Principi geometrici nei sistemi costieri trasgressivi. Parte 1a: processi di migrazione del litorale: Geologica Romana, v. 38, p. 63-77.

Tosi, L., 1994, L'evoluzione paleoambientale tardoquaternaria del litorale veneziano nelle attuali conoscenze: Il Quaternario, v. 7, p. 589-596.

Trincardi, F., and Field, M.E., 1991, Geometry, lateral variability, and preservation of downlapped regressive shelf deposits: eastern Tyrrhenian margin, Italy: Journal of Sedimentary Petrology, v. 61, p. 75–90.

Trincardi, F., Correggiari, A., and Roveri, M., 1994, Late Quaternary transgressive erosion and deposition in a modern epicontinental shelf: the Adriatic Semi-enclosed Basin: Geo-Marine Letters, v. 14, p. 41-51.

Trincardi, F., Asioli, A., Cattaneo, A., Correggiari, A., and Langone, L., 1996, Stratigraphy of the late-Quaternary deposits in the Central Adriatic basin and the record of short-term climatic events: Mem. Ist. Ital. Idrobiol., v. 55, p. 39–70.

Trincardi, F., and Correggiari, A., 2000, Quaternary forced regression deposits in the Adriatic basin and the record of composite sea-level cycles. In: Hunt, D., Gawthorpe, R. (Eds.), Depositional Response to Forced Regression: Geological Society Special Publication, v. 172, p. 245-269.

Trincardi, F., Cattaneo, A., Correggiari, A., and Sultan, N., 2004, Evidence of soft-sediment deformation, fluid escape, sediment failure and regional weak layers within the late-Quaternary mud deposits of the Adriatic Sea: Marine Geology, v. 213, p. 91–119.

Trincardi, F., Foglini, F., Verdicchio, G., Asioli, A., Correggiari, A., Minisini, D., Piva A, Remia, A., Ridente D., and Taviani, M., 2007, The impact of cascading currents on the Bari Canyion System SW-Adriatic Margin (Central Mediterranean): Marine Geology, v. 246, p. 208-230.

Trincardi, F., Argnani, A., and Correggiari, A., 2011a, Note illustrative della Carta Geologica dei Mari Italiani alla scala 1:250.000 - Foglio NL 33-7 Venezia. S.EL.CA., Firenze, IT, p. 151.

Trincardi, F., Argnani, A., and Correggiari, A., 2011b, Note illustrative della carta geologica dei mari italiani alla scala 1:250.000, S.EL.CA, fogli Ancona NK 33 - 1/2, Bari NK 33-6 e Vieste NK 33- 8/9.

Trincardi, F., Argnani, A., and Correggiari, A., 2011c, Carta Geologica dei Mari Italiani per il bacino adriatico a scala 1:250000 CARTA SUPERFICIALE - CARTA DEL

SOTTOFONDO - NOTE ILLUSTRATIVE di 6 fogli, ISPRA Istituto Superiore per la Protezione e la Ricerca Ambientale-Servizio Geologico d'Italia. Ente realizzatore: Istituto di Scienze Marine-Consiglio Nazionale delle Ricerche.

Trincardi, F., Campiani, E., Correggiari, A., Foglini ,F., Maselli, V., Remia, A., 2013, Bathymetry of the Adriatic Sea: The legacy of the last eustatic cycle and the impact of modern sediment dispersal: Journal of Maps, v. 10, p. 151-158.

Van Wagoner, J.C., Mitchum, M.R., Campion, K.M., and Rahmanian, V.D., 1990, Siliciclastic sequence stratigraphy in well logs, cores, and outcrops: American Association of Petroleum Geologists Methods in Exploration Series, v. 7, p. 55.

Vezzoli, G and Garzanti, E., 2009, Tracking paleodrainage in pleistocene foreland basin: Journal of Geology, v. 117, p. 445-454.

Vidal, L., Bickert, T., Wefer, G., and Röhl, U., 2002, Late Miocene stable isotope stratigraphy of SE Atlantic ODP Site 1085: relation to Messinian events: Mar Geol, v. 180, p. 71–85. doi:10.1016/S0025-3227(01)00206-7.

Waelbroek, C., Labeyrie, L., Michel, E., Duplessy, J.C., McManus, J.F., Lambeck, K., Balbon, E., and Labracherie, M., 2002, Sea level and deep water temperature changes derived from benthic foraminifera isotopic records: Quaternary Science Reviews, v. 21, p. 295-305.

Weltje, G.J., and Prins, M.A., 2003, Muddled or mixed? Inferring palaeoclimate from size distributions of deep-sea clastics: Sedimentary Geology, v. 162, p. 39-62.

Weltje, G.J., and Tjallingii, R., 2008, Calibration of XRF core scanners for quantitative geochemical logging of sediment cores: theory and application: Earth Planet Sci. Lett., v. 274, p. 423–438.

Wilhelms-Dick, D., Westerhold, T., and Röhl, U., 2012, A comparison of mm scale resolution techniques for element analysis in sediment cores: J Anal Atom Spectrom, v. 27, p. 1574–1584.

Yarincik, K.M., Murray, R.W., and Peterson, L.C., 2000, Climatically sensitive eolian and hemipelagic deposition in the Cariaco Basin, Venezuela, over the past 578,000 years: results from Al/Ti and K/Al: Paleoceanography, v. 15, p. 210–228.

Zecchin, M., Gordini, E., and Ramella, R., 2015, Recognition of a drowned delta in the northern Adriatic Sea, Italy: stratigraphic characteristics and its significance in the frame of the early Holocene sea-level rise: The Holocene, v. 25, p. 1027–1038.

Ziegler, M., Jilbert, T., De Lange, G.J., Lourens, L.J., Reichart, G.J., 2008, Bromine counts from XRF scanning as an estimate of the marine organic carbon content of sediment cores: Geochem. Geophys. Geosyst., v. 9, Q05009.

Ziegler, M., Lourens, L.J., Tuenter, E., and Reichart, G.J. 2009, Anomalously high Arabian Sea productivity conditions during MIS 13: Clim. Past. Discuss., v. 5, p. 1989–2018.

Zuffa, G.G., 1980, Hybrid arenites: Their composition and classification: Journal of Sedimentary Petrology, v. 50, p. 21–29.

Zuffa, G.G., 1987, Unravelling hinterland and offshore palaeogeography from deep-water arenites, In Leggett, J.K. and Zuffa, G.G., eds, Marine Clastic Sedimentology: Models and Case Studies, p. 39–61.

APPENDIX A

Location of the cores

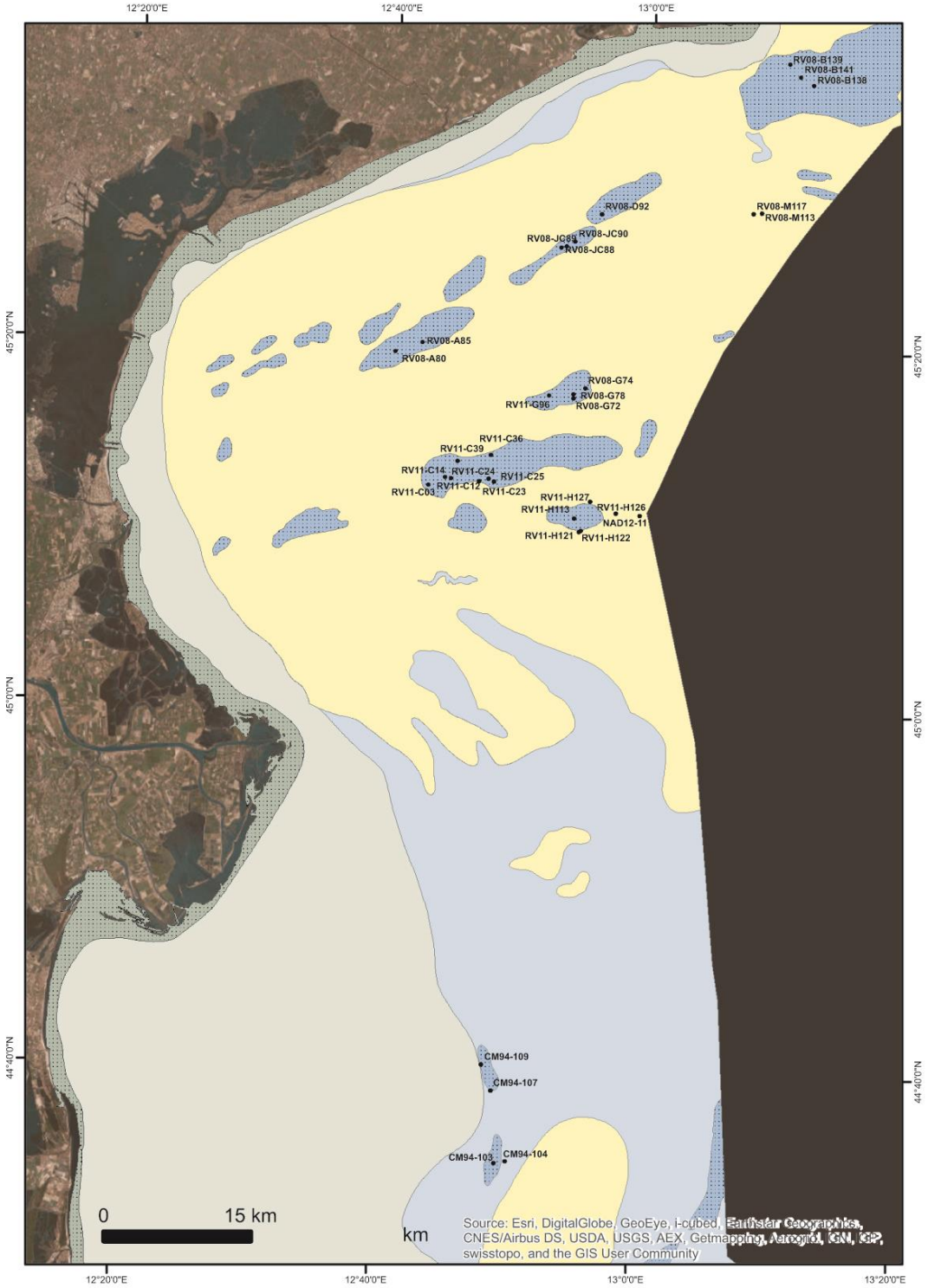

Log legend


Clay

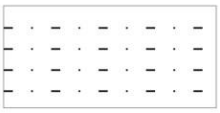
Silt

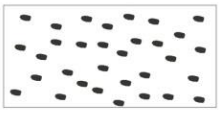
Sand


Peat

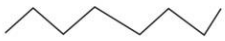
Erosional surface


Bioclasts


Frustules carbonaceous


Organic matter

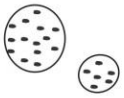
Sand pocket

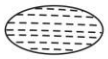
Clay chip

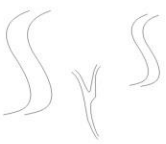
Bioturbation

Grainsize bar

CM94_103

Area: Adriatic Sea
Date: 01/09/1994
Lat: 44°34’58’’.32
Long: 12°49’36.84
Water depth (m): 34.7

Coring device: Vibrocorer ROSSFELDER P-5B
Core lenght (cm): 385
Core diameter (mm): 90

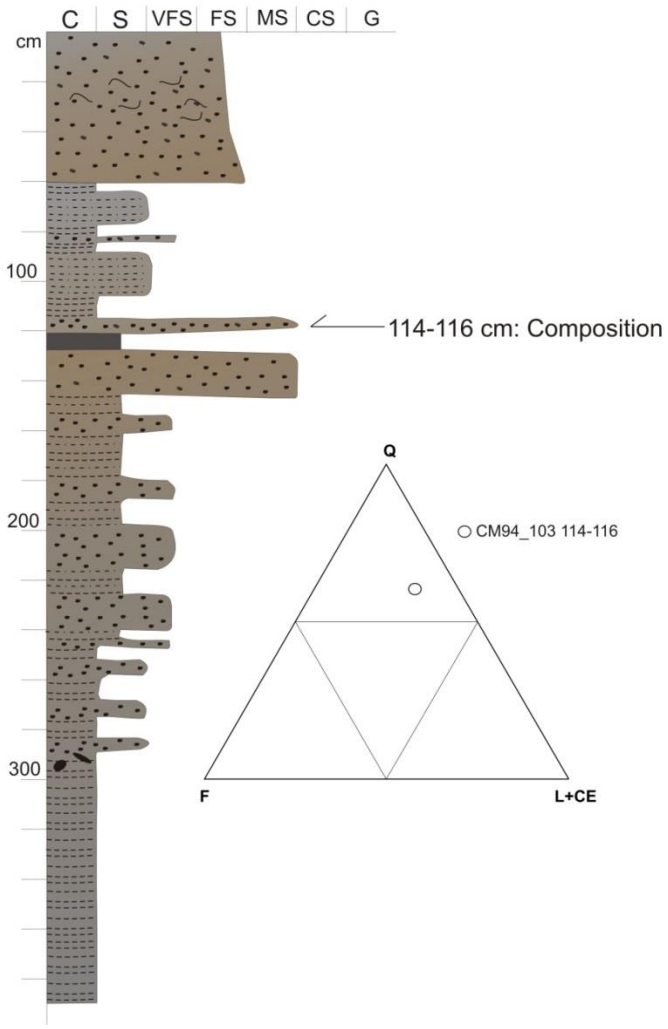

CM94_104

Area: Adriatic Sea
Date: 01/09/1994
Lat: 44°35'07.08
Long: 12°50'28.68
Water depth (m): 36

Coring device: Vibrocorer ROSSFELDER P-5B
Core lenght (cm): 265
Core diameter (mm): 90

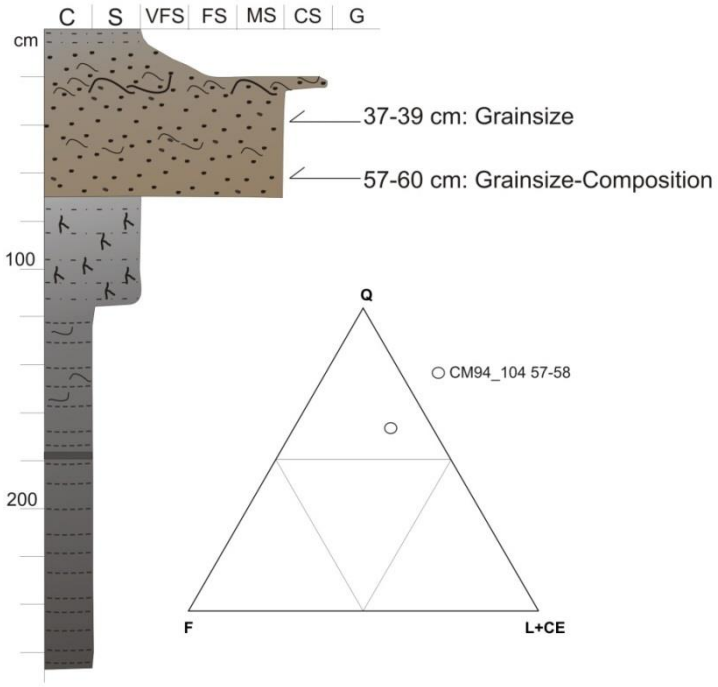

	Gravel	Sand	Mud (silt+clay)	Silt	Clay	D50
CM94_104 37-39	0.0	82.8	16.2	11.5	5.7	-
CM94_104 58-60	0.0	77.6	22.5	17.8	4.7	-

CM94_107

Area: Adriatic Sea
Date: 01/09/1994
Lat: 44°38'58''.62
Long: 12°49'13''.56
Water depth (m): -

Coring device: Vibrocorer ROSSFELDER P-5B
Core lenght (cm): 390
Core diameter (mm): 90

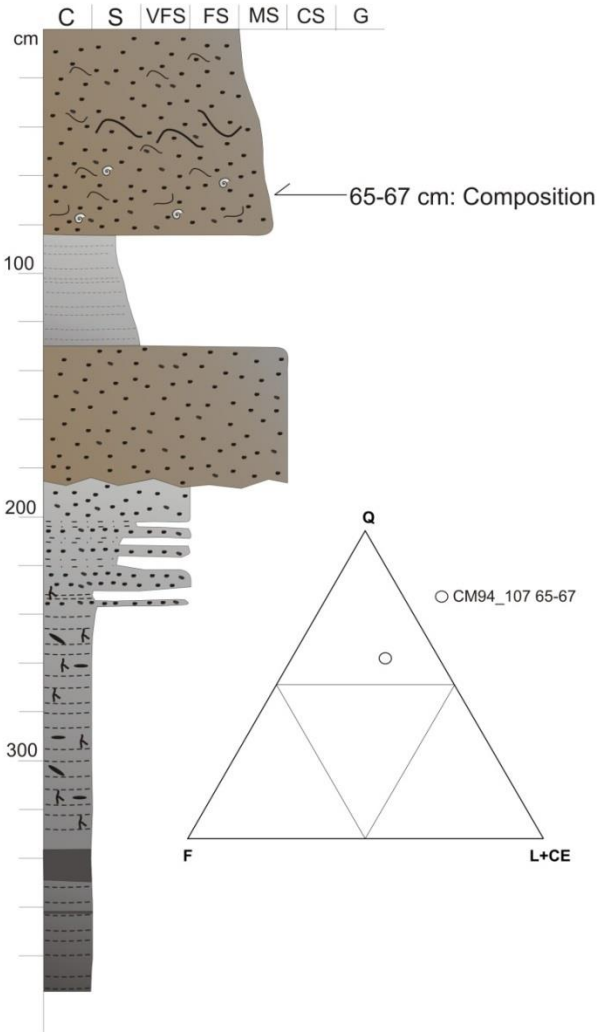

CM94_109

Area: Adriatic Sea
Date: 01/09/1994
Lat: 44°40'24.60
Long: 12°48'28.08
Water depth (m): 34

Coring device: Vibrocorer ROSSFELDER P-5B
Core lenght (cm): 290
Core diameter (mm): 90

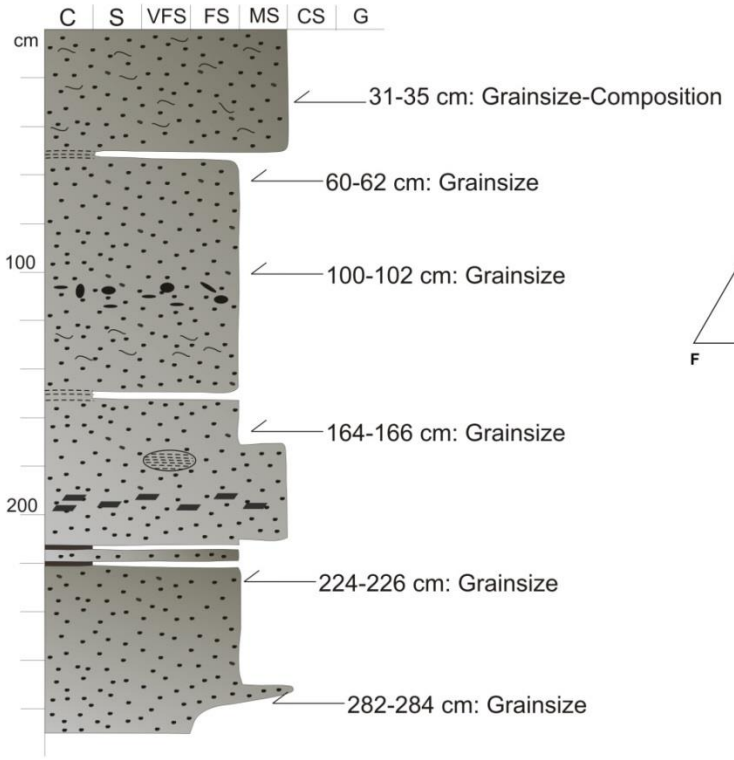

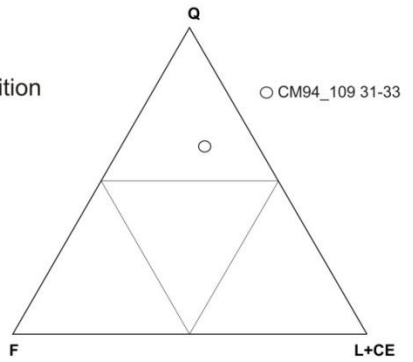

	Gravel	Sand	Mud (silt+clay)	Silt	Clay	D50
CM94_109 33-35	0.0	91.6	8.5	5.9	2.6	-
CM94_109 60-62	0.0	68.7	31.2	22.6	8.6	-
CM94_109 100-102	0.0	95.6	4.4	3.7	0.7	-
CM94_109 164-166	0.0	86.2	13.8	12.1	1.7	-
CM94_109 224-226	0.0	95.9	4.1	4.1	0.0	-
CM94_109 282-284	0.0	97.3	2.7	2.7	0.0	-

NAD12-11

Area: Adriatic Sea
Date: 22/05/2012
Lat: 45°10'53''.68
Long:12°59'40''.04
Water depth (m): 34

Coring device: Vibrocorer ROSSFELDER P-5B
Core lenght (cm): 220
Core diameter (mm): 90

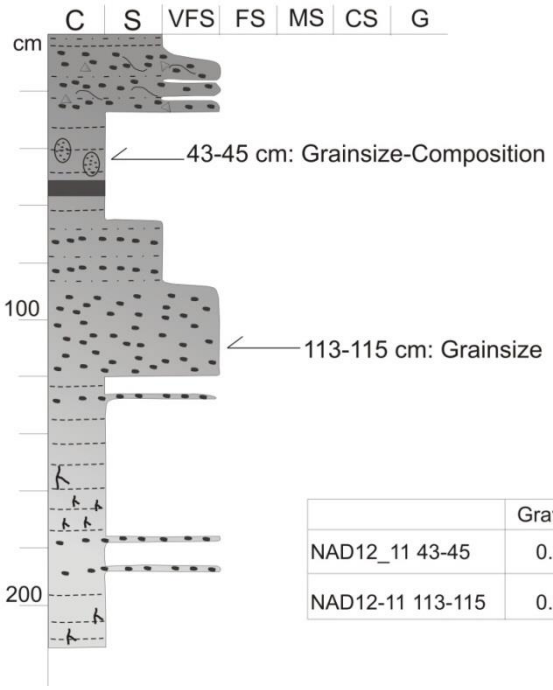

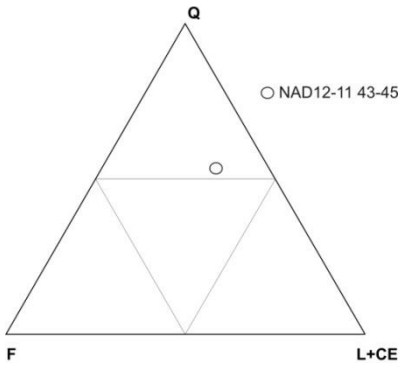

	Gravel	Sand	Mud (silt+clay)	Silt	Clay	D50
NAD12_11 43-45	0.0	82.8	11.2	11.2	0.0	-
NAD12-11 113-115	0.0	62.6	37.4	37.4	0.0	-

RV11_H113

Area: Adriatic Sea
Date: 30/10/2011
Lat: 45°10'40.82
Long: 12°54'35.36
Water depth (m): 29.2

Coring device: Vibrocorer ROSSFELDER P-5B
Core lenght (cm): 335
Core diameter (mm): 90

Magnetic Susceptibility

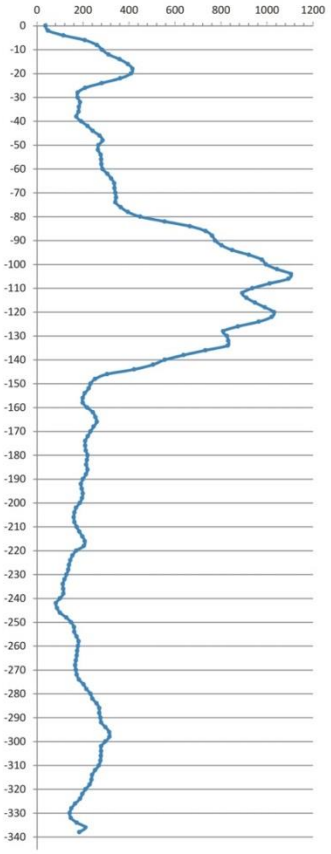

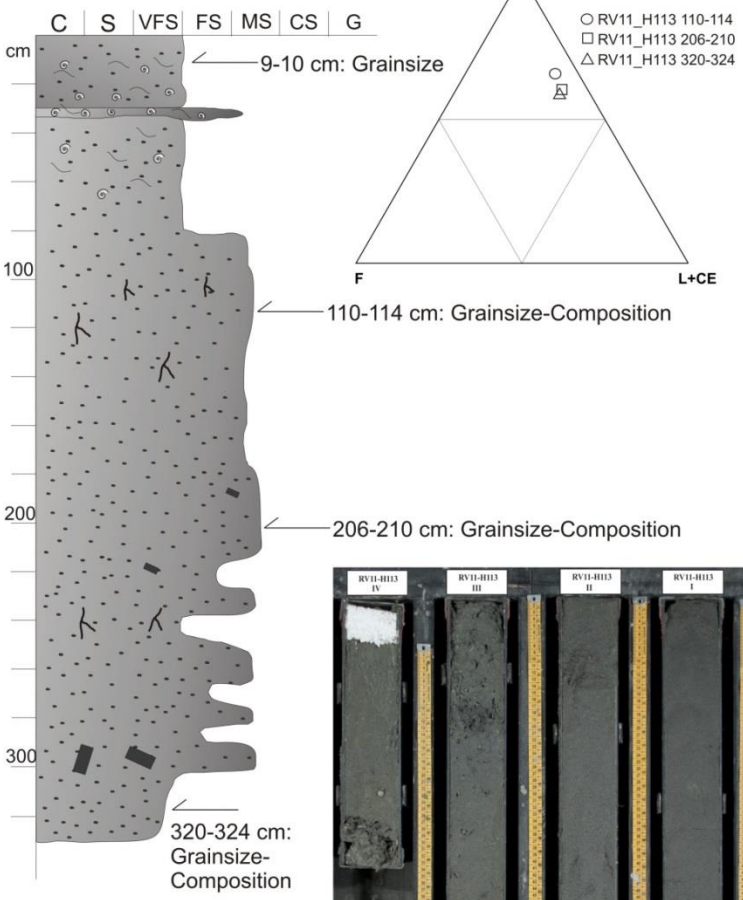

	Gravel	Sand	Mud (silt+clay)	Silt	Clay	D50
RV11_H113 9-10	0.2	90.8	8.9	8.9	0.0	154.0
RV11_H113 110-114	0.0	95.1	4.9	4.9	0.0	214.6
RV11_H113 206-210	0.0	89.4	10.6	10.6	0.0	144.8
RV11_H113 320-324	0.0	85.6	14.4	14.4	0.0	115.6

RV11_H121

Area: Adriatic Sea
Date: 31/10/2011
Lat: 45°09'55.54
Long: 12°54'57.16
Water depth (m): 30.0

Coring device: Vibrocorer ROSSFELDER P-5B
Core lenght (cm): 380
Core diameter (cm): 90

Magnetic Susceptibility

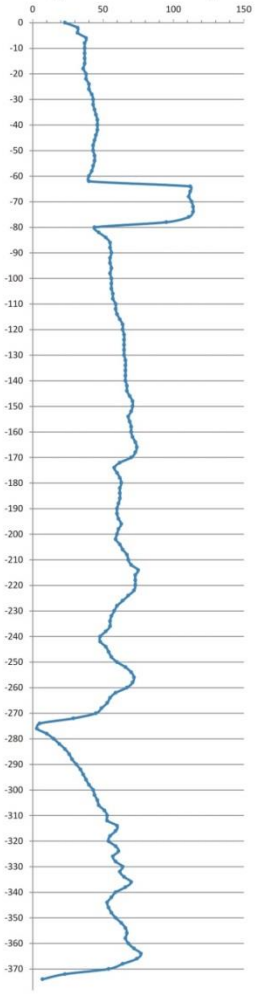

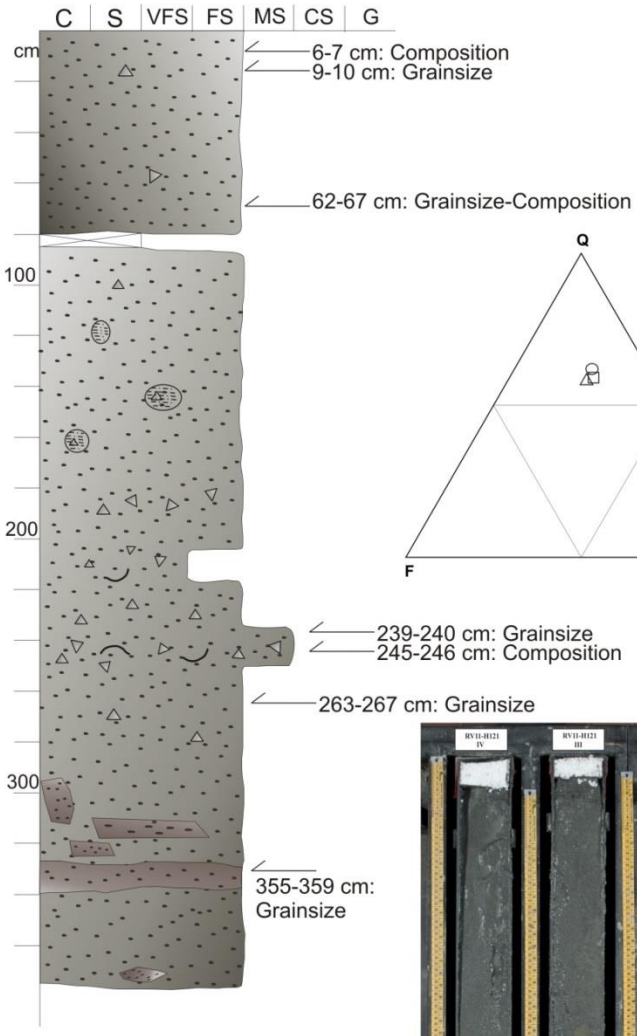

	Gravel	Sand	Mud (silt+clay)	Silt	Clay	D50
RV11_H121 9-10	0.1	95.3	4.6	4.6	0.0	182.8
RV11_H121 62-66	0.0	93.7	6.3	6.3	0.0	199.2
RV11_H121 239-240	0.0	93.0	7.0	7.0	0.0	200.7
RV11_H121 263-267	3.0	86.2	10.9	10.9	0.0	173.8
RV11_H121 355-359	0.0	94.5	5.5	5.5	0.0	197.8

RV11_H122

Area: Adriatic Sea
Date: 31/10/2011
Lat: 45°09'59.24
Long: 12°55'05.32
Water depth (m): 30.0

Coring device: Vibrocorer ROSSFELDER P-5B
Core lenght (cm): 190
Core diameter (mm): 90

Magnetic Susceptibility

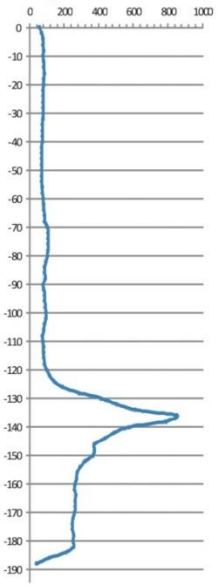

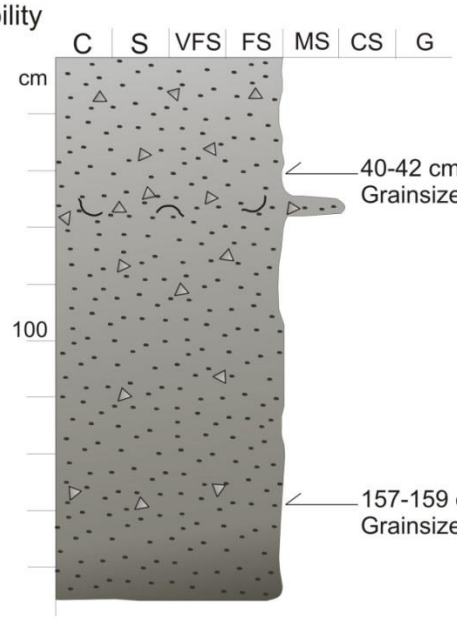

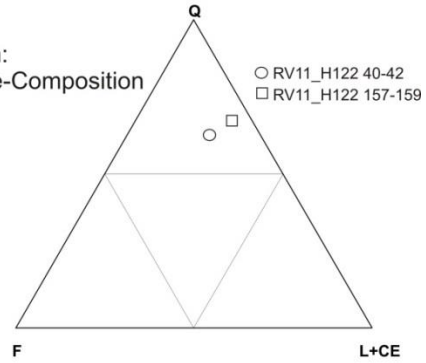

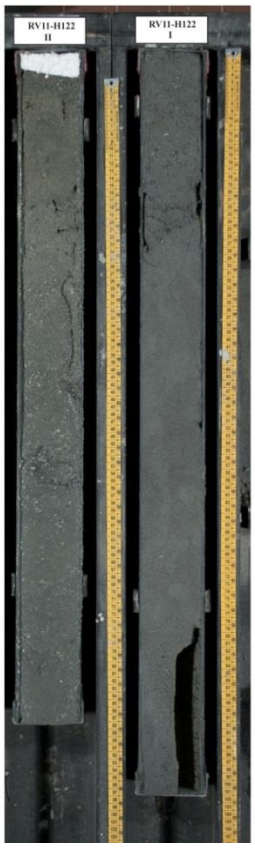

	Gravel	Sand	Mud (silt+clay)	Silt	Clay	D50
RV11_H122 40-42	1.6	87.6	10.8	10.8	0.0	-
RV11_H122 157-159	0.1	94.9	5.0	5.0	0.0	-

RV11_H126

Area: Adriatic Sea
Date: 31/10/2011
Lat: 45°11'00.53
Long: 12°57'48.69
Water depth (m): 31

Coring device: Vibrocorer ROSSFELDER P-5B
Core lenght (cm): 390
Core diameter (mm): 90

Magnetic Susceptibility

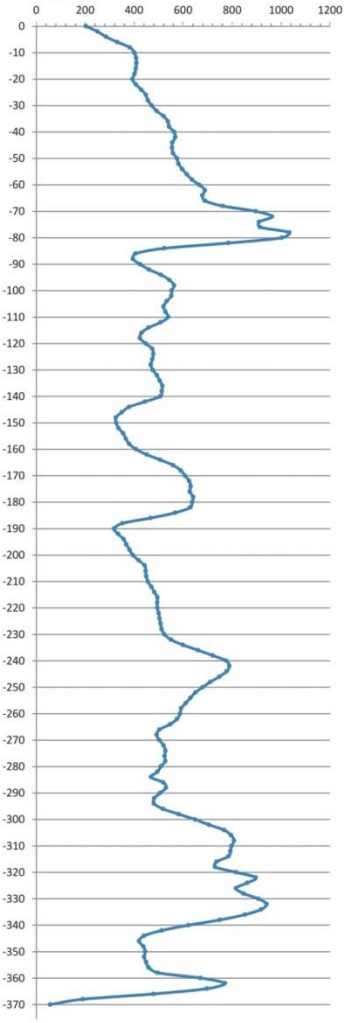

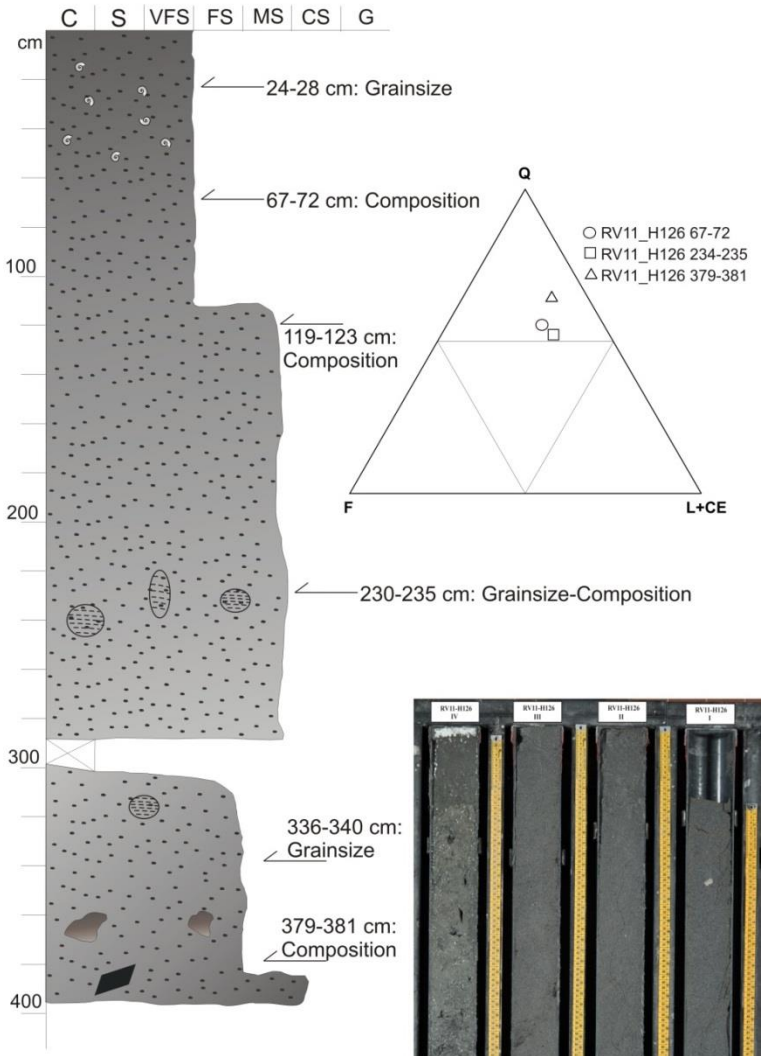

	Gravel	Sand	Mud (silt+clay)	Silt	Clay	D50
RV11_H126 24-28	2.9	80.0	17.1	17.1	0.0	-
RV11_H126 119-123	0.0	95.8	4.2	4.2	0.0	-
RV11_H126 230-234	0.0	96.3	3.7	3.7	0.0	-
RV11_H126 336-340	0.0	97.5	2.5	2.5	0.0	-

RV11_H127

Area: Adriatic Sea
Date: 31/10/2011
Lat: 45°11'36.96
Long: 12°55'48.38
Water depth (m): 30

Coring device: Vibrocorer ROSSFELDER P-5B
Core lenght (cm): 470
Core diameter (mm): 90

Magnetic Susceptibility

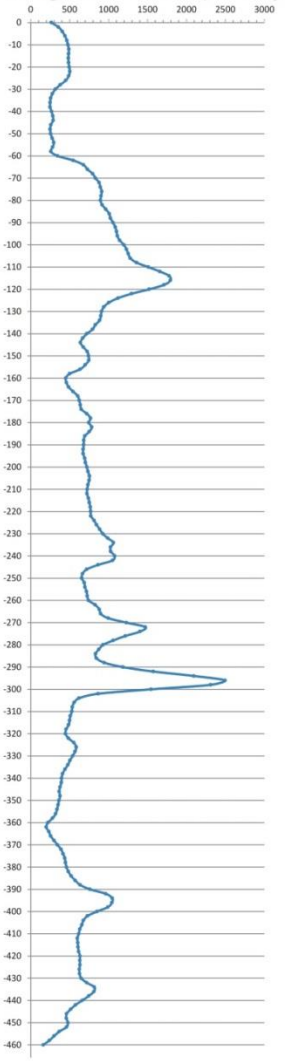

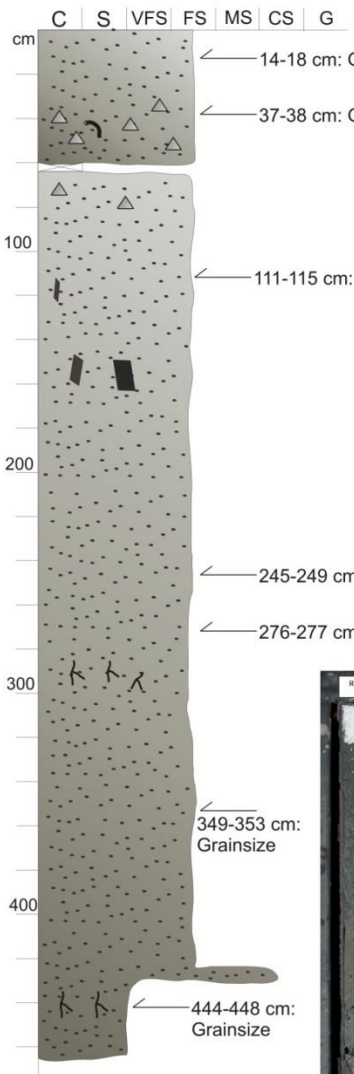

14-18 cm: Grainsize

37-38 cm: Grainsize

111-115 cm: Grainsize-Composition

245-249 cm: Grainsize

276-277 cm: Composition

349-353 cm: Grainsize

444-448 cm: Grainsize

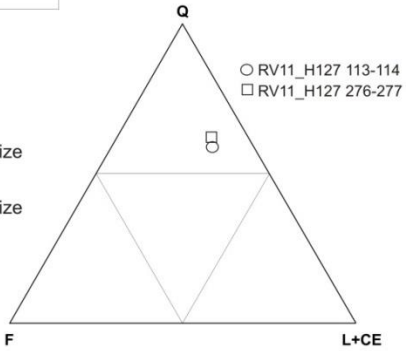

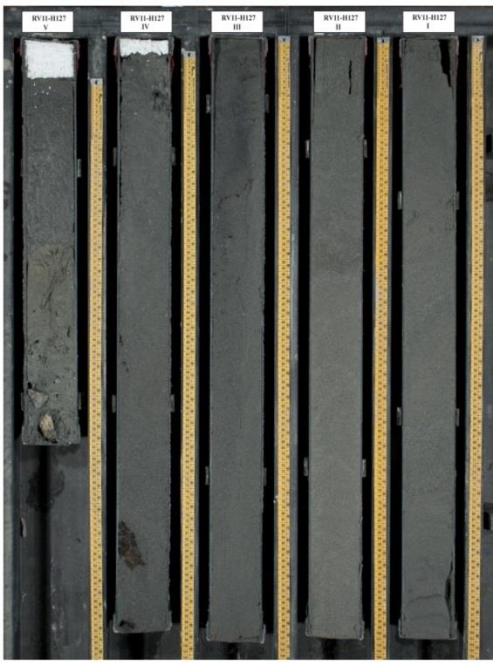

	Gravel	Sand	Mud (silt+clay)	Silt	Clay	D50
RV11_H127 14-18	1.6	93.6	4.8	4.8	0.0	192.2
RV11_H127 37-38	0.3	78.3	21.4	21.4	0.0	171.9
RV11_H127 111-115	0.2	96.7	3.1	3.1	0.0	182.6
RV11_H127 245-249	0.0	97.0	3.0	14.4	0.0	230.9
RV11_H127 349-353	0.0	95.9	4.1	4.1	0.0	150.2
RV11_H127 444-448	0.0	81.6	18.4	18.4	0.0	105.9

RV11_C03

Area: Adriatic Sea
Date: 02/10/2011
Lat: 45°12'19.62
Long: 12°43'09.60
Water depth (m): 25

Coring device: Vibrocorer ROSSFELDER P-5B
Core lenght (cm): 318
Core diameter (mm): 90

Magnetic Scusceptivity

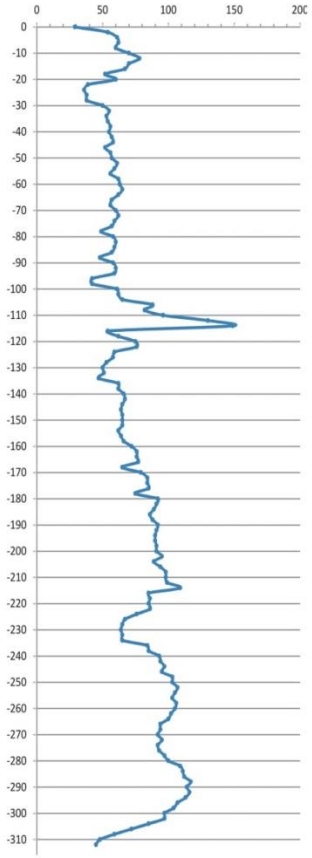

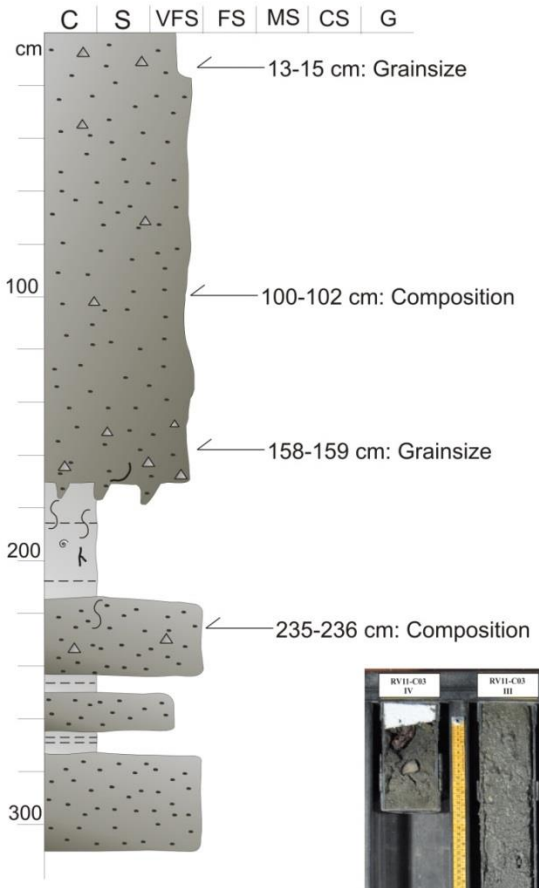

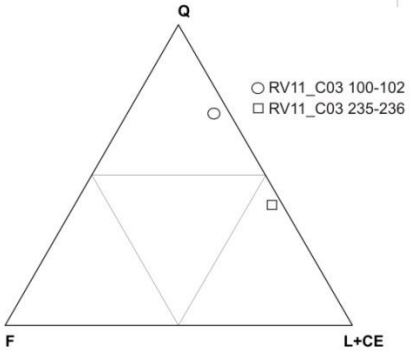

	Gravel	Sand	Mud (silt+clay)	Silt	Clay	D50
RV11_C03 13-15	1.9	92.7	0.9	0.9	0.0	218.6
RV11_C03 158-159	1.1	93.6	5.3	5.3	0.0	191

RV11_C12

Area: Adriatic Sea
Date: 03/10/2011
Lat: 45°12'47.46
Long: 12°44'25.41
Water depth (m): 25

Coring device: Vibrocorer ROSSFELDER P-5B
Core lenght (cm): 300
Core diameter (mm): 90

Magnetic Susceptibility

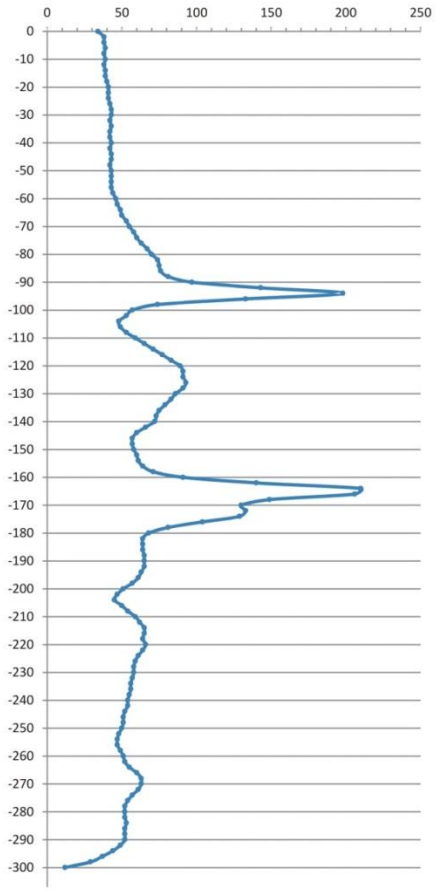

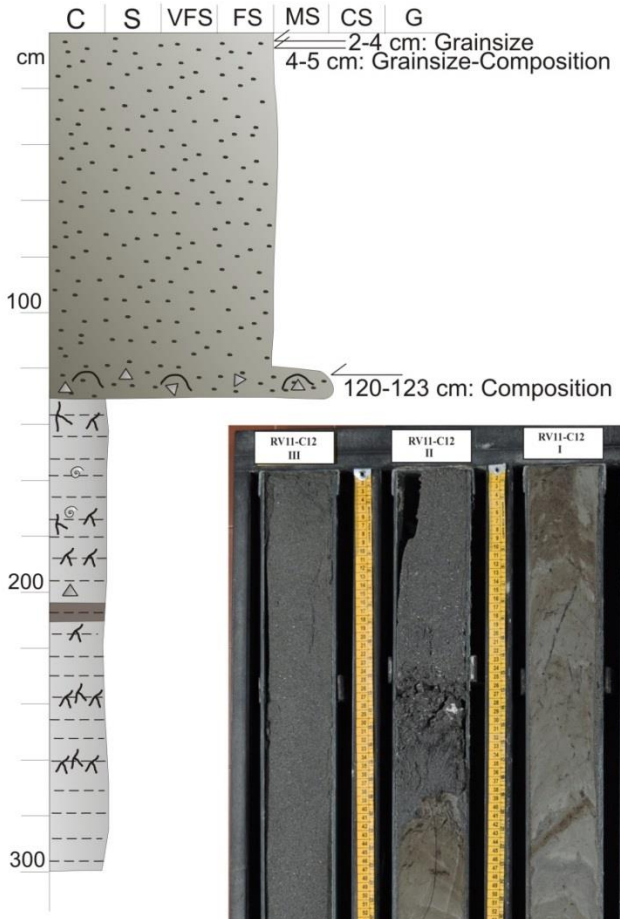

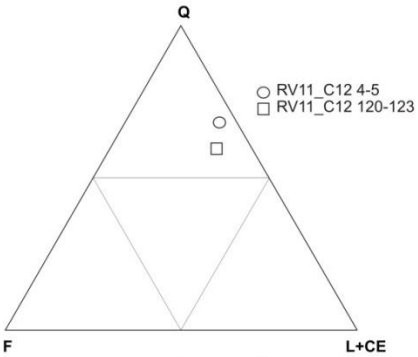

	Gravel	Sand	Mud (silt+clay)	Silt	Clay	D50
RV11_C12 2-4	0.3	96.9	2.8	2.8	0.0	211.9
RV11_C12 4-5	0.0	96.4	3.6	3.6	0.0	171.8

RV11_C14

Area: Adriatic Sea
Date: 03/10/2011
Lat: 45°12'44.14
Long: 12°44'54.14
Water depth (m): 25

Coring device: Vibrocorer ROSSFELDER P-5B
Core lenght (cm): 330
Core diameter (mm): 90

Magnetic Susceptibility

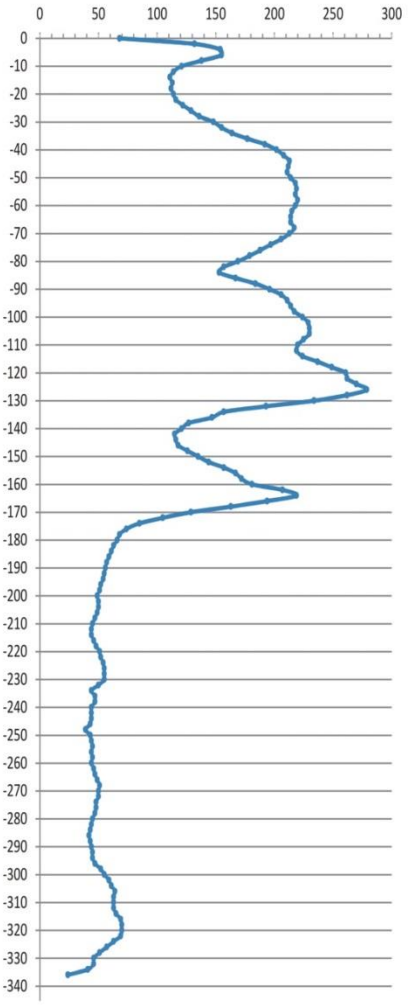

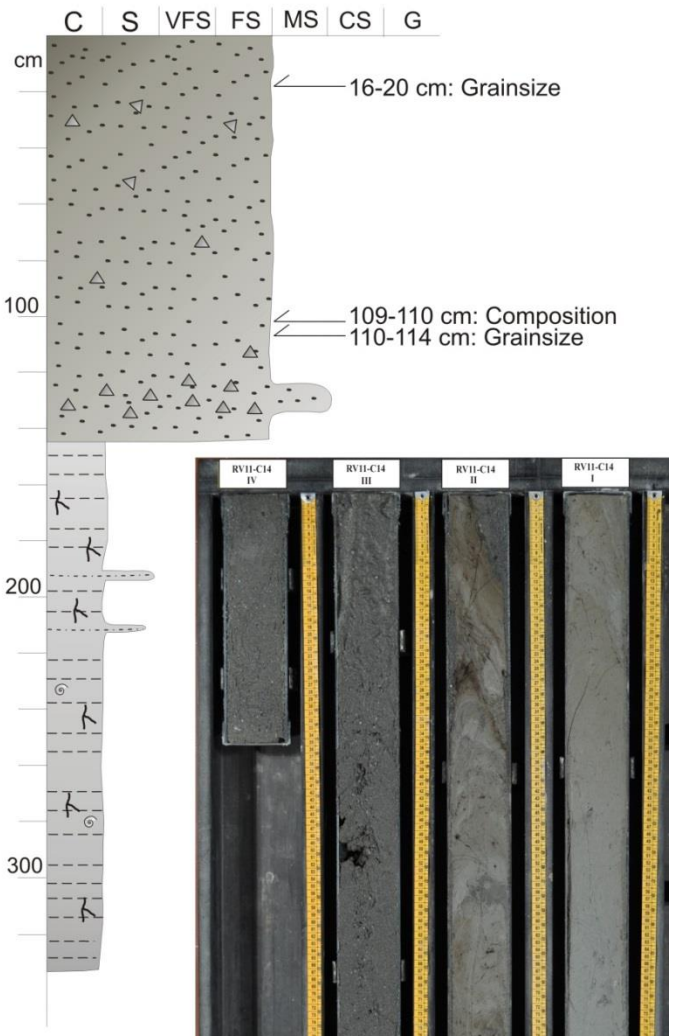

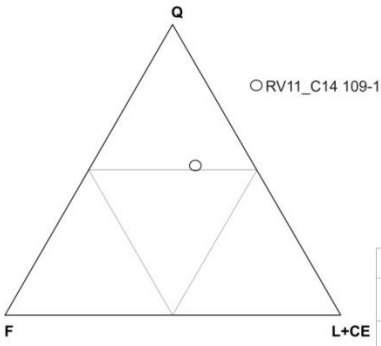

	Gravel	Sand	Mud (silt+clay)	Silt	Clay	D50
RV11_C14 16-20	0.2	95.8	4.0	4.0	0.0	203.3
RV11_C14 110-114	0.0	97.5	2.4	2.4	0.0	211.0

RV11_C23

Area: Adriatic Sea
Date: 04/10/2011
Lat: 45°12'37.04
Long: 12°45'05.93
Water depth (m): 27

Coring device: Vibrocorer ROSSFELDER P-5B
Core lenght (cm): 362
Core diameter (mm): 90

Magnetic Susceptibility

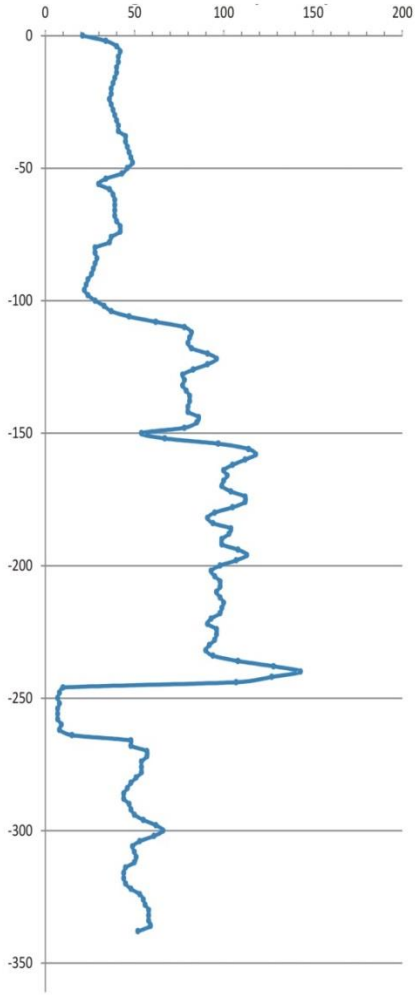

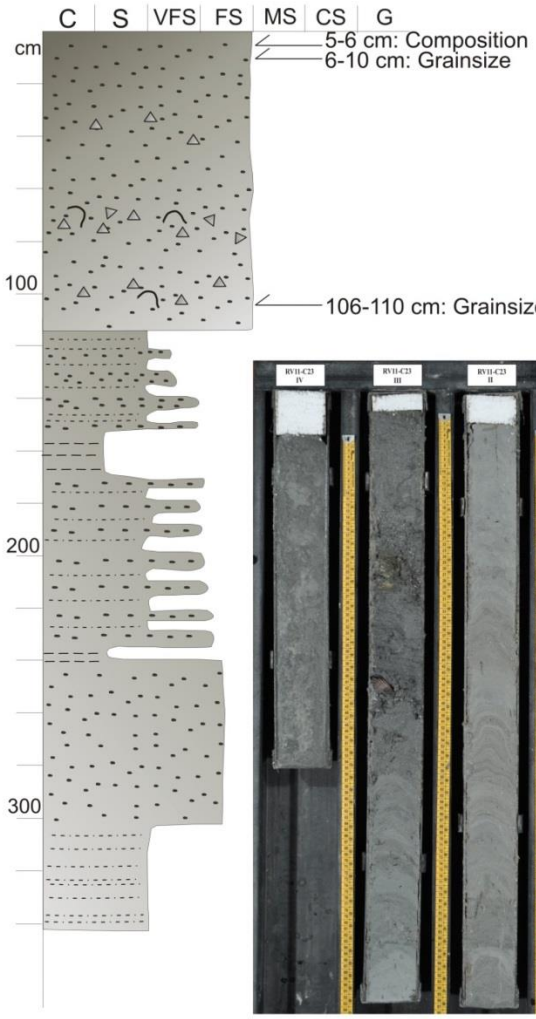

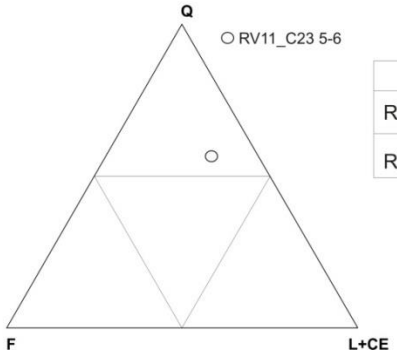

	Gravel	Sand	Mud (silt+clay)	Silt	Clay	D50
RV11_C23 6-10	0.0	85.1	14.9	14.9	0.0	69.75
RV11_C23 106-110	0.0	53.6	46.4	46.4	0.0	171.1

RV11_C24

Area: Adriatic Sea
Date: 04/10/2011
Lat: 45°12'44.08
Long: 12°47'48.03
Water depth (m): 26

Coring device: Vibrocorer ROSSFELDER P-5B
Core lenght (cm): 220
Core diameter (mm): 90

Magnetic Susceptibility

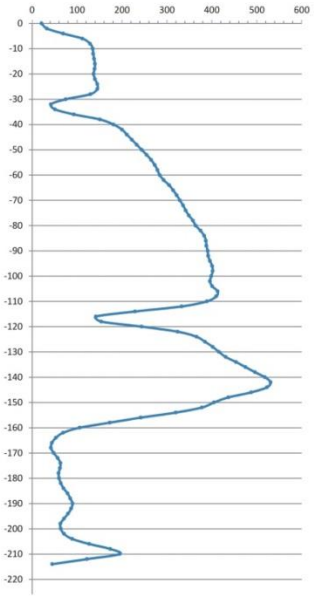

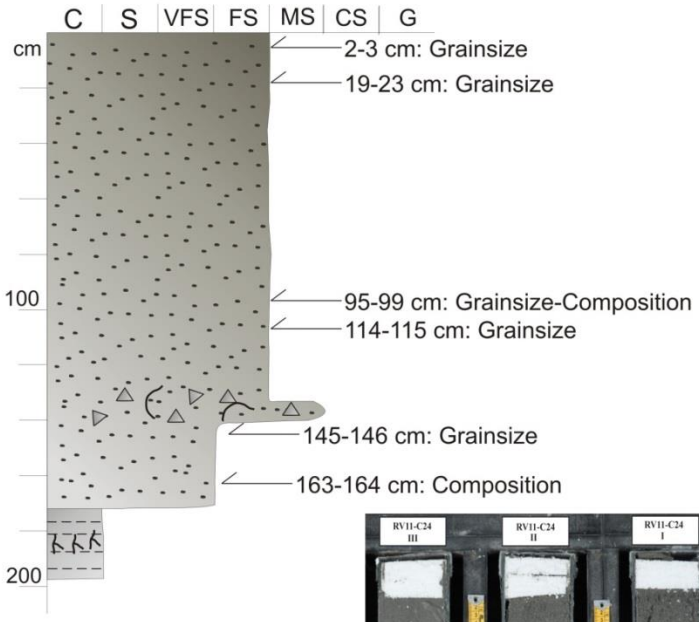

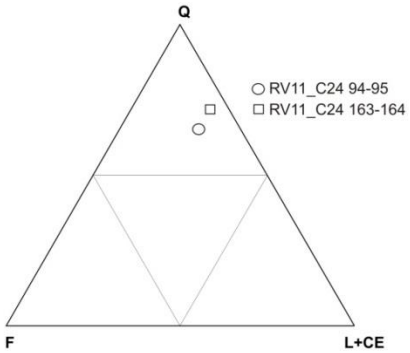

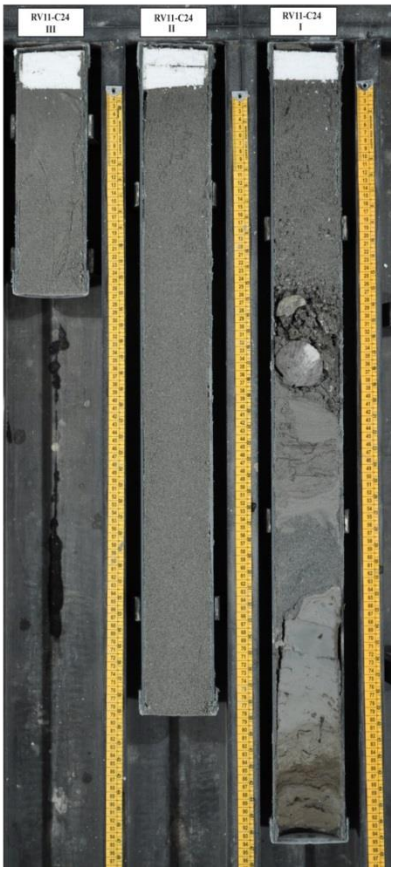

	Gravel	Sand	Mud (silt+clay)	Silt	Clay	D50
RV11_C24 2-3	0.0	64.9	35.4	35.4	0.0	82.26
RV11_C24 19-23	0.1	93.6	6.4	6.4	0.0	212.4
RV11_C24 95-99	0.0	92.5	7.4	7.4	0.0	223.4
RV11_C24 114-115	0.0	91.0	9.0	9.0	0.0	223.9
RV11_C24 145-146	3.0	63.9	33.1	33.1	0.0	81.42

RV11_C25

Area: Adriatic Sea
Date: 04/10/2011
Lat: 45°12'36.46
Long: 12°48'13.49
Water depth (m): 26

Coring device: Vibrocorer ROSSFELDER P-5B
Core lenght (cm): 180
Core diameter (mm): 90

Magnetic Susceptibility

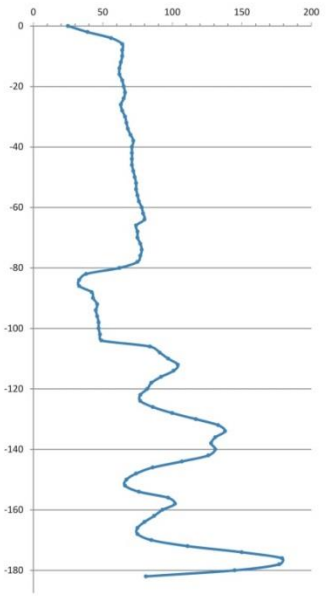

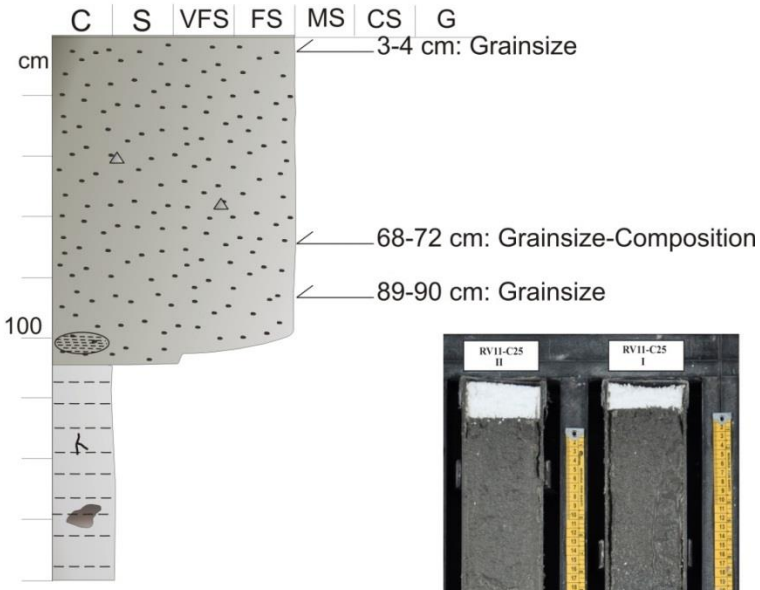

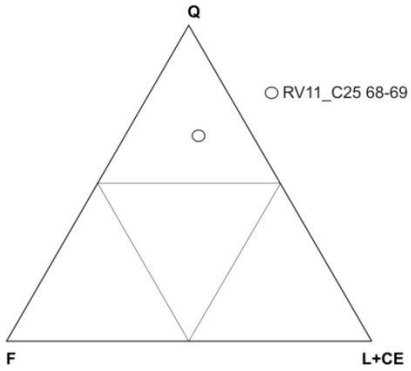

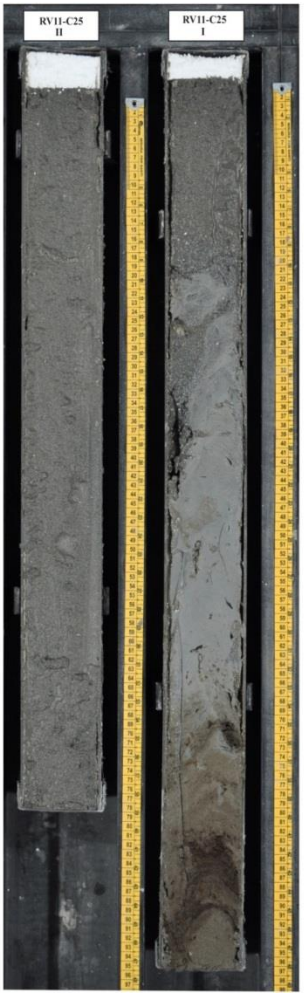

	Gravel	Sand	Mud (silt+clay)	Silt	Clay	D50
RV11_C25 3-4	0.0	92.4	7.6	7.6	0.0	154.4
RV11_C25 68-72	0.1	96.4	3.5	3.5	0.0	220.5
RV11_C25 89-90	0.6	95.1	4.3	4.3	0.0	222.1

RV11_C36

Area: Adriatic Sea
Date: 05/10/2011
Lat: 45°14'04.88
Long: 12°47'57.89
Water depth (m): 25.5

Coring device: Vibrocorer ROSSFELDER P-5B
Core lenght (cm): 420
Core diameter (mm): 90

Magnetic Susceptibility

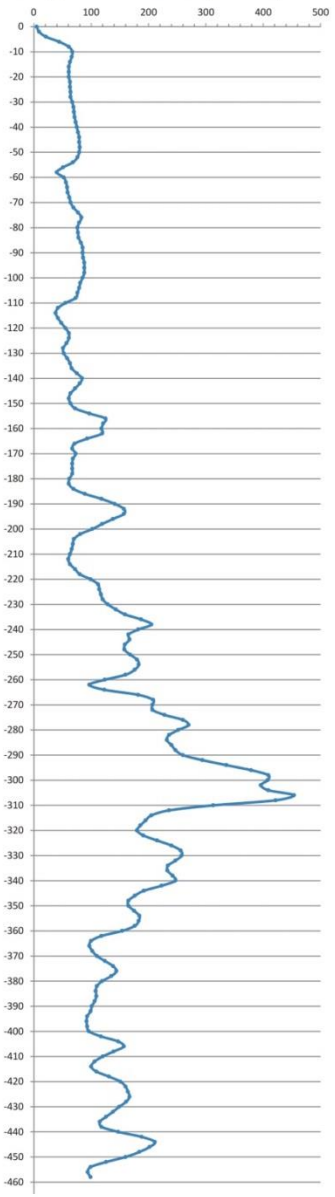

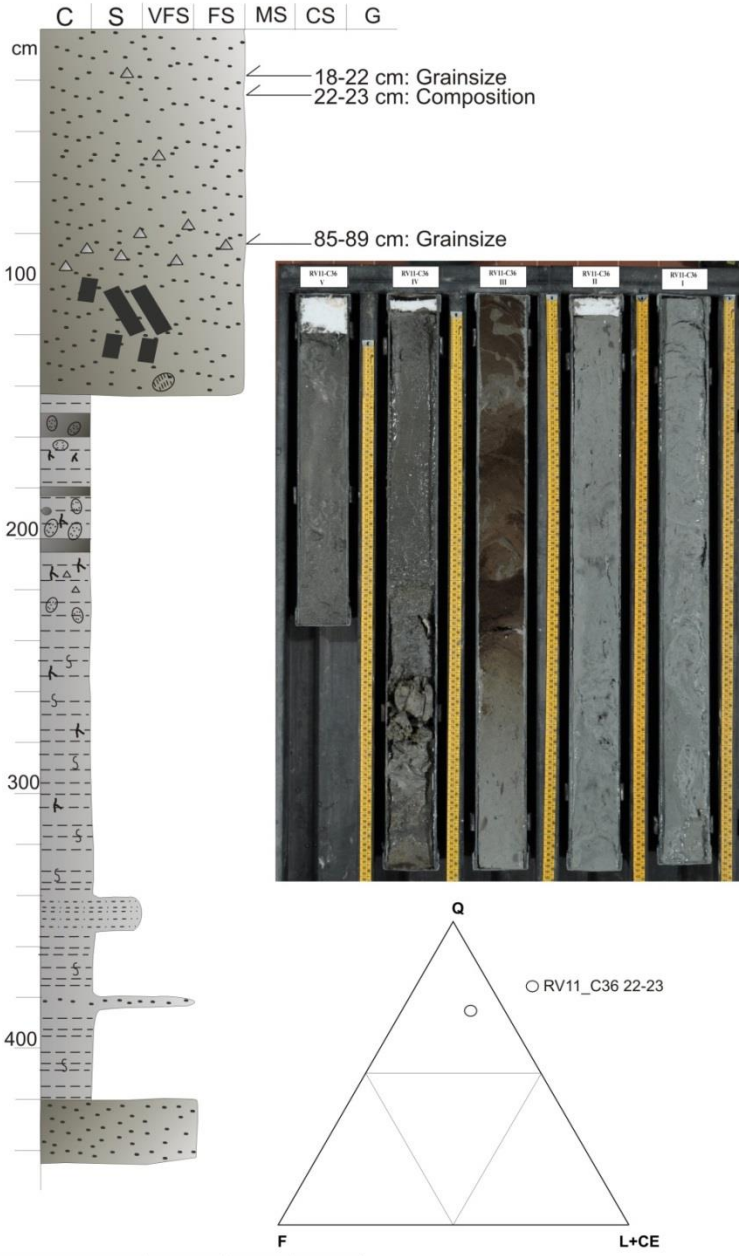

	Gravel	Sand	Mud (silt+clay)	Silt	Clay	D50
RV11_C36 18-22	0.0	92.3	7.7	7.7	0.0	176.1
RV11_C36 85-89	0.5	94.7	4.8	4.8	0.0	201.3

RV11_C39

Area: Adriatic Sea
Date: 5/10/2011
Lat: 45°13'41.43
Long: 12°45'21.30
Water depth (m): 25

Coring device: Vibrocorer ROSSFELDER P-5B
Core lenght (cm): 320
Core diameter (mm): 90

Magnetic Susceptibility

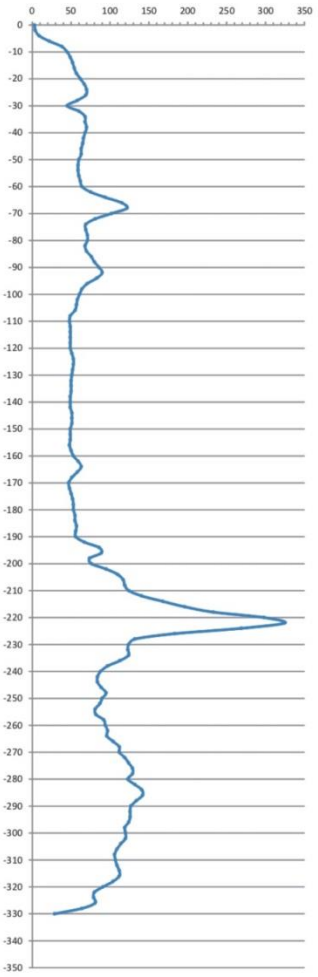

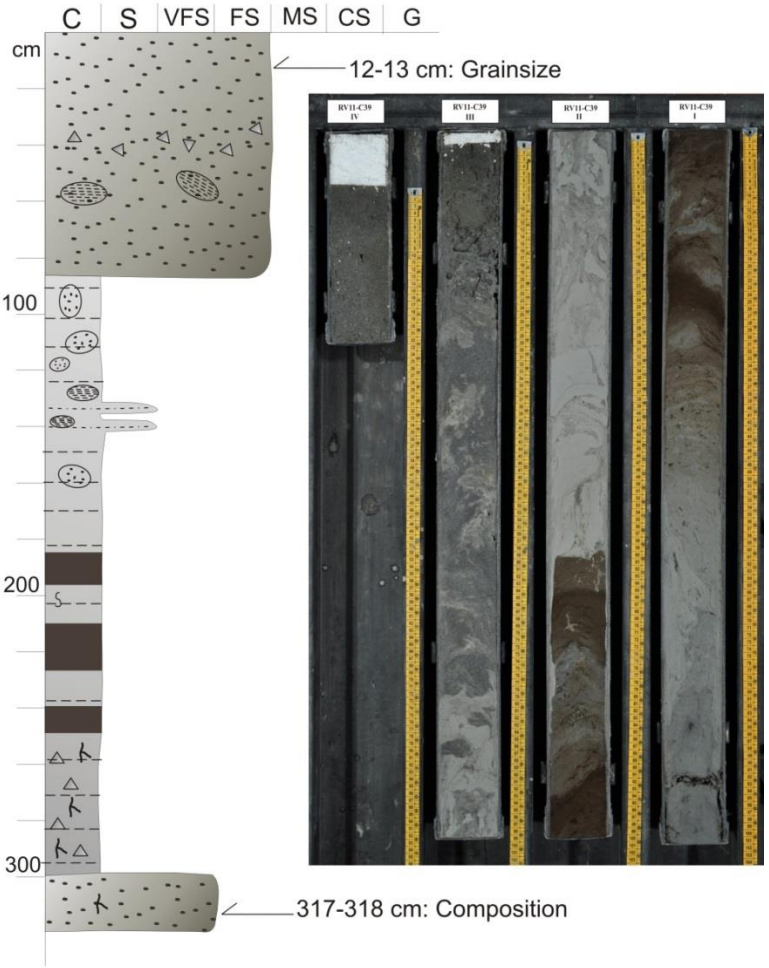

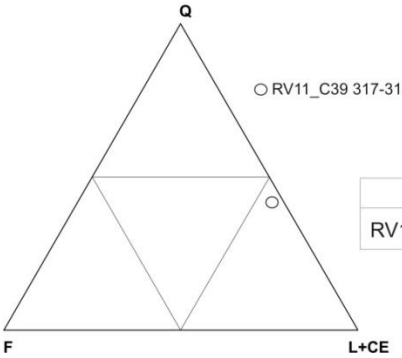

	Gravel	Sand	Mud (silt+clay)	Silt	Clay	D50
RV11_C39 12-13	0.4	95.3	4.3	4.3	0.0	231.3

RV11_G96

Area: Adriatic Sea
Lat: 45°17'31.88
Long: 12°54'16.94
Water depth (m): 30.5

Coring device: Vibrocorer ROSSFELDER P-5B
Core lenght (cm): 265
Core diameter (cm): 90

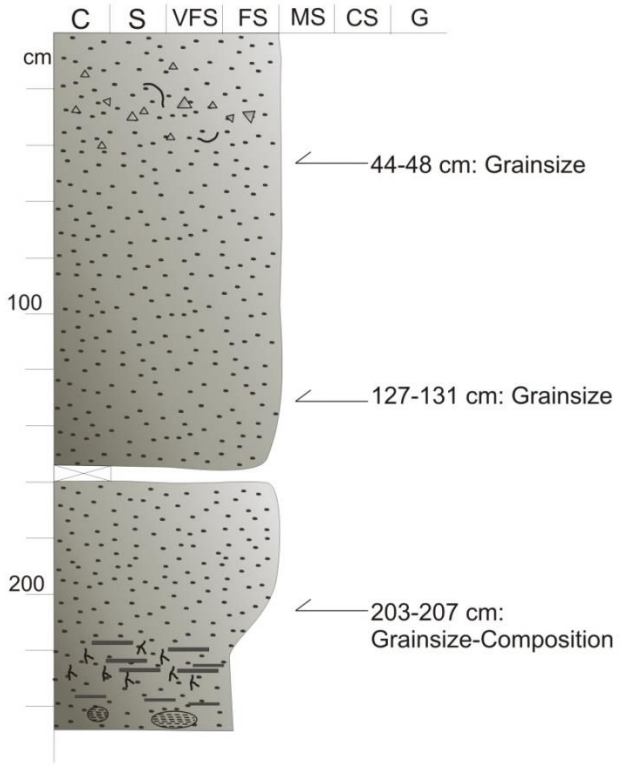

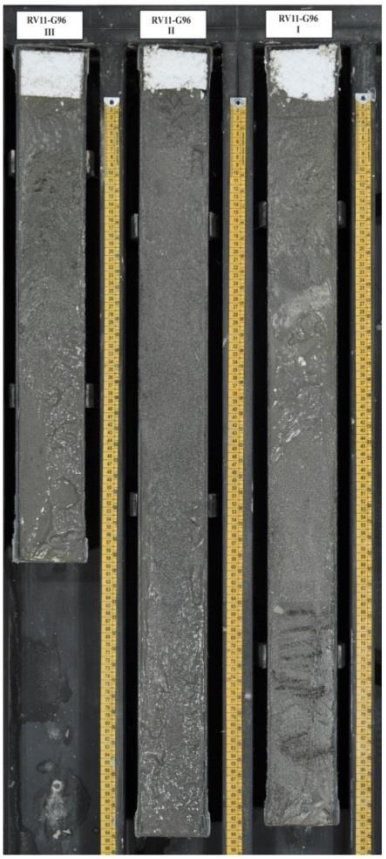

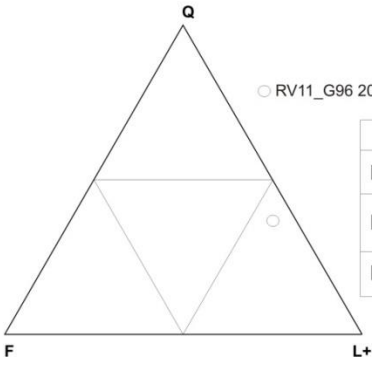

	Gravel	Sand	Mud (silt+clay)	Silt	Clay	D50
RV11_G96 44-48	0.0	90.5	9.5	9.5	0.0	117.0
RV11_G96 127-131	0.0	96.2	3.8	3.8	0.0	182.1
RV11_G96 203-207	0.0	90.6	9.4	9.4	0.0	114.2

RV08_G72

Area: Adriatic Sea
Date: 10/2008
Lat: 45°17'18.62
Long: 12°54'16.37
Water depth (m): 30

Coring device: Vibrocorer ROSSFELDER P-5B
Core lenght (cm): 370
Core diameter (mm): 90

Magnetic Susceptivity

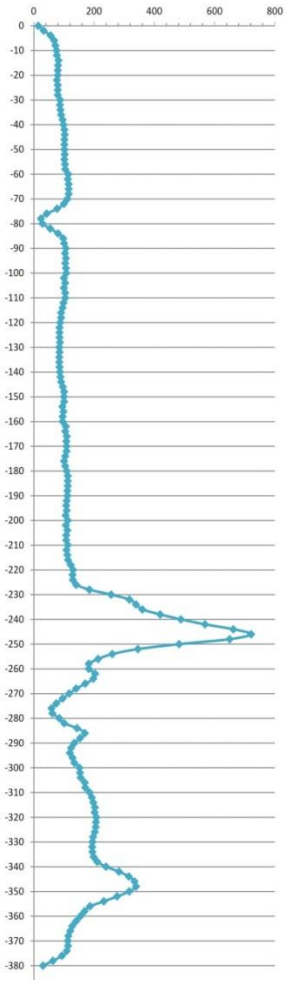

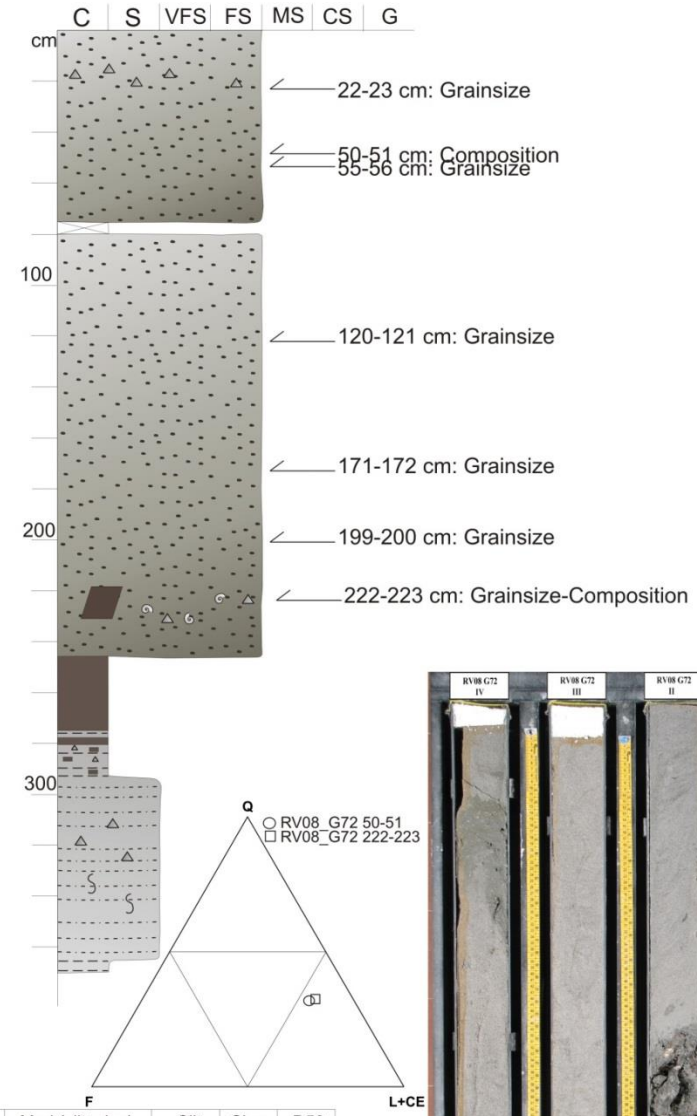

	Gravel	Sand	Mud (silt+clay)	Silt	Clay	D50
RV08_G72 22-23	2.0	78.3	19.8	19.8	0.0	126.4
RV08_G72 55-56	0.0	95.0	5.0	5.0	0.0	158.7
RV08_G72 120-121	0.0	93.6	6.4	6.4	0.0	132.1
RV08_G72 171-172	0.0	94.2	5.8	5.8	0.0	138.8
RV08_G72 199-200	0.0	92.0	8.0	8.0	0.0	134.3
RV08_G72 222-223	0.0	86.7	13.3	13.3	0.0	112.6

RV08_G74

Area: Adriatic Sea
Date: 10/2008
Lat: 45°17'52.94
Long: 12°55'10.67
Water depth (m): 29.5

Coring device: Vibrocorer ROSSFELDER P-5B
Core lenght (cm): 410
Core diameter (mm): 90

Magnetic Susceptibily

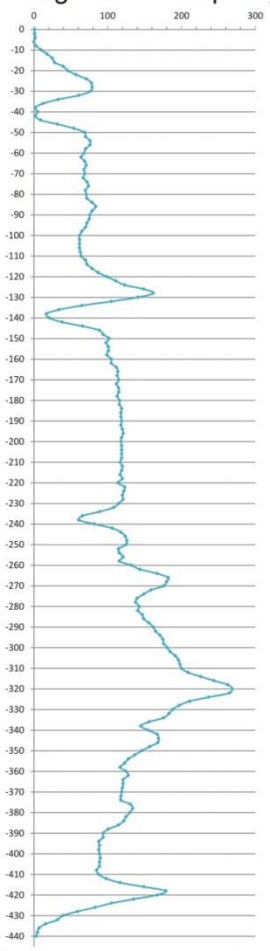

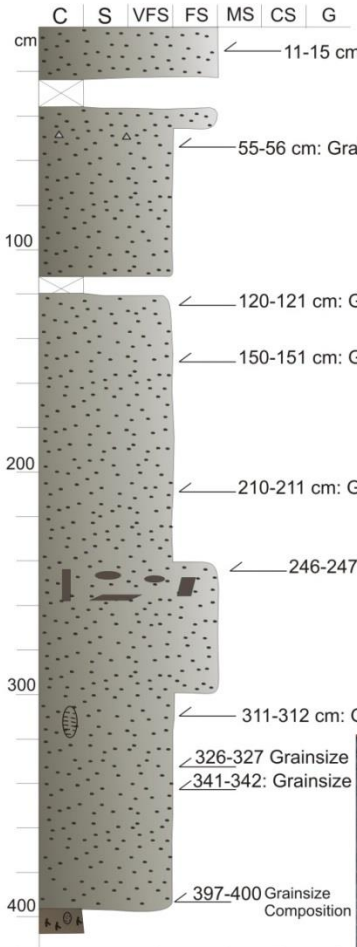

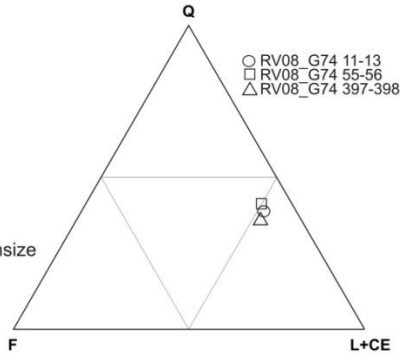

	Gravel	Sand	Mud (silt+clay)	Silt	Clay	D50
RV08_G74 14-15	0.0	92.3	7.7	7.7	0.0	152.7
RV08_G74 56-57	0.2	93.0	6.8	6.8	0.0	148.0
RV08_G74 120-121	0.4	86.2	13.4	13.4	0.0	146.5
RV08_G74 150-151	0.0	97.2	2.8	2.8	0.0	138.9
RV08_G74 210-211	0.0	97.0	3.0	3.0	0.0	133.3
RV08_G74 246-247	0.0	94.7	5.3	5.3	0.0	130.9
RV08_G74 311-312	0.0	96.0	4.0	4.0	0.0	222.6
RV08_G74 326-327	0.0	83.0	17.0	17.0	0.0	88.6
RV08_G74 341-342	0.0	83.8	16.2	16.2	0.0	91.4
RV08_G74 399-400	0.0	96.6	3.4	3.4	0.0	194.0

RV08_G78

Area: Adriatic Sea
Date: 10/2008
Lat: 45°17'26.36
Long: 12°52'21.94
Water depth (m): 29

Coring device: Vibrocorer ROSSFELDER P-5B
Core lenght (cm): 250
Core diameter (cm): 90

Magnetic Susceptibility

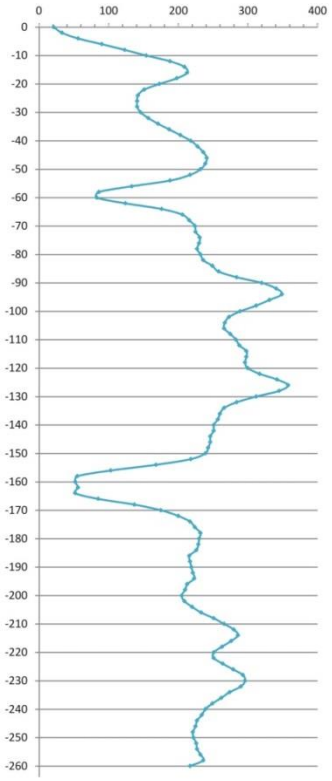

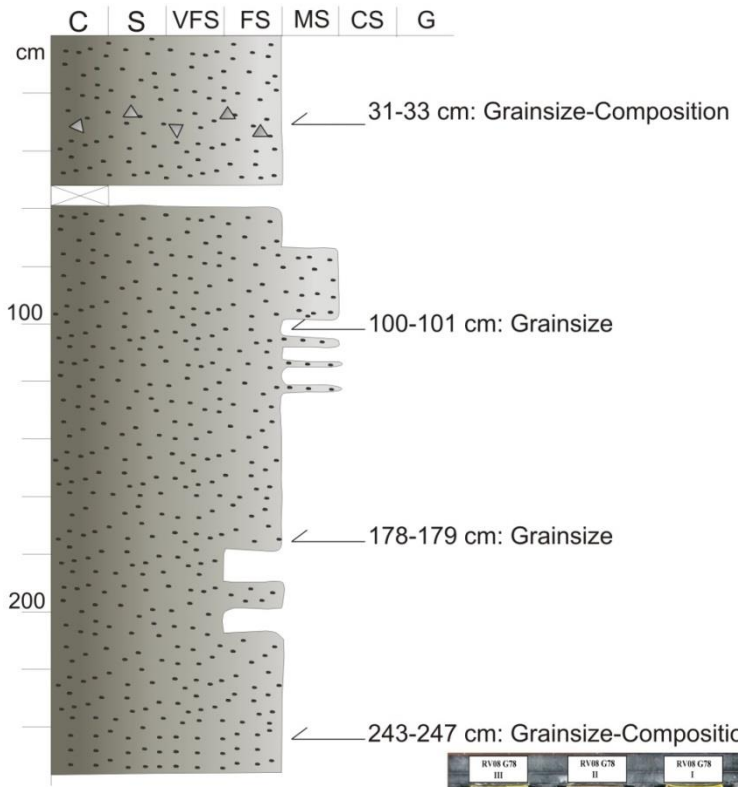

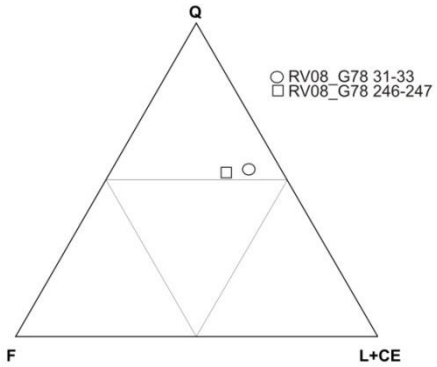

	Gravel	Sand	Mud (silt+clay)	Silt	Clay	D50
RV08_G78 32-33	1.3	75.6	23.1	23.1	0.0	109.0
RV08_G78 100-101	0.0	51.6	48.4	48.4	0.0	64.1
RV08_G78 178-179	0.0	95.6	4.4	4.4	0.0	152.6
RV08_G78 243-244	0.0	90.9	9.1	9.1	0.0	108.3

RV08_A80

Area: Adriatic Sea
Date: 10/2008
Lat: 45°19'39.33
Long: 12°40'14.18
Water depth (m): 20.5

Coring device: Vibrocorer ROSSFELDER P-5B
Core lenght (cm): 300
Core diameter (mm): 90

Magnetic Susceptibility

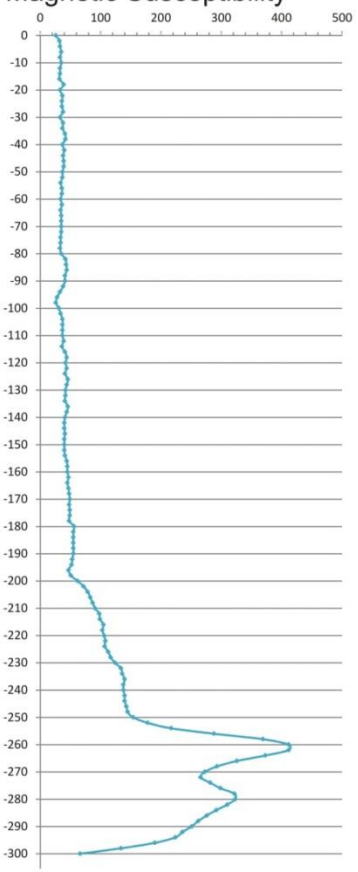

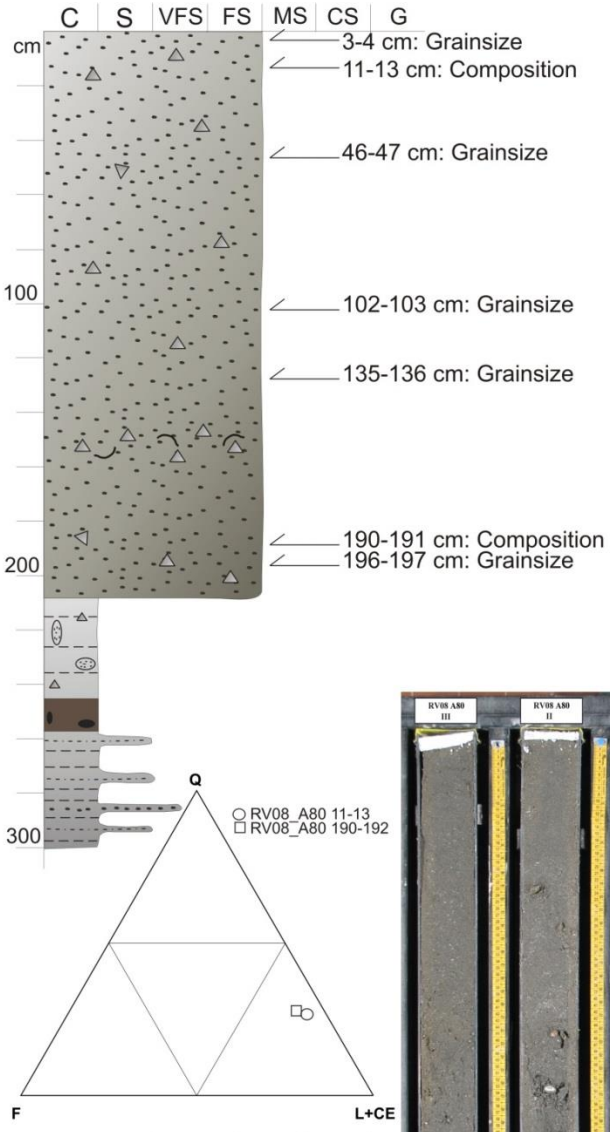

	Gravel	Sand	Mud (silt+clay)	Silt	Clay	D50
RV08_A80 3-4	0.0	98.2	1.8	1.8	0.0	209.7
RV08_A80 46-47	0.5	98.2	1.2	1.2	0.0	209.1
RV08_A80 102-103	0.0	98.9	1.1	1.1	0.0	198.8
RV08_A80 135-136	0.4	98.3	1.4	1.4	0.0	189.5
RV08_A80 196-197	2.7	94.6	2.7	2.7	0.0	200.5

RV08_A85

Area: Adriatic Sea
Date: 10/2008
Lat: 45°20'11.33
Long: 12°42'21.18
Water depth (m): 20.5

Coring device: Vibrocorer ROSSFELDER P-5B
Core lenght (cm): 436
Core diameter (mm): 90

Magnetic Suscaptibility

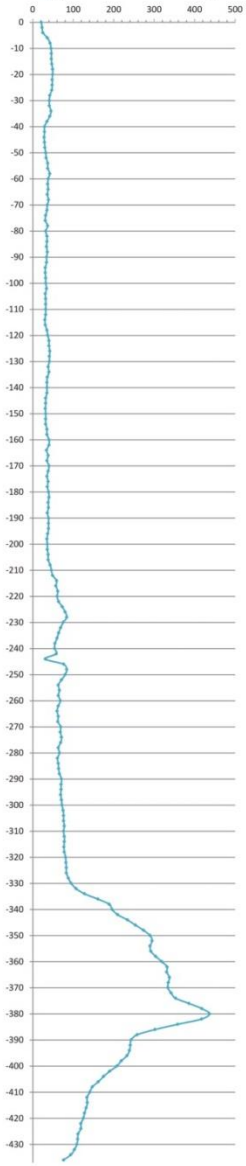

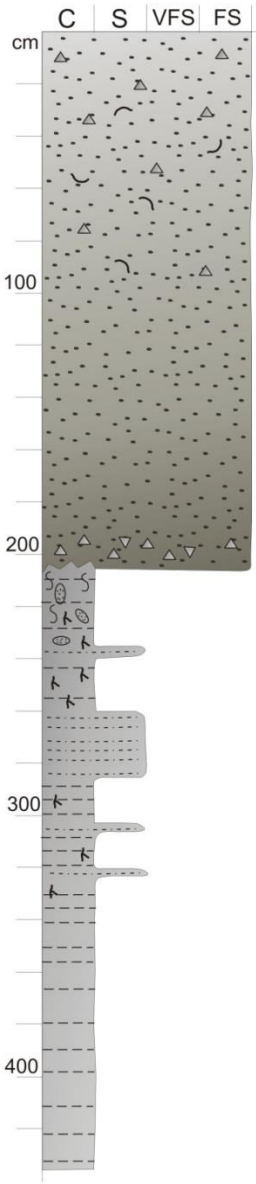

3-6 cm: Grainsize-Composition

94-95 cm: Grainsize

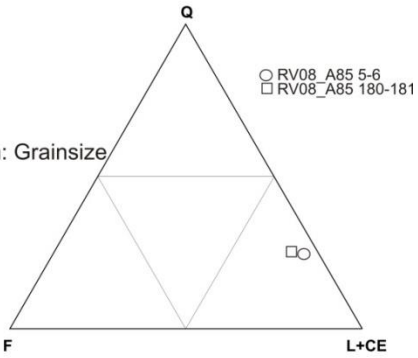

180-185 cm: Grainsize-Composition

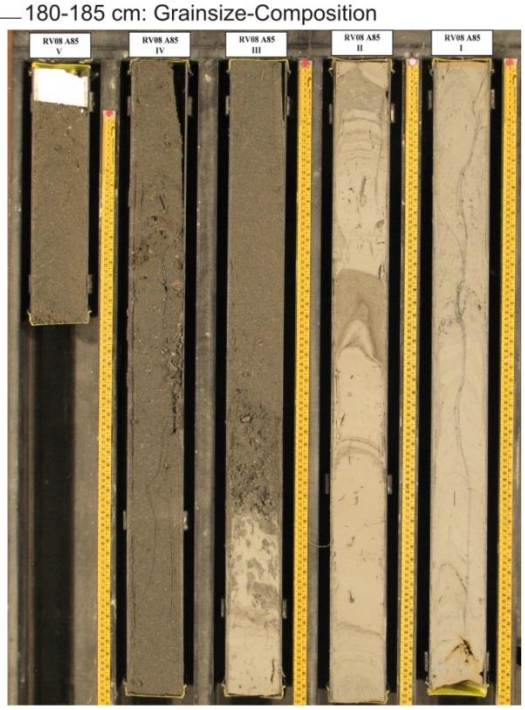

	Gravel	Sand	Mud (silt+clay)	Silt	Clay	D50
RV08_A85 3-4	0.3	99.3	0.4	0.4	0.0	205.7
RV08_A85 94-95	1.1	98.0	0.9	0.9	0.0	200.7
RV08_A85 184-185	0.3	97.4	2.3	2.3	0.0	196.1

RV08_JC88

Area: Adriatic Sea
Date: 10/2008
Lat: 45°25'36.75
Long: 12°53'03.06
Water depth (m): 21

Coring device: Vibrocorer ROSSFELDER P-5B
Core lenght (cm): 325
Core diameter (mm): 90

Magnetic Susceptibily

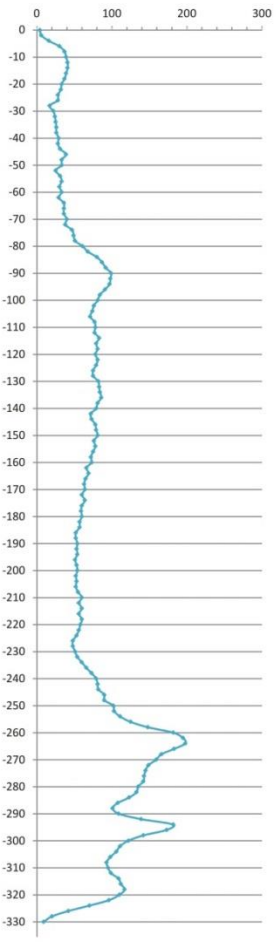

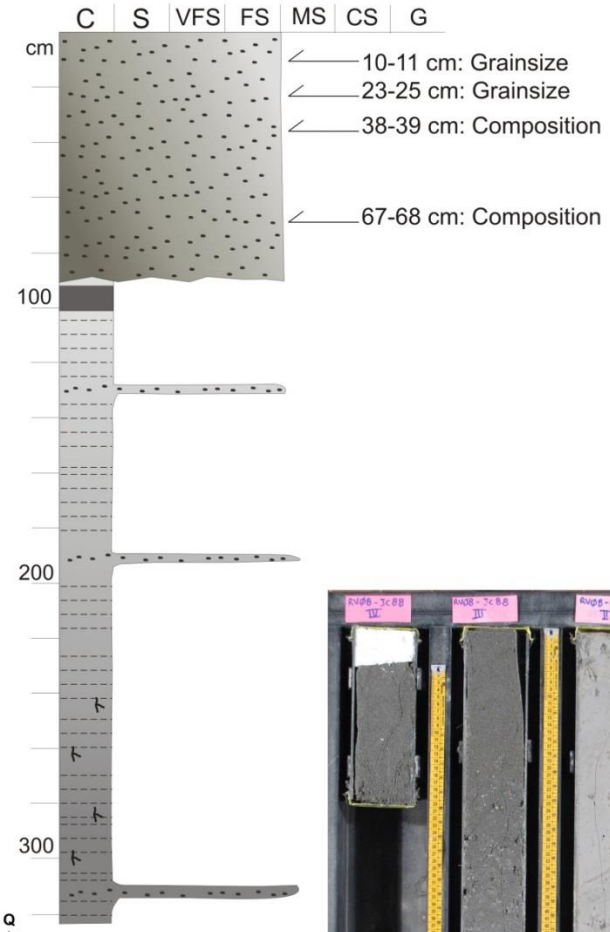

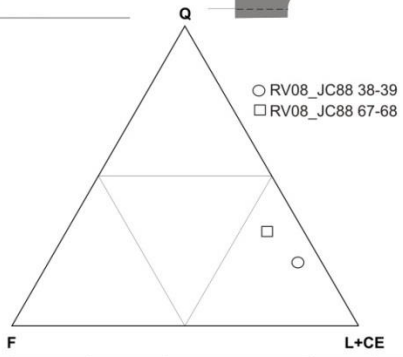

	Gravel	Sand	Mud (silt+clay)	Silt	Clay	D50
RV08_JC88 10-11	0.0	97.4	2.6	2.6	0.0	237.0
RV08_JC88 23-25	0.0	96.2	3.8	3.3	0.5	210.0

RV08_JC89

Area: Adriatic Sea
Date: 10/2008
Lat: 45°25'36.75
Long: 12°53'03.06
Water depth (m): 21

Coring device: Vibrocorer ROSSFELDER P-5B
Core lenght (cm): 325
Core diameter (mm): 90

Magnetic Susceptibility

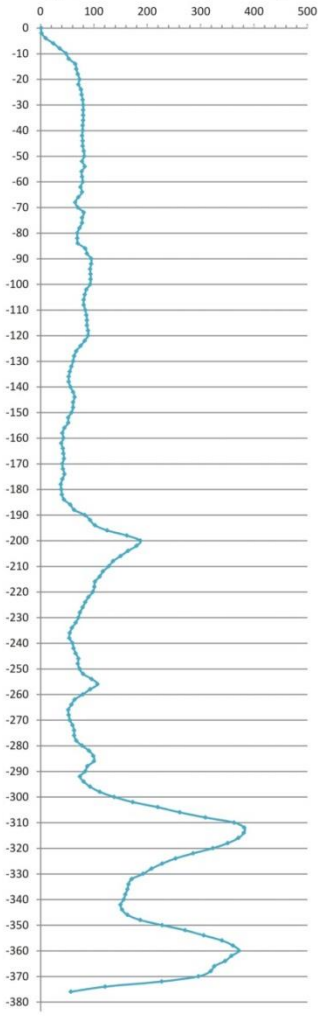

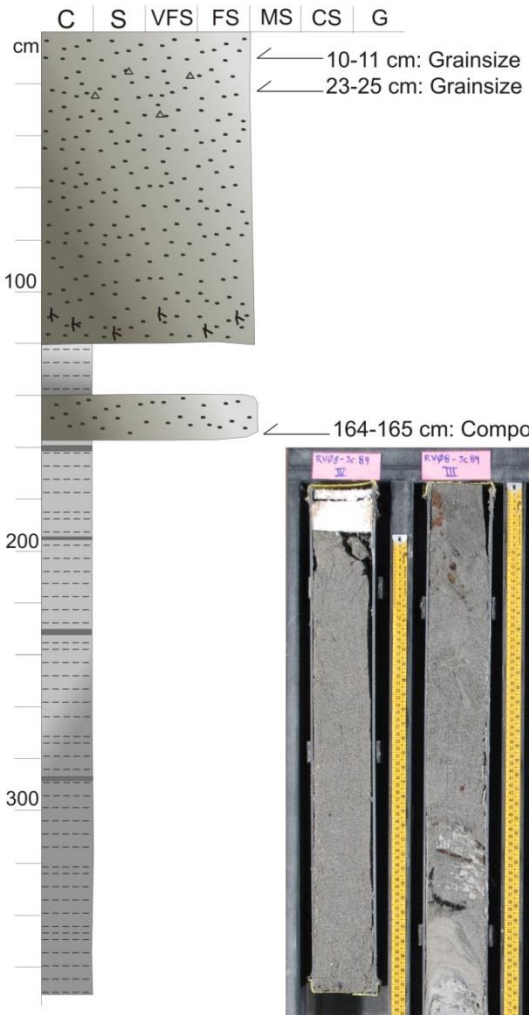

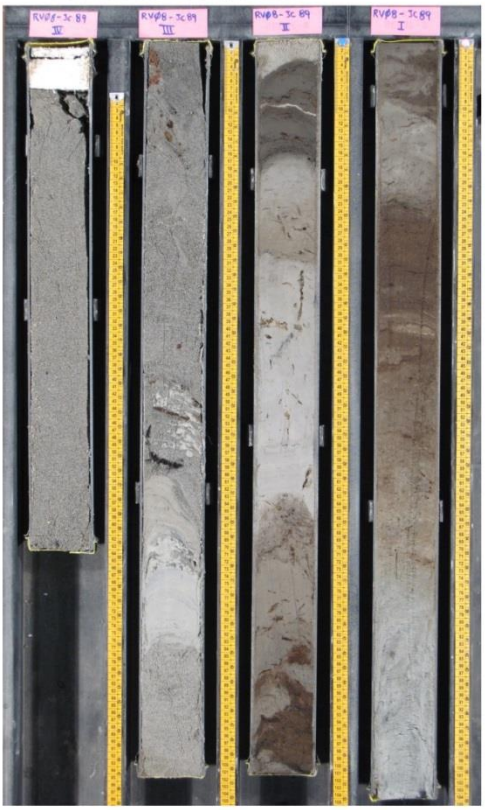

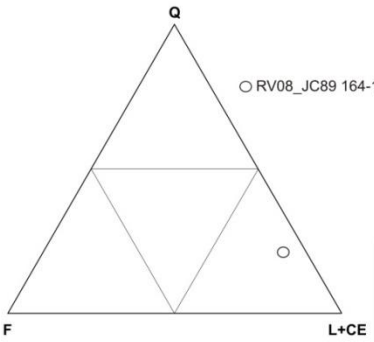

	Gravel	Sand	Mud (silt+clay)	Silt	Clay	D50
RV08_JC88 10-11	0.0	97.4	2.6	2.6	0.0	237.0
RV08_JC88 23-25	0.0	96.2	3.8	3.3	0.5	210.0

RV08_JC90

Area: Adriatic Sea
Date: 10/2008
Lat: 45°25'56.51
Long: 12°54'06.82
Water depth (m): 21

Coring device: Vibrocorer ROSSFELDER P-5B
Core lenght (cm): 460
Core diameter (mm): 90

Magnetic Susceptibility

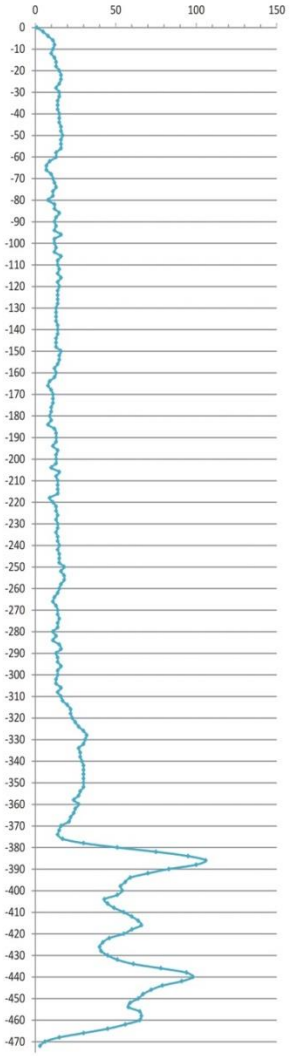

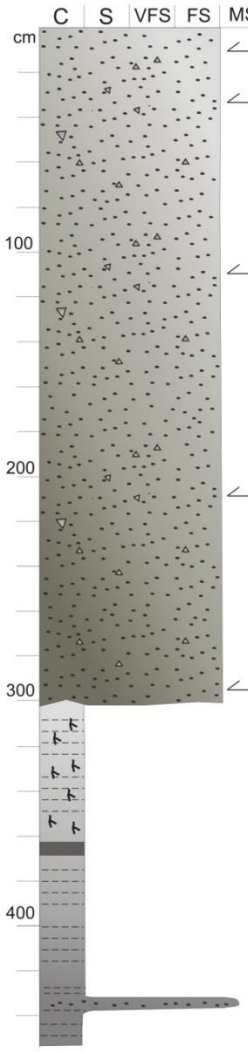

10-12 cm: Composition

36-37 cm: Grainsize

112-114 cm: Composition

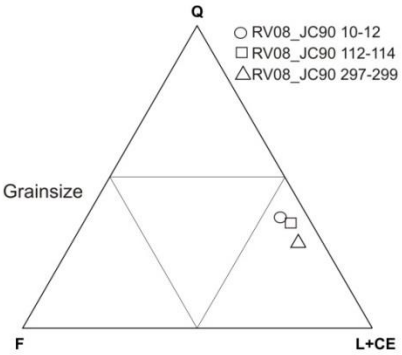

210-212 cm: Grainsize

297-300 cm: Grainsize-Composition

	Gravel	Sand	Mud (silt+clay)	Silt	Clay	D50
RV08_JC90 36-37	0.0	97.4	2.6	2.6	0.0	-
RV08_JC90 210-211	0.0	98.4	1.6	1.6	0.0	-
RV08_JC90 300-301	0.0	99.2	0.8	0.8	0.0	-

RV08_D92

Area: Adriatic Sea
Date: 10/2008
Lat: 45°27'30.01
Long: 12°56'08.92
Water depth (m): 21

Coring device: Vibrocorer ROSSFELDER P-5B
Core lenght (cm): 263
Core diameter (mm): 90

Magnetic Susceptibility

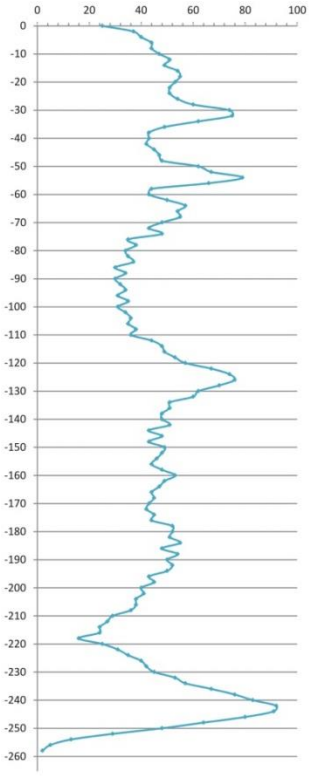

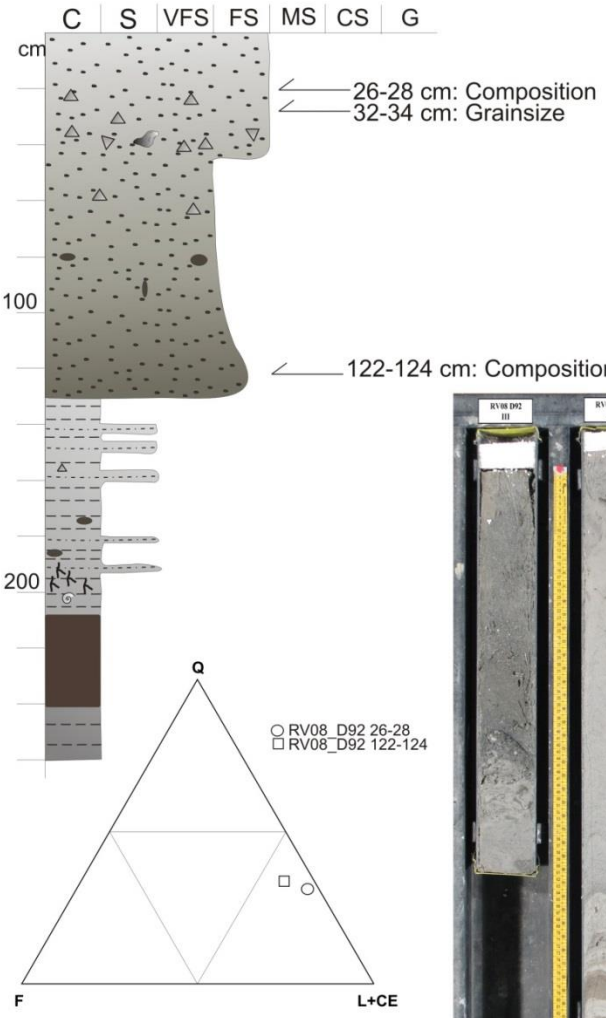

	Gravel	Sand	Mud (silt+clay)	Silt	Clay	D50
RV08_D92 33-34	4.3	82.7	13.0	13.0	0.0	161.7

RV08_M113

Area: Adriatic Sea
Date: 10/2008
Lat: 45°27'45.79
Long: 13°08'39.70
Water depth (m): 24

Coring device: Vibrocorer ROSSFELDER P-5B
Core lenght (cm): 125
Core diameter (mm): 90

Magnetic Susceptibility

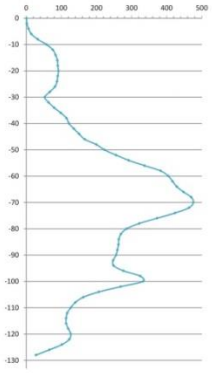

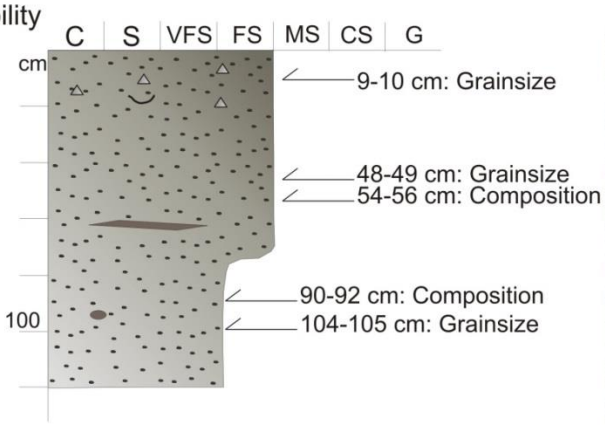

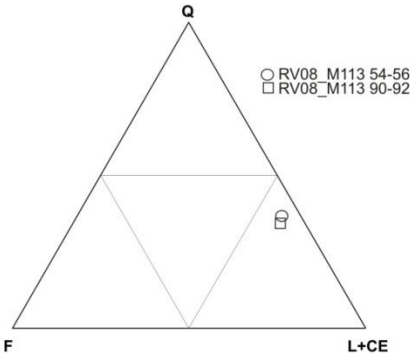

	Gravel	Sand	Mud (silt+clay)	Silt	Clay	D50
RV08_M113 9-10	1.2	85.3	13.5	13.5	0.0	147.6
RV08_M113 48-49	0.0	93.5	6.5	6.5	0.0	146.4
RV08_M113 104-105	0.0	88.6	11.4	11.4	0.0	155.4

RV08_M117

Area: Adriatic Sea
Date: 10/2008
Lat: 45°27'42.12
Long: 13°08'00.35
Water depth (m): 24

Coring device: Vibrocorer ROSSFELDER P-5B
Core lenght (cm): 195
Core diameter (mm): 90

Magnetic Susceptibility

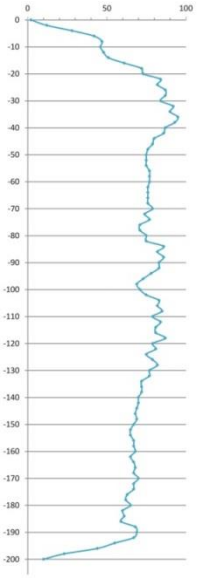

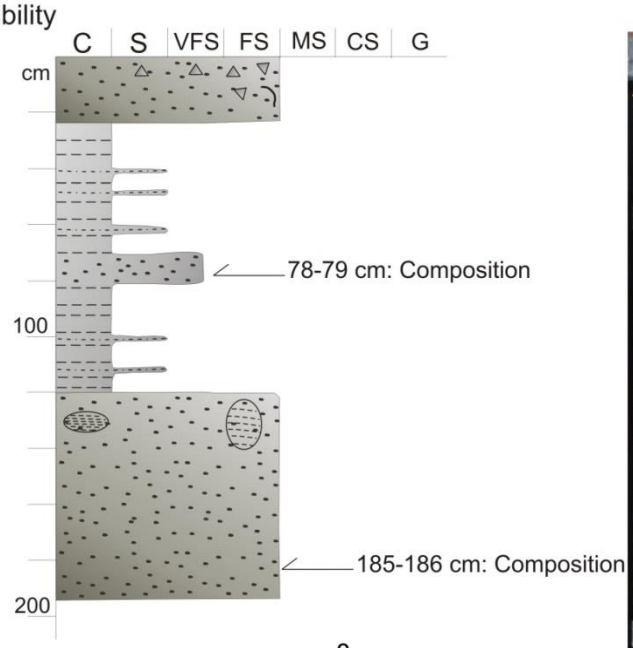

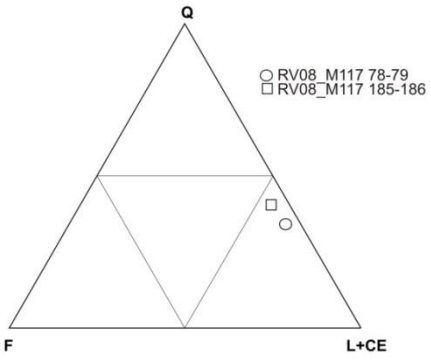

RV08_B138

Area: Adriatic Sea
Date: 10/2008
Lat: 45°34'52.01
Long: 13°12'33.13
Water depth (m): 14.4

Coring device: Vibrocorer ROSSFELDER P-5B
Core lenght (cm): 422
Core diameter (mm): 90

Magnetic Susceptivility

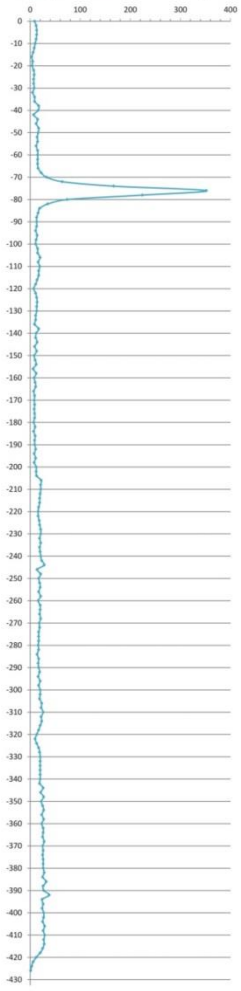

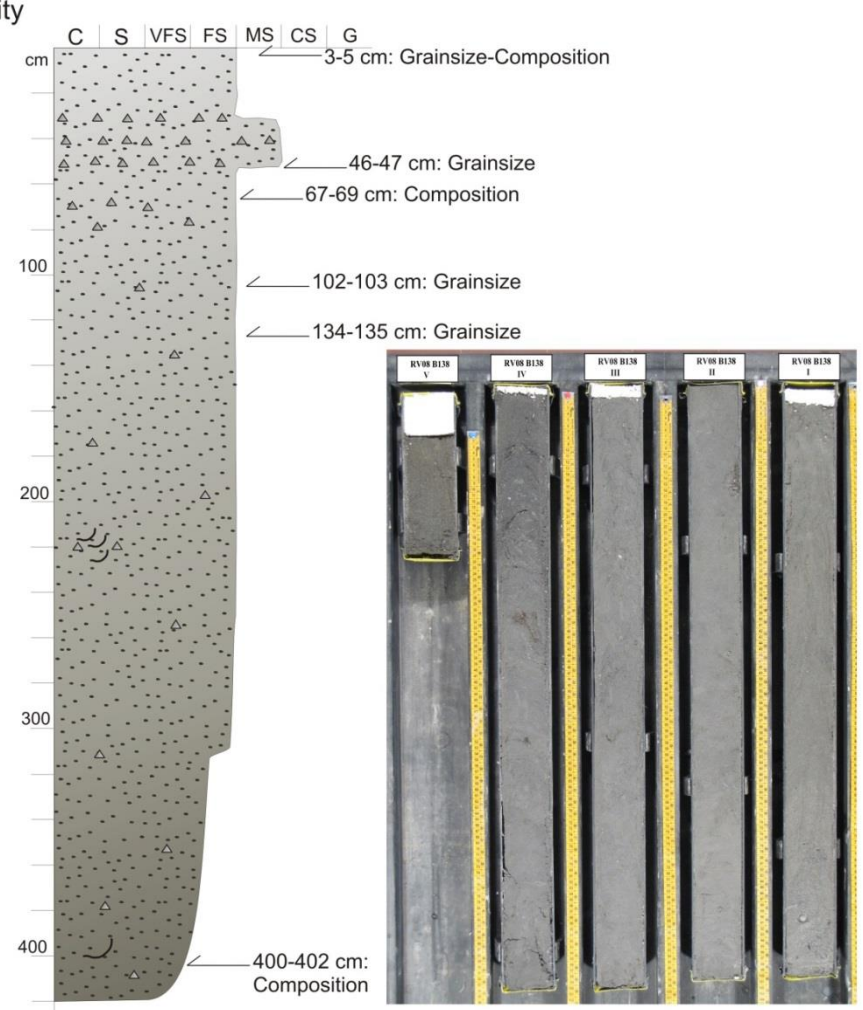

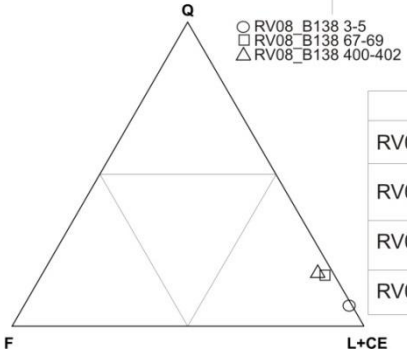

	Gravel	Sand	Mud (silt+clay)	Silt	Clay	D50
RV08_B138 3-4	0.0	99.0	1.0	1.0	0.0	188.1
RV08_B138 46-47	0.0	35.9	64.1	50.8	13.3	58.27
RV08_B138 102-103	0.1	71.3	28.6	16.3	12.3	90.17
RV08_B138 135-136	0.0	47.2	52.8	36.4	16.4	55.23

RV08_B139

Area: Adriatic Sea
Date: 10/2008
Lat: 45°36'01.73
Long: 13°10'39.54
Water depth (m): 13.2

Coring device: Vibrocorer ROSSFELDER P-5B
Core lenght (cm): 90
Core diameter (mm): 90

Magnetic Scusceptibility

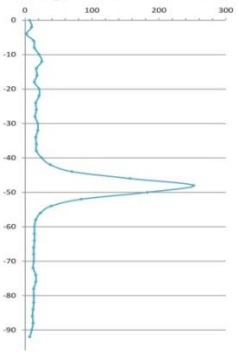

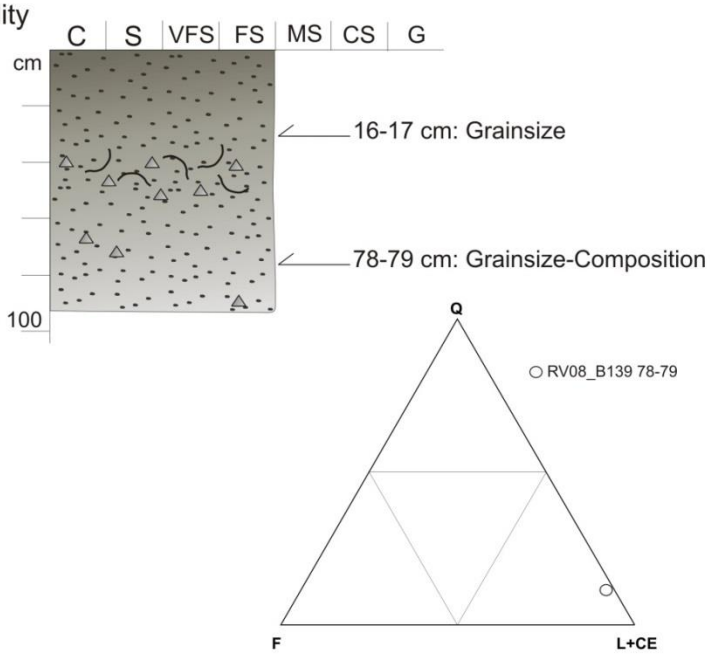

	Gravel	Sand	Mud (silt+clay)	Silt	Clay	D50
RV08_B139 16-17	0.5	98.6	0.9	0.9	0.0	195.0
RV08_B139 78-79	0.7	98.0	1.3	1.3	0.0	188.0

RV08_B141

Area: Adriatic Sea
Date: 10/2008
Lat: 45°35'18.97
Long: 13°11'29.94
Water depth (m): 14

Coring device: Vibrocorer ROSSFELDER P-5B
Core lenght (cm): 133
Core diameter (mm): 90

Magnetic Susceptibitily

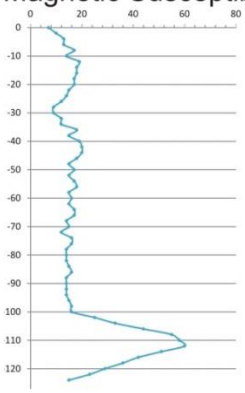

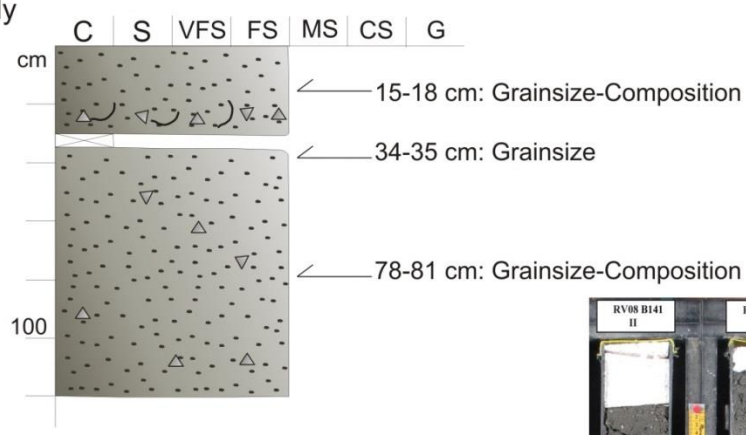

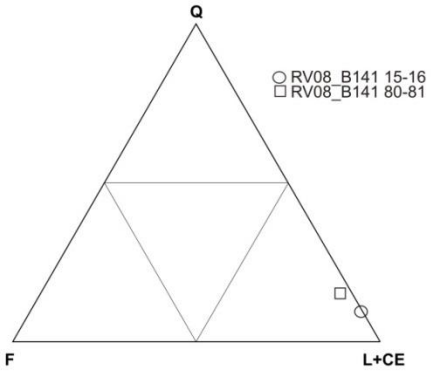

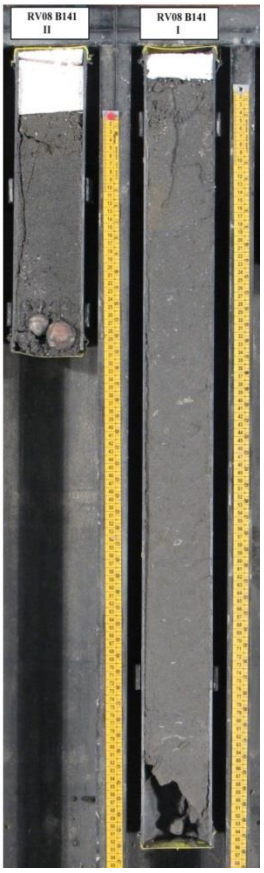

	Gravel	Sand	Mud (silt+clay)	Silt	Clay	D50
RV08_B141 17-18	0.2	98.8	1.0	1.0	0.0	169.6
RV08_B141 34-35	0.0	92.2	7.8	7.8	13.3	123.4
RV08_B141 78-79	0.0	92.9	7.1	7.1	12.3	114.3

APPENDIX B

Location of the cores

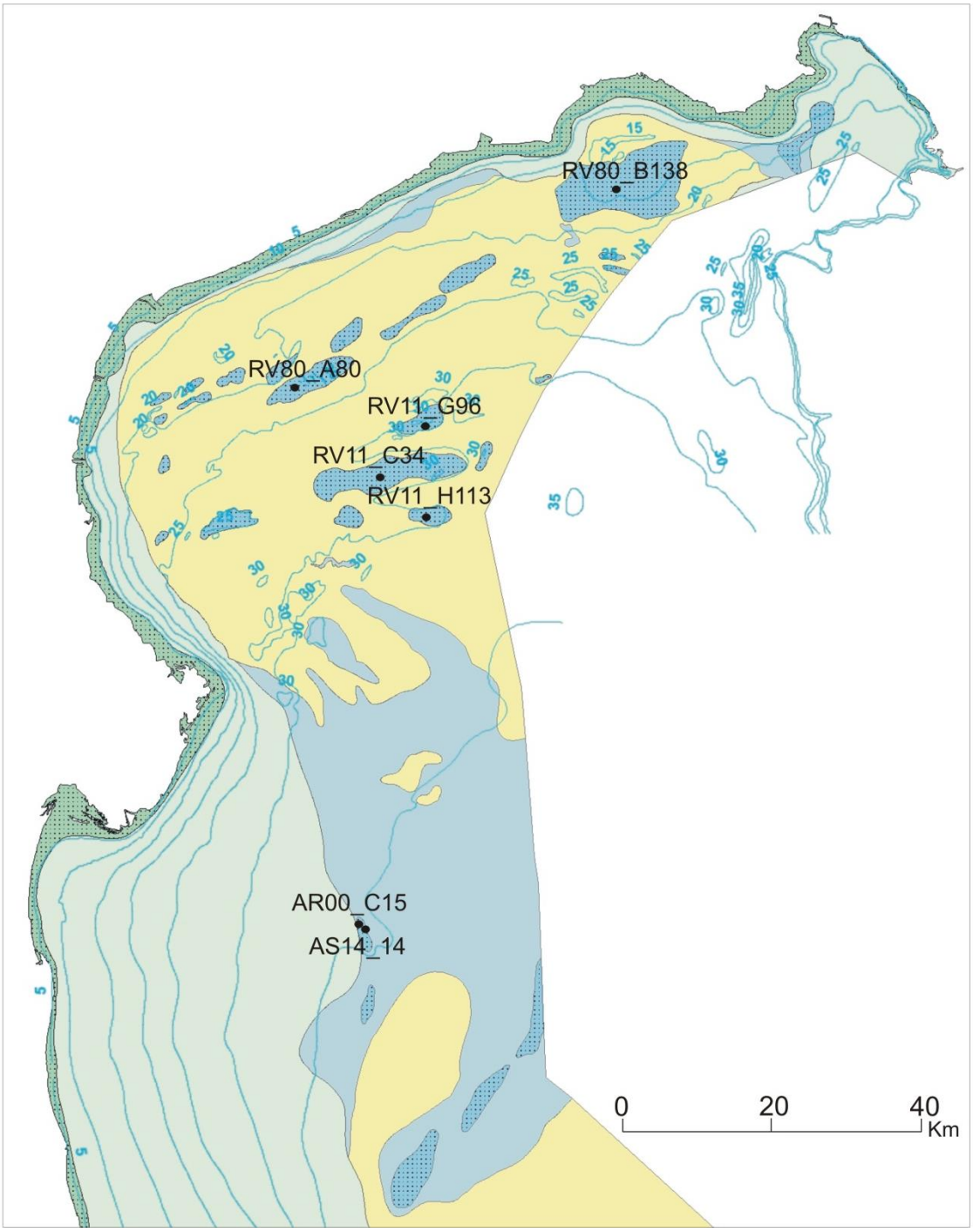

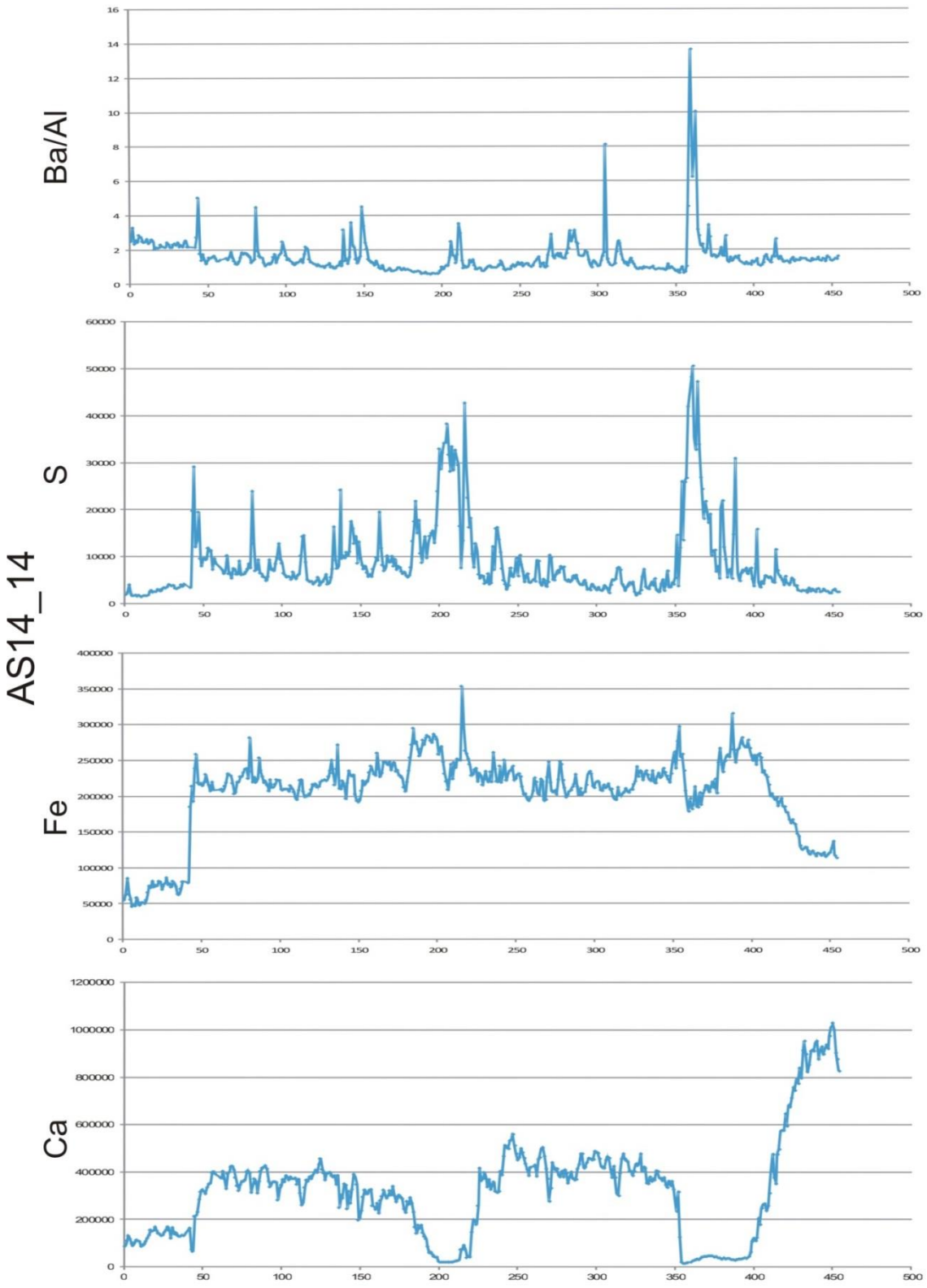
AS14_14
Ba/Al
S
Fe
Ca

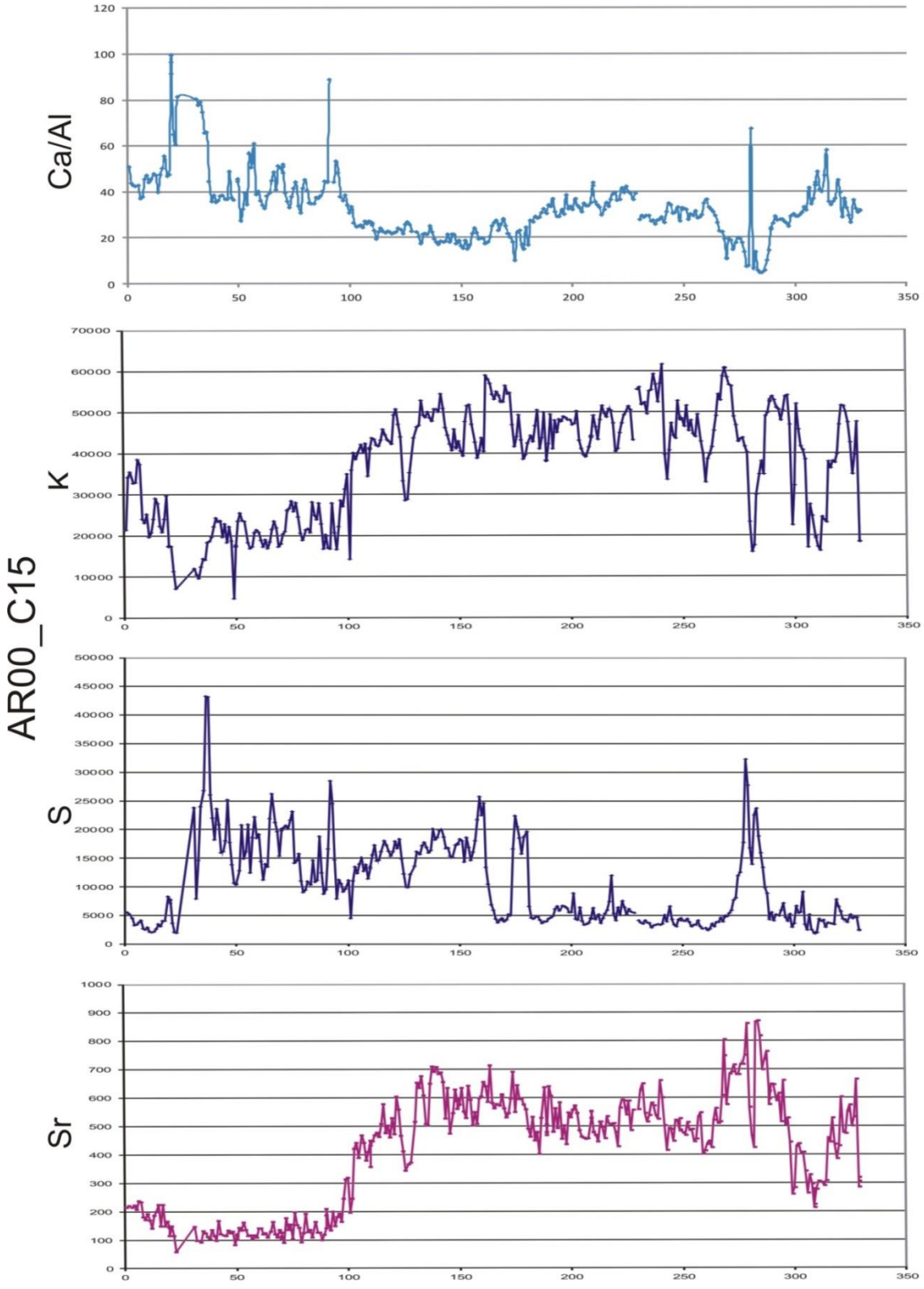
AR00_C15
Ca/Al
K
S
Sr

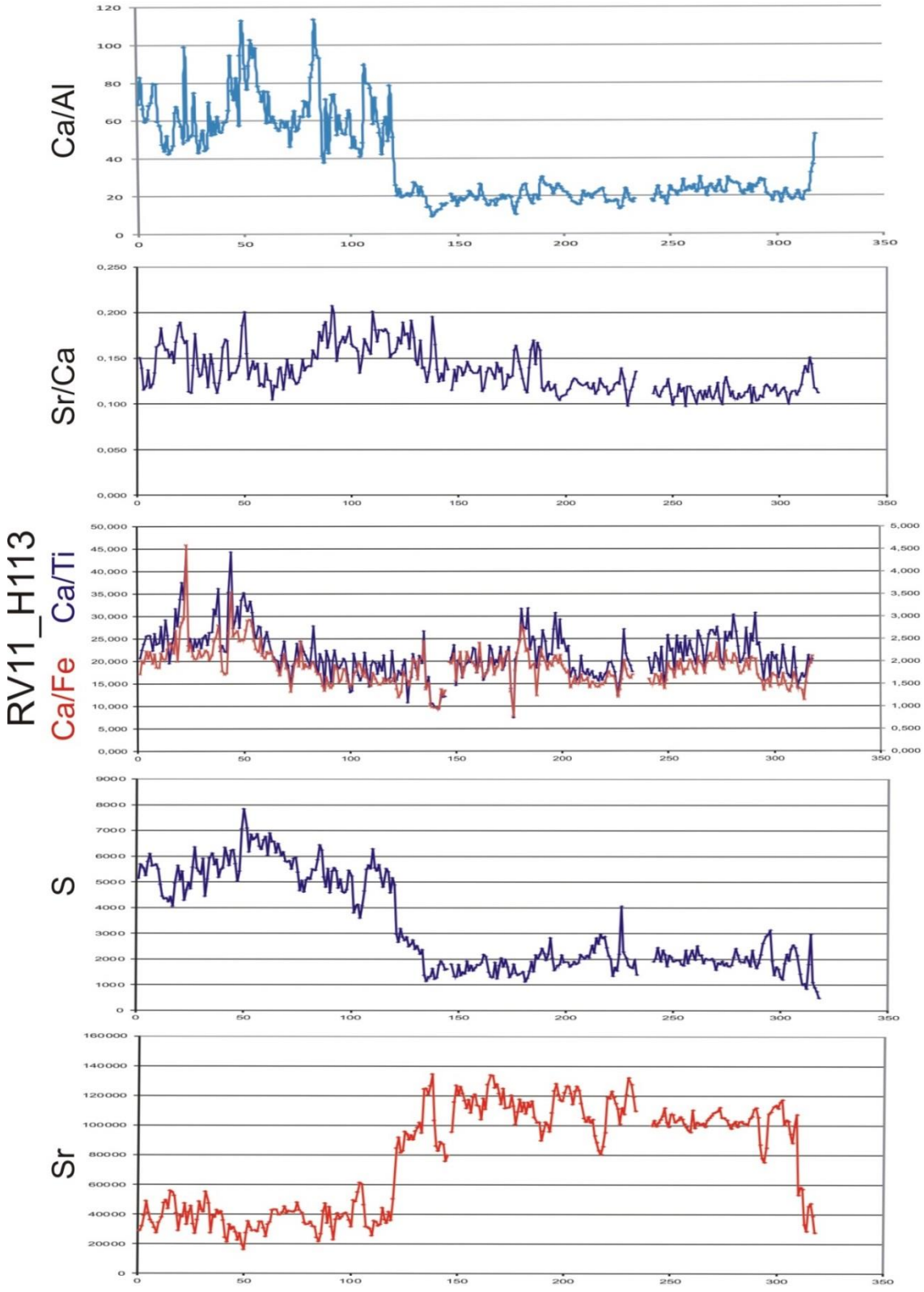
RV11_H113
Ca/Al
Sr/Ca
Ca/Fe
Ca/Ti
S
Sr

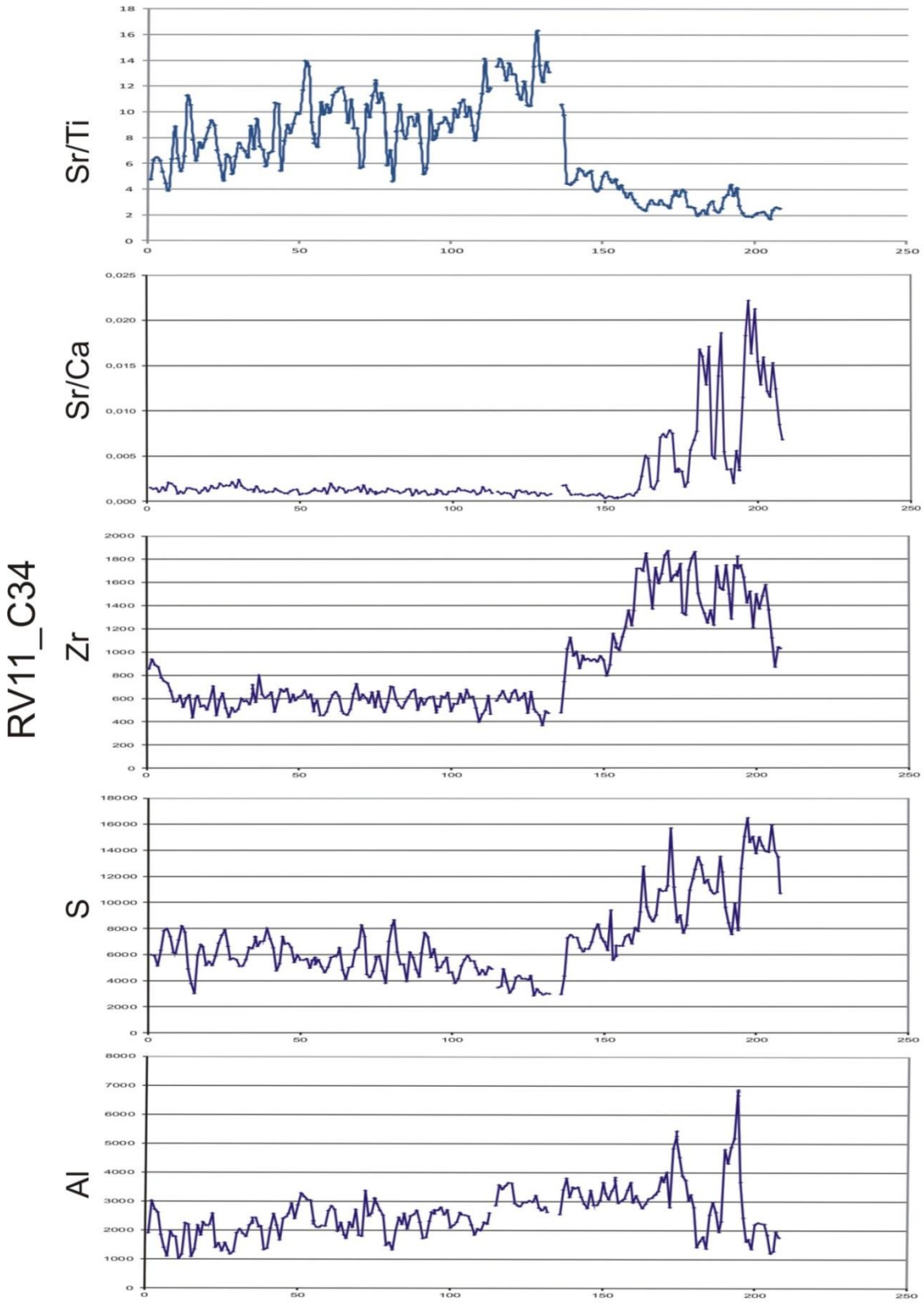
RV11_C34
Sr/Ti
Sr/Ca
Zr
S
Al

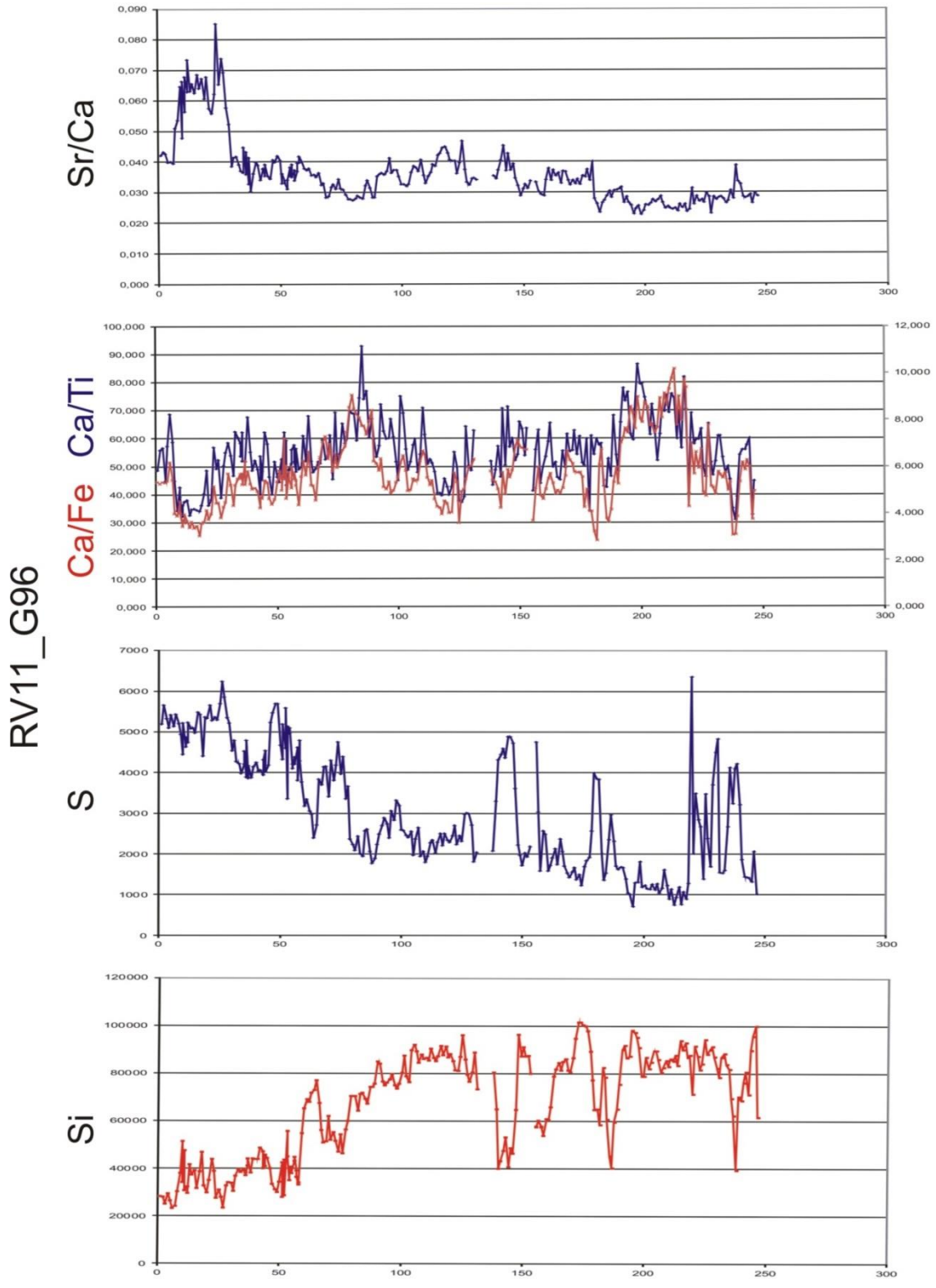
RV11_G96
Sr/Ca
Ca/Fe
Ca/Ti
S
Si

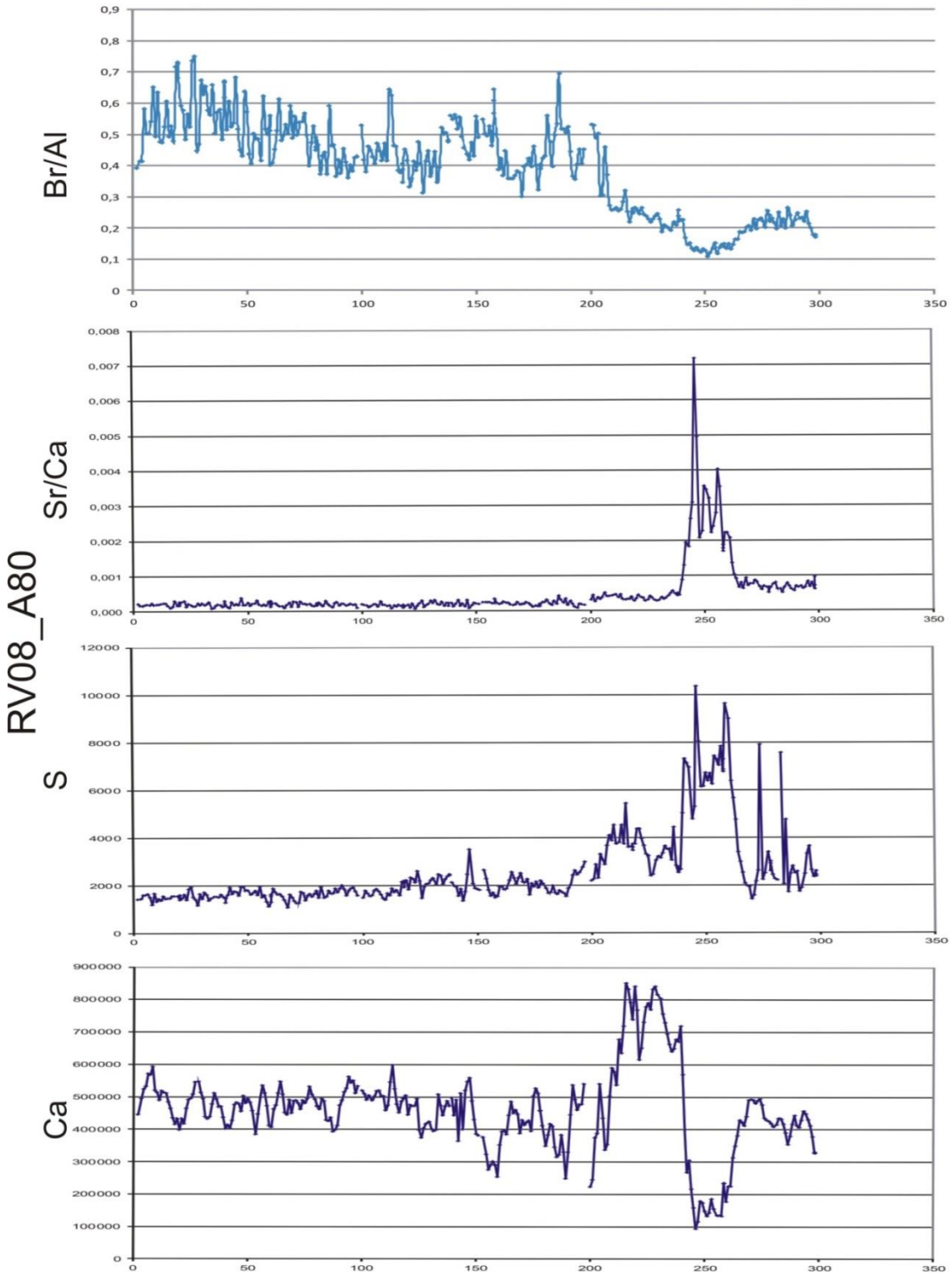
RV08_A80
Br/Al
Sr/Ca
S
Ca

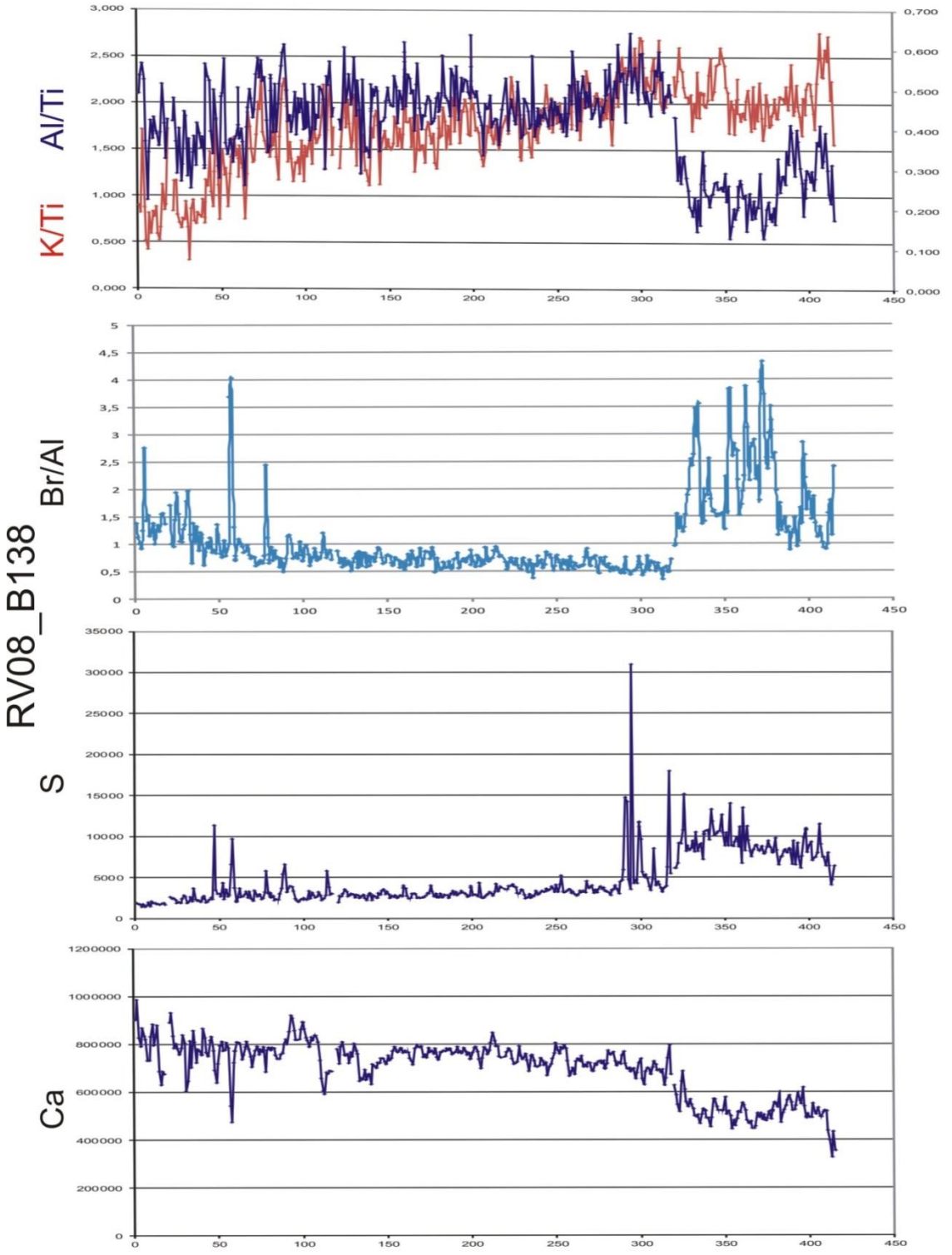
RV08_B138
K/Ti
Al/Ti
Br/Al
S
Ca